From human-intention recognition to compliant control using dynamical systems in physical human-robot interaction

Thèse N° 9120

MAHDI KHORAMSHAHI

2019

ÉCOLE POLYTECHNIQUE
FÉDÉRALE DE LAUSANNE

Words are never 'only words';
they matter because they define the contours of what we can do.
— Slavoj Žižek

To Laura

Acknowledgments

During my PhD, I had the opportunity to meet and benefit from many great people without whom this thesis would not have been written. Therefore, I am glad to begin this dissertation by expressing my sincere gratitude to them.

First and foremost, my deepest gratitude goes to my thesis director Prof. Aude Billard for her valuable suggestions, insightful criticism, and constant support throughout my academic life at Learning Algorithms and Systems Laboratory (LASA). I am undoubtedly grateful to her for giving me the freedom to pursue my own ideas while providing me with constructive feedback and guidance. I would like to thank her for accepting nothing less than excellence from me.

I would like to extend my gratitude to the member of my review committee: Prof. Abderrahmane Kheddar, Prof. Nathanaël Jarrasé, and Prof. Auke Ijspeert, for their time and effort, and their insightful comments and feedback on my thesis draft. Furthermore, I am grateful to Prof. Ronan Boulic who served as the president of my committee.

I would like to thank the senior members of LASA for passing down a legacy of scientific exploration, concrete ideas, and comradeship. I am grateful to Mohammad Khansari and Klas Kronander whose previous works shaped the way that I think and helped me to have a better scientific approach during my PhD. Furthermore, I would like to thank Ashwini Shukla and Jose Medina for their support and sharing their knowledge with me. As Isaac Newton puts it: "If I have seen further it is by standing on the shoulders of Giants."

Next, I would like to thank those with whom it was a never a dull moment in the lab. I am grateful to Nili, Nadia, and Guillaume for all the excitements, fun moments, their sincere friendship, and their emotional support. A big thanks certainly also goes to Nicolas for his kind-hearted friendship and organizing many social events. Other big thanks go to my officemates for being fun and supportive: Nicolas, Walid, and Joel.

I would like to thank my other colleagues, with whom I have shared moments of deep anxiety but also of big excitement: Iason, Sina, Felix, Denys, Andrew, Ajung, Murali, Wissam, João, Lucia, Hang, Miao, Ravin, Sahar, Suphi, and Seungsu. Many warm thanks go to the new generation for keeping LASA lively and cheerful: Baptiste, Athanasios, Konstantinos, David, Lukas, Leonardo, Illaria, Anais, Saurav, Michael, Kunpeng, Farshad, Salman, and Bernardo. I

Abstract

Human ability to coordinate one's actions with other individuals to perform a task together is fascinating. For example, we coordinate our action with others when we carry a heavy object or when we construct a piece of furniture. Capabilities such as (1) force/compliance adaptation, (2) intention recognition, and (3) action/motion prediction enables us to assist others and fulfill the task. For instance, by adapting the compliance, we not only reject undesirable perturbations that undermine the task but also incorporate others' motions into the interaction. Complying with partners' motions allows us to recognize their intention and consequently predict their actions. With the growth of factories involving humans and robots working side by side, designing controllers and algorithms with such capacities is a crucial step toward assistive robotics. The challenge, however, is to attain a unified control strategy with predictive/adaptive capacities at the task, motion, and force-level which ensures a stable and safe interaction. To this aim, this thesis proposes a state-dependent dynamical system-based approach for prediction and control in physical human-robot interactions.

In the first part of this dissertation, we focus on the human capacity to predict their partners' motion. More specifically, we investigate mechanisms of spatio-temporal coordination between two partners. We employ a simple scenario called "the mirror game" where two individuals (human, robot, or avatar) imitate each other's motions. Our empirical assessment reveal that the intention-based prediction of the leader's motions allows the follower to compensate for perception-action delays and to improve the tracking performance in terms of temporal coordination and confidence.

In the second part of this dissertation, we propose an adaptive mechanism that enables the robot to recognize the intention of a human user. We utilize state-dependent dynamical systems for motion planning and impedance control to deliver safe and compliant human-robot interaction. We consider a series of tasks (possible human intentions) encoded by dynamical system. Applying a similarity metric between the real velocities (induced by the human) and desired velocities generated by the dynamical systems, the robot is thus able to recognize the human's intention and switch to the intended task. We provide a rigorous experimental and analytical evaluation of our method yielding an interaction behavior that is safe and intuitive for the human.

Finally, we tackle the compliance adaptation capability. We propose an admittance controller

Abstract

that reacts only when human-intentional forces are detected. Intentional and accidental forces are distinguished by measuring the persistency of the external forces, through a computation of the autocorrelation/energy of the force patterns. The overall controller exhibits variable stiffness where high stiffness allows the robot to reject the external disturbances and execute the task autonomously whereas low stiffness enables the robot to comply with human intentional forces. We demonstrate that our control architecture is effective in delivering satisfactory tracking and compliant behavior through a series of robotic experimentations.

Keywords: Physical human-robot interaction, intention recognition, task adaptation, motion prediction, compliance and motion control, dynamical systems, impedance and admittance control.

Résumé

La capacité humaine de coordonner nos actions avec celles des autres pour mener à bien une tâche ensemble est fascinante. Par exemple, nous coordonnons nos actions avec les autres lorsque nous transportons un objet lourd ou lorsque nous devons assembler un meuble. Les capacités de (1) adaptation des forces/compliance, (2) reconnaissance de l'intention et (3) prédiction du mouvement/des actions nous permettent de porter assistance aux autres et de réaliser la tâche. Par exemple, en adaptant la compliance, nous pouvons non seulement rejeter les perturbations indésirables qui pourraient compromettre le succès de la tâche, mais aussi incorporer les mouvements des autres dans l'interaction. S'adapter de manière souple aux mouvements du partenaire nous permet de reconnaître ses intentions et par conséquent de prédire ses actions. Avec l'avènement des usines où humains et robots travaillent côte à côte, la mise en place de contrôleurs et d'algorithmes qui incluent de telles capacités apparaît comme une étape cruciale vers la robotique d'assistance. Le défi consiste à atteindre une stratégie de contrôle unifiée avec des capacités de prédiction/adaptation au niveau de la tâche, du mouvement et des forces qui garantisse une interaction stable et sécurisée. Dans ce but, cette thèse propose une approche basée sur les systèmes dynamiques invariants pour la prédiction et le contrôle dans les interactions physiques humain-robot.

Dans la première partie de cette thèse, nous explorons la capacité humaine de prédire les mouvements d'un partenaire. En particulier, nous étudions les mécanismes spatio-temporels de coordinations entres deux partenaires. Nous exploitons un scénario minimaliste appelé le Jeu du Miroir, où deux individus (humains, robots ou avatars) imitent réciproquement leurs mouvements. Notre évaluation empirique révèle que la prédiction des mouvements du meneur, basée sur l'intention, permet au suiveur de compenser les délais de perception-action et d'améliorer les performances de suivi en termes de coordination temporelle et de confiance.

Dans la seconde partie de cette thèse, nous proposons un mécanisme d'adaptation qui permet au robot de reconnaître l'intention d'un utilisateur humain. Nous exploitons les systèmes dynamiques invariants pour la planification du mouvement et le contrôle d'impédance pour fournir une interaction humain-robot sécurisée et souple. Nous considérons une série de tâches (ou intentions humaines possibles) encodée par des systèmes dynamiques. En appliquant une métrique de similarité entre la vitesse réelle (causée par l'humain) et la vitesse désirée générée par les systèmes dynamiques, le robot est alors capable de reconnaître l'intention du partenaire humain et de passer à la tâche correspondant à cette dernière. Nous

Résumé

fournissons une évaluation expérimentale et analytique rigoureuse de notre méthode, qui permet d'obtenir un comportement sécurisé et intuitif pour l'être humain.

Enfin, nous abordons la capacité d'adaptation de la compliance. Nous proposons un contrôleur d'admittance qui réagit uniquement lorsque des forces d'origine humaine sont détectées. Les forces intentionnelles et accidentelles sont distinguées en mesurant la persistance des forces externes, par un calcul de l'autocorrélation/énergie des motifs de forces. Le contrôleur final dispose d'une rigidité variable. Une rigidité importante permet de rejeter les perturbations externes et d'exécuter la tâche de manière autonome, alors qu'une rigidité faible permet au robot de s'adapter en souplesse aux forces humaines volontaires. Nous démontrons que notre architecture de contrôle est efficace pour fournir un suivi satisfaisant et un comportement adaptatif lors d'une série d'expériences robotiques.

Mots-clés : Interaction physique humain-robot, reconnaissance d'intention, adaptation à la tâche, prédiction de mouvement, compliance et contrôle de mouvement, systèmes dynamiques, contrôle d'impédance et d'admittance.

Contents

Contents

List of Figures

Notations

Abbreviations

pHRI	Physical human-robot interaction
DS	Dynamical system(s)
DoF	Degrees-of-freedom
CWT	Continuous wavelet transform
XWT	Cross wavelet transform
GMM	Gaussian mixture model
RT	Reaction time

Symbols

Spaces

$\mathbb{R}^n$	set of n-dimensional real numbers
$\mathbb{R}^+$	set of positive real numbers

Variables

q	Joint configuration
x	Robot's position
$\dot{x}_r$	Robot's real velocity
$\dot{x}_d$	Robot's desired velocity
F_e	External force
F_c	control force

Functions and operators

$f(.)$	State-dependent dynamical system
$\nabla_x V(x)$	Gradient of a scalar function w.r.t. x
$\lvert . \rvert^2$	Norm-squared
v^T	Transpose of a vector (i.e., v)
$log(.)$	The natural logarithmic function
∂	Partial derivative
$\mathcal{D}$	Differential (of a map)

1 Introduction

History is on the cusp of a robotic revolution. It is estimated that it will transform the global economy over the next 20 years. By physically collaborating with humans, robots aim at reducing human effort further in performing repetitive and cumbersome tasks. Many domains will benefit from such assistance offered by robots: manufacturing, home applications, as well as medical and social services. Manufacturing is a particular domain where such repetitive and cumbersome tasks are ubiquitous; e.g., pick-and-place, polishing, brushing, and transferring heavy loads. However, until the last decade, robots were designed only to operate autonomously with minimum human interaction in an isolated workspace. Therefore, the collaboration between industrial robots and humans was limited. For instance, an industrial robot is indeed able to lift and orient a heavy object to be operated by a human worker; e.g., to be polished or welded. However, the safety and performance of such systems are limited as traditional robots do not react or adapt to human behavior. This excludes many collaborative tasks which, as humans, we perform through physical interactions with one another. To overcome this, in the last two decades, tremendous amount of work was dedicated by roboticists toward collaborative robots.

In contrast to industrial robots, the new generation of robots aim at physically interacting with humans in a shared workspace; i.e., to interact in direct contact with humans or via a jointly manipulated objected. These **co**llaborative ro**bot**s are often referred to as **cobot**s or co-robots. The capacity to interact physically with humans allows cobots to be adaptive and reactive toward the human user. For example, by following the human guidance, a robot can orient and position a heavy object as intended by the human user. The ability to react to human guidance and to continuously rely on human leadership enables the robot to perform complex tasks. In this fashion, the human supervises the execution of the task and modifies the robotic behavior. Consider an example where a human supervises a robot polishing a surface and changes the polishing patterns by physically demonstrating his/her desired behavior. This leaves the repetitive and cumbersome aspects of the task to the robot while the human acts as a leader on a decision-making level. Given the multifarious applications of physically interactive cobots, it is not a surprise that their popularity is on the rise. Robotic Industries

Association (RIA) estimated that collaborative robots will make up about 34% of all robot sales in 2025. Currently, it is only 3%. However, reaching an effective collaboration through physical interaction imposes several challenges especially for control and motion-planning.

The safety of the human user is of paramount importance as collaborative robots are expected to come into direct contact with human beings. The safety can be addressed both from a mechanical design and a control perspective. Force-limited robots, equipped with force-torque sensors, are designed to detect and react properly to abnormal interaction forces. For instance, in coming into high-impact contacts with humans, the robot stops by sensing an abrupt change in interaction forces. Moreover, to reduce potential mechanical impact, cobots are designed to be lighter, with soft and round surface areas on the body parts. From a control perspective, safety can be ensured through active compliance offered by the controller. Traditionally, the sole purpose of a robot in an industrial setting was to precisely repeat a pre-defined trajectory where high-gain position control is favored. Such control strategy is unsafe in coming into contact with humans. Without any reactivity toward human, this strategy is prone to generating high mechanical impacts due to heavy robotic arms and high speed movements. As a solution, compliant control has been proposed to control the dynamics of the interaction where the robot appears as a mass-spring-damper to the external world. Instead of solely minimizing the tracking error, this controller minimizes a combination of tracking error and applied forces to the environment. Therefore, compliant control allows for safe interaction with a human-user while executing a reference trajectory; i.e., the robot moves in the direction of human applied-forces and smoothly returns to its reference trajectories when human retreats. However, this compliant behavior is limited to the force-level. The human-induced motions are damped and "forgotten" as the human retreats from the interaction. This turns the robot into a *passive follower* toward human guidance. Advanced motion-planners with prediction and adaptive capabilities can overcome this limitation and extend the robotic compliant behavior to the motion and task-level. In this manner, the robot also complies to human-intended motions and tasks which renders the robot as a *proactive follower*.

Cobots are aimed to be versatile in terms of number of tasks that they can perform. This is considered in their flexible design which allows to use different end-effectors and tools. For instance, the robot can perform pick-and-place using a gripper and change its tool to a polisher for polishing tasks. This enables cobots to be used in diverse locations and setting; both stationary or with mobile platforms. Therefore, it is necessary for the robot to be able to learn new tasks in a simple and efficient way. *Learning from demonstration* is a suitable approach where the robot learns new tasks from human-guided motions. The literature of robot learning offers an abundance of machine learning techniques to encode such desired motions into a motion-planner. Having learned a new task and using compliant control, the robot can physically collaborate with its human partner. Yet, it is another challenge for the robot to modify its task or switch across tasks during the interaction. This is a crucial step toward ***proactivity***; i.e., the robotic capability to recognize the human intentions and comply to human desired behaviors by adapting robotic motions and tasks. In this line of thought, the proactivity is achieved through adaptation of different components; i.e., force-generation,

motion-generation, and task-selection. Such adaptation toward human intention remains an unsolved challenge, specially due to environmental uncertainties. Cobots are expected to operate in natural environments, which compared to the highly controlled industrial settings, elicit a higher level of uncertainties. The human behavior can be the main source of such uncertainties. For instance, the human motions might be noisy and not a clear representative of the intended task. In some cases, the human intention might abruptly change or the applied forces might be accidental and detrimental to the stability of the task. Therefore, a seamless robotic interaction requires a control architecture which accounts for all these situations. This thesis tackles these challenges by providing solutions toward human-intention recognition, motion and task-adaptation, and intentional forces recognition.

Proactivity can be achieved in two forms. In the first form, the robot adapts its task according to the human interaction; namely motion-adaptation. In the other form, the robot adapts its task by means of switching to another task that resembles the human input; namely task adaptation. Both forms impose new challenges for stable and efficient motion planning. For instance, a parameterized motion-generator that is adaptable and remains stable under the variation of its parameters. It is also required that the motion generator encodes for different tasks and allows for smooth and stable transition across them. Given the adaptability of the motion-generation, human-intention recognition is still required for a meaningful adaptation toward an assistive behavior. The robotic literature offers methods to identify the underlying intention of an observed motion. Reviewing this literature in Section 2, we point out that such proposed methods are often offline whereas the intentions are required to be recognized online as the human physically interacts with the robot. In short, online intention-recognition along with task-adaptation and motion-adaptation are the key challenges in reaching a proactive robotic behavior.

The recent advancements in motion-planning and control are significant contributions in achieving robotic proactive behavior. For instance, state-dependent Dynamical Systems (DS) offers a powerful tool for motion-planning aspects of the interaction. Khansari-Zadeh and Billard (2011b) proposed a learning approach for encoding demonstrations in a DS in a stable manner; i.e., avoiding spurious attractors and divergent behavior. The first advantage of this approach is its generalization to unseen contexts. For example, the robot can perform a reaching motion from an unseen initial condition. The other advantage is the reactivity of the motion planning which arises from the state-dependency of DS. Upon perturbations, instead of returning to the initial planned trajectory, the robot re-plans with respect to the new state. This enables the robot to intelligently reacts to human interactions. This approach is also suitable for incremental learning methods where the robot gradually learns a new task during the interaction. As exploited in this thesis, DS-based motion planning lays a strong foundation for further development with regard to adaptive behavior.

To address the compliant-control aspect of the interaction, compliant control strategies are of great interest. The impedance control has been proposed by Hogan (1988) in order to achieve compliant interaction with the environment. The robot can track a given trajectory

while exhibiting a compliant behavior toward external perturbations. Indeed, the robot might deviate from the original trajectory, but in the absence of perturbations, the robot can execute its task autonomously. Furthermore, without a desired trajectory, the robot follows human forces acting as a passive follower. Having a dynamical system (as a motion-planner) and an impedance controller in the control loop allows for a reactive motion planning. This has been shown by Kronander and Billard (2016) to lead to a reliable passive interaction with the environment. The robot acts as an active leader that allows for physical interaction with the human as the follower. As demonstrated in this thesis, by adding adaptive capabilities, the impedance and admittance can be utilized to reach proactive behavior in physical interactions.

The goal of this thesis is to provide a unified control framework that understands the human co-worker intention and adapts to it through physical interaction; more specifically, a framework which addresses intention recognition, task and motion adaptation, and compliant interaction with humans. In our first endeavor toward intention recognition, in Chapter 3, we study the human-follower behavior at the kinematic level in a leader-follower setting. We use the Mirror Game framework proposed by Noy et al. (2011) where one individual leads the task by creating his/her own desirable motions while the other individual is instructed to follow the leader's motion synchronously. Our investigations confirm that the follower proactive behavior can be explained by an adaptive dynamical system. Therefore, in the follow-up contributions, we extend this adaptation property to physically interactive robots. More specifically, we extend the DS-impedance control framework to reach motion and task-adaptation capabilities. In Chapter 4, we propose a DS formulation that allows the robot to modify its task through transformations such as translation, rotation, and scaling. Through an adaptive mechanism, the robot captures the human intended motions during the physical interaction and proactively executes them. In Chapter 5, we propose another DS formulation that encodes for several tasks with stable and smooth transition properties. Beside versatile motion-generation, this formulation also allows for intention recognition. Through human-induced motions, the robot recognizes the human-intended task and proactively executes it. Furthermore, we tackle another challenge in reaching a robust adaptive behavior for physically interactive robots with regard to disturbances and unintentional forces. In chapter 6, we offer an algorithm that distinguishes between intentional and accidental forces; allowing the robot to reject undesirable disturbances and adapt to intentional inputs. Each contribution is illustrated by a conceptual graph in Fig. 1.1. Such motion and compliance adaptation allows the robot to change roles from a stiff leader to a compliant leader, and to a passive or proactive follower; see Evrard and Kheddar (2009) as pioneer work for role adaptation.

In the following, we present the outline of the thesis along with the contributions. Later in Section 1.2, we introduce further the approaches taken in this thesis.
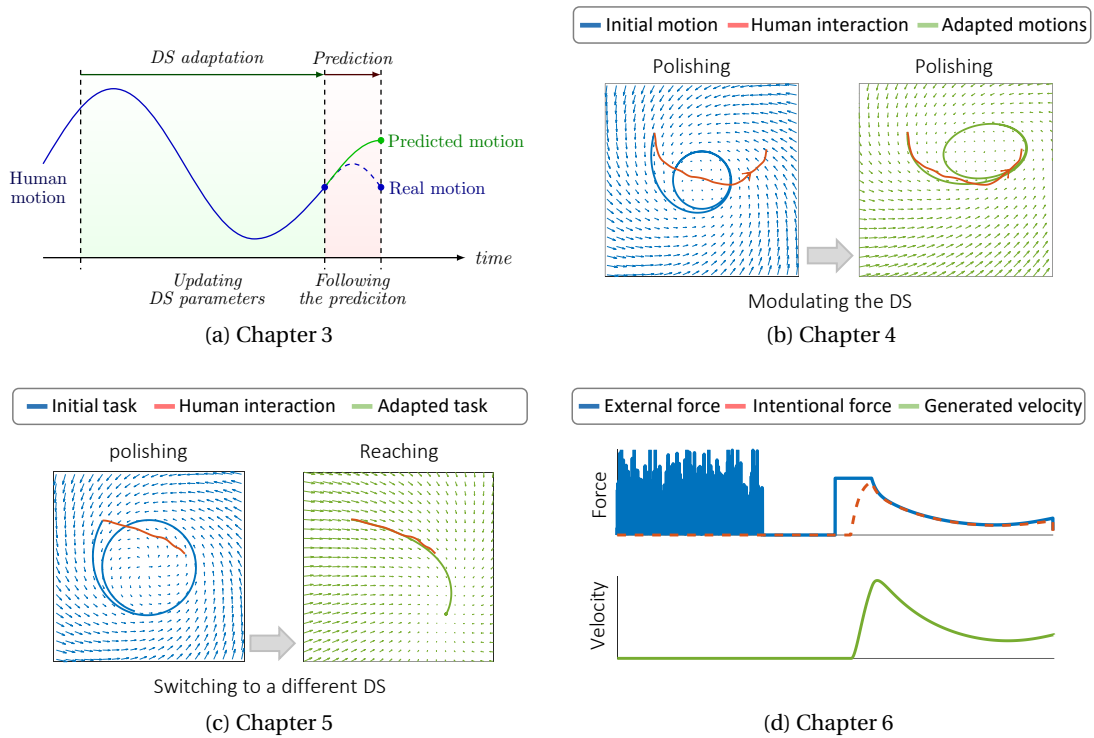
Figure 1.1 – An abstract illustration for the main contribution of each chapter. a) In Chapter 3 we show that an adaptive dynamical system can account for human proactive motion coordination. b) In Chapter 4, we implement such adaptive behavior where robot modifies the DS with respect to human interactions. c) In Chapter 5, we introduce another adaptive mechanism where the robot switches between tasks in order to comply with human intended task. d) In Chapter 6, we introduce a detection and reaction strategy toward human guidance based on an admittance control approach.

1.1 Main contribution and thesis outline

Here, we present the outline and briefly list the main contribution of this dissertation. Fig. 1.2 summarizes the outline and the main key points of each chapter in relation to one another. In Chapter 2, we review the state of art and we provide a series of mathematical formulations used in this thesis. Chapter 3 focuses on non-physical interactions between human subjects where we mainly focus on understanding and modeling human following capacities. We confirm that individuals follow a prediction of their leaders' motions rather than the current observation. Specifically, we show that using an adaptive dynamical system as the predictive model can explain the follower's behavior. Moreover, we show that the capacity to recognize the leader's intention improves the tracking behavior.

To put our findings from the human studies in practice, in Chapter 4, we propose an online motion-adaptation for robotic task using dynamical systems. This method allows a human user to modify a robotic task encoded by DS through physical interaction. Moreover, in Chap-
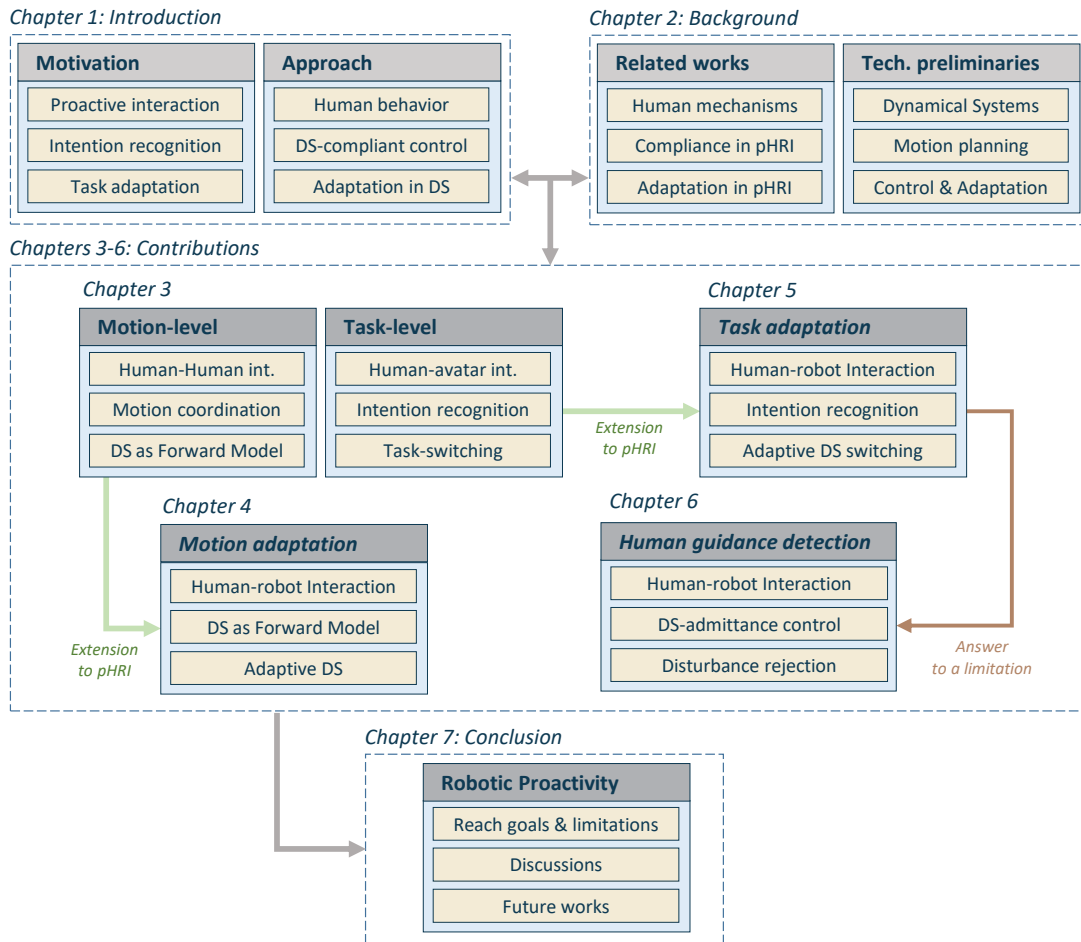
Figure 1.2 – Thesis structure with key point of each chapter.

ter 5, we offer a task-adaptation mechanism enabling the robot to switch across dynamical systems in order to comply to human intentions. We provide rigorous mathematical analysis and experimental evaluation for our methods in terms of stability, convergence, and optimality.

In Chapter 6, we introduce a novel algorithm to distinguish between human intentional forces and accidental disturbances. Moreover, we present and evaluate a DS-based admittance control with regard to stability, passivity and adaptability toward human intention. The last chapter provides a brief discussion for limitations and possible future research.

1.1.1 Publications

Main portion of this dissertation has been published in peer-reviewed journals and conferences. The studies on human following behavior presented in Chapter 3 has been published in Khoramshahi et al. (2014), Khoramshahi et al. (2016), and Khoramshahi et al. (2015). The

motion-adaptation method presented in Chapter 4 has been published in Khoramshahi et al. (2018). The task-adaptation method in Chapter 5 has been published in Khoramshahi and Billard (2018). The content of Chapter 6 is under review in a robotic journal at the time of this writing.

In collaboration with other colleagues, the author shared authorship of several peer-reviewed publication during his PhD. Tangential to Chapter 3, social motor coordination of schizophrenia patients has been studied and published in Cohen et al. (2017b), Słowiński et al. (2017), and Cohen et al. (2017a). Human perception toward their robotic partners has been presented in Raffard et al. (2018). Realism and efficacy for robotic facial expressions has been investigated and published in Raffard et al. (2016). Moreover, compliant in catching flying objects was explored and published in Salehian et al. (2016).

1.2 Approach

In the section, we detail further on the approach taken in this thesis. The main aspect of our approach is the usage of state-dependent dynamical systems; to model and understand the human behavior, to provide compliant behavior, to achieve adaptive motion-planning, and recognition and reaction to the intentional human-guidance.

1.2.1 Underlying mechanisms in Human following behavior

Inspiration from human studies can be of great value in designing new controllers and algorithms for robots that are aimed to physically interact with us and assist us with our daily tasks. To understand the underlying mechanisms of human proactive following behavior, we initially focus on human-human motion coordination. We studied scenarios where one participant is designated to lead the motion and the other is instructed to synchronize with the leader. Our data analysis confirms that an adaptive dynamical system can explain the proactivity in the follower's behavior. More specifically, by adapting the dynamical system to the leader's motions, the follower can predict the leader's actions. This allows the follower to 1) compensate for his/her sensory-motori delays, and 2) be a proactive follower; i.e., following the predicted motions rather than following the delayed observations.

Furthermore, through an avatar-human mirror game experiment, we study the effect of intention-recognition on motion-planning. In this experiment, an avatar-leader systematically switches between different tasks. We show that when human-followers are provided with cues about the leader's intention, they deliver a better tracking performance. In short, two main mechanisms are involved for proactive following behavior. First, the adaptive capacity to modify the task at hand to accommodate for the leader's modifications. Second, the capacity to smoothly switch to another task that resembles the leader's behavior. Inspired by these two studies, we propose two different formulations for dynamical systems for adaptive motion-generation in pHRI.

1.2.2 Compliant interaction using dynamical systems

As humans, we benefit from compliance in our interaction with one another. This compliance enables us to communicate our intention through motions that we induce to our partners. Sebanz and Knoblich (2009) suggest that the human follower complies with the actions of others which allows intention recognition, and subsequently, action coordination. Due to the follower's compliant behavior, the leader is able to communicate his/her intention through interaction-forces (van der Wel et al., 2011; Sawers et al., 2017) and movements (Sartori et al., 2011). Similarly, compliant behavior, ranging from passive (due to the mechanical design) to active (due to the control design), is a key requirement for robots to interact with humans (Billard, 2017). Active compliance has been of particular interest to engineers for achieving safe and intuitive physical interaction (De Santis et al., 2008). To have a clearer definition of compliance in this thesis, consider the general control feedback loop depicted in Fig.1.3. In this hierarchical feedback loop, the robot can exhibit compliant behavior at different levels. These levels are as follows:

1. *Compliance at the force-level*: the robot is designed to fulfill a particular motion, however, it remains compliant toward small perturbations due to the external forces; e.g., impedance and admittance control (Hogan, 1988).

2. *Compliance at the motion-level*: the robot is designed to execute a particular task, however, it allows for variation of motions that still fulfill the task; e.g., the reactive motion planning using DS and impedance control proposed by Kronander and Billard (2016).

3. *Compliance at the task-level*: the robot switches or adapts to a task that complies with the intention of its human partner; see Bussy et al. (2012a).
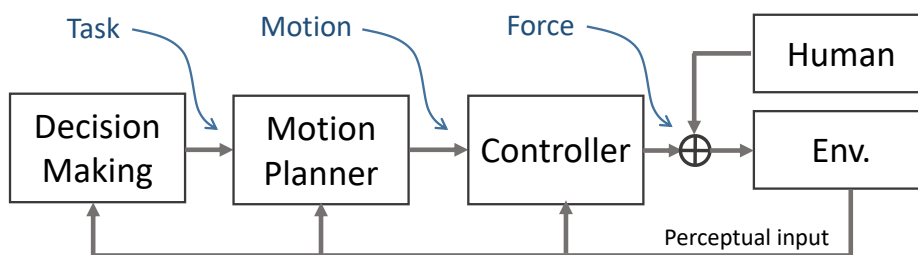
Figure 1.3 – A generic control design approach to physical human-robot interaction where, based on a decided task, corresponding motions are generated, and consequently, corresponding forces are applied. Each block takes proper perceptual input into consideration to achieve a desirable behavior.

As mentioned, having DS and impedance control in the main loop (as proposed by Kronander and Billard (2016)) naturally provides compliance at the motion-level; i.e., if the robot's state is perturbed, the state-dependent DS re-plans the desired motion. This property allows the

human to temporarily modify the robot's motions. Nevertheless, such modifications are lost as the human retreats from the interaction as the DS is not adapted accordingly. An incremental learning approach has been proposed to accommodate for online demonstrations of the human user; see Kronander et al. (2015) where the DS is locally modulated (i.e., scaling and rotation) using Gaussian process. Such methods are efficient in an off-line setting as they treat the new demonstrations as a batch. However, in an on-line setting, the robot requires to constantly adapt to changes in the leader's motion or intention. To overcome this, we propose a globally modulated DS where rotation, scaling, and translation are possible. Using a simple adaptation mechanism for modulation parameters, the robot exhibits compliance at the motion-level; i.e., the robot instantly adapts the target location of a reaching motion or adapts the polishing patterns on a surface.

Having several homogeneous models encoding for different tasks not only improves the robot's versatility (as the robot can execute several tasks) but also allows for task-identification as the robot can infer the underlying task for a given observed motion. Recently Maeda et al. (2017b) proposed a probabilistic model that encodes for different tasks and acts as an inference tool for intention recognition. Nevertheless, such methods are required to perform motion-generation and intention-recognition simultaneously during the physical interaction with human. To tackle this limitation, we propose a DS formulation for encoding several tasks with the possibility of smooth transitions. Moreover, we propose an adaptive mechanism to recognize the human intention and smoothly switch to the most similar task. Preserving the passivity properties of the DS-based impedance control, the human user can physically interact with the robot and demonstrate his/her intentions. In this formulation, the dynamical systems are used both for motion-generation and intention-recognition resulting in an intuitive and seamless interaction. This extends the DS compliant capabilities to the task-level where the robot switches to the human-intended task. We evaluate our adaptive approaches mathematically and experimentally.

1.2.3 Adaptability in dynamical systems

As mentioned earlier, we employ state-dependent dynamical systems for motion-generation to perform a specific task. It has been shown by Khansari-Zadeh and Billard (2011b) that such models can be leaned efficiently from demonstrations. The generated motions using the learned models are guaranteed to be smooth and stable; i.e., converging to the designated attractor or limit cycle. Moreover, such models exhibit generalization to the unseen contexts; i.e., intra/extrapolating the demonstrations over the state-space. Furthermore, Kronander and Billard (2016) show that having the DS-based motion-generator inside the control loop leads to reactive motion planning. This enables the impedance-controlled robot to comply with external forces and re-plan the motion based on the human interactions. In order to extend the compliance capacities of dynamical system, as introduced in the previous section, we take an adaptive approach in thesis. However, endowing motion-generators with adaptive capacity introduces new challenges relevant and crucial to physical human-robot interaction. It is

important to guarantee the performance of the control loop under the variation of the adaptive parameters. In the following, we introduce these concerns from control theory perspective.

Smoothness: To avoid abrupt and jerky motions that might endanger the safety and the quality of the interaction, the generated motions are ought to be smooth. In an adaptive scenario, we need to ensure that the generated trajectories remain smooth in two distinct cases: 1) under arbitrary values for the adaptive parameters and 2) under the time-variation of the parameters. To preserve the original smoothness of the dynamical system, we limit our global modulation to diffeomorphisms; see Neumann and Steil (2015) and Perrin and Schlehuber-Caissier (2016) for similar approaches in using diffeomorphism for motion-generation. In the case of the task-adaptation, we use a weighted combination of several dynamical systems where the smoothness is guaranteed under arbitrary variation of the coefficients. Similar linear combination of primitive dynamics has been used widely in the literature of motion-generation; see Thoroughman and Shadmehr (2000) and Lim et al. (2005).

Stability: Beside smoothness, it is crucial to guarantee that the generated motions are not divergent under arbitrary variations of the adaptive parameters. However, such stability analysis is not straight-forward for the general case; see Daafouz and Bernussou (2001) for the Lyapunov analysis of a linear system with time-varying parametric uncertainties. Unlike general cases, it is unnecessary to assume that the parameters are uncertain as they are governed by the adaptive mechanism. With such consideration, we derive the necessary conditions for the stability of the motion-generation.

Convergence: Given a human interaction over a time-period, it is desired to observe a converging behavior for the adaptation parameters; e.g., the parameters asymptotically converge to a fix-point. It is trivial to see that unnecessary fluctuations or diverging behavior lead to an undesirable motion-generation. In the context of pHRI, we investigate whether 1) the parameters change properly with respect to the adaptation signal and 2) they converge to a fixed-point after the human retreats from the interaction. Considering the adaptation dynamics, the converge is often subjected to the quality of the adaptation signal; i.e., human-induced error in this thesis. In other word, the human demonstration is required to be rich enough to lead to a proper adaptation; e.g., in the case of task-adaptation, a switching occurs if the human demonstration differs from the current task and resembles another. This is often formulated as persistent excitation condition; see Åström and Wittenmark (2013) for mathematical formulations.

Optimality: Furthermore, it is vital to show that the converged parameters are optimal; i.e., with respect to a cost function that accounts for some aspects of the interaction. Oftentimes, the adaptive law is derived from a cost-function such as energy or tracking error. In this thesis, we relate our adaptation mechanism to cost functions concerned with human-induced errors; i.e., the difference between the planned velocities by the robot and the demonstrated velocities by the human-user. In other words, by reducing the human-induced error through

parameter adaptation, we capture the human-intention allowing the human to retreat from the interaction.

Passivity: As the human physically interacts with the robot and injects energy, the passivity of the system becomes crucial. The passivity of DS-based impedance control has been throughly investigated by Kronander and Billard (2016). Following the same lines, we ensure the passivity of our control architectures in this thesis; see also Shahriari et al. (2017) for similar approaches in ensuring the passivity under the parameter adaptation.

Human effort: In the evaluation of our adaptation methods, we consider the human effort required to demonstrate his/her intention to the robot through the physical interaction. As the robot is controlled compliantly, the observed stiffness and damping by human influence the required effort for physical interaction. To decrease this effort, we propose an approach based on variable-admittance control to lower the stiffness toward human guidance. Therefore, we develop an algorithm to detect intentional human-guidance forces.

Tracking behavior: To execute a task, it is necessary to track the generated motions by the DS precisely. This applies when the human is not present in the interaction as the robot requires to comply with human forces which induces tracking error. Unfortunately, in DS-based impedance control, both tracking performance and compliant behavior are controlled using the same impedance gain; i.e., the damping term. High gains favor tracking precision, and low gains are suitable for human interactions. We show that our proposed DS-based admittance control with human-guidance detection can be a solution for this case.

1.2.4 Admittance control for compliance and tracking decomposition

As mentioned earlier, the impedance gain in DS-based impedance control leaving us with a trade-off; i.e., high gains lead to higher precision preferable for execution of the task, while low gains lead to lower stiffness behavior agreeable for the human user. It is clear to see that a seamless interaction requires both behaviors; i.e., to be a stiff leader and reject the disturbances and to be compliant toward other intentions. To overcome this, we propose a novel control architecture to provide proper compliance and motion-control based on the human guidance. We assume that the robot is controlled in velocity (either using pure high-gain velocity controller or via velocity-based impedance controller), and position and force feedback are available. In order to obtain reactive motion planning, we employ our state-dependent dynamical systems. Using the admittance block, we compute the velocities resulting from the external forces. In doing so, we allow for a variable admittance ratio. This controller structure can be seen as an interplay of two separated control loops: one which aims to provide precise tracking behavior, and another which aims to provide proper compliance behavior; i.e., to reject the disturbances using lower admittance ratios or to allow for human interaction using higher ratios.

1.2.5 Recognition of intentional vs. accidental forces

To benefit from variable-admittance control introduced in the previous section, we adapt the admittance ratio according to the nature of the external forces. Intuitively speaking, accidental forces need to be rejected (in order to fulfill the task autonomously) while intentional forces must be incorporated into the robotic behavior; e.g., complying to the human intention to switch from one task to another. Therefore, the challenge is to distinguish between the forces intended by human and undesirable disturbances. We use a similar approach to those proposed in the literature to distinguish between intended and unexpected contacts; see Haddadin et al. (2008); Berger et al. (2015); Kouris et al. (2018). Following the same line of thoughts, we rely on the persistency of interaction forces to detect the human guidance. This shows an analogy to the literature of collision avoidance where 1) high-frequency components in the haptic channel (e.g., sudden changes in forces) can contribute to a safe interaction with the environment, and 2) low-frequency components (e.g., persistent forces) can be utilized for human-guidance detection, role distribution, and human-intention detection.

This eventually brings us a seamless interaction using two robotic behaviors: the leader role where the robot rejects the external perturbations and focuses on the autonomous execution of the task, and the follower role where the robot ignores the task and complies to human intentional forces. An example of such interactions is illustrated in Fig. 1.4 where the robot is initially executing a reaching task autonomously and maintaining the target position. In doing so, the robot is a non-compliant/stiff-leader so as to reach a desirable tracking performance and rejecting the undesirable disturbances. Detecting human guidance, the robot becomes compliant in selective directions, allowing the human to modify only locally its motion. As such, the robot appears as a compliant leader, as it still carries on with the initial task. If the human guidance persists, the robot increases its compliance until it becomes a passive-follower. This allows the human to take over the leadership of the task which subsequently allows the human to demonstrate a desired behavior to the robot. Next, the robot starts to follow a prediction of the human intention which renders the robot as a proactive-follower. The human, accepting the robot's prediction and proactivity, retreats from the interaction allowing the robot to become autonomous (stiff-leader) and to focus on tracking behavior.
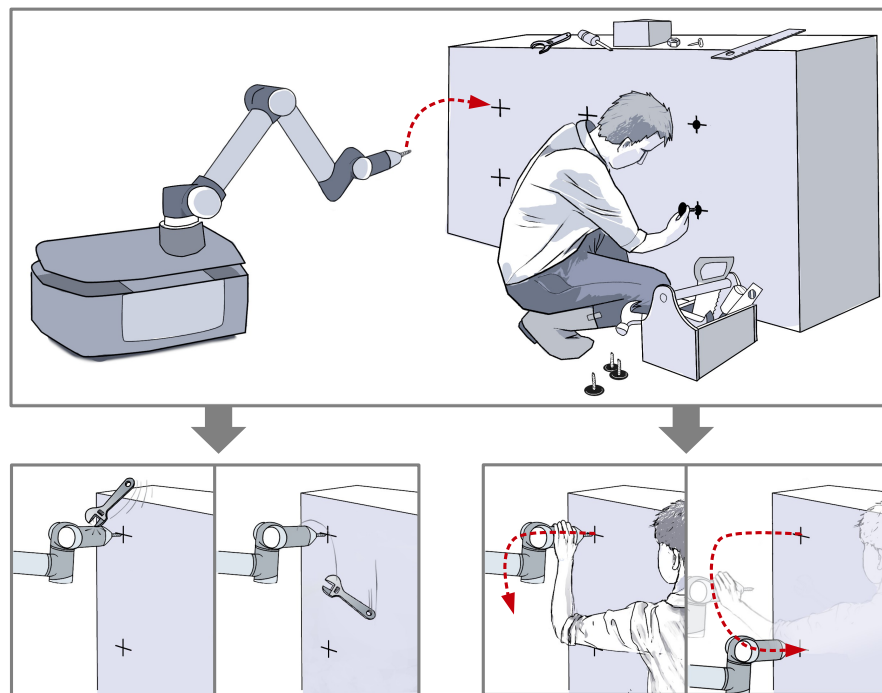
Figure 1.4 – An illustration of human robot collaboration where the robot reacts intelligently to external perturbation. In the **first** scenario, the robot rejects the undesirable disturbances for a better tracking performance; i.e., to maintain the drilling point and to avoid damaging the object and the tool. In the **second** scenario, the robot detects and complies with the human guidance; i.e., the robot becomes compliant and passive where the human can easily move the tool and demonstrate his/her intention. Moreover, the robot recognizes the intention and moves to the next drilling point to perform the task autonomously.

2 Background and related work

As introduced in the previous chapter, the goal of this thesis is to endow physically collaborative robots with proactive behavior toward their human coworkers. This chapter provides a review on the state-of-the-art and technical preliminaries necessary to establish and define fundamental concepts for the solutions proposed in the following chapters of this thesis. The literature on human-robot interaction is interdisciplinary and ranges from engineering and computer science to neuroscience, cognitive science, and other social sciences and humanities (psychology, ethics, and philosophy). This literature is strongly inspired by the ways humans interact with one another, especially non-verbally. In this thesis, we focus in particular on the motion coordination and control aspects of human-robot interactions. We primarily concentrate on related works which helps us with the design of proactive robotic behavior; i.e., recognizing the human intention, predicting the future actions, and providing assistance.

Interaction between a human and a robot includes several mechanisms responsible for decision making, motion-planning and control; both on human and robot-side. Understanding the mechanisms involved in the human-side and exploiting recent advancements in robotic and control are of particular importance to this thesis. For such mechanism, consider the generic model for physical human-robot interaction (pHRI) illustrated in Fig. 2.1. In this figure, the human and the robot are jointly acting on the environment to bring about their desired changes. The human acts based on a mental state; i.e., the desired goal or task which is determined by the "internal drives" or affected by the intention of others. The action coordination mechanism plans and applies the proper actions. To better coordinate, the forward model enables the human to predict the future state and actions of other. On right-side of the figure, the robotic behavior is primarily governed by the task which is concerned with safety, assistance and the intentions of the human partner. In a feedforward manner, the task translates into motions and consequently into forces that are applied to the environment. However, in a feedback fashion, each block is affected by the sensory inputs and recognized intentions of the human partner. The following sections of this chapter are dedicated to provide reviews on related work specific to each component of this schema. More specifically, the related work is organized as follows:
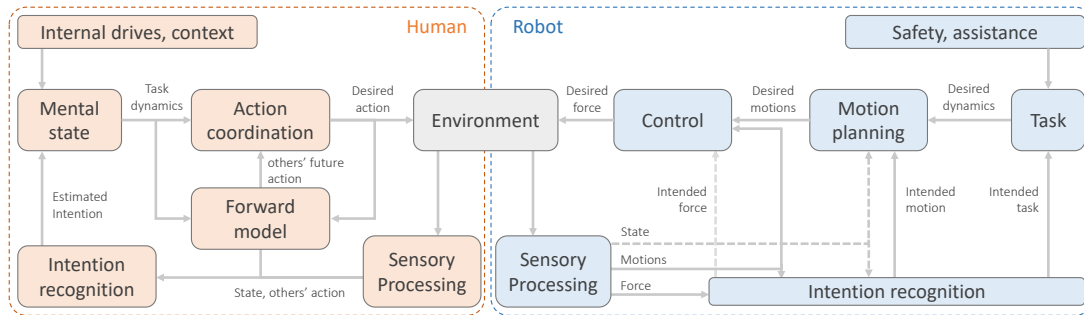
Figure 2.1 – A generic model for physical human-robot interaction. The human-side of the model is adopted from Oztop et al. (2005). In Section 2.1, we review the related works on human mechanisms involved for interaction and coordination with others. In Section 2.2, we review the literature of pHRI related to mechanisms and concepts illustrated on the robot-side of the model.

- **Human-side:** In Section 2.1, we summarize the works dedicated to a better understanding of human capacities for motion coordination. These studies are mostly concerned with human-human interactions. This body of work is related in particular to the dynamical system model for human following behavior that we introduce in Chapter 3 and later use in Chapter 4.

- **Robot-side:** In Section 2.2, we present methods for compliant and proactive human-robot interactions. We review in particular methods for control, motion planning, prediction, and intention recognition which are related to the robotic implementations in Chapters 4, 5, and 6.

In each part, we situate our approach, presented in Section 1.2, in relation to the state-of-the-art. Finally, in Section 2.3, we present the technical preliminaries necessary for analyses and designs presented in proceeding chapters.

2.1 Inspirations from human proactive following behavior

Social motor coordination has received much interest in the recent years as a central part of social interaction; see Schmidt et al. (2011) as a review. It refers to our ability to coordinate our movements with other individuals to perform a task in the context of a *joint action* as opposed to an *individual action*. Sebanz et al. (2006) define a *joint action* as "any form of social interaction whereby two or more individuals coordinate their actions in space and time to bring about a change in the environment". Moreover, the cognitive and socio-psychological aspects of such coordination have been studied thoroughly; see Sebanz et al. (2006) and Knoblich et al. (2011). Interpersonal coordination provides an important foundation for social interaction. For instance, Hove and Risen (2009) show that the degree of interactional synchrony of bodily movements of co-actors during social interaction is a significant predictor of subsequent

affiliation ratings and cooperation between individuals. Performing tasks with others often requires recognizing what they intend, predicting their next actions, and adapting one's behavior accordingly. To better understand the mechanisms at the basis of joint action, cognitive and neural scientists have mostly studied the underlying processes separately, including those responsible for joint attention (Tomasello, 1995), action observation/prediction (van Schie et al., 2008; Sebanz and Knoblich, 2009), action coordination (Marsh et al., 2009), synchrony (Valdesolo et al., 2010), and task sharing (Sebanz et al., 2005). Supported by a vast literature on psychology and neuroscience, Sebanz et al. (2006), Vesper et al. (2010) and Vesper et al. (2017) proposed architectures in which these mechanisms enable individuals to coordinate with others. In the following, we review such mechanisms in relation to the work developed in this thesis.

- **Task-sharing**: In an interaction, individuals require to have a representation of the task. Tasks are often identified by their end-goal and a set of possible actions. A goal is a specific state of the environment and actions are the means by which the environment can be changed; e.g., motions and forces. To coordinate efficiently, it is important for an individual in an interaction to infer the others' intended goals. For instance, we convey our intentions to other using gaze (Kourtis et al. (2014) and Brennan et al. (2008)).

- **Role-Assignment**: Knowing the task, the individual can take on different roles. For example, one individual can be responsible for early part of the motion while the rest is performed by the other; see Reed et al. (2006b). Negotiations over such roles or distribution of task-load can be perform through the interaction as it is reviewed in later sections. We also exhibit the ability to continuously adapt our roles between leader and follower as suggested by Konvalinka et al. (2010). Furthermore, dyads can reach a state where both parties follow and lead at the same time; see Sebanz et al. (2006).

- **Task-monitoring**: This process monitors if the actions are taken as planned and to what extent the goal of the task is achieved. Monitoring is crucial to detect deviations from the intended goal so that partners can quickly react and adapt. Furthermore, large deviations from a task can serve as an indicator when the intended goal changes.

- **Action-observation**: For a successful interaction, it is necessary for an individual to observe the actions of his/her partner. Action observation enables us not only to predict the future actions but also to recognize the intended task/goal of our partners. We often communicate our intention through subtle kinematics changes (Sartori et al., 2009, 2011) or through the haptic channel (Takagi et al., 2017).

- **Action-prediction** Knowing what our partners will do allows for precise temporal coordination (Vesper et al., 2010) and proactive coordination (Pickering and Clark, 2014). Several internal forward models were proposed to explain the human capability to predict other's actions. In the following sections, we review these works in further details. Recognizing other's intentions and goals facilitates action-prediction. Sebanz

and Knoblich (2009) argues that this mechanism can be just a by-product of prediction about others' goal.

- **Action-coordination** Knowing the intended task and its representation along with the current state and prediction of our partner's action, we adjust our actions in time and space to get closer to the final goal. Moreover, we choose actions that are

    - *Assistive*: actions that result in a lower effort, and to a greater extent, a lower need for coordination.
    - *Predictable*: actions that are less variable and easier to predict for others.
    - *Expressive*: actions that express new intentions or other changes in the interaction.

    Vesper et al. (2010) refer to these aspects as *coordination smoothers* and explain that synchrony can serve as a smoother. Moreover, human dyads control their compliance for stability of the interaction (Ganesh et al., 2014). Proper compliant behavior and haptic communication allow the partners to negotiate their roles and goals (Melendez-Calderon, 2012; Takagi et al., 2017; van der Wel et al., 2011).

Inspired by these mechanisms, we take a dynamical system approach toward physical human-robot interaction (pHRI). Robotic tasks in pHRI can be encoded using dynamical systems which allows for task-monitoring, intention recognition, and task switching. Through adaptation in dynamical systems, the robot can predict human actions and reach a proactive behavior. Finally, through DS-based compliant control, the robot coordinates its action in an assistive manner.

2.1.1 Intention recognition

We mentioned previously that an efficient interaction requires a model for the task; see Sebanz and Knoblich (2009). Using such a model, the individual can predict the motions of their partners and act proactively. Nevertheless, in a realistic multi-task/goal scenario, it is crucial to infer the intended task/goal of others. Our ability to infer the intention of others from contextual information is fascinating. To name a few, we rely on gaze cues, gestures, facial expressions, kinematics, and haptics. In the following, we provide a brief review for those mechanisms.

An essential contextual cue that humans exploit for intention recognition is the gaze behavior. The ability to follow another's gaze is central to the joint action (Volcic and Lappe, 2009) via its roles in joint attention (D'Entremont et al., 1997) and action observation (Flanagan and Johansson, 2003). The cooperative eye hypothesis (Tomasello et al., 2007) suggests that the visual characteristics of human eyes, such as the shape and color of the sclera, iris, and pupil, evolved to make it easier to follow others' gaze directions. According to this hypothesis, evolution enhances cooperative social interactions by providing a new social function; i.e., using gaze as a means to share our intentions. A growing number of studies have investigated

the use of gaze as a form of non-verbal communication in a variety of social interactions; e.g., to complement speech (Kendon, 1967), and as a mechanism to orient others' attention (Frischen et al., 2007). The ability to orient and follow other's gaze-direction enables joint attention (Emery et al., 1997), which plays an important role in our social cognition (Tomasello, 1995). Recent neurological studies have revealed that some visual cells are sensitive to gaze direction (Perrett et al., 1985); these cells overlap with neural pathways representing facial expression (Engell and Haxby, 2007). Moreover, eye contact modulates the activation of the social brain (Senju and Johnson, 2009). This suggests that the ability to generate gaze patterns and respond to gaze as a means of conveying intentions recruits common neural substrates (Itier and Batty, 2009; Bavelas et al., 2002). It has also been reported that gaze behavior is crucial for joint action (Sebanz et al., 2006; Sebanz and Knoblich, 2009). Orienting the gaze at the right location at the right time improves coordination with other individuals. Furthermore, gaze direction is necessary in establishing a closed-loop dyadic interaction, which enables a better coordination in joint actions (Volcic and Lappe, 2009). In Chapter 4, we use simulated gaze cues of an avatar in a leader-follower setting to study the human gesture following behavior. In this approach, we investigate how intention recognition affects motion coordination. Through quantitative assessments, we show that the human ability to proactively coordinate with a leader relies on the recognition of the intended task.

Intentions can be recognized by observing other's actions in terms of movement. In an early work, Johansson (1973) propose a method to study the perception of bodily movements where they use point-lights to represent important joints of a moving person. They show that 10 to 12 points are adequate to evoke the impression of a human walking, running, or dancing. Follow-up studies show that even gender (Richardson and Johnston, 2005), emotion (Atkinson et al., 2004), and identity (Loula et al., 2005) of the actor can be inferred from such low-dimensional kinematic data. Furthermore, in joint-action scenarios where two agents are represented by light-points, observers can recognize the task and predict the actions; see Manera et al. (2010) and Manera et al. (2011b). The underlying neural mechanism for this capacity is controversial, as two main hypotheses are competing. One group of researchers argue that observed actions are simulated by the motor cortex (more specifically by the *mirror-neuron system*) to infer the intention; see Fogassi et al. (2005). Others (Brass et al., 2007) explain intention-recognition via areas outside the motor cortex which are often considered as responsible for *theory of mind* and *mentalization*; i.e., the capacity to infer the latent *mental state* of others. Ansuini et al. (2014) and De Lange et al. (2008) argue that the two views are intertwined, and intentions become visible – as opposed to latent – in the kinematic behavior.

Individual can facilitate the interaction by predicting and communicating their intention using the kinematics behavior. Sartori et al. (2009) show that individuals change their kinematics when they intend to communicate their intention in a simple reaching task. Becchio et al. (2008) also demonstrate that acting socially or individually affect the kinematics. Sartori et al. (2011) and Manera et al. (2011a) show that subjects can distinguish between different intentions behind a reaching motion; namely, to cooperate, to compete, or to perform an action individually. Frith and Frith (2006) postulate that, at the most basic level, we can

predict how a movement will finish. Therefore, we can infer the intended end-goal of an observed movement. Wolpert et al. (2003) argue that such early prediction about other's intention are tested as the motion progress. Becchio et al. (2012) and Lewkowicz et al. (2013) go one step further and propose that early intention recognition affects the motion planning in joint actions. In Chapter 5, we take a similar approach to intention recognition in pHRI. The robot relies on kinematics information provided by the human-user. By simulating different dynamical systems, each encoding for a specific task, the robot forms a prediction for the human-intended task. Such predictions are immediately reflected in the motion-planning allowing for intention communication and convergence to the intended task.

2.1.2   Action prediction and the role of internal predictive models

As mentioned, action prediction plays a crucial part in the ability to be proactive. Predicting what others are going to do next allows individuals to adjust their actions accordingly. One line of research has been dedicated to *internal forward models* to explain such prediction capabilities. Internal models, as proposed by Prinz (1997), allow an individual to predict the consequences of his/her own actions. Wolpert et al. (2003) proposed an approach in which the internal models are used for motion control purposes. In their model, both self-action production and others-action understanding are explained by the same mechanism. Therefore, such internal models (which were initially proposed to predict the consequence of one's own action) were used for action understanding. Townsend et al. (2017) proposed a computational model where internal models are used to infer the intention of other from their movements. Sebanz and Knoblich (2009) argue that individuals in an interaction also acquire a forward model for the joint performance. They further explain that, in presence of such joint models, the error during the interaction can be processed efficiently; i.e., they can help distinguishing between errors occurring at the level of the task and at the level of individual motions.

Several other studies (Wolpert et al., 1998; Krakauer and Mazzoni, 2011) have suggested that the main role of a forward internal model might be to overcome time delays from decision making, perception and action. Furthermore, results from Foulkes and Miall (2000) and Miall and Jackson (2006) also suggest the presence of a delay component in the internal process for motion generation. Moreover, they provide estimations for this sensory delay and its effect on motion-coordination. Smith predictor (Smith, 1959) is one such mechanism which maintains an internal model of the dynamics combined with an estimate of sensory delay. Haken et al. (1985) uses such delay to explain the fact that in their finger-tapping experiments, anti-phase motion falls into synchronized motion after a certain frequency. Haken et al. (1985) study was limited to individual-action settings where the subject is required to coordinate between left and right index fingers. However, in the last decade, such phenomena are studied in joint-action as well. Thus, the idea of synchrony as solution to compensate for delays is extended to joint-action scenarios. For instance, Naeem et al. (2012) show phase and frequency locking behaviors even in the absence of visual feedback. They suggest that individuals acquire a

model for the interaction which enables them for such synchronous behavior.

In summary, this literature pinpoints that human proactive behavior requires prediction capacities which entail internal forward models. A long-standing goal in pHRI is to endow robots with similar prediction capacities as to reach robotic proactive behavior. Therefore, a relevant approach is to draw inspiration from human and develop predictive models for physically collaborating robots. In this thesis, we take this approach by leveraging state-dependent DS. Thus, to reach robotic proactivity, we tackle the two following challenges. **First**, we investigate whether state-dependent DS can account for such internal forward models. More precisely, whether human proactive behavior can be explained by an adaptive DS. **Second**, we employ an adaptive state-dependent DS both as the motion-planner and the forward internal model for robotic proactivity toward human-users.

In Chapter 3, we investigate the **first** problem. We take the established delayed-internal-model hypothesis and we use tools from adaptive control and dynamical systems to realize our interaction model. Our model is consistent with the hypothesis that the adaptation in motor behavior is a direct result of updates in the internal model; see Krakauer and Mazzoni (2011). In other words, in a leader-follower setting, the follower incrementally builds a model of the leader's motion and executes its own motion by using forward prediction based on the internal model; i.e., proactive following behavior. Chapter 4, we tackle the **second** challenge. We implement an adaptive DS for a robotic arm to reach proactivity in interaction with a human-user; i.e., the robot gradually adapts the DS based on the human motion. Therefore, instead of passively following the human motions, the robot execute the generated motions based on the adapted DS.

Finally, motivated by the view developed in Wolpert et al. (2003) that action production and action observation are performed by the same mechanism, we propose a unified dynamical system approach for both motion generation and task identification in Chapter 5. In this case, the observed actions of the human is interpreted using the same dynamical system as for motion planning. As proposed by Sebanz and Knoblich (2009), the interaction errors between a robot and a human are interpreted based on the dynamical model representing the task; i.e., small errors are treated as tracking error and covered by the compliant control, and large errors are considered as a change in the human intention and compensated by the adaptation mechanism.

2.1.3   Physical interaction and the role of haptic and compliant behavior

Many coordination tasks require the individuals to be physically coupled to each other. In such condition, each partner perceives the forces exerted by the others. It has been shown that tasks can be completed faster when two humans physically interacts; see Reed et al. (2004) and Reed et al. (2006a) for reaching and Gentry et al. (2005) for periodic tasks. Moreover, Sallnäs and Zhai (2003) show that error rate decreases for virtual hand-overs when haptic feedback is present. Similarly, Groten et al. (2010) show that tracking performance for a carrying task

improves when haptic feedback is provided to the partners. Moreover, the desired forces can be tracked more precisely as investigated by Masumoto and Inui (2013). Several other works argue that such advantage are not always present and might be affected by other aspect of the interaction. For instance, Takagi et al. (2016) demonstrate that the force reproduction accuracy is strongly biased by facing the partner. Takagi et al. (2018) also reveal that the performance is affected by both the coupling stiffness and the partners' individual skills. Furthermore, Skewes et al. (2015) suggest that the overall performance is affected by adaptability of the partner; i.e., humans coordinate better with adaptive but irregular partners than predictable but non-responsive partners indicating that adaptability is more important than predictability.

Forces applied by partners are not always in agreement. Madan et al. (2015) categorize them into 1) harmonious, 2) conflicting, and 3) passive behavior. One reason for conflicting forces is to reject disturbances as proposed by Reed et al. (2005) and Reed and Peshkin (2008). Melendez-Calderon et al. (2015) show that dyad increase their oppositional forces when they are faced with perturbations. However, beside using this haptic feedback to control the final desired force and reject disturbances, individuals might use this modality for other purposes. van der Wel et al. (2011) suggest that dyads amplify their forces to generate a haptic information channel where they can communicate their intentions. More specifically, Sawers et al. (2017) and Takagi et al. (2017) demonstrate that individuals communicate their movement goals through forces. Chauvigné et al. (2017) also argue that the follower in interaction infers the intended motions based on the forces applied by the leader. Furthermore, Ranasinghe et al. (2015) show that, beside goals and motions, the individual communicate their level of confidence by modulating their impedance. For instance, a passive behavior can be an indicator that the follower is not confident in his/her prediction about the leader intention.

Several studies indicate that haptic channel is also used to negotiate over roles and strategies. For example, Oguz et al. (2010); Stefanov et al. (2009) demonstrate that partners use conflicting forces to negotiate over the roles. Likewise, Groten et al. (2009) show that dyads negotiate over a fair distribution of the required effort. Using the notion of game theory, Braun et al. (2009) also argue that individuals agree upon their roles and task distribution through force exertion; i.e., to reach a Nash equilibrium. It has been shown by Ganesh et al. (2014) that individuals adapt their behavior toward each other when physical interaction is mutually beneficial. For instance, the partner with lower-force variability produces stronger forces for better force tracking performance as investigated by Masumoto and Inui (2015). Moreover, Reed et al. (2006a) demonstrate that dyads develop a strategy where one contributes to acceleration and the other to deceleration of a carried object. In a similar work, Reed et al. (2006b) show that dyads develop a temporal strategy where one performs the early parts of the motion and the other the late parts. They discuss that such strategies reduce the variability and make the partners more predictable to each other.

Recent development in robotic platform enable the researchers to investigate human arm impedance properties; see Mussa-Ivaldi et al. (1985); Shadmehr and Mussa-Ivaldi (1994); Burdet et al. (2001). Ikeura and Inooka (1995) demonstrate that human behavior can be

represented by an impedance model where the damping parameter is variable; i.e., low for slow movement and high for fast movements. Todorov and Jordan (2002) and Franklin et al. (2008) show that in interaction with a passive environment, humans apply forces in order to minimize a combination of tracking error and effort. This naturally leads to an impedance control, as proposed by Burdet et al. (2014) and Yang et al. (2011). Wang et al. (2008) use a human haptic model to implement an impedance controller. Jarrassé et al. (2012) extend this framework to multi-agents settings where individuals share the cost and agree upon a fair task-distribution. Therefore, human physical interaction is often regarded as two parts: 1) an adaptive planner that generates reference trajectories and set-points 2) a compliant controller (such as impedance) that generates proper forces to track the reference trajectories while allowing for perturbations.

In summary, we benefit from compliant behavior in our physical interaction with others. The compliance enables action perception, intention recognition, and adaptation in humans. For instance, due to the follower's compliant behavior, the leader is able to communicate his/her intention through interaction-forces and movements. Moreover, the human follower complies with the actions of others (i.e., *compliance at the motion and force-level*) which allows intention recognition and subsequently action coordination (i.e., *compliance at the task-level*). In consistency with the literature, in Chapter 4 and 5, we propose compliant controllers with adaptive motion-planner. More specifically, we show that DS-based impedance control along with adaptive dynamical system is efficient in recognizing the intention of a human-user through the physical interactions. In Chapter 6, we take a similar approach to the reviewed works indicating that individuals communicate and infer each other's goal through interaction forces. Thus, to distinguish between intentional and accidental forces, we simulate the intended movement behind a perceived external force. Observing a persistent simulated movement, the robot complies to the external forces.

2.1.4   The mirror game as a framework to study human motion coordination

Despite the fundamental finding of the previous studies on human motion control, they are limited to single human setting; i.e., a single subject coordinating its action with an external signal such as an audio beat. Joint activities have been rarely studied, mainly due to the lack of an experimental paradigm. Noy et al. (2011) adapted the mirror-game - a fundamental practice in improvisational theater - as an experimental system for studying joint interactions between two subjects. In this game, two or more players imitate each others' motions with or without a designated leader. In their first study, two players imitate each other's motions along one-dimensional parallel tracks (Noy et al., 2011). Therefore, the dynamics of the two players can be investigated quantitatively through their kinematic recordings. Using this setup, they showed that players exhibit moments of "togetherness" by generating complex, smooth, synchronized motions without a designated leader.

After its debut in 2011, the Mirror Game has been widely used in the literature. Zhai et al. (2014)

used this setup to design interactive virtual players for rehabilitation purposes. Gueugnon et al. (2016) studied the acquisition of socio-motor improvisation. Slowinski et al. (2014) pointed out the kinematic characteristics of the players. By comparing position and velocity distributions of the motions, they showed that individuals move differently; i.e. with a specific *motion signature*. Affiliation and attachment between individuals in relation to social interaction using the mirror game was studied by Levy-Tzedek et al. (2017) and Feniger-Schaal and Lotan (2017). *Togetherness* and other physiological markers in this game were investigated by Noy et al. (2015) and Hart et al. (2014). Słowiński et al. (2017) and Cohen et al. (2017b) utilized this framework to study motion-coordination in Schizophrenia and pin-point some of its biomarkers. Himberg et al. (2018) examined the relationship between subjective sense of *connectedness* in groups and motion synchronization in the mirror game.

The efficacy and simplicity of the mirror game in quantification of human interactions make it a suitable tool for the first part of this thesis; i.e., investigation of proactive motion coordination in humans. Thus, we selected this tool to investigate human following behavior in the context of non-physical interactions. In Chapter 3, we use the mirror game setup in two studies. In the first study, we develop a mathematical model that can explain the follower's proactive behavior in the context of a human leader-human follower interaction. In the second study, we explore the effect of intention recognition on motion coordination in a mirror game between a human follower and an avatar leader.

Finally, it is crucial to note that any physical interaction imposes a set of constraints on the motion of each partner which we discussed in the previous subsection. Nevertheless, in the mirror game setup used in Chapter 3, the motion of both the leader and follower are free from any physical coupling/constraints. The motivation behind this choice is twofold. First, the focus of this chapter is to investigate the follower's prediction capacity (at the motion-level) facing a leader who can create complex motions that are not limited to point-to-point movements. Second, the offered models and frameworks in the literature (often derived from theories on human arm movements such as the minimum jerk model) are limited to point-to-point movements (with known initial and final positions) and do not scale to dyadic interactions where the leader's motions are unconstrained and unknown.

2.1.5 Avatars as programmable leaders for human-followers

We are currently witnessing a growing number of applications for humanoid robots, androids, and computer simulated avatars in the context of social interactions; see Meadows (2007), Ishiguro (2007), and Sakamoto et al. (2007). For instance, Sakamoto et al. (2007) suggest that in telecommunication, androids can elicit a strong feeling of presence in the operator. Furthermore, to enhance the social interaction with such artificial agents, researchers have tried to improve both the visual and behavioral aspects of android and avatars; see Minato et al. (2004). Among others, gaze behavior is an effective element to enhance social interactions (Minato et al., 2005, 2006). By using an appropriate gaze behavior, a robot can establish the

Figure 2.2 – Two subjects playing the mirror game in a leader-follower setup.

participants' roles in a conversational setting and increase the sense of affiliation among the individuals (Mutlu et al., 2009, 2012). Robotic gaze aversion (i.e., the intentional redirection away from the face of the human partner in the interaction) is also perceived by humans as intentional and thoughtful, which can effectively shape the interaction (Andrist et al., 2014). Garau et al. (2001) and Garau et al. (2003) have also investigated different gaze behaviors in avatars where inferred (from voice) gaze behavior enhanced the behavioral realism. It has also been shown that the duration of a gaze cue, in a social interaction setting, plays a significant role on the level of co-presence (Bente et al., 2007). Previous studies have shown that, during verbal communication, active gaze behavior improves avatar liveliness and human-similarity; see Garau et al. (2003), Bente et al. (2007), and Bailenson et al. (2006). For example, gaze dynamics (shifts, aversion, and fixation) can influence the sense of affiliation (Mason et al., 2005). In another study, human gaze has been tracked to orient the avatar gaze in order to create eye-contact leading to the sense of awareness of others' gazes in virtual interaction settings (Steptoe et al., 2008). Moreover, responsive gaze behavior from an avatar can elicit in a human partner the feeling of being looked at (Yoshikawa et al., 2006). Despite numerous studies on the realism of avatars (MacDorman et al., 2009; Mori et al., 2012), and the realism of simulated gazes in virtual environments (Garau et al., 2003), little is known about the effects of avatar gazes in social motor coordination. In particular, it is unclear whether in joint action settings, avatars can effectively simulate natural gaze behavior, and whether human partners can benefit from it.

Similarity is believed to be an important factor for affiliation/attraction (Byrne, 1961; Lydon et al., 1988). Thus, it would be interesting to see if the same principle can be applied to the avatar-robot (or human-robot) interaction, where a different aspect of similarity – gaze cues in our case – can boost affiliation. To increase realism in animated avatars, several models of gaze have been proposed; see Ramaiah et al. (2013) as an example where the avatar head moves between poses according to the desired gaze behavior. To create human-inspired

interactions, the avatar gaze has been programmed to be reactive to the human gaze that is tracked with wearable devices (Kipp and Gebhard, 2008) or cameras (Fu et al., 2008). Moreover, as the avatar's hand was used for the mirror game, models suggested for human eye-hand coordination can be helpful in increasing behavioral similarity between avatars and humans. However, such proposed models in the literature are highly task-dependent; see Liesker et al. (2009) for search, Bowman et al. (2009) for sequential target contact, Coen-Cagli et al. (2009) for drawing, and Lazzari et al. (2009) for rhythmical pointing tasks. Therefore, in Chapter 3, to keep the analysis simple, robust, and interpretable, we limit our gaze-hand model to a simple delay of $500ms$. This model is indeed in line with previous findings in Volcic and Lappe (2009) and Khoramshahi et al. (2014). The results of Chapter 3 confirm that gaze cues preceding hand movements help the human partner with the action-prediction process which consequently improves the coordination. Furthermore, and tangential to the mainline of this thesis, in Appendix A, we show that such gaze behavior also helps the human partner with the perception of human-likeness. This shows that similarity-affiliation effect persists in the case of motor coordination with an avatar utilizing simple gaze behavior.

2.2 Intention recognition through physical human-interaction

The applications of pHRI are multifarious: carrying and installing heavy objects (Kim et al., 2017a; Lee et al., 2007), hand-over (Strabala et al., 2013), cooperative manipulation and manufacturing (Peternel et al., 2014; Cherubini et al., 2016), and assistive tele-operation (Peternel et al., 2017a). While the field of pHRI is rapidly expanding, the role of most robots in the interaction falls into two extreme cases:

1) *Passive followers* (PF): whereby reducing the interaction forces and spatial error (i.e., *compliance at the force-level*), the robot provides a passive following behavior. This approach has the advantage that the human can lead the task (i.e., decide on the desired trajectory), however, the robot cannot provide power/effort in the direction of the uncertainties (i.e., due to the human intentions). Carrying heavy loads in collaboration with human (Bussy et al., 2012b) is the rudimentary example where the robot only provides support in the direction of gravity but fails to assist in the human-intended direction of movement where it even increases the total mass.

2) *Active leaders* (AL): where the robot executes a pre-defined task while allowing for safe interactions with environment and tolerating for small perturbations; i.e., achieving compliance at motion and force-level as proposed by Kronander and Billard (2016)), this approach has the advantage of minimizing the human effort. Nonetheless, if the robot is pre-programmed to accomplish only one task, any human efforts to perform a different task (in the course of the interaction) will be rejected.

Evrard and Kheddar (2009) and Li et al. (2015) proposed different control architectures that explicitly modulate the role of the robot (between follower and leader). However, one could

aim for approaches that benefit from the advantages of both PF and AL. For example, the robot passively follows the human guidance initially and predicts the future desired motions by recognizing the underlying task. Then, the robot takes over the leadership by executing the recognized task. This capacity to act upon predicted motions results in a proactive behavior toward human leadership. To achieve this, many predictive models for human behavior have been proposed. For instance, Petrič et al. (2016) proposed to use Fitts' law to predict human movements. As another case, Leica et al. (2017) suggested a model based on mechanical-impedance that predicts human motions based on the interaction forces. Other approaches were suggested to learn the dynamics of the collaboration (including control and prediction dynamics) (Rozo et al., 2013; Ghadirzadeh et al., 2016). Moreover, most of the approaches in the literature tackle the prediction problem in the framework of impedance control. In the next section, we review the related literature on impedance control as we use this approach throughout this thesis. Moreover, to reach proactive and adaptive behavior we address the prediction capabilities at three different levels:

- Motion-level: In Chapter 4, we adapt the robotic motion (generated by DS) to those demonstrated by a human user; i.e., the robot complies to the intended motions.

- Task-level: In Chapter 5, through physical interaction, we recognize the intended task of a human-user; i.e., the robot complies to the intended tasks.

- Force-level: In Chapter 6, using admittance control and processing the external forces, we distinguish between intentional and accidental forces; i.e., the robot complies to intentional forces.

Regarding our approach toward proactivity in pHRI, in the following, we review the related literature for impedance control, DS-based motion planning, motion-adaptation, task-adaptation, and human-guidance detection.

2.2.1 Compliant control: from passive-follower to compliant-leader

A conservative approach toward pHRI is to ensure a passive interaction; e.g., the kinetic energy of the robot dissipates over time. The control strategies proposed by Hogan (1988) provide straightforward formulations (impedance and admittance) for such passive and compliant interactions. We review the technical details of impedance and admittance control in Section 2.3. In its simple form, the robot renders a mass-spring-damper behavior around a reference trajectory; e.g., a set-point with zero-velocity. Having proper parameters (i.e., inertia, damping and stiffness matrix), one can achieve passive interaction with the environment. Considering only the damping part allows the robot to passively follow the external forces; i.e., *passive-follower*. This is useful for transportation tasks (especially for mobile platforms as in Kang et al. (2010)) or manipulation tasks where a different and more suitable inertia and damping is rendered for the human user as in Duchaine and Gosselin (2007). However, this

way, the robotic behavior is limited to a passive-follower where the robot appears as a static mass-damper or a mass-spring-damper.

Based on the advancement of variable impedance control (Vanderborght et al., 2013), many approaches aim for the dynamic optimization of impedance parameters to achieve a desirable compliant behavior during human-robot interaction (Duchaine and Gosselin, 2007). Duchaine and Gosselin (2007) show that varying the compliant behavior can improve the interaction from the user point-of view. To go further and achieve a human-like compliant behavior, Ganesh et al. (2010) proposed an adaptation method based on human motor behavior which was shown to be effective in human-robot interaction settings by Gribovskaya et al. (2011).

Instead of a set-point, the robot can exhibit the compliance behavior around a reference trajectory; i.e., a compliant-leader in the interaction. This trajectory can be pre-computed (Ferraguti et al., 2013), or can be generated reactively depending on the state of the robot (Kronander and Billard, 2016). Beside the optimization of the impedance parameters, other approaches aim to achieve a desirable behavior by optimization of the impedance set-points; see Maeda et al. (2001) and Corteville et al. (2007). To be effective, this approach requires motion estimation and planning under human-induced uncertainties which is tackled in the literature by means of optimal and adaptive control (Medina et al., 2012; Li et al., 2016, 2017), machine learning techniques (Calinon et al., 2014; Medina et al., 2011), and more specifically reinforcement learning (Modares et al., 2016). These works, to some extent, rely only on a local anticipation of human motions which, nevertheless, lowers the human effort (Evrard and Kheddar, 2009) and increases transparency (Jarrassé et al., 2008). Regarding this literature, human-intention recognition is only addressed at the motion and force-level (see Fig.1.3). However, the proactivity of robotic systems can tremendously benefit from adaptation at the task-level where the robot adapts its task to those intended by the human-user. In Chapter 5, we contribute to this literature by recognizing and adapting to the human-intended task.

In Chapter 6, we explore the advantages of admittance control for pHRI application; i.e., the robot senses the interaction forces and responds with proper velocities. This controller is widely used in the literature of pHRI: collaborative assembly (Cherubini et al., 2016), insertion tasks (Mol et al., 2016). By responding to human forces, the robot can provide a simple following behavior as in Duchaine and Gosselin (2007). Moreover, human trajectory estimation can provide proactive following behavior (Jlassi et al., 2014). Duchaine and Gosselin (2009) and Ranatunga et al. (2017) proposed a method to adapt to human stiffness as to generate cooperative movements. Admittance control is also suitable for whole body control of robots such as arm-based platform (Dietrich et al., 2012). Hashtrudi-Zaad and Salcudean (2001) argue that performances of this controller depend on the stiffness of the environment and propose a method to switch an impedance controller to have the accuracy of admittance control in free motion with the robustness of the impedance controller. Campeau-Lecours et al. (2016) also argue that admittance control is suitable to perceive the environment and human intentions and to respond accordingly. They mention that the behavior is acceptable if the reference

trajectories are highly dynamics. Moreover, the performance of impedance controller in terms of tracking performance and compliant behavior is contradictory; i.e., high impedance gains result in precise tracking performance but stiff behavior toward the environment whereas low gains provide compliant interaction but poor tracking performance. However, in admittance control, the tracking performance (often provided by high-gain velocity controller) and compliant behavior (controlled by the admittance block) are decoupled and work in parallel. Therefore, admittance control provides a simple solution toward compliant leader behavior: the resulted velocities from the external force can be simply added to task-specific velocities. This idea is used in Corteville et al. (2007) and Shahriari et al. (2017). In Chapter 6, we use the same approach to combine task-specific motion planning with proper compliant behavior.

2.2.2 Reactive motion planning using dynamical systems

To endow robots with leader behavior, we employ state-dependent dynamical systems as motion generators. Such DS can be learned through human demonstrations and provide stable and convergent trajectories (Khansari-Zadeh and Billard, 2011b). The state-dependency of DS provides a reactive behavior; i.e., the external perturbations to the state result in a different desired velocity. Moreover, considering the storage-function related to the DS leads to simpler design of passive interaction with the environment while performing a task (Kronander and Billard, 2016). Furthermore, DS provides a strong framework for adaptive motion generation. To do so, the dynamics can be modulated based on a external signals; e.g., Gribovskaya et al. (2011) use external forces to perform a collaborative task, Sommer et al. (2017) use contact information to avoid obstacle, Medina et al. (2016) use the load-share to obtain a fluid hand-over, and Khoramshahi et al. (2018) use tracking error to refine a DS based on human guidance. DS provide a computationally light motion planning which allows for smooth transient behaviors. However, tracking a trajectory potentially undermines the passivity of the system. Energy tank-based controllers were employed to relax the conservative condition on the passivity (Ferraguti et al., 2015; Schindlbeck and Haddadin, 2015; Kronander and Billard, 2016); i.e., the robot can be temporally active and injects energy into the environment while, on average-over-time, stays passive. Generating motion using dynamical systems with their corresponding storage functions (as proposed by Kronander and Billard (2016)) allows us to investigate and control the passivity of the whole system easier. Same approach is used by Shahriari et al. (2017) to include the energy due to the motion planning using Dynamic Movement primitives. The literature of robotic compliant control clearly shows the efficacy of the proposed methods to generate a "single" desired behavior (e.g., compliant leader, passive or proactive follower). However, it falls short from providing robots with intelligence mechanism for detecting the proper behavior and switching mechanisms that are proved to be safe and stable.

Taking advantage of state-dependency of such dynamical systems, we are able to propose three different adaptive strategies in this thesis. In Chapter 4, by adapting DS parameter, encoding for geometrical transformation, the robot complies to human demonstrated motions. In this

case, the robot acts as an *adaptive leader*. In Chapter 5, we propose an adaptive mechanism to switch smoothly from one DS to another, each encoding for a different task, to comply to human interactions. During such adaptation, the robot acts as an *proactive follower* where, as it complies to human forces, it forms prediction about human-intended task. In Chapter 6, DS-based admittance control allows for transition between leader and follower behavior. In presence of human-guidances, the robot acts a proactive follower whereas, in the absence of such guidances, it acts as a leader with proper tracking performance and disturbance rejection capabilities.

2.2.3   Motion-adaptation based on physical human-interaction

As mentioned before, the impedance parameters (e.g., inertia, damping, and stiffness) allow for adaptation methods to achieve various control objectives: to adapt to human forces (Abu-Dakka et al., 2015), human compliant behavior (Ganesh et al., 2010), or human intended set-point (Corteville et al., 2007). While these approaches are very effective to locally and temporally adapt to the human physical-interactions, they are limited in adaptation to human intention with regard to the underlying task. On the other hand, incremental learning approaches focus on the learning of a task as a whole through several interactions with the environment or the human user; see Abi-Farraj et al. (2017), Maeda et al. (2017a), and Lee and Ott (2010). Several techniques can be envisioned to accommodate the new experiences. For instance reinforcement learning can be used to learn the dynamics of physical interaction with human Ghadirzadeh et al. (2016), or learn to stay in contact with a surface properly (Hazara and Kyrki, 2016). In Jlassi et al. (2014), optimal control is used to improve the trajectories for heavy load-carrying with a human. These methods can learn from small corrections made by the human during each interaction in order to achieve their goal; see Sauser et al. (2012). These demonstrations can take place through physical interaction with the robot; see Cho and Jo (2013), Ewerton et al. (2016), Tykal et al. (2016), and Lee and Ott (2011) for kinesthetic teaching. However, the fact that in most current approaches the learning and execution phases are disjoint and defined by the human supervisor limits reaching a seamless interaction.

The interaction can be more effective if the robot learns proper motion regarding different human intentions and during the execution phase, the robot only adapts to the proper already-learned motion based on human interaction. Simple robotic tasks, such as polishing and pick-and-place, can be improved by adapting to the intention of the human user. For example, adapting to the human desired forces can improve the quality of a polishing task as shown by Kabir et al. (2017), Oba et al. (2016), and Schindlbeck and Haddadin (2015). This task can be improved further by adapting to the human desired patterns. In another example, adaptive behavior was provided for pick-and-place task where the target locations were determined using visual guidance (Quintero et al., 2015) or natural language (Schulz, 2017). In Kastritsi et al. (2018), use varying stiffness to reshape the movement primitives. In Chapter 4, we propose adaptive motion planning for such tasks based on the physical interactions. To do so, we employ parameterized dynamical systems (DS) which show flexibility toward numerous

possible human-intentions. For instance, in Peternel et al. (2017b); Gams et al. (2014) the parameters of a time-dependent DS are adapted to achieve a desired force during human-robot interaction. However, an adaptive time-dependent DS captures only the temporal aspect of the input signal (e.g., phase lags and offsets). In Chapter 4, to capture the spatial aspect of the human intention (e.g., where to polish or pick/place), we employ state-dependent dynamical systems (Khansari-Zadeh and Billard, 2011b). By treating the human as a state-dependent reference model (with the intended parameters), we propose and analyze our adaptive mechanism in Chapter 4.

2.2.4   Intention-recognition and task-adaptation

The amount of previous efforts addressing adaptation at a task level is sparse. Bussy et al. (2012a) employed a velocity threshold to trigger a new task (e.g., switching from "stop" to "walk" while carrying an object). As reported, such hard switching results in abrupt movements which are required to be filtered to reach human-like motions. Pistillo et al. (2011) proposed another framework (based on dynamical systems) where the robot switches between tasks if it is pushed by its human-user to different areas of its workspace. Although this approach leads to a reliable and smooth transition between tasks, such human-intention recognition strategy (i.e., based on the location of the robot in the workspace) is not efficient; e.g., each task needs a considerable volume of the workspace to be functional, and the robot cannot switch between different tasks in the same area of the workspace. Moreover, there has been recent interesting methods to encode several tasks in one model Ewerton et al. (2015); Calinon et al. (2014); Lee et al. (2015), and disjointly, several works to recognize and learn the intention of the human Aarno and Kragic (2008); Bandyopadhyay et al. (2012); Wang et al. (2018); Ravichandar and Dani (2015). Only recently, Maeda et al. (2017b) and Tanwani and Calinon (2017) proposed probabilistic models that not only encode for different tasks, but also act as an inference tool for intention recognition. Furthermore, in another recent work, Noohi and Žefran (2017) proposed a interaction model that allows for intention-recognition based on interaction forces. However, they do not address the online and physical interaction between the human and the robot. The goal of Chapter 5 is to address these issues and provide a smooth transition between tasks with an efficient human-intention recognition strategy that allows for seamless physical interaction between a human and a robot.

2.2.5   Human-guidance recognition

Human-guidance is a central topic in collaborative robots. The human can supervise the robot task and through his/her guidances modifies the task. Nevertheless, for a robust collaboration, it is crucial for the robot to distinguish between human-guidances and other possible disturbances. Human-guidance can be given through several modalities and contextual information such as vision, natural-language processing, etc. However, in this thesis, we focus on the haptic channel, namely relying on the external forces sensed by the robot, as literature presented in Section 2.1.3 emphasizes the central role of the haptic channel in performing

physical joint actions. Benefiting from human-guidances in collaborative robots imposes two challenges. First, it is essential for the robot to distinguish between human-guidances and other undesirable interaction forces. Second, a reaction strategy which ensures the stability and performance of the system is crucial. Among solutions proposed in the literature, admittance control is suitable to detect and react to human guidances while performing a task. This controller can provide the proper behavior by filtering/modifying measured forces. This is not the case in impedance control where the input is a displacement. The literature of collision detection exploits this fact. The robot rejects small external forces and delivers a satisfactory tracking behavior. It only reacts to forces detected as collision. Detection algorithms rely on the assumption that collisions result in a fast rate of change in different quantities such as input power (De Luca et al., 2006), generalized momentum (He et al., 2015) and external forces (Haddadin et al., 2008; Cho et al., 2012). The collision is detected if the magnitude of such signals surpasses a certain threshold. This threshold can be adapted over time based on the evolution of the force signal as proposed in Makarov et al. (2014). More elaborated methods use the difference between real and nominal dynamics (Landi et al., 2017). Kouris et al. (2018) suggest to use frequency domain approaches to distinguish unexpected collisions from voluntary contact during human-robot collaborations. Interestingly, they conclude that admittance control provides the fastest reaction behavior. Reaction strategies are also of interest to our work where the robot switches from active to passive mode; as in Li et al. (2018) where the robot switches from position control to a passive torque-control upon collision with a human user. In contrast, we use a unified control architecture (i.e., DS-based admittance controller with human-guidance detection) which allows us to smoothly switch back and forth between active and passive modes.

Even though detection of human-leadership is structurally similar to collision detection, there are a few important differences. First, a human joining the interaction does not necessarily result in high rate of changes in force or energy. Second, it is required to detect not only the human joining the interaction, but also leaving it. Interactions with the environment are usually considered passive while the human is an active agent who intends to inject energy into the system. The literature on variable compliance control offers different approaches where the controller adapts to detected human intentions (Lecours et al., 2012; Kim et al., 2017b; Ranatunga et al., 2015; Corteville et al., 2007). However, such works are limited to a single role for the robot, and human-interaction detection is not used to switch from leader to follower. In Chapter 6, we assume human-guidance forces are consistent (as opposed to noises, oscillations and short-lived disturbances like shocks). We rely on these properties to detect human-guidance forces instead of fast rate of changes in the literature of collision detection.

In Chapter 6, we tackle the problem of switching between leader and follower behaviors. In a closely related work, Evrard and Kheddar (2009) propose to use a homotopy variable to linearly combine the two behaviors. However, the authors do not offer a solution to adjust this variable based on the contextual informations and to guarantee the stability. In a follow-up work, Bussy et al. (2012a) utilize a manual switch from proactive follower to leadership. In

this thesis, we combine the leader and follower behaviors through generated velocities by dynamical systems and admittance loop. Furthermore, we provide an adaptation/estimation for such homotopy variable while guaranteeing the stability of the system.

2.3 Technical preliminaries

We briefly review technical materials presented in this thesis. All reviewed materials are either previously published or from standard text books. We start by defining dynamical systems and their properties such as stability and passivity. Then, we discuss different configurations where a DS can be used for motion planning in robotic application. Moreover, we quickly present a learning to learn a DS from demonstration based on Gaussian Mixture Models. To cover strategies for motion/compliance control, we present the dynamics of a generic robotic manipulator, and we discuss impedance and admittance control. Furthermore, we review the DS-based impedance control. Later, we present a short introduction to basic methods in Adaptive Control. Finally, we review some performance measurement related to pHRI.

2.3.1 Dynamical systems

Dynamical systems (DS) are widely used in this thesis for motion planning, analysis of stability, passivity, and convergence behavior. The materials presented here are adopted from Khalil (1996); refer to the original textbook for further details. To have a clear definition for DS, let us start with a general form as

$$\dot{x} = f(x, t, u) \tag{2.1}$$

where $x \in \mathbb{R}^d$ represents the state of the system, t denotes time, and u is the control input. In control input is designed as a combination between state-feedback and feed-forward signal; i.e., $u = u(x, t)$. In this case, the closed-loop dynamics are

$$\dot{x} = f(x, t, u(x, t)) = \tilde{f}(x, t) \tag{2.2}$$

The general dynamics are explicitly time-dependent. However, in this thesis, we are concerned only with state-dependent systems formulated as

$$\dot{x} = f(x) \tag{2.3}$$

where $f : \mathbb{R}^d \mapsto \mathbb{R}^d$ is a continuous function. Such DS are referred to as *autonomous* since the evolution of the state ($\dot{x}$) only depends on the state itself (x). A state (x^*) is said to be the *equilibrium point* if $f(x^*) = 0$. The stability of an equilibrium point over a region ($\mathcal{D} \subseteq \mathbb{R}^d$) can be guaranteed under a Lyapunov function ($V(x) : \mathbb{R}^d \mapsto \mathbb{R}$) with the following properties.

1. $V(x)$ vanishes at the equilibrium point: $V(x^*) = 0$

2. $V(x)$ is continuous and positive definite in $\mathcal{D}$: $V(x) > 0 \quad \forall x \in \mathcal{D} \setminus x^*$

3. $\dot{V}$ is negative definite in $\mathcal{D}$: $\dot{V}(x) < 0 \quad \forall x \in \mathcal{D} \setminus x^*$

In this case, $x = x^*$ is *locally asymptotically stable*.

A DS is called *conservative* if it is the gradient of a *potential energy function* as follows.

$$f(x) = -\nabla_x V(x) \tag{2.4}$$

where $V(x)$ is a scaler positive definite function that vanishes at $x = x^*$. The stability of $\dot{x} = f(x)$ is immediate by considering $V(x)$ as the Lyapunov function leading to $\dot{V} = -||\nabla_x V(x)||^2$. An autonomous DS can expressed as

$$f(x) = -\nabla_x V(x) + \tilde{f}(x) \tag{2.5}$$

where $\tilde{f}$ represent the nonconservative part of $f(x)$ that cannot be expressed based on the gradient a potential function. The stability of the system using $V(x)$ as the Lyapunov function results in

$$\dot{V}(x) = \nabla_x V(x)^T \dot{x} = \nabla_x V(x)(-\nabla_x V(x) + \tilde{f}(x)) = -||\nabla_x V(x)||^2 + \nabla_x V(x)^T \tilde{f}(x) \tag{2.6}$$

The asymptotic stability can be achieved if $\nabla_x V(x)^T \tilde{f}(x) < ||\nabla_x V(x)||^2$.

For the notion of passivity, consider the following dynamical system.

$$\begin{cases} \dot{x} = f(x, u) \\ y = h(x, u) \end{cases} \tag{2.7}$$

In this system, $u \in \mathbb{R}^m$ denotes the input, and $y \in \mathbb{R}^m$ the output signal. The map $u \mapsto y$ is *passive* if there exists a storage function $W(x)$, bounded from below, such that

$$\int_0^t u^T(s) y(s) ds > W(x(t)) - W(x(0)) \tag{2.8}$$

The left-hand side can be considered as the energy supplied to the system and the right-hand side the stored energy. The inequality shows that the part of input energy is dissipated and the system does not generate energy by itself. Alternatively, one can ensure passivity by proving

$$\dot{W}(x) \leq u^T y \tag{2.9}$$

where $W(x)$ requires to differentiable with respect to x. This is useful notion in pHRI as the human injects energy into the robotic system and it is crucial to show that this energy dissipates and does not lead to unstable behaviors. Typically in the analysis of passivity, W is designed based on the mechanical energy of the robot. For further consistency, the external forces applied to the robot are considered as the input u, the robot velocity as output
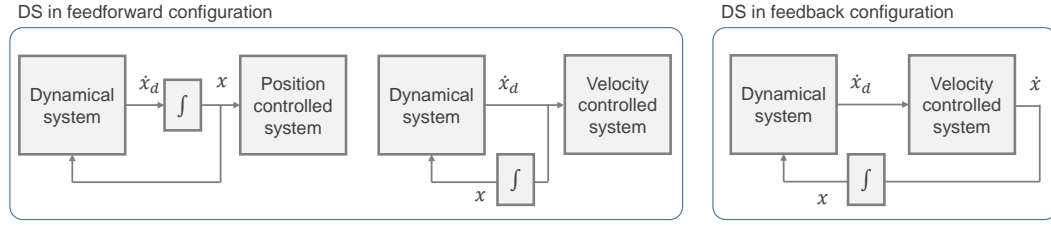
Figure 2.3 – Motion generation using dynamical system (left) DS in feedforward configuration where motion-generation is independent of robot's dynamics. (right) DS in feedback configuration where motion-generation reacts to robot's behavior.

y rendering $u^T y$ as the mechanical power.

2.3.2   Motion generation using dynamical systems

In this section, we focus on motion-generation for robotic application. Consider a stable DS f, and an initial condition $x_d(0)$. Using this DS, we can generate the desired trajectory by the following forward integration.

$$\begin{cases} x_d(t) = x_d(0) + \int_0^t f(x_d(\tau))d\tau \\ \dot{x}_d(t) = f(x_d(t)) \end{cases} \tag{2.10}$$

This numerical solution of initial initial value problem (the desired position x_d) is sent to a position-controlled robot as depicted in Fig. 2.3. It is also possible to send ($\dot{x}_d$) as the reference if the robot is velocity controlled. Moreover, one can use both x_d and $\dot{x}_d$ as the reference. As illustrated, the DS is used in a feedforward configuration in these cases; i.e., the state of the system does not affect the motion generation process.

Fig. 2.3 also shows DS in a feedback configuration where the state of the system affects the motion planning. The general equation for the closed loop system can be formulated as

$$\begin{cases} \dot{x}_d = f(x) \\ \dot{x} = H(x, \dot{x}, \dot{x}_d, u_e) \end{cases} \tag{2.11}$$

where H represents the dynamics of the velocity-controlled system, and u_e an external disturbance. Having perfect tracking $\dot{x} = \dot{x}_d$ (which often achieved by high-gain control) is equivalent to feedforward configuration. However, in compliant scenarios where $\dot{x}$ can deviate from $\dot{x}$, the two configurations are fundamentally different. In such scenarios, the DS provides a reactive motion-planning based on the perturbed states (x) due to external forces u_e; e.g., human interaction with the robot. One candidate for such compliant controller is the impedance controller. Having DS (as the motion generator), impedance controller (as the compliant controller), and robot dynamics in closed loop brings us to DS-impedance control which we introduce later in the next section.

The main challenge in DS-based motion planning is to design a DS such that it generates task-specific motion. For example, consider reaching motions for pick-and-place with obstacle avoidance where the robot is required to follow motions 1) starting from any initial condition in a reasonable region, 2) avoiding the obstacle, and 3) converging to the target position. Khansari-Zadeh and Billard (2011b) propose a method to learn such task by encoding a set of demonstration in a stable dynamical system. In this method, to go beyond simplicity of linear dynamical system and generate complex motions, we consider the following nonlinear dynamical systems.

$$f(x) = \sum_{k=1}^{K} h_k(x)(A_k x + b_k) \tag{2.12}$$

where $A_k \in \mathbb{R}^{d \times d}$ represent the linear dynamics, $b_k \in \mathbb{R}^d$ an offset, $h_k(x) \in \mathbb{R}^+$ state-dependent activation function. This nonlinear system is constructed by the linear combination of K locally linear DS facilitating the stability analysis and the learning procedure. To have a stable convergence for x^*, the following condition is sufficient.

$$A_k + A_k^T \prec 0 \quad \text{and} \quad b_k = -A_k x^* \quad \forall k \tag{2.13}$$

To obtain a learning process, we assume that the demonstrations (a pair of x and $\dot{x}$) are sampled from the following Gaussian Mixture Model.

$$P(x, \dot{x}; \mu_k, \Sigma_k) = \sum_{k=1}^{K} \pi_k \mathcal{N}(x, \dot{x}; \mu_k, \Sigma_k) \tag{2.14}$$

where $\mathcal{N}$ is a normal distribution with mean μ_k and covariance Σ_k, prior probability of π_k. Moreover, the means and covariances can be decomposed as follows.

$$\mu_k = \begin{pmatrix} \mu_{k,x} \\ \mu_{k,\dot{x}} \end{pmatrix}, \qquad \Sigma_k = \begin{pmatrix} \Sigma_{k,x} & \Sigma_{k,x,\dot{x}} \\ \Sigma_{k,\dot{x},x} & \Sigma_{k,\dot{x}} \end{pmatrix} \tag{2.15}$$

Using this joint distribution, $\dot{x}$ can be estimated based on x as the maximum posterior mean of the conditional probability density:

$$\dot{x} = \arg\max_{\dot{x}} P(\dot{x}|x) = \sum_{k=1}^{K} \frac{\pi_k P(x|k)}{\sum_{i=1}^{K} \pi_i P(x|i)} (\mu_{k,\dot{x}} + \Sigma_{k,\dot{x},x}(\Sigma_{k,x})^{-1}(x - \mu_{k,x})) \tag{2.16}$$

By comparison to 2.12, we can relate the GMM model to the DS model as

$$\begin{cases} A_k = \Sigma_{k,\dot{x},x}(\Sigma_{k,x})^{-1} \\ b_k = \mu_{k,\dot{x}} - A_k \mu_{k,x} \\ h_k(x) = \frac{\pi_k P(x|k)}{\sum_{i=1}^{K} \pi_i P(x|i)} \end{cases} \tag{2.17}$$

The GMM parameters can be initially guessed using *Expectation Maximization* and tune

further to minimize the error between demonstrated and generated velocities. The reader is referred to Khansari-Zadeh and Billard (2011a) for further details such as an alternative optimization based on Cholesky decomposition of covariance matrices. Furthermore, Khansari-Zadeh and Khatib (2017) propose another learning approach to learn the potential functions directly suitable to to design conservative DS.

2.3.3   Robotic arm control

Let us begin with the dynamics of a N-DoF robotic manipulator specified in the joint state as

$$M(q)\ddot{q} + C(q,\dot{q})\dot{q} + g(q) = \tau_c + \tau_e \tag{2.18}$$

where $q \in \mathbb{R}^N$ is the joint position and its time-derivatives $\dot{q}$ and $\ddot{q}$ denote velocity and acceleration respectively. $M(q) \in \mathbb{R}^{N \times N}$ represent the inertia, $C(q,\dot{q}) \in \mathbb{R}^{N \times N}$ the coriolis and centrifugal forces and $g(q) \in \mathbb{R}^N$ the forces generated by gravity. τ_c denote the control torques exerted by the actuators, and τ_e the external forces applied by the environment; including humans and other robots. Moreover, by compensating for gravity, we can write

$$M(q)\ddot{q} + C(q,\dot{q})\dot{q} = \tilde{\tau}_c + \tau_e \tag{2.19}$$

where $\tau_c = \tilde{\tau}_c + g(p)$ with $\tilde{\tau}_c$ being the new control input. In these dynamics, the inertia matrix is positive definite ($M > 0$) and $\dot{M} - 2C$ is skew-symmetric.

The mapping from the joint-space ($q \in \mathbb{R}^N$) to the task-space (i.e., the end-effector pose $x \in \mathbb{R}^6$) is given by the forward kinematics of the robot as $x = G(q)$ where G is defined the geometrical model of the robot. Therefore, the Jacobian of this mapping ($J(q) \in \mathbb{R}^{6 \times N}$) satisfies $\dot{x} = J(q)\dot{q}$. Furthermore, the equation dynamics can be describe the in task-space as

$$M_x(q)\ddot{x} + C_x(q,\dot{q})\dot{x} = F_c + F_e \tag{2.20}$$

where F_c and $F_e \in \mathbb{R}^6$ respectively represent the control and the external wrench applied to the end-effector satisfying $\tilde{\tau}_c = J^T(q)F_c$ and $\tau_e = J^T(q)F_e$. $M_x(q) \in \mathbb{R}^{N \times N}$ represent the end-effector inertia, $C_x(q,\dot{q}) \in \mathbb{R}^{N \times N}$ the end-effector damping due to the Coriolis and centrifugal forces. For derivation of M_x and C_x and further details on task-space formulation see Khatib (1987). Furthermore, In this thesis, we assume that the actuator (F_c), force-sensor (F_e), and motion-sensing (x) are co-located.

Impedance control

Impedance control is an efficient candidate to compliant control the desired robotic motions. The general structure of this controller is depicted in Fig. 2.4. Consider the desired and real trajectory x_d and x, respectively with their time-derivatives. The tracking error is computed as $e = x - x_d$. The following impedance law considers a dynamical relation between the error (e)
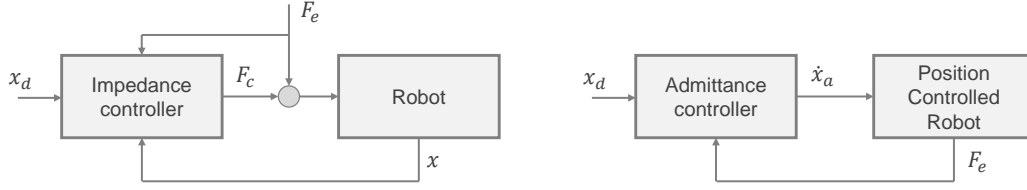
Figure 2.4 – Impedance and admittance control structure.

and external force (F_e).

$$M_d\ddot{e} + D_d\dot{e} + K_d e = F_e \tag{2.21}$$

To realize this impedance behavior for the robot's dynamics in Eq. 2.20, we can use the following controller.

$$F_c = (M_x M_d^{-1} - \mathbb{1}_6)F_e - (M_x M_d^{-1})(D_d\dot{e} + K_d e) + M_x\ddot{x}_d + C_x\dot{x} \tag{2.22}$$

The force sensing is only required if we aim to render a different inertia matrix. In case of $M_d = M_x$, the impedance control simplifies to

$$F_c = -D_d\dot{e} - K_d e + M_x\ddot{x}_d + C_x\dot{x} \tag{2.23}$$

The passivity of this controller can be investigated by considering $W = \frac{1}{2}\dot{e}^T M_d\dot{e} + \frac{1}{2}e^T K e$. The rate of change of this storage function is

$$\begin{aligned} \dot{W} &= \dot{e}^T(-D_d\dot{e} - K_d e + F_e) + e^T K\dot{e} \\ &= F_e^T\dot{e} - \dot{e}^T D_d\dot{e} \end{aligned} \tag{2.24}$$

In this equation $D_d > 0$. This shows that the system is passive with respect to the port $(F_e, \dot{e})$. More precisely, from the controller point of view, the mapping $\dot{e} \mapsto F_e$ is passive. Note that in impedance, the environment induce and error ($\dot{e}$) and robot response with a force (F_e).

The impedance can be implemented at the velocity level where the error dynamics are designed to be

$$M_d\ddot{e} + D_d\dot{e} = F_e \tag{2.25}$$

leading to the following controller.

$$F_c = -D_d\dot{e} + M_x\ddot{x}_d + C_x\dot{x} \tag{2.26}$$

In this case, the passivity of $\dot{e} \mapsto F_e$ can be shown using $W = \frac{1}{2}\dot{e}^T M_d\dot{e}$.

Admittance control

Admittance control is suitable for position/velocity-controlled robot; i.e., systems that are not equipped with torque control. Thus, we assume that the robot is position control. The general structure of this controller is illustrated in fig 2.4. In this case, an admittance block translates the external forces into a proper deviation from the nominal trajectory; i.e., $e = x_a - x_d$ where x_d is the desired reference trajectory and x_a is the admittance-generate velocity sent to the position controller. To satisfy the relation between F_e and e as in Eq.2.21, we need to compute $\ddot{x}_a$ as

$$\ddot{x}_a = \ddot{x}_d + M_d^{-1}(F_e - D_d(\dot{x}_a - \dot{x}_d) - K_d(x_a - x_d)) \tag{2.27}$$

Having the desired acceleration, in an discrete implementation of admittance controller, we update the admittance states by the following integration.

$$\dot{x}_a(t + \Delta t) = \dot{x}_a(t) + \ddot{x}_a(t)\Delta t$$
$$x_a(t + \Delta t) = x_a(t) + \dot{x}_a(t)\Delta t \tag{2.28}$$

Gmerek and Jezierski (2012) use this implementation to control a 1-DoF robotic arm. Using $W = \frac{1}{2}\dot{e}^T M_d \dot{e} + \frac{1}{2}e^T K e$, one can similarly show that the mapping $F_e \mapsto \dot{e}$ is passive. This controller can also be implemented in at the velocity level. Note that in the computation of acceleration ($\ddot{x}_a$), the desired trajectory is used; i.e., $\dot{x}_d$ and x_d. For simpler notation and implementation, we can directly take e as the admittance state and integrated forward the following dynamics

$$\ddot{e} = M_d^{-1}(F_e - D_d\dot{e} - K_d e) \tag{2.29}$$

and send $x_a = e + x_d$ as the desired reference. Moreover, similar to the impedance controller, the admittance control can be implemented at the velocity level. It is crucial to note that the admittance control introduce delays in the control loop due to the time-integrations. Ott et al. (2010) discuss the the performances of the two controller and proposes a unified framework for switching across the two modes. In short, impedance in suitable for interaction with stiff environment but results in poor tracking performance in free motion whereas admittance delivers better tracking performance but results in instability in contact with stiff environment.

DS-based impedance control

This controller can be seen as an velocity-based impedance controller where the reference velocity is planned by DS. Consider the following implementation for the position of the end-effector ($x \in \mathbb{R}^3$)

$$F_c = -D(\dot{x} - f(x)) \tag{2.30}$$

where the damping matrix $D \in \mathbb{R}^{3 \times 3}$ is positive definite and $f(.) : \mathbb{R}^3 \mapsto \mathbb{R}^3$ the state-dependent dynamical system. Under this control, the overall dynamics of the robot become

$$M_x(q)\ddot{x} + (D + C_x(q, \dot{q}))\dot{x} - Df(x) = F_e \tag{2.31}$$

This controller is proposed by Kronander and Billard (2016) and investigated in great details. Here, we briefly overview some of the relevant properties of this controller relevant to this thesis.

To show the passivity of the overall system, we assume that the DS is derived from a potential function as follows.

$$f(x) = -\nabla_x V(x) \tag{2.32}$$

Furthermore, we assume that $Df(x) = df(x)$ where $d \in \mathbb{R}^+$; e.g., D has a eigenvector in direction of $f(x)$ with eigenvalue of $d \in \mathbb{R}^+$. Note that this can be achieved by having $D = d\mathbb{I}_3$. Nevertheless, we can design damping matrices where we have a different damping coefficient for directions orthogonal to $f(x)$. Mathematically speaking, $Dv = d^\perp v$ for non-zero $v \in \mathbb{R}^3$ such that $v^T f(x) = 0$ where $d^\perp \in \mathbb{R}^+$ is the orthogonal damping coefficient.

Under aforementioned assumptions, we consider the following storage function to investigate the passivity of the overall system.

$$W(x, \dot{x}) = \frac{1}{2}\dot{x}^T M_x \dot{x} + dV(x) \tag{2.33}$$

The rate of this function is

$$
\begin{aligned}
\dot{W} &= \dot{x}M_x\ddot{x} + \frac{1}{2}\dot{x}^T \dot{M}_x \dot{x} + d\nabla_x V(x)^T \dot{x} \\
&= \frac{1}{2}\dot{x}^T(\dot{M} - 2C)\dot{x} + F_e^T \dot{x} - \dot{x}D\dot{x} + \dot{x}^T Df(x) - d\nabla_x V(x)^T \dot{x} \\
&= F_e^T \dot{x} - \dot{x}^T D\dot{x} + d\dot{x}^T f(x) - df(x)^T \dot{x} \\
&= F_e^T \dot{x} - \dot{x}^T D\dot{x}
\end{aligned}
\tag{2.34}
$$

which shows the mapping $\dot{x} \mapsto F_e$ is passive. Moreover, this analysis shows that the unperturbed system converges to the fixed point where $W(x, \dot{x}) = 0$. This is trivial to show that this is the case for the attractor of the DS; i.e., $V(x) = 0$ and $\dot{x} = 0$.

The tracking performance of the impedance controller for execution of a task can be investigated using Eq.2.31 as follows by defining the error as $\dot{e} = \dot{x} - f(x)$.

$$
\begin{aligned}
\ddot{e} &= \ddot{x} - f'(x)\dot{x} \\
&= M_x^{-1}(F_e - C_x\dot{x} - D\dot{e}) - f'(x)\dot{x}
\end{aligned}
\tag{2.35}
$$
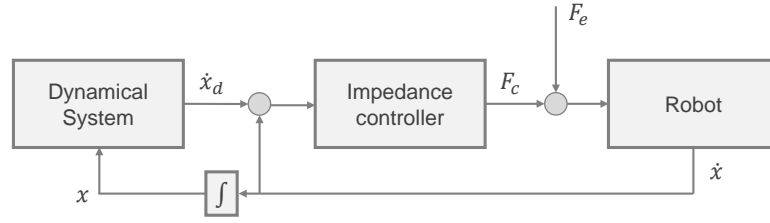
Figure 2.5 – DS-based impedance control. The DS used as a motion generator in a feedback loop with the controller and the environment. This leads to an active motion generation meaning the generated motion is influenced by the real state of the robot (i.e., the real position x). the motion generators provides desired velocity ($\dot{x}_d$) only corresponding to a single and fixed dynamical system (i.e., the static representation of only one task).

which brings us to the following error dynamics

$$M_x \ddot{e} + D\dot{e} = F_e - (C_x + f'(x))\dot{x} \tag{2.36}$$

where $f' = \partial f(x)/\partial x \in \mathbb{R}^{3 \times 3}$. To have stable dynamics on the left-hand-side, it is necessary to have $M^{-1}D \succ 0$. However, the other terms (especially the external forces) which can be seen as disturbances introduce biases. The control gain (D) can be increased in order to reduce the effect of such disturbances and improve tracking behavior. However, one should note that in discrete control loop, there is upper-bound for the stability of the system. Discretization of Eq.2.35 with Δt, ignoring the disturbances, and studying the eigenvalues provides us with an approximation of this upper-bound; i.e., $D < 2M\Delta t^{-1}$

In this controller, the observed damping for the human-user ($D_h \in \mathbb{R}^{3 \times 3}$) can be computed as

$$D_h = -\frac{\partial F_e}{\partial \dot{x}} = D \tag{2.37}$$

It can be seen that the resulting damping solely depends on the controller. To reduce the human effort in the interaction, lower controller gain should be used.

Earlier, we assumed that D has an eigenvector in the direction Furthermore, using Rayleigh quotient ($\mathcal{R} : \mathbb{R}^{3 \times 3} \times \mathbb{R}^3 \mapsto \mathbb{R}$) we can compute the damping effect in the direction of the desired velocity velocity generated by the dynamical system.

$$\mathcal{R}(D_h, f(x)) = \frac{f(x)^T D_h f(x)}{f(x)^T f(x)} = \frac{f(x)^T D f(x)}{f(x)^T f(x)} = \frac{f(x)^T d\, f(x)}{f(x)^T f(x)} = d \tag{2.38}$$

Similarly, we can show that the damping effect in the orthogonal direction is $d^\perp$.

Furthermore, the stiffness ($K_h \in \mathbb{R}^{3 \times 3}$) can be derived as

$$K_h = -\frac{\partial F_e}{\partial x} = -D\frac{\partial f(x)}{\partial x} = -Df'(x) \tag{2.39}$$

It can be seen that the stiffness is not only affected by the control gain D, but also by the properties of the DS (i.e., $f'(x)$ which denotes the convergence rates of the DS). The stiffness in a particular direction, namely x_s with unit norm, can be calculated by the following Rayleigh quotient.

$$\mathcal{R}(K_h, x_s) = x_s^T K_h x_s = -x_s^T D f'(x) x_s \tag{2.40}$$

For instance, in a case with $D = d\mathbb{I}_3$ and $f(x) = -kx$ with $k \in \mathbb{R}^+$. we have the apparent stiffness of dk in all directions.

2.3.4 Adaptation

Adaptive control was proposed initially to deal with parameter uncertainty in the plant dynamics. It is suitable for pHRI where human intention introduce uncertainties for the robot. In this thesis, we are concerned with model-reference adaptive control; intuitively, the human intention is considered as the reference model. The main approach in adaptive control is to first determine a control structure, and derive the error function. The next step is to construct a Lyapunov function based on the error function and derive the adaptation law. In the following, we review two distinct structure for adaptive control; i.e., direct and indirect method as illustrated in Fig. 2.6.

Direct adaptive control

In this approach, we directly adapt the control parameters without estimating the actual parameters of the model. To explain this, let us adopt a classical example from adaptive control textbook to a pHRI setting. To do this, we start with one-dimensional dynamics of a robotic system as

$$m\ddot{x} + b\dot{x} = F_c \tag{2.41}$$

where m is the mass and b is the mechanical damping. For the reference model, we assume the human in the interaction has the following desired behavior

$$m\ddot{x}_h + b_h\dot{x}_h + k_h x = 0 \tag{2.42}$$

where $\ddot{x}_h$ and $\dot{x}_h$ are the desired human acceleration and velocity respectively. In this equation, $b_h, k_h > 0$ are the *unknown* damping and stiffness coefficients of the human which determine the desired motion for a given state x (i.e., the reference signal) toward the origin (i.e., $x^* = 0$). Furthermore, we assume the following controller to reach the origin.

$$F_c = -d\dot{x} - kx \tag{2.43}$$
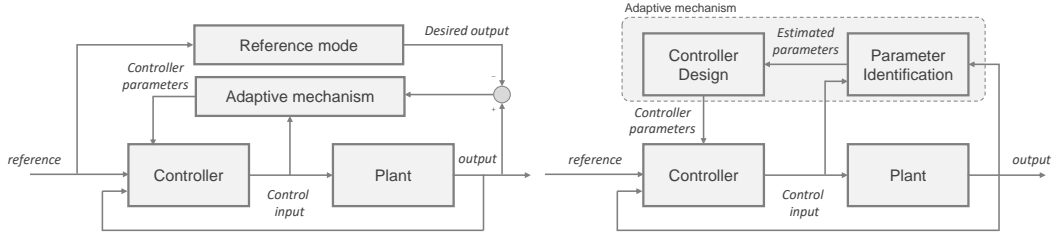
Figure 2.6 – General approaches to adaptive control. (left) In direct method, the parameters of the controller are adapted directly, where as in (right) indirect method, the unknown parameters of the system are first estimated and take into account to update the controller.

To relate to DS-impedance control, one can imagine $f(x) = -d^{-1}kx$ is used where k and d are the *adaptive* parameters of the controller. Having the control structure determined, we define the following error function

$$\dot{e} = \dot{x} - \dot{x}_h \tag{2.44}$$

where by minimizing this error, the robot follows the human-desired motions. The dynamics for this error function can derived as

$$
\begin{aligned}
m\ddot{e} &= m\ddot{x} - m\ddot{x}_h \\
&= (F_c - b\dot{x}) - (-b_h\dot{x}_h - k_h x) \\
&= (-d\dot{x} - kx - b\dot{x}) - (-b_h(\dot{x} - \dot{e}) - k_h x) \\
&= -b_h\dot{e} + (b_h - b - d)\dot{x} + (k_h - k)x
\end{aligned}
\tag{2.45}
$$

Based on the appeared coefficients, we consider the following Lyapunov function.

$$V(\dot{e}, d, k) = \frac{1}{2}(m\dot{e}^2 + \frac{1}{\epsilon}(b_h - b - d)^2 + \frac{1}{\epsilon}(k_h - k)^2) \tag{2.46}$$

where $\epsilon \in \mathbb{R}^+$ is an arbitrary constant. It is trivial to show that at $V = 0$, we achieve our control objective. The derivative of this function is

$$
\begin{aligned}
\dot{V} &= m\dot{e}\ddot{e} - \frac{1}{\epsilon}(b_h - b - d)\dot{d} - \frac{1}{\epsilon}(k_h - k)\dot{k} \\
&= -b_h\dot{e}^2 + (b_h - b - d)(\dot{x}\dot{e} - \frac{1}{\epsilon}\dot{d}) + (k_h - k)(x\dot{e} - \frac{1}{\epsilon}\dot{k})
\end{aligned}
\tag{2.47}
$$

We can ensure that $\dot{V} < 0$ by choosing the following adaptation law

$$
\begin{cases}
\dot{d} = & -\epsilon\dot{x}\dot{e} \\
\dot{k} = & -\epsilon x\dot{e}
\end{cases}
\tag{2.48}
$$

As it can be seen, we directly adapt the control parameters (k and d) without identifying the human model (k_h and b_h).

Indirect adaptive control

In indirect adaptive control, we first identify the unknown parameters. Then, we design the control parameters based on the estimated parameters. Here, we review an example where estimate the unknown parameters of the human model in Eq. 2.42. To this end, we assume a similar model as follows

$$m\ddot{x} + \tilde{b}\dot{x} + \tilde{k}x = 0 \tag{2.49}$$

where $\tilde{b}$ and $\tilde{k}$ are the adaptive parameters. Assuming the same error function ($\dot{e} = \dot{x} - \dot{x}_h$), we can write

$$
\begin{aligned}
m\ddot{e} &= m\ddot{x} - m\ddot{x}_h \\
&= -\tilde{b}\dot{x} - \tilde{k}x + b_h\dot{x}_h + k_h x \\
&= -b_h\dot{e} - (\tilde{b} - b_h)\dot{x} + (\tilde{k} - k_h)x
\end{aligned}
\tag{2.50}
$$

Similarly, we can choose the following Lyapunov function

$$V(\dot{e}, \tilde{b}, \tilde{k}) = \frac{1}{2}\left(m\dot{e}^2 + \frac{1}{\epsilon}(\tilde{b} - b_h)^2 + \frac{1}{\epsilon}(\tilde{k} - k_h)^2\right) \tag{2.51}$$

which result in the following derivative

$$\dot{V} = -b_h\dot{e}^2 + (\tilde{b} - b_h)(\frac{\dot{\tilde{b}}}{\epsilon} - \dot{e}\dot{x}) + (\tilde{k} - k_h)(\frac{\dot{\tilde{k}}}{\epsilon} - \dot{e}x) \tag{2.52}$$

By choosing the following adaptation law, we can ensure that $\dot{V} < 0$.

$$
\begin{cases}
\dot{\tilde{b}} = & -\epsilon \dot{x}\dot{e} \\
\dot{\tilde{k}} = & -\epsilon x\dot{e}
\end{cases}
\tag{2.53}
$$

Even though the adaptation rules are similar to those in Eq.2.48, we should note that the control structures are different.

MIT rule

Here, we shortly introduce an alternative to the Lyapunov method to derive the adaptive rule. Having the error function, one can consider the following cost function.

$$J(\tilde{k}, \tilde{b}) = \frac{1}{2}\dot{e}^2 \tag{2.54}$$

The parameters can be adapted by following the direction of the negative gradient of J as follows.

$$\dot{\tilde{k}} = -\epsilon\frac{\partial J}{\partial \tilde{k}} \quad \text{and} \quad \dot{\tilde{b}} = -\epsilon\frac{\partial J}{\partial \tilde{b}} \tag{2.55}$$

In our previous example, we can write

$$\dot{\tilde{k}} = -\epsilon \dot{e} \frac{\partial \dot{x}}{\partial \tilde{k}} \quad \text{and} \quad \dot{\tilde{b}} = -\epsilon \dot{e} \frac{\partial \dot{x}}{\partial \tilde{b}} \tag{2.56}$$

To compute these sensitivity we can write

$$\dot{x} = \frac{-\tilde{k}}{mp + \tilde{b}} x \tag{2.57}$$

where $p = \frac{d}{dt}$. This leads to the following adaptation rule.

$$\begin{cases} \dot{\tilde{b}} = & -\epsilon (\frac{1}{mp+\tilde{b}} \dot{x}) \dot{e} \\ \dot{\tilde{k}} = & -\epsilon (\frac{1}{mp+\tilde{b}} x) \dot{e} \end{cases} \tag{2.58}$$

This is similar to the Lyapunov based method with the introduction of the low pas filters. The induced delay due to these filters make the MIT rule only locally stable assuming that the adaptation rate ϵ is small. However, this method is preferred over the Lyapunov approach when the computation of error dynamics is not straightforward. For further details on MIT rule, the reader is referred to Jain and Nigam (2013).

For convergence of adaptive systems certain conditions are necessary. These condition are often revealed by investigation the adaptation dynamics. For instance, adaptation in Eq. 2.53 stops when $x = 0$ and $\dot{x} = 0$. Thus, it is necessary to have *rich* signals to trigger the adaptation. This is often referred to as *Persistence Excitation* in the literature of adaptive control. The reader is referred to Åström and Wittenmark (2013) for such further details.

2.3.5 Assessments

In this section, we briefly present several metrics to assess an interaction. We start by measuring synchrony between two time-series. This is relevant to Chapter 3 where we assess the human following behavior. Later, we present the notion of power, energy, and autocorrelation which are used in the robotic implementations reported in Chapter 5 and 6.

Synchrony in the time domain

Having two times series $x[k]$ and $y[k]$ for $n = 1, .., N$, we assess the synchrony based on Root-Mean-Square error as follows

$$E_{\text{RMS}} = \sqrt{\frac{1}{N} \sum_{k=1}^{N} (x[k] - y[k])^2} \tag{2.59}$$
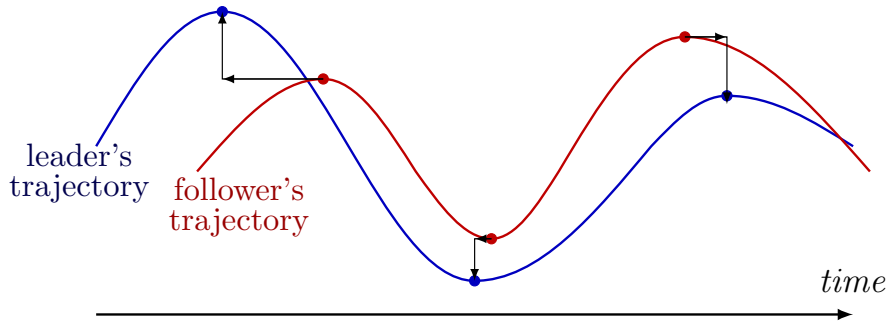
Figure 2.7 – Synchrony assessment based on temporal and spatial error from zero-velocity points. Horizontal arrows show temporal errors and vertical arrows show spatial error.

This is can also be useful for assessing the performance of a controller in term of motion-tracking.

Furthermore, the lag between two time-series can be computed based on cross-correlation as follows.

$$R_{xy}(l) = \sum_{k=-\infty}^{\infty} x[k-l]y[k] \tag{2.60}$$

where l is a shift in time; i.e., a delay between x and y. The value of l that results in highest R_{xy} can be considered as the lag between the two time series. It is trivial to see for similar time series, this is obtained at $l = 0$.

However, in most application, not all moments of the interaction have the same level of importance. For example, in the mirror game, we focus on zero-velocity points as illustrated in Fig. 2.7. Two types of error can be extracted from zero-velocity points: *temporal error* (as used in Noy et al. (2011)) and *spatial error*. For each zero-velocity point in the follower's trajectory, we consider the time-nearest zero-velocity instant of the leader's trajectory but with the same direction (minimum or maximum). Then we calculate temporal/spatial error based on the time/position difference. This results in two distributions for temporal and spatial errors. In the temporal-error distribution, the positive/negative accounts for leading/lagging behaviors. In Chapter 3, we utilize these distributions to model the human following behavior. Moreover, we can use the average of the temporal error distribution as a measure for the reaction time of the follower. This is also employed in Chapter3 to investigate the effect of intention-recognition on motion-coordination.

Synchrony in the wavelet domain

The synchrony between two motions can be assessed in time-frequency domain. To this end, we use Continuous Wavelet Transform (CWT) by using the Morlet wavelet as follows.

$$\psi(\eta, \omega_0) = \pi^{-1/4} e^{i\omega_0\eta} e^{-1/2\eta^2} \tag{2.61}$$

where η is a dimensionless time, and ω_0 is a dimensionless frequency that is used for feature selection purposes. Moreover, the wavelet kernel can be stretched in time using $\eta = st$ where s in a new dimensionless time. Given a time-series $x[n]$ for $n = 1, ..., N$ with unit time step δt, we can compute its continuous time wavelet as follows.

$$W_x(n, s) = (\frac{\delta t}{s})^{1/2} \sum_{k=1}^{N} x[k] \psi(\frac{\delta t}{s}[n-k], \omega_0) \tag{2.62}$$

Therefore, the wavelet power can be defined as $|W_x(n, s)|^2$, and the local phase can be defined using the complex part of W_x as

$$\phi(n, s) = \arg(W_x(n, s)) = \text{atan2}(\mathbb{Im}(W_x(n, s)), \mathbb{Re}(W_x(n, s))) \tag{2.63}$$

The cross wavelet transform (XWT) of two time series can be computed as follows

$$W_{xy}(n, s) = W_x(n, s) W_y^*(n, s) \tag{2.64}$$

where $*$ denotes the complex conjugation. The cross wavelet power is defined as $|W_{xy}(n, s)|^2$ and phase as $\arg(W_{xy}(n, s))$. Furthermore, to find areas in time and frequency with high common power, we can compute the *wavelet coherence* as follows.

$$R_{xy}^2(n, s) = \frac{|W_{xy}(n, s)|^2}{|W_x(n, s)|^2.|W_y(n, s)|^2} \tag{2.65}$$

This can be seen as a localized correlation coefficient in time-frequency domain. Considering a null-hypothesis that the signals are generated by a given background power spectrum, we can assess the statistical significance of the computed powers. For such further details, the reader is referred to Grinsted et al. (2004). In this thesis, we use this analysis in Chapter 3.

Power and energy

Given the robot dynamics in Eq. 2.24, the associated powers with the controller ($P_c \in \mathbb{R}$) and the external forces ($P_e \in \mathbb{R}$) are

$$P_c = F_c^T \dot{x} \quad \text{and} \quad P_e = F_e^T \dot{x} \tag{2.66}$$

We compute these entities to assess the physical interaction in Chapter 5 and 6. Moreover, the accumulated energy based on such power can be computed as follows.

$$E_e(t) = \int_0^t P_e(\tau) d\tau \tag{2.67}$$

or in the discrete form

$$E_e(n) = \sum_{k=0}^{n} P_e[k] \tag{2.68}$$

where $P_e[k]$ is the external power sample at time-step k.

Autocorrelation

The correlation of a time-series with itself results in its *autocorrelation* as follows.

$$R_{xx}(l) = \sum_{k \in \mathbb{Z}} x(k)x(k-l) \tag{2.69}$$

For the time-series defined over $[-\infty, ..., n]$, and $l \geq 0$, we can write

$$R_{xx}(l) = \sum_{k=-\infty}^{n} x(k)x(k-l) \tag{2.70}$$

Moreover, the autocorrelation at $l = 0$ leads to the energy of the signal (E_x) as follows.

$$R_{xx}(0) = \sum_{k=-\infty}^{n} |x(k)|^2 = E_x \tag{2.71}$$

autocorrelation can be used to assess the similarity of a signal to a shifted version of itself. In Chapter 6, we will use this notion of to distinguish between accidental and intentional forces.

3 Human-follower proactivity

As introduced in Chapter 1, our first step toward robotic proactivity is to understand and draw inspirations from human behavior. Furthermore, in Chapter 2.1, we reviewed possible mechanisms which contributes to human proactivity behavior. Following the same line of thoughts, in this chapter, we investigate human proactivity in motion-coordination with a leader. In our understanding of human behavior, we are interested in using models that are applicable to robotics systems. Therefore, in Section 3.2, we use an adaptive state-dependent dynamical system to explain human-following behavior. This approach is then extended in Chapter 4 to reach proactivity in robotic systems. Beside motion-adaptation, in Section 3.3, we show that the human follower recognizes and adapt to the leader's intended-task. This finding inspires the robotic task-adaptation strategy in Section 5 suggesting that it is beneficial for robots to coordinate at the task-level with their human partner.

3.1   Introduction

Many daily tasks involve spatio-temporal coordination between two agents. Study of such coordinated actions in human-human and human-robot interaction has received increased attention of late as reviewed in Section 2.1. In this Chapter, we use the *mirror paradigm* to study motion-coordination in a leader-follower setting. In this game, two agents are facing each other with a handle/marker to move on a virtual horizontal line. The players are instructed to play the game such that the designated follower should follow the designated leader's hand motions. The leader is instructed to make "rich" motions (namely successive oscillations with variation in amplitude and frequency) while taking into account the follower's capacity to follow (i.e. slow down when needed to allow the follower to catch up). The related work for this framework is reviewed Section 2.1.4.

The main goal of this chapter is to investigate the follower's behavior. In the first experiment (Section 3.2), we are interesting in modeling the motion of the follower, given a particular motion of the leader. We propose a mathematical model consistent with the internal model hypothesis and the delays in the sensorimotor system; see Section 2.1.2. A qualitative compar-

ison of data collected in four human dyads shows that it is possible to successfully model the motion of the follower.

In the second experiment (Section 3.3), we investigate if the leader-intention recognition (in a multi-task scenario) contributes to follower's motion-coordination. For this purpose, we use a robotic avatar which provides early gaze cues with regard to its intended task. Producing structured and repetitive yet random motions, the avatar acts as the leader in the interaction and the participants are the followers. We propose time-domain and wavelet-domain analysis to study the effect of intention recognition. We confirm that individuals can exploit gaze cues to predict other's intended tasks and to better coordinate their motions with their partners, even when the partner is a computer-animated avatar. The related work for use of avatar for interaction with human-partner is reviewed in Section 2.1.5.

3.2 Motion adaptation in human-following behavior

In this section we propose a dynamical system approach to explain the follower's proactive behavior in following a leader's motions; i.e. a mathematical model which accurately describes the main qualitative features of the data. To model the behavior of the follower in this leader-follower setup, we first take a qualitative approach.

Eight subjects (paired in four different dyads) participated in a mirror game experiment. Each dyad made three trials at the game, each one lasting 60 seconds. The data consist of the 1D end-effector positions (the two balls position on the strings) recorded at a rate of 100 samples per second. In Fig. 3.1, one sample of leader-follower motion is illustrated. At the beginning, the follower shows an expected delay in his motion. Up to $15sec$, the tracking is satisfactory until the leader "*suddenly*" changes the location of the oscillation, and the follower shows a tendency to oscillate according to the last observed max and min points. This creates an interesting pattern in the follower's motion; i.e., undershooting and overshooting. These observations imply that the follower uses an internal model which helps him/her to compensate for the delay. This forward modeling, however, worsens the tracking when the leader suddenly changes the dynamics of the motion and hence no longer matches the follower's expected model. In this case, the follower must build again an internal model of the leader's motion. Therefore, we hypothesize that the human follower adapts his/her motion rather than purely tracks the delayed observations. In the following, we consider these observations to drive our modeling approach.

3.2.1 Predictive models for proactive following behavior

Consider the control architecture in Fig. 3.2 for the follower's behavior in interaction with a leader. Receiving the leader's trajectory ($x_l(t)$) as the input, this cognitive mechanism generates the follower's trajectory ($x_f(t)$) as the output. This mechanism can be seen as three sub-systems placed in series: *sensory system*, *internal modeling*, and the *motor system*. Physio-
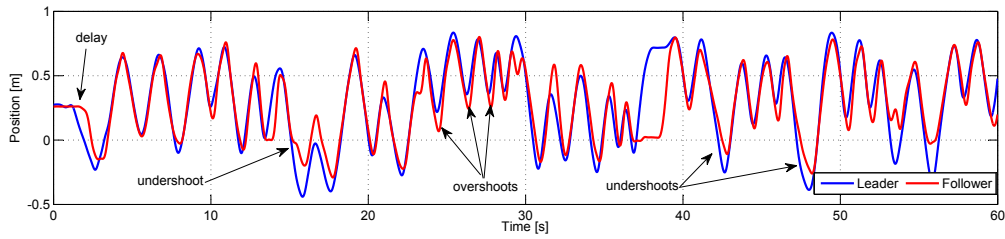
Figure 3.1 – A sample of experimental recording from the leader-follower setup in the mirror game. Arrows indicate noticeable patterns in the follower's behavior. The y-axis is the linear 1-DoF displacement of the participants' hands (horizontal line orthogonal-to-sagittal plane).
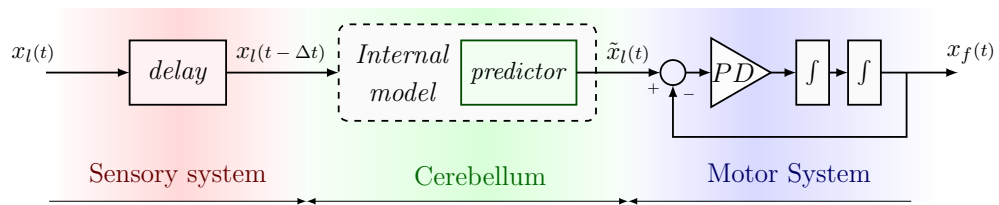
Figure 3.2 – Using dynamical system as the internal predictive model to explain human-proactivity in following the leader's motions.

logical sensory-motor systems have significant feedback delays. In our proposed mechanism, this is represented by a delay in the *sensory* sub-mechanism. The *internal model* plays the role of the cerebellum in controlling for the timing of the agent's response. We adapt this internal model to the delayed perceived motion ($x_l(t - \Delta t)$) and by forward integration, we estimate the follower's current position ($\tilde{x}_l(t)$). This estimation of current position is used as the set-point for the *motor system* where the motor system is represented by a 2nd-order closed-loop control system.

Relying on the delayed sensory data ($x_l(t - \Delta t)$) and using it as the set-point for the motor system limits human tracking performance. In contrast, modeling the leader's motion and using this to predict the leader's motion would not only improve tracking performance, but also lower control effort (no need to focus continuously our attention to visual feedback). There are myriad of studies attesting that humans benefit from these two aspects of forward modeling (Wolpert et al. (1998); Krakauer and Mazzoni (2011)). In our cognitive mechanism, we use a dynamical system to model and predict the leader's motion; see Fig. 3.3. The parameters of the dynamical system are updated by using previous data-points falling into a *memory window* (of length T). Once the model is updated, it is used to predict the current leader's position based on the leader's position and velocity at $t - \Delta t$. Memory length T and delay Δt are the model's parameters. These parameters can be tuned to achieve a desired behavior.

3.2.2 Parameterized dynamical systems

It is desirable to select a model of control which can capture the qualitative properties of the data, while producing dynamics close to humans. The oscillatory nature of the task and the smoothness of human motion can be realized by a 2nd-order dynamical system of the form:

$$\ddot{x}_l = \theta_1 + \theta_2 x_l + \theta_3 \dot{x}_l \tag{3.1}$$

where the dynamical system parameters (θ_1, θ_2, and θ_3) can be updated to model the leader's motion; see Fig. 3.3. This model can be rewritten in the general form presented in Eq 2.12 by assuming the state as $z = [x_l, \dot{x}_l]^T$ which leads to:

$$\dot{z} = Az + b \tag{3.2}$$

where

$$A = \begin{bmatrix} 0 & 1 \\ \theta_2 & \theta_3 \end{bmatrix} \quad \text{and} \quad b = \begin{bmatrix} 0 \\ \theta_1 \end{bmatrix} \tag{3.3}$$

Having this model for the leader's motion, we can predict the future by forward integration of the model. To do this, we use the last observation as the initial condition for the numerical integration as follows.

$$\begin{cases} \tilde{x}_l(t-\Delta t) = x_l(t-\Delta t) \\ \dot{\tilde{x}}_l(t-\Delta t) = \dot{x}_l(t-\Delta t) \end{cases} \Rightarrow \begin{cases} \ddot{\tilde{x}}_l(t-\Delta t) = \theta_1 + \theta_2 \tilde{x}_l(t-\Delta t) + \theta_3 \dot{\tilde{x}}_l(t-\Delta t) \\ \dot{\tilde{x}}_l(t-\Delta t + dt) = \dot{\tilde{x}}_l(t-\Delta t) + \ddot{\tilde{x}}_l(t-\Delta t)\, dt \\ \tilde{x}_l(t-\Delta t + dt) = \tilde{x}_l(t-\Delta t) + \dot{\tilde{x}}_l(t-\Delta t)\, dt \end{cases} \tag{3.4}$$
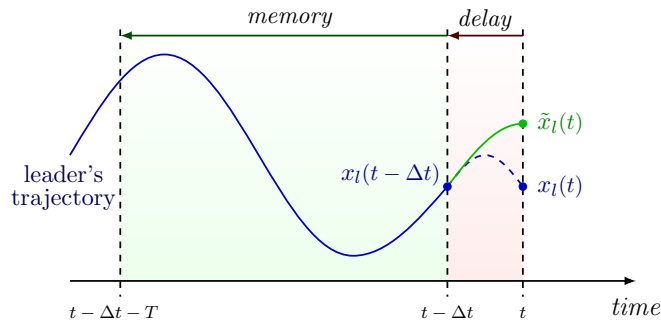
Figure 3.3 – Memory and delay as the two hyper-parameters of the internal model. Memory controls the amount of previous data being used for updating, while delay controls prediction horizon.

3.2.3 Adaptation using the least-square method

Being linear with respect to the parameters is a great advantage for this model as it enables us to use a simple learning method; i.e. Minimum-Least-Square (LS) method. In this method, the regressor matrix is

$$
S = \begin{bmatrix}
1 & x_l(t - \Delta t) & \dot{x}_l(t - \Delta t) \\
1 & x_l(t - \Delta t - dt) & \dot{x}_l(t - \Delta t - dt) \\
\vdots & \vdots & \vdots \\
1 & x_l(t - \Delta t - T) & \dot{x}_l(t - \Delta t - T)
\end{bmatrix}
\tag{3.5}
$$

and the target vector is

$$
Y = \begin{bmatrix}
\ddot{x}_l(t - \Delta t) \\
\ddot{x}_l(t - \Delta t - dt) \\
\vdots \\
\ddot{x}_l(t - \Delta t - T)
\end{bmatrix}
\tag{3.6}
$$

In such a discrete implementation, $S \in \mathbb{R}^{N \times 3}$ and $Y \in \mathbb{R}^N$ where $N = T/dt + 1$ assuming T is divisible by dt. Therefore, using LS method, the parameter vector ($\Theta = [\theta_1 \ \theta_2 \ \theta_3]^T$) is calculated as follows.

$$
\Theta = (S^T S)^{-1} S^T Y
\tag{3.7}
$$

Having the model parameters updated, we can integrate forward to compensate the delay and predict the leader's current position ($\tilde{x}_l(t)$). During forward integration, we can saturate position, velocity, and acceleration based on the assumption that these quantities are limited on the leader's side. These saturations prohibit the model from generating fast, and unreasonable motions. Finally, the prediction ($\tilde{x}_l(t)$) is used as the desired trajectory for a 2nd-order dynamical system where a hand-tuned PD-controller performs satisfactorily; see Fig. 3.2.

Using LS method, we should consider cases where $S^T S$ is not invertible. More specifically, cases where rank of S is lower than 3. To study this, we can consider cases where column of the regressor matrix ($S = [S_1, S_2, S_3]$) are either zero or linearly dependent. In the following cases, c_1, c_2, c_3 represent non-zero arbitrary coefficients, and $0_{N \times 1}$ a zero vector of size N.

- $S_1 = 0_{N \times 1}$

  This case cannot take place as the first column of S is defined to be a vector of ones.

- $S_2 = 0_{N \times 1}$

  This case represent that the leader's position is constant at zero; i.e., $x_l = 0$. Thus, we have $\dot{x}_l = 0$ and $\ddot{x}_l = 0$. For this case, the model (Eq. 3.4) predicts the leader's motion using $\Theta = [0, 0, 0]$.

- $S_3 = 0_{N \times 1}$

  This case represents the case where the leader's velocity is zero; i.e., $\dot{x}_l = 0$. Thus, we have $\ddot{x}_l = 0$. In Eq. 3.4, a correct prediction can be obtained using $\Theta = [0, 0, 0]$ for this case.

- $c_1 S_1 + c_2 S_2 = 0$

  This case is created when the leader's position is constant and non-zero; i.e., $x_l = -c_1/c_2$. In this case, we have $\dot{x}_l = 0$ and $\ddot{x}_l = 0$. Thus, the model (Eq. 3.4) can predict the leader's motion using $\Theta = [0, 0, 0]$.

- $c_1 S_1 + c_3 S_3 = 0$

  This represents the case where the leader's velocity is constant and non-zeros; i.e., $\dot{x}_l = -c_1/c_3$. In this case, we have $\ddot{x}_l = 0$. Therefore, $\Theta = [0, 0, 0]$ results in a correct prediction in Eq. 3.4.

- $c_2 S_2 + c_3 S_3 = 0$

  This represent a 1st-order dynamics behavior in leader's motion; i.e., $\dot{x}_l = -c_2/c_3 x_l$. In this case, we have $\ddot{x}_l = -c_2/c_3 \dot{x}_l$. In this singular case, the model can predict the leader's motion using $\Theta = [0, 0, -c_2/c_1]$.

- $c_1 S_1 + c_2 S_2 + c_3 S_3 = 0$

  This case also represents a 1st-order dynamics; i.e., $\dot{x}_l = -c_1/c_3 + c_2/c_3 x_l$. Similar to the previous case, we have $\ddot{x}_l = -c_2/c_3 \dot{x}_l$. Thus, $\Theta = [0, 0, -c_2/c_1]$ leads to a correct prediction.

It can be seen that all these special cases can be handled by ensuring small values for the parameters; i.e., $\theta_1 = \theta_2 = \theta_3 = 0$ which means $\dddot{x}_l = 0$. This set of parameters leads to a predictive First-Order-Hold scenario. We can use damped/regularized LS to push the estimated parameters to handle the aforementioned singular cases. We use the following formulation to adaptively change the regularization term (μ) with respect to the regressor matrix condition number ($\kappa(S)$).

$$\begin{cases} \kappa = \frac{\lambda_{max}(S^T S)}{\lambda_{min}(S^T S)} \\ \mu = \mu_0(1 - e^{-\alpha \kappa}) \\ \Theta = (S^T S + \mu I)^{-1} S^T Y \end{cases} \tag{3.8}$$

In Fig. 3.4, the performance of our method is tested for typical trajectories; i.e. different dynamics of motion. In Fig. 3.4a, we consider the constant position case. Based on the delay, during the first 0.3 seconds of the simulation, we do not have sensory input and it is not reasonable to move. After $0.3s$, the model is updated and its prediction is tracked by the 2nd-order dynamics motor system. Dealing with discrete PD controller, we have a lag of 2 samples between prediction and command generation by the model. For the constant velocity case (Fig. 3.4b) and first-order dynamics (Fig. 3.4c), the model performs satisfactorily. Having
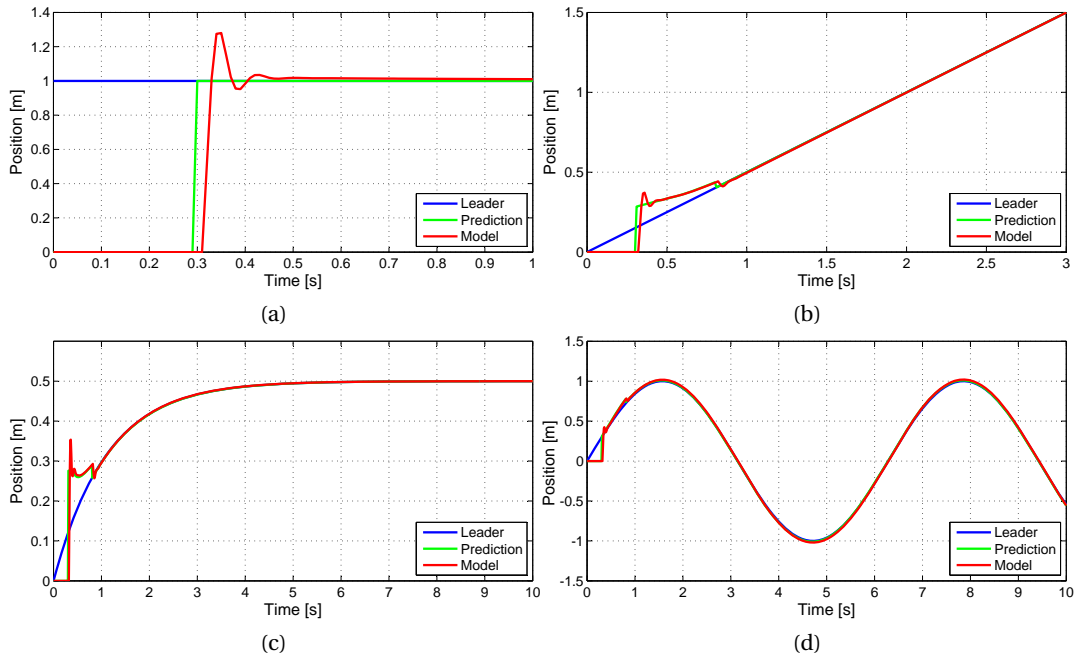
Figure 3.4 – Performance of the internal model to follow typical trajectories. The first three trajectories cause singularity for the LS method. In these simulations, we have $dt = 0.01s$, $\Delta t = .3s$, $T = .5$, $\mu_0 = 10$, and $\alpha = 1$. For the discrete PD controller, we have $K_p = K_d = .5$

few data-points in the beginning of each simulation makes the prediction unreliable. Finally, in Fig. 3.4d, the proposed model is tested against sinusoidal trajectory. It is interesting to note that this trajectory is dynamically consistent with our model, and setting the damping in LS to zero will lead to $\Theta = [0 \; \omega^2 \; 0]$ where ω is the oscillation frequency. Moreover, Fig. 3.4 shows that the proposed method can also follow the changes in the motion dynamics; e.g. from oscillation to reaching.

3.2.4 Results

In order to tune our model to human performance, especially to account for the observed overshoot and undershoot, we focus on zero-velocity points. Two types of error can be extracted from zero-velocity points: *temporal error* (as used in Noy et al. (2011)) and *spatial error*. For each zero-velocity point in the follower's trajectory, we consider the time-nearest zero-velocity instant of the leader's trajectory but with the same direction (minimum or maximum); see Fig. 2.7. Then we calculate temporal/spatial error based on the time/position difference.

With the features presented above, we study the human performance in Fig. 3.5a. Interestingly, for the temporal error, most of the probability mass is present in the region with positive error. This shows that the follower's trajectory is lagging most of the time. The distribution in the negative part of temporal error shows that the follower sometimes changes the direction of

motion sooner than the leader. This, again, speaks in favor of an internal model that guides the change in motion direction. Another interesting property of this graph is that almost all the delays are below $300ms$. We can use this observation and fix the delay in our model to $\Delta t = 300ms$.

The distribution of spatial error is very close to a normal distribution with mean $0.005m$ and standard deviation of $0.13m$. Similar distributions can be achieved by tuning our proposed model on the data-set. It is desirable to determine a set of parameters that match best the model-follower and human-follower distributions. To do this, we must extract feature vectors from the temporal and spatial distributions. We do this by counting the frequency of data-points in the following bins.

$$w_h^t = \begin{bmatrix} 4.6\% & 0.6\% & 1.3\% & 2.9\% & 5.1\% & 7.2\% & 18.4\% & 36.1\% & 14.9\% & 3.6\% & 1.1\% & 4.1\% \end{bmatrix}$$

$$-0.5 \quad -0.4 \quad -0.3 \quad -0.2 \quad -0.1 \quad 0 \quad 0.1 \quad 0.2 \quad 0.3 \quad 0.4 \quad 0.5 \quad \textit{Temproal error [s]}$$

$$w_h^s = \begin{bmatrix} 2.6\% & 0.7\% & 1.5\% & 4.2\% & 11.6\% & 31.5\% & 27.8\% & 11.8\% & 3.9\% & 1.4\% & 1.1\% & 1.8\% \end{bmatrix}$$

$$-0.25 \quad -0.2 \quad -0.15 \quad -0.1 \quad -0.05 \quad 0 \quad 0.05 \quad 0.1 \quad 0.15 \quad 0.2 \quad 0.25 \quad \textit{Spatial error [s]}$$
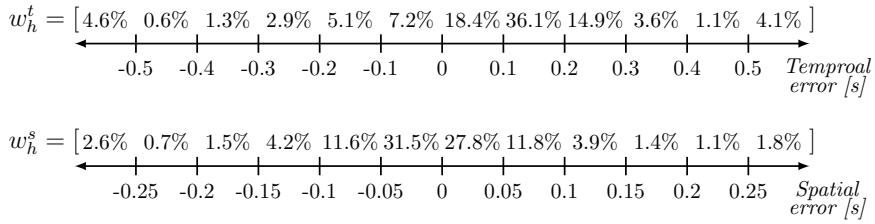
Here, w_h^t and w_h^s are the coarse representation of the temporal and spatial error distribution for human performance. Same feature vectors can be extracted for any model; i.e. w_m^t and w_m^s. Having these feature vectors, to tune model parameters, we can use the following cost function; i.e. Hellinger statistical distance.

$$H(w_h, w_m) = \frac{1}{\sqrt{2}} \parallel \sqrt{w_h} - \sqrt{w_m} \parallel_2 \tag{3.9}$$

where w_h and w_m represent the human and model temporal or spatial error distribution.

Now that we formalized our tuning problem as a multi-objective optimization, we search for the best combination of our model's parameters; i.e. *delay* and *memory*. This search
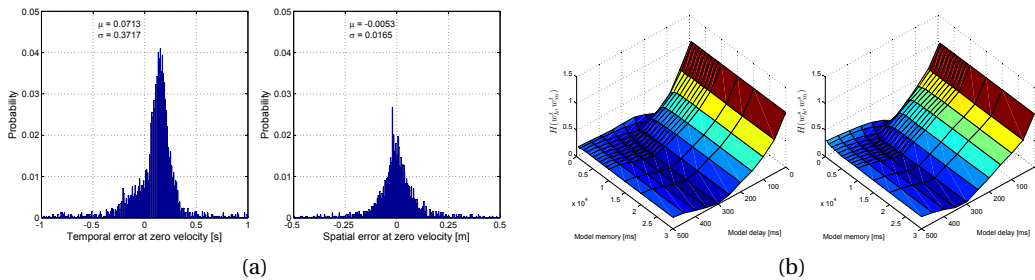
Figure 3.5 – (a) Probability distribution of temporal and spatial error in zero-velocity points for human follower in mirror game setup. (b) Grid search for delay and memory parameters. Statistical difference between human and model follower in (left) temporal and (right) spatial error.
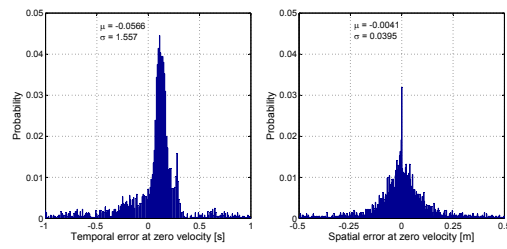
Figure 3.6 – Probability distribution of temporal and spatial error at zero-velocity points for model-follower in the mirror game setup with tuned parameters (300ms for delay and 5s for memory).
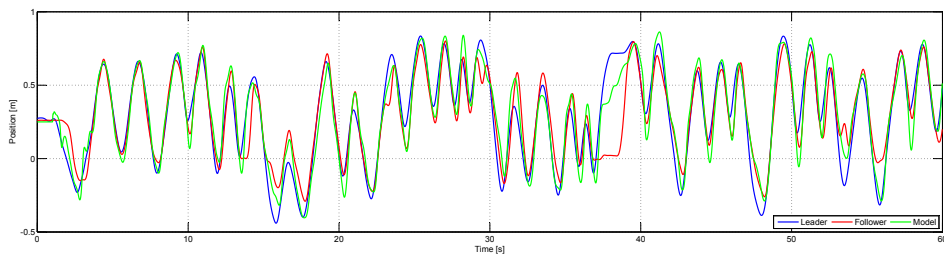
(a) Example 1.
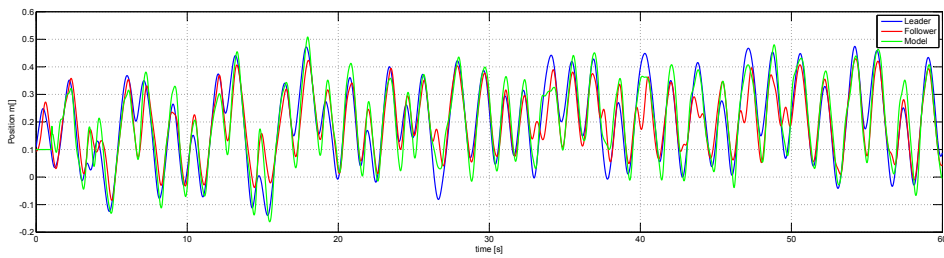
(b) Example 2.

Figure 3.7 – Model performance for Leader-follower setup. In these two examples, the model's performance (green) is compared to the human-follower (red) in tracking the human-leader (blue).

is illustrated in Fig. 3.5b. As it can be seen, these cost functions are consistent with each other. Moreover, they are more sensitive to changes in the *delay* parameter than in the *memory* parameter. The best choice for *delay* is 300ms which is consistent with our previous hypothesis from Fig. 3.5a. This delay is also in agreement with the previous studies in human reaction time to changes in direction Mateeff et al. (1999). Having 300ms for *delay*, these cost functions are almost insensitive to *memory*. Here, we pick 5s for *memory* where the cost functions exhibit less sensitivity to the other parameter; i.e. robustness.

The temporal and spatial error distribution of our model with tuned parameters are illustrated in Fig. 3.6. As it can be seen, the temporal and spatial error distribution graphs are highly similar to those for human-follower in Fig. 3.5a. In both graphs, the maximum and cut-off delay (a point which contains 90% of the temporal error distribution) are alike. In both human and the model, the temporal distribution in the negative part (where the follower switches

direction sooner than the leader) is also similar.

Fig. 3.7 shows the performance of the model on the experimental data (leader's trajectory). Our model's output matches the human-follower trajectory most of the time. It however accounts relatively poorly for the overshoots and undershoots. This is likely due to the fact that these are caused by previous max and min points of trajectory and our dynamical model can only model the offset (center of oscillations). Improving our model to take these into account, we might be able to create these pattern more accurately.

In this section, we studied the human ability to coordinate on the motion level. More precisely, the ability to predict the leader's motions and proactively coordinate the motions. We showed that an adaptive dynamical system can explain this capability. In the next section, we focus the human ability to coordinate on the task level. We show that recognizing the underlying intended-task contributes to a higher coordination performance.

3.3 Task-adaptation in human-following behavior

In this section, we focus on the ability of a human to coordinate on the task-level. More specifically, we investigate whether intention-recognition (i.e., recognizing the leader's intended task) contributes to motion-coordination. In context of human-human interaction, we provide our partners with contextual cues regarding our intention. For instance, such these cues can be provided through gaze. The ability to follow one another's gaze plays an important role in our social cognition; especially when we *synchronously* perform tasks together. Here, we investigate how gaze cues can improve performance in a simple coordination task (i.e., the *mirror game*), whereby two players mirror each other's hand motions. A systematic control over the gaze of one player allows us to influence the intention-recognition performance of the other player. To do this, we employ a robotic avatar where we can control its gaze behavior. We use a computer-generated avatar that simulates the humanoid robot iCub (Tikhanoff et al., 2008), a 53-DOF humanoid robot as shown in Fig 3.10. We contrast two conditions, in which the avatar provides or not explicit gaze cues that indicate the next location of its hand.

In the following, we present the avatar leader's behavior in terms of motion-generation (where the avatar switches across different tasks) and gaze behavior (where the avatar provides gaze cues with regard to its intended task to help the human-follower).

3.3.1 Avatar task-switching

In the experiment, the avatar is the leader and programmed to create motion patterns generated by different underlying tasks; i.e., different sinusoidal oscillations each specified in terms of amplitude and offset. The avatar leads the interaction by moving its right arm on a virtual horizontal line orthogonal-to-sagittal plane. The parameters of the trajectories (offsets, amplitudes, frequencies, and random transitions) are hand-tuned based on human trajectories
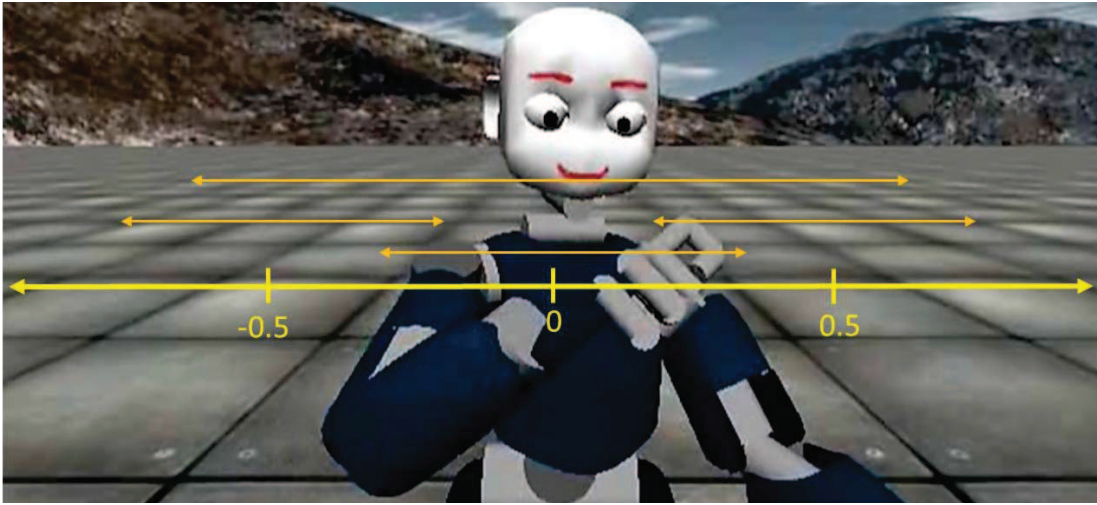
Figure 3.8 – Switching across tasks using an avatar. Modes of oscillations comprise random motions of the avatar's hand. Three small oscillations (one to the left, center, right of the torso with amplitude of 0.3) and one large oscillation (amplitude of 0.7). Number of oscillations in each mode and transition to the next mode are random. The symmetric reachable range of the hand is scaled to [-1,+1], and it into the avatar's coordinates.

of the previous section, hence they display dynamics that are qualitatively close to human natural-dynamics. We use a standard inverse kinematics solver to control the motion of the 6 degrees of freedom of the right arm of the robot, so as to accurately follow the desired hand trajectory. In our inverse kinematics solver, we also consider human-like postures (motion of the shoulder and elbow).

To generate leading motion patterns, we first scale the reachable range of the avatar' hand to $[-1, +1]$ as illustrated in Fig. 3.8. This reachable range, with respect to the body sagittal plane, is asymmetric. Then, we considered four different tasks (i.e., modes of oscillation) as depicted in the same figure. Each mode has a different combination of offsets and amplitudes as follows:

$$
\begin{bmatrix} offset \\ amplitude \end{bmatrix} \in \left\{ \begin{bmatrix} 0 \\ .3 \end{bmatrix}, \begin{bmatrix} -.5 \\ .3 \end{bmatrix}, \begin{bmatrix} .5 \\ .3 \end{bmatrix}, \begin{bmatrix} 0 \\ .7 \end{bmatrix} \right\} \tag{3.10}
$$

To avoid that the human-follower learns the task-switching patterns and uses this as as a predictor, we use random switching patterns. The number of oscillations in each task is a random number between 2 and 5 (inclusive and uniform) except for the large oscillation where the number of oscillations is fewer (one or twice). Starting a task, velocity of the oscillation is also selected randomly (1 or 1.3m/s) increasing the difficulty of the game. Moreover, upon completion, the next mode is randomly (and uniformly) chosen. This results in a random trajectory in each trial as shown in Fig 3.9.
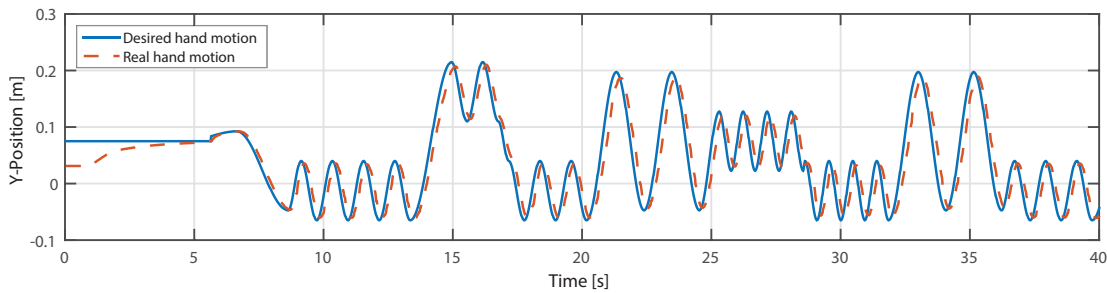
Figure 3.9 – A sample of generated motion for the avatar's hand. Tracking performance of the PD controller in this simulator is considered satisfactory. It is visible that the generated motion is composed of different modes (combination of offset and amplitude).

Figure 3.10 – The simulated iCub robot. The robot is acting as the leader in the mirror game, generating random sinusoidal trajectories. (Left) the gaze is fixated on the hand. (Right) the gaze precede the hand. The blue arrows show the next hand movement and the green arrows show the current gaze fixation point.

3.3.2   Avatar gaze cues

To help the human-follower with the intention-recognition, the avatar provides gaze cues for the its next task-switching. The head and eyes of the robot are controlled so as to generate the desired gaze behavior. The gaze direction is generated mostly by the eye movement, and the head movement was used to create a more natural and human-like behavior. To have a control condition that can act as a baseline in our analysis, we use the case where the avatar does not provide the follower with a gaze cue; i.e., the gaze and hand moves synchronously, see Fig 3.10. In the *gaze cue* condition, the eyes precede the hand motion; the hand's trajectory was used for the gaze, but with $500ms$ lag. In the *no-gaze cue* condition, the eyes are locked on the hand and move in synchrony with the hand, see Fig 3.10. In our analysis, this condition serves as the baseline for participants' performances.

To control the gaze, we used the default gaze inverse-kinematic solver provided by the iCub simulator (Pattacini, 2011). In this solver, both head and eye movements are used to generate the gaze fixation point; i.e., 3 degrees of freedom for the eyes (azimuth, elevation, and vergence
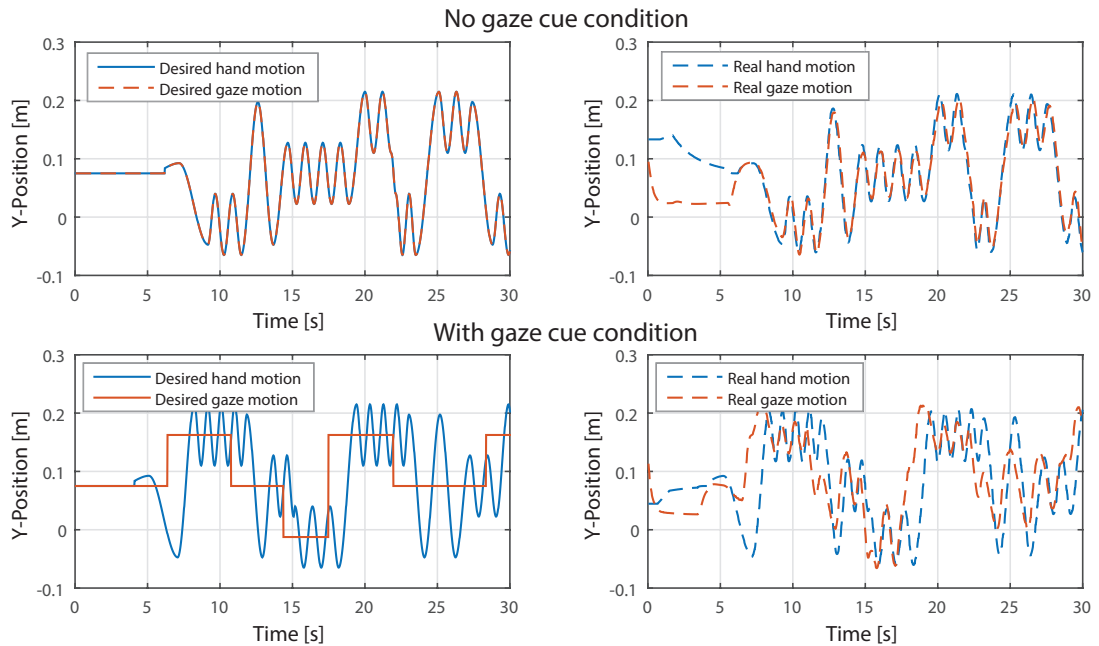
Figure 3.11 – An example of desired trajectories for the avatar's hand and gaze in the two conditions.

angles) and 3 degrees for the head (pitch roll and yaw angles). Parameters used to generate smooth and human-like gaze behavior are reported in in Fig. 3.11. It can be seen that the real gaze-trajectory differs from the desired one. This is due to the gaze controller being affected/perturbed by the hand motion. However, the leading behavior, which provides gaze cues, is preserved; the gaze moves sooner to the new offset and oscillates synchronously with the hand, and has a smaller amplitude.

The choice of parameters affects the level of difficulty of the game; switching quickly between different modes of oscillation results in fast and highly transitory motions which are harder to follow. By varying the parameters (speed and complexity of the motion) prior to the experiment, we adjusted the difficulty of the game to amplify the effects of gaze cues; at a higher level of difficulty, only relying on the hand motions does not result in a satisfactory tracking performance. Thus, we expected participants to pay attention to gaze cues and exploit this information throughout the game and, in particular, during the phases where the difficulty was the highest, specifically when the avatar changes direction of motion very rapidly. To avoid compounds due to unnatural dynamics of motion, we provided the avatar with motions that follows closely the typical dynamics of human hand motions (which we observed in Section 3.2.1) in terms of range and frequency.

Figure 3.12 – The experimental setup. The avatar is displayed on a big screen (46 inches). The avatar led the mirror game and the participant followed the avatar's hand motions. The participant held a marker for motion tracking purposes.

3.3.3   Experimental setup: the human-avatar mirror game

In our experiment, participants were asked to follow the motion of the avatar, see Fig 3.12. To track the motion of the human's hand, we asked the subject to hold a marker, which enabled us to track their motion using OptiTrack system NaturalPoint (2018) (120Hz for sampling rate, and accuracy of 0.1mm). For this, we recruited 37 participants (26 males and 11 females) from the EPFL campus (Bachelor, Master's, and PhD students). Their average age was 23.1 (4.7) [18-39] (values are presented in the form mean (standard deviation) [min-max]). Each participant took part in one session that lasted a maximum of 10 minutes. No inclusion/exclusion criteria were used for the recruitment and all participants successfully completed the session. As a consequence, no data had to be removed from the experiment. They also provided written informed consent to take part in this experiment.

Each participant participated in both conditions. In order to remove the order effects, we divided the participants into two groups: one group was exposed to the "*no-gaze cue*" condition first, and the other was exposed to the "*gaze cues*" condition first. See Fig 3.13 for our experimental protocol. In each condition, subjects played four consecutive trials, each 30 seconds long. Having played in both conditions, the participants were asked to answer a short questionnaire. This led to a total of 344 recorded trajectories ($30s$ long each) for the analysis. Upon completion of all the trials, we asked the participants five short questions about their impressions of the difficulty and realism (similarity to human behavior) of the avatar; see Appendix A for further details on the results obtained from the questionnaire.

As mentioned before, our experiment has two conditions. In the *no-gaze cue* condition, the eyes are locked on the hand and move in synchrony with the hand. In the *gaze cue* condition, the gaze precedes the hand motion by $500ms$. To pinpoint significant within-
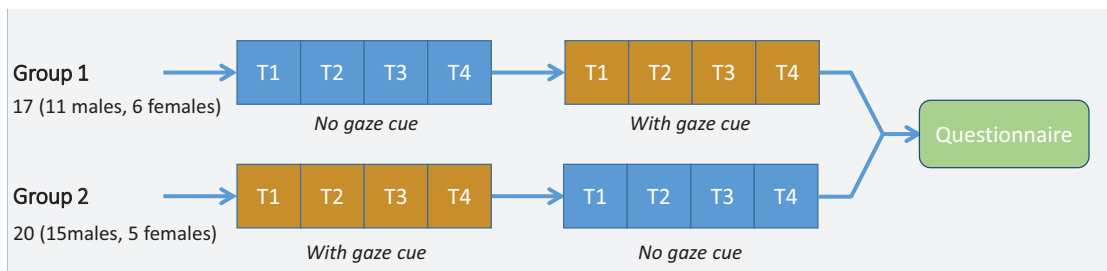
Figure 3.13 – The protocol used for the experiment. Subjects were divided into two groups and participated in the experiment with a different ordering of conditions followed by a short questionnaire.

subject contrasts across the conditions, repeated measures ANOVA is performed. The reaction time, the perception of difficulty, and the perception of similarity are the three dependent variables which we measured in the two conditions; i.e., "*no-gaze cue*" and "*gaze cues*". The condition and the order of the conditions are used as within-subject factors; i.e. independent variables. Moreover, a separate analysis includes further the effect of age and gender where age is split into tree balanced groups as reported in Appendix A.
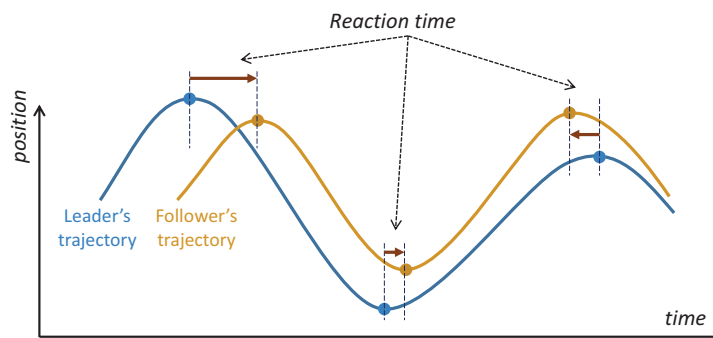
Figure 3.14 – Extraction of reaction time based on zero-velocity points in the leader and follower trajectories. In this conceptual example, we have positive reaction times (the leader/follower is leading/lagging) in the first two cases, and a negative reaction time (the leader/follower is lagging/leading) in the last case.

3.3.4   Results

We first present the results of our questionnaire. Then, we investigate the results obtained from the motion capture systems. Afterward, we crosscheck the subjects' performances with their impressions reported in the questionnaire. Finally, we present the results acquired from the frequency-domain analysis of the recorded participants' motions.
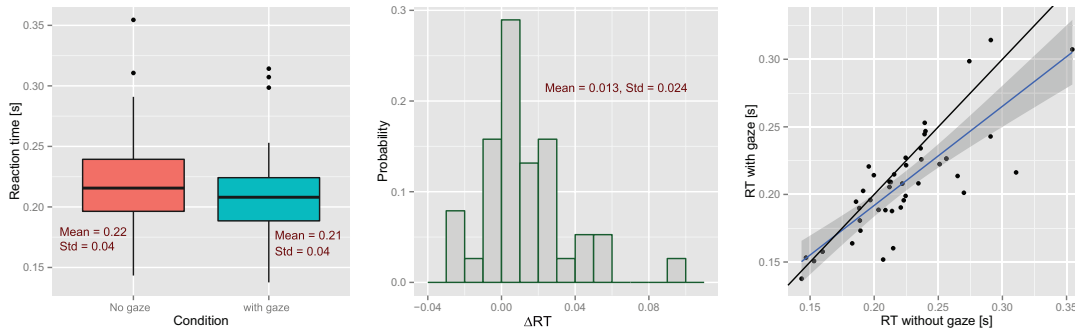
Figure 3.15 – Overall analysis of the recorded motions. (Left) Boxplots of subjects' reaction times in each condition. (Center) histogram of ΔRT. (Right) RT in the *gaze cues* condition vs. RT in the *no-gaze cue* condition. Each dot represents a participant. Black line is the unity line and the blue line in the result of the linear regression.

Human-follower's reaction time

Now, we turn to the objective and quantifiable results on the effect of gaze on the subjects' tracking performances. To this end, we analyze the data on the relative velocity of participants and the avatar's hand motions. In the previous section, we show that the human tracking performance can be captured by the temporal differences between the leader and the follower trajectories. Here we use the same measure; see Fig 3.14. For each set of leader-follower trajectories obtained from a trial, we calculate the temporal differences between the leader and the follower only across the peaks (i.e., zero-velocity points). We choose the average to compare the tracking performance across the two conditions, i.e., average reaction-time (RT). We refer to the within-subject RT contrast across the condition as RT improvement defined as

$$\Delta RT = RT_n - RT_g \tag{3.11}$$

where RT_n and RT_g represent the participants' reaction times in "*no-gaze cue*" and "*gaze cues*" conditions respectively. A positive value for this variable shows that the participant had a better performance in the presence of the gaze cues.

Fig 3.15 shows the overall results using this metric. Fig 3.15(Left) shows the boxplots for reaction times in each condition where participants, on average, show faster reactions with gaze cues than without. The analysis of variance shows a significant improvement in reaction times due to the gaze cues [$F(1,35) = 9.445$, $p = 0.004$]. Moreover, a marginally significant effects due to age was detected [$F(2,32) = 2.996$, $p = 0.064$]. Fig 3.15(Center) shows the distribution of ΔRT. The results of the Wilcoxon test suggest that the average of this distribution ($13\,ms$) is significantly greater than zero. The last subplot, Fig 3.15(Right), shows the performance of each individual change in the presence of the gaze cue. The black line indicates the unity line (the null hypothesis). As can be seen, the data is skewed to the favorable side of this line (alternative hypothesis). The blue line illustrates the linear regression of the data. The slope of this regression implies that individuals with lower performances (higher RT in the "no gaze"
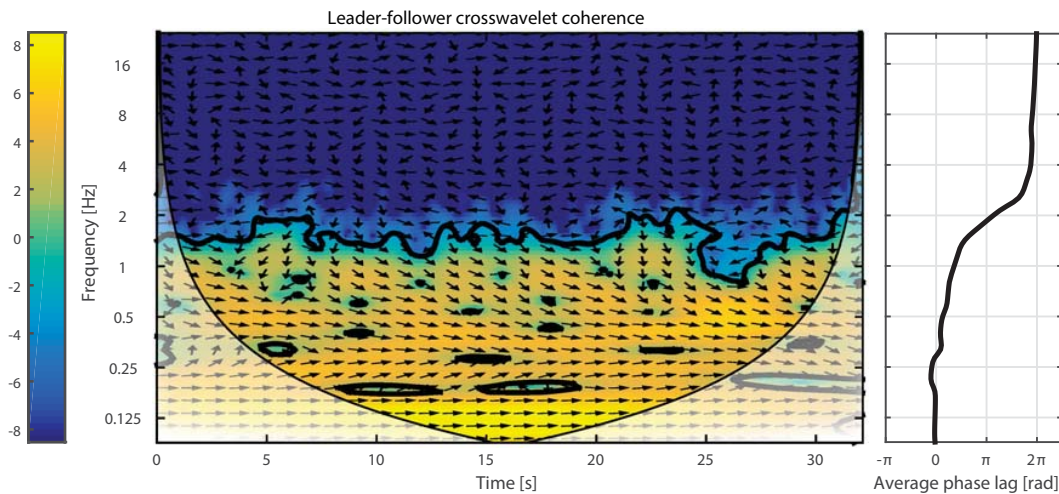
Figure 3.16 – Cross-wavelet analysis. Right: Cross-wavelet coherence between the leader and the follower in one of the trials. Power of frequency components at each time is color coded; i.e., blue/yellow for weak/strong components, respectively. Moreover, the arrows indicate the leader-follower phase relation for each frequency over time. Left: Average phase-lag for each frequency extracted from the main plot.

condition) benefit more from gaze cues. For more detail on the statistical analysis regarding effect of condition-order, age, and gender, the reader is referred to Appendix A.

Human-follower's phase lag

Thus far, for our analysis, we used a metric based on the computation of zero-velocity points only. Although this metric provides a good estimation of the reaction time and enables us to put forward significant differences across the conditions. However, it does not provide an assessment for the different aspects of joint action; i.e., action prediction, temporal coordination, and joint planning. To overcome this and check the effect of gaze in more detail, we apply frequency-domain techniques reviewed in Section 2.3.5. This method allows for a more refined analysis where the leader-follower interaction is presented as a frequency-phase relation. This helps us to understand how gaze cues improve the coordination. A cross-wavelet transform is applied to the leader-follower trajectories by using a Matlab toolbox provided by Grinsted et al. (2004). In this transform, the Morelet wavelet with conventional temporal resolution ($\sigma = 6$) is used.

The results of cross-wavelet coherence for one of the trials are illustrated in Fig 3.16. In cross-wavelet coherence, each point at a certain time and frequency has two components: power and angle. The power, which is color-coded in the figure, shows the strength of that frequency at that moment. The angle, however, shows the phase-lag between the leader and the follower. The arrows, pointing to the right, indicate a perfect synchrony, whereas arrows tilting up-

ward/downward show a leading/lagging behavior in the follower; upward/downward arrows signify 90 degrees phase lead/lag. To quantify the temporal correspondence, we extract the average phase-lag at each frequency; see Fig 3.16(Right). We observe that, in low frequencies, there is a satisfactory synchronization that deteriorates as frequency increases. There is an interesting point when the graph passes 90 degrees, i.e., an asynchronous interaction. Similar to linear filters, this frequency ($2Hz$ in this example) can be considered as the *bandwidth* of the interaction; i.e., a frequency beyond which the synchronous interaction cannot be maintained. Moreover, after a certain frequency, the estimation of phase lag is not reliable as the power of that frequency drops in the cross-wavelet coherence plot.

The average phase-lag can be extracted for each subject for the two conditions, i.e., with and without gaze. Such graphs, for one of the subjects, are plotted Fig 3.17a. It can be seen that, for both cases, synchrony reduces as frequency increases. However, the interaction has a lower lag for each frequency in the presence of the gaze. This can be assessed easier by looking at the difference of two graphs in the lower plot in Fig 3.17a. This plot clearly shows that, for this participant, the presence of the gaze improves the interaction over all frequencies.

We apply this procedure to all participants and study the average behavior that is plotted in Fig 3.17b. Investigating the 95% confidence interval does not show a significant improvement (with zero improvement as the null hypothesis). However, scaled standard deviations are plotted for comparison across the frequency spectrum. As mentioned before, the average phase for high frequencies is not reliable, which, in this figure, results in wide intervals. It can be seen that improvements take place in three different regions. Interestingly, each region accounts for a different underlying process in joint actions. These processes are as follows:

Task-level coordination: low-frequency region ($1/8 - 1/4 Hz$) accounts for the task-switching; see Fig 3.9 where the task=switching creates a low-frequency components in the trajectory. By providing a gaze cue to the next location of the oscillations, the avatar improves the synchrony in the interaction in this frequency interval. Therefore, intention recognition (using the gaze cues) allows the individuals to coordinate better on the task-level.

Motion-level coordination: mid-frequency region ($1/2 - 1 Hz$) accounts for the oscillatory motions in each task. The improvement in this range supports the hypothesis that, in the *gaze cues* condition, the follower can synchronously follow one mode of oscillation, which has a random number of repetitions, until the next gaze cue. Therefore, intention recognition (using the gaze cues) improves in-task motion coordination.

Transition-level coordination: high-frequency region (around $2Hz$) accounts for fast and transitory motions when the task is abruptly changed. The improvement in this region shows that, in presence of gaze cues, individuals have a lower reaction time when the task is switched. Therefore, intention recognition (using the gaze cues) allows the follower for a more synchronous transition across tasks. However, compared to the previous regions, this result is not reliable due to the wider confidence intervals.
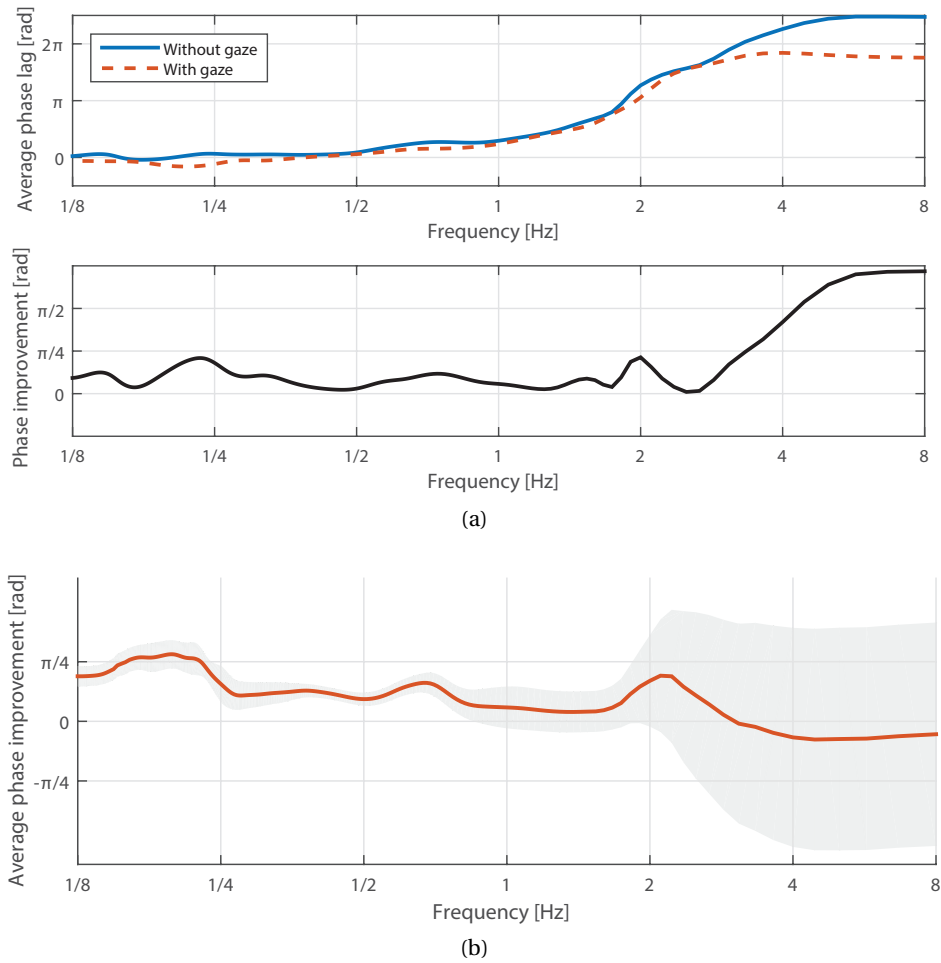
Figure 3.17 – Frequency-phase profiles. a) Top: Average phase-lag vs. frequency of one of the participants in both conditions; with and without gaze. Bottom: Phase improvement vs. frequency of one of the participants due to the presence of the gaze cues. b) Effect of gaze on the synchrony of the interaction across frequency (averaged over all subjects). The red graph indicates the average improvement due to the gaze cues. Gray area indicates the scaled 95% confidence intervals.

3.4 Discussion and conclusion

In this chapter, we studied the human proactivity at two levels; i.e., motion and task-level. At the motion-level, we showed that the human follower adapts its motion based on leader's trajectories rather than pure tracking of the such delay observations. To this end, we introduced a cognitive mechanism capable of producing human-like motions for the mirror game setup. In this model, we used adaptive dynamical system as an internal predictive model. We built this model based on qualitative assumptions and observations from human data recordings. Moreover, using quantitative methods, we tuned our model's hyper-parameters to fit the human data. We showed that simple dynamical models can be used explain and

reproduce the follower's motion in the leader-follower setting of the mirror game.

At the task-level, we showed that the human follower recognizes the underlying task and uses the avatar gaze cues to better predict the task-transitions. To this end, we used the mirror game paradigm where the human subject imitates the hand motions of an animated avatar. The use of avatar-leader (instead of a human-leader) enables us to systematically control for task-switching and gaze-cues. To test our hypotheses, we implemented a simple gaze behavior where an avatar provides a human subject with task-relevant cues. In a within-subject study, we recorded the performance of participants in the presence and absence of gaze cues. Our main result shows that gaze cues significantly improve participants' reaction times to the avatar's movements. A wavelet analysis of the interactions provided us with a better understanding of different underling aspects/processes reported for motion-coordination. Frequency-domain techniques helped us to model the follower's behavior as a frequency-dependent-phase relation that, compared to time domain analyses, is easier to interpret. Both metrics captured the beneficial effects of gaze cues. Due to a higher effect size in this metric (the entire frequency domain), however, a larger sample size is required to reach substantial statistical power in order to draw significant conclusions.

In the next two chapters, we put our findings from these experiments in practice. In Chapter 4, we use the idea of parameterized adaptive dynamical systems to achieve a robotic behavior that proactively follows a human-leader. In Chapter 5, we focus on robotic system that recognizes the underlying intended-task from human demonstrated motions.

4 Robotic motion adaptation through physical human-interaction

In the previous chapter, we showed that the proactivity of a human-follower can be explained by an adaptive dynamical system. Our results confirm that the follower adapts his/her internal model based on the leader's motion. To be proactive, the follower relies on the predictions of the adapted model rather than passively following the leader's motions. In this chapter, we put this idea in practice. We present an adaptive motion planning approach for impedance-controlled robots to modify their tasks based on human physical interactions. We use a parameterized time-independent dynamical system for motion generation where the modulation of such parameters allows for motion flexibility. To adapt to human interactions, we update the parameters of our dynamical system in order to reduce the tracking error (i.e., between the desired trajectory generated by the dynamical system and the real trajectory influenced by the human interaction). The related work for this chapter is reviewed in Section 2.1.2 and 2.2.3. In the following, we present our adaptive method and we provide analytical analysis and several simulations of our method. Finally, we investigate our approach through real world experiments with a 7-DOF KUKA LWR 4+ robot performing tasks such as polishing and pick-and-place.

4.1   Introduction

As introduced in Chapter 1, collaborative robots are aimed to assist us with tasks that are repetitive and burdensome such as polishing surfaces and pick-and-place. Over the past four decades, the problem of control and motion planning for such tasks has been studied rigorously for traditional industrial settings. However, recent advances in robotics aim to utilize robots in everyday settings, such as small factories and home applications. Therefore, having a human in proximity of robots who intends to modify the robotic behavior through physical interactions introduces new challenges; not only from a control perspective to ensure safety and passivity but also regarding motion planning to recognize the underlying intentions and react accordingly. Interacting with a human who might have different intentions/goals can be done in several fashions: using control panels, remote controllers or other extra interfaces. However, a seamless behavior can be achieved if the robot reacts in accordance with human
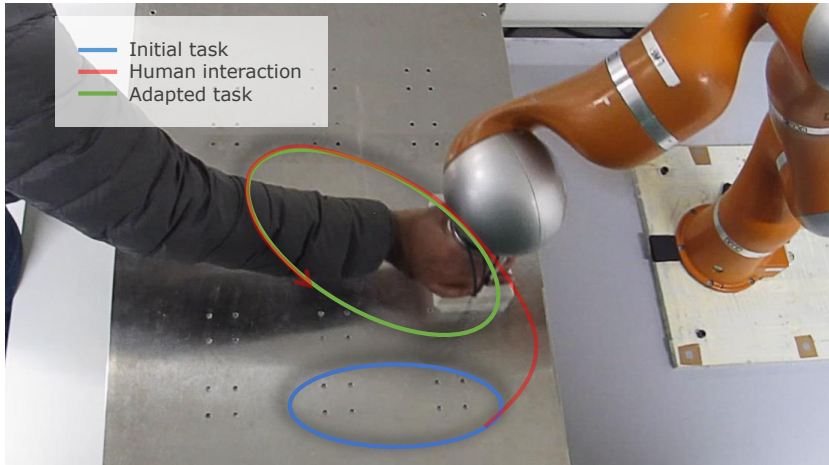
Figure 4.1 – Online motion adaptation in a polishing task where the human demonstrates his/her intention through physical interaction and the robot adapts the task accordingly.

physical interactions. Therefore, it seems desirable to have robots that are not only compliant in their interaction, but also adaptive to the intention of their users. In this chapter, we focus on motion adaptation under a specific task; e.g., polishing a flat surface as illustrated in Fig. 4.1. To do this, we extended our adaptive DS from Chapter 3. In that chapter, we showed that adaptation of the motion-planner leads to proactive following behavior. By extending this idea to physically interacting robot we achieve two robotic behavior in this chapter:

- **Compliant leader**: the robot executes the task autonomously but allows for human physical interaction.

- **Proactive follower:** during the physical interaction, the robot adapts its motion-planner with respect to the human demonstrations. Thus, the robot complies with human forces and follows the predicted motions.

The control architecture of this chapter is depicted in Fig. 4.2. The mathematical formulation for robotic arm control and DS-based impedance controller are presented in Section 2.3.3 and 2.3.3. In the following, we present the mathematical formulation for motion generation and motion adaptation using parameterized dynamical systems.

4.2 Motion generation using parameterized dynamical systems

We presented the background on motion planning using dynamical systems in Section 2.3.2. For the purposes on this chapter, let us consider a desired behavior encoded using state-dependent DS as

$$\dot{z} = \hat{f}(z) \tag{4.1}$$
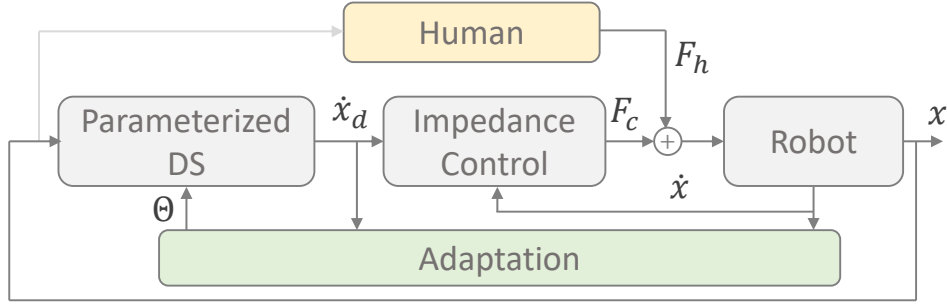
Figure 4.2 – Control loop of an adaptable dynamical system. The human and the robot physically interact by applying F_h and F_c respectively. The impedance controller applies proper forces to track the desired velocity $\dot{x}_d$ generated by the dynamical systems. The adaptation mechanisms update the DS parameters (Θ) based on the DS-generated velocity ($\dot{x}_d$) and human-influenced real velocity ($\dot{x}$).

In this formulation, $z \in \mathbb{R}^m$ is the canonical state and $\hat{f}(.) : \mathbb{R}^m \to \mathbb{R}^m$ is the canonical DS. We assume that the canonical DS is globally stable to an attractor or a limit cycle under a continuously differentiable Lyapunov function. To reshape the generated motion by the DS, we consider a diffeomorphism $M(.;\Theta) : \mathbb{R}^m \to \mathbb{R}^m$ with p free parameters ($\Theta = [\theta_1 \cdots \theta_p]$ with $\Theta \in \Omega_\Theta$). We formulate the canonical state (z) as the transformation of the actual state ($x \in \mathbb{R}^m$) as follows:

$$z = M(x;\Theta) \tag{4.2}$$

Time-differentiation of this mapping results in

$$\dot{z} = \mathcal{D}M_x(x;\Theta)\dot{x} + \mathcal{D}M_\Theta(x;\Theta)\dot{\Theta} \tag{4.3}$$

where the differential $\mathcal{D}M_x \in \mathbb{R}^{m \times m}$ is invertible. Furthermore, we neglect the second term by assuming the variation of parameters is slow. Using Eq. 4.1 and 4.2, we can write

$$\dot{x} = [\mathcal{D}M_x(x;\Theta)]^{-1}\hat{f}(M(x;\Theta)) \tag{4.4}$$

This formulation might appear complex and non-applicable for robotic implementation. Let us consider a special case for the transformation.

$$M(x;\Theta) = SR(x + \bar{x}) \tag{4.5}$$

In this transformation, the state is translated by $\bar{x} \in \mathbb{R}^m$, rotated by $R \in \mathcal{SO}(m)$, and scaled by a diagonal matrix ($S \in \mathbb{R}^{m \times m}$) with positive entries. The differential of this mapping is

$$\mathcal{D}M_x(x;\Theta) = SR \tag{4.6}$$

In this case the dynamics in Eq. 4.4 become

$$\dot{x} = R^{-1}S^{-1}\hat{f}(SR(x + \bar{x})) \tag{4.7}$$

For the implementations of this chapter, it is sufficient to consider a 2-dimensional case ($x \in \mathbb{R}^2$). In this case the transformed DS is

$$f(x,\Theta) = \begin{bmatrix} \cos\theta_3 & \sin\theta_3 \\ -\sin\theta_3 & \cos\theta_3 \end{bmatrix} \begin{bmatrix} \theta_4^{-1} & 0 \\ 0 & \theta_5^{-1} \end{bmatrix} \hat{f}(\begin{bmatrix} \theta_4 & 0 \\ 0 & \theta_5 \end{bmatrix} \begin{bmatrix} \cos\theta_3 & -\sin\theta_3 \\ \sin\theta_3 & \cos\theta_3 \end{bmatrix} (x + \begin{bmatrix} \theta_1 \\ \theta_2 \end{bmatrix})) \tag{4.8}$$

In this parameterized DS, θ_1 and θ_2 are the translation parameters along x_1 and x_2 respectively. θ_3 represent the rotation, and θ_4 and θ_5 account for scaling along x_1 and x_2 respectively. In the following, we use this DS to generate motion for two different tasks; i.e., polishing and pick-and-place tasks.

4.2.1 Polishing task

To generate polishing patterns on a surface ($x = (x_1, x_2)^T$),we use a DS described in the polar coordinates (r and θ) as $\dot{r} = -\alpha(r - r_0)$ and $\dot{\phi} = \omega$ where $r^2 = x_1^2 + x_2^2$ and $\phi = \text{atan2}(x_2, x_1)$. $\omega \in \mathbb{R}^+$ is the desired angular velocity, $\alpha \in \mathbb{R}^+$ is the desired radial velocity and $r_0 \in \mathbb{R}^+$ is the desired radius of rotation. Fig. 4.3 shows the vector field for this dynamical system along with generated motions. This figure also shows how this DS can be transformed (scaled, rotated, and translated) to create different polishing patterns. Furthermore, in Fig. 4.4, we illustrate the transformation of a simple circular motion to a complex cyclic motion through smooth modification of transformation parameters. We can observe that the generated trajectories are smooth.
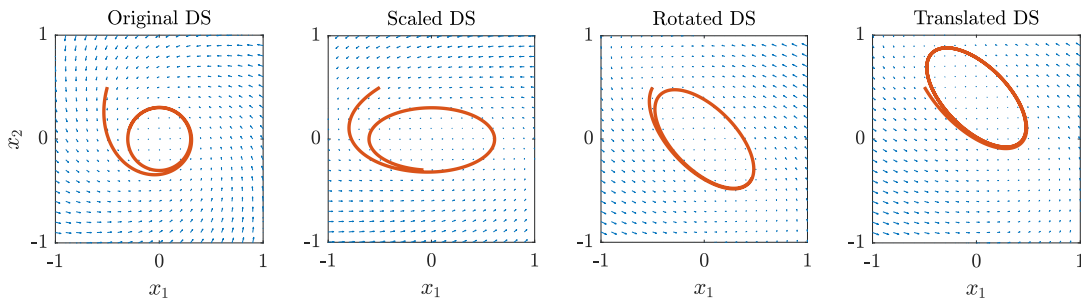
Figure 4.3 – DS motion-generation for polishing task. The first DS shows the original case where $r_0 = 0.3$, $\omega = 1$, and $\alpha = 1$. In the subsequent plots, the original DS is transformed step-by-step to reach a different polishing pattern. In the final transformations, we have $\Theta = [0, -0.4, \pi/4, 0.5, 1]$. These examples are simulated numerically for illustration purposes.
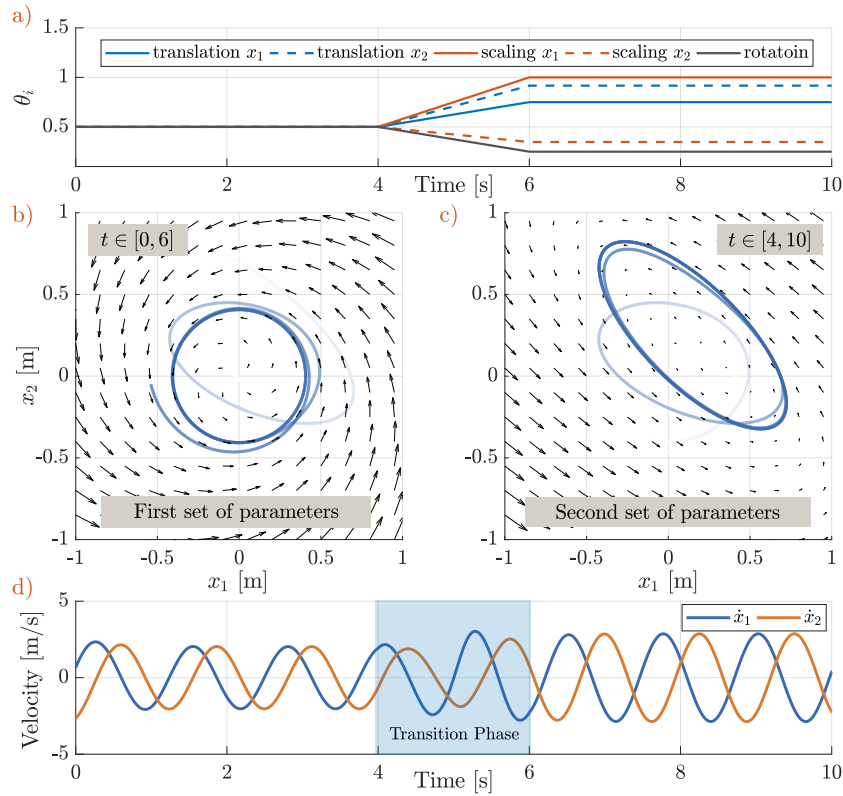
Figure 4.4 – The effect of variation of the adaptive parameters on the DS and the generated trajectories. **(a)** Normalized parameters. **(b)** Vector field of DS before and **(c)** after the transformation. The faded parts of the trajectories indicate the transition. **(d)** generated trajectories which are smooth. To generate this example, we manually modulate the transformation parameters. In Section 4.3, we show how such parameters can be adapted with respect to human interactions.

4.2.2 Pick-and-place

In order to generate pick-and-place motion for the end-effector position, we use linear dynamics described by $\dot{x}_d = -K_p(x_r - \bar{x})$ where $K_p \in \mathbb{R}^3$ is diagonal with positive entries, and $\bar{x}$ is the target location which is an adaptive parameter. We use three instances of the same dynamics to generate 1) approaching the picking location 2) going through a via-point 3) approaching the placing location. These dynamical systems are illustrated in Fig. 4.5. We switch to the next dynamics when we are close enough to the attractor (i.e., $||x_r - \bar{x}|| < \delta_p$). Moreover, we go through the via point between each pick and place. In our experimental scenario, we only consider adaptation for picking and placing targets.
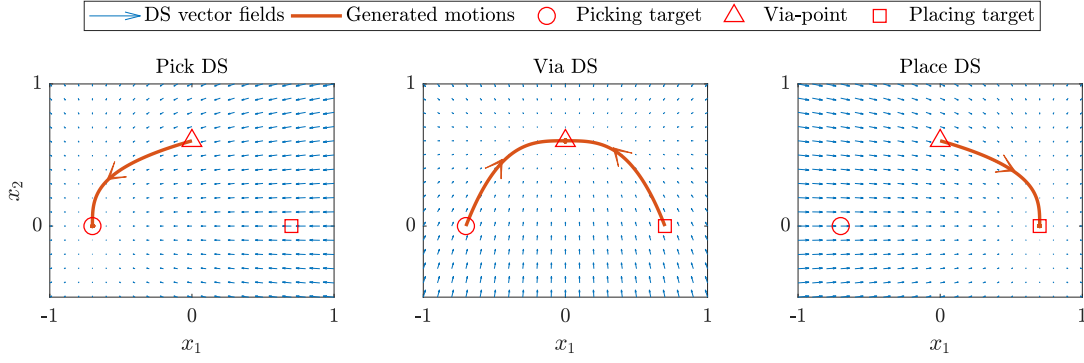
Figure 4.5 – Using dynamical systems to perform a repetitive pick-and-place task. The robot switches to the next DS when the target of the current DS is reached. Between each pick and place motion, the robot goes through a via-point to avoid potential collisions. These examples are simulated numerically for illustration purposes.

4.3 Motion adaptation in parameterized dynamical systems

We construct our adaptive law based on a minimization of the tracking error described as

$$J(\Theta; K, \Delta t_s) = \frac{1}{2}\dot{e}^T\dot{e} \tag{4.9}$$

where

$$
\begin{aligned}
\dot{e}(t) &= \frac{1}{K}\sum_{k=0}^{K-1}[\dot{x}_d(t - k\Delta t_s) - \dot{x}(t - k\Delta t_s)] \\
&= \frac{1}{K}\sum_{k=0}^{K-1}[f(x(t - k\Delta t_s); \Theta) - \dot{x}(t - k\Delta t_s)]
\end{aligned} \tag{4.10}
$$

is the error between the desired velocity (generated by DS) and the real velocity (influenced by human interaction) over K points spaced with Δt_s in the past. For example, having $K = 1$ brings us back to the instantaneous error. Intuitively, by reducing this error, we adapt the DS to generate the same movements as demonstrated by the human. We obtain this by following the gradient of the cost-function as follows.

$$\frac{\partial J}{\partial \theta_i} = \frac{1}{K}e^T\sum_{k=0}^{K-1}\frac{\partial f(x(t - k\Delta t_s); \Theta)}{\partial \theta_i} \tag{4.11}$$

To have the sensitivity of the DS to the parameters, we use the following simple approximation.

$$\frac{\partial f(x; \Theta)}{\partial \theta_i} = \frac{f(x; \Theta_{\neq i}, \theta_i + h) - f(x; \Theta_{\neq i}, \theta_i - h)}{2h} \tag{4.12}$$

where h is the step size of the gradient, and $\Theta_{\neq i}$ denotes all other parameters (except θ_i) that are kept fixed to their current value. Having the gradient, we update the ith parameter as

follows.

$$\theta_i(t) = \theta_i(t - \Delta t) - \epsilon \frac{\partial J}{\partial \theta_i} \Delta t \tag{4.13}$$

where ϵ and $\Delta t \in \mathbb{R}^+$ are the adaptation and update rate respectively.

4.3.1   Convergence behavior

The convergence behavior of our method can be investigated by assuming the following form for the real velocity.

$$\dot{x} = (1 - \alpha)\dot{x}_d + \alpha f(x; \Theta^*) + \eta(t) \tag{4.14}$$

where $\alpha \in [0, 1]$ is a rate at which the human takes the robot away from its desired behavior ($\dot{x}_d = f(x; \Theta)$) and demonstrates his/her intention which we assume follows the same dynamical system but with a different set of parameters (Θ^*). $\eta(t)$ accounts for un-modeled behaviors (caused by the controller and the human). If we linearize $f(x; \Theta)$ with respect to Θ around Θ^*, we obtain:

$$f(x; \Theta) = f(x; \Theta^*) + \frac{\partial f(x; \Theta)}{\partial \Theta}(\Theta - \Theta^*) + H(x; \Theta) \tag{4.15}$$

where $H(.)$ denotes the higher-order terms. The instantaneous error between desired velocity and the desired one can be computed suing Eq. 4.14 as

$$
\begin{aligned}
f(x; \Theta) - \dot{x} &= f(x; \Theta^*) - (1 - \alpha)f(x; \Theta) - \alpha f(x; \Theta^*) - \eta(t) \\
&= \alpha(f(x; \Theta) - f(x; \Theta^*)) - \eta(t)
\end{aligned}
\tag{4.16}
$$

Using Eq. 4.15, we have

$$
\begin{aligned}
f(x; \Theta) - \dot{x} &= \alpha\left(\frac{\partial f(x; \Theta)}{\partial \Theta}(\Theta - \Theta^*) + H(x; \Theta)\right) - \eta(t) \\
&= \left(\alpha \frac{\partial f(x; \Theta)}{\partial \Theta}\right)(\Theta - \Theta^*) + \left(\alpha H(x; \Theta) - \eta(t)\right)
\end{aligned}
\tag{4.17}
$$

Therefore, the extended error function in Eq. 4.10 can be simplified into:

$$\dot{e}(t) = S(\Theta - \Theta^*) + d(t) \tag{4.18}$$

where

$$
\begin{cases}
S = \frac{\alpha}{K} \sum\limits_{k=0}^{K-1} \partial f(x(t - k\Delta t_s); \Theta)/\partial \Theta \\
d(t) = \frac{1}{K} \sum\limits_{k=0}^{K-1} \alpha H(x(t - k\Delta t_s); \Theta) - \eta(t - k\Delta t_s)
\end{cases}
\tag{4.19}
$$
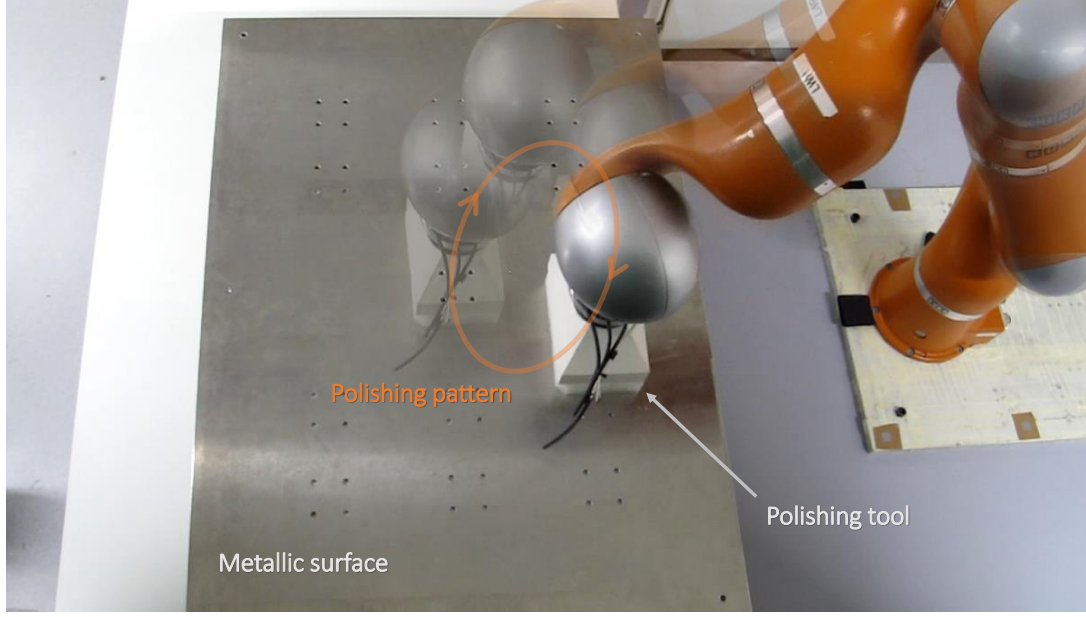
Figure 4.6 – The robotic setup for the adaptive polishing task. The robot comes in contact with a flat metallic surface and follows the DS-generated motions. The end-effector of the robot is equipped with a polishing tool.

Given the assumption that the disturbance term $d(t)$ is negligible (more precisely, $\partial d/\partial \Theta \simeq 0$ and $S^T d \simeq 0$) the dynamics of the adaptation (Eq. 4.13) can be approximated by

$$\dot{\Theta} = -\epsilon S^T S (\Theta - \Theta^*) \tag{4.20}$$

where $S^T S \in R^{p \times p}$ is a positive semidefinite matrix. Given the fact that the number of parameters is higher than the dimension of the error signal ($p > m$), the rank of $S^T S$ is limited to m. However, the convergence to Θ^* can take place if the condition for *Persistence Excitation (PE)* (Åström and Wittenmark (2013)) holds as follows.

$$\exists \delta \quad \forall t \exists T > 0 \quad s.t. \quad \int_t^{t+T} S(\tau)^T S(\tau) d\tau > \delta I_m \tag{4.21}$$

This guarantees the convergence of the parameters in average over time. This means that the average of $S^T S$ over time is strictly positive definite providing a sufficient condition for stability in Eq.4.20. To provide better conditions for *PE* we aim to use a higher number of data-point (i.e., K and Δt_s) over a period of time that captures the behavior of both DS and human demonstration. Moreover, the human can improve the convergence by providing demonstration that results in lower $||d(t)||$; i.e., demonstrations that can be expressed by the DS (with lower $||\eta(t)||$ in Eq.4.14) and desirable parameters (Θ^*) that are close to the current ones (which results in smaller $||H(x;\Theta)||$ in Eq.4.15).
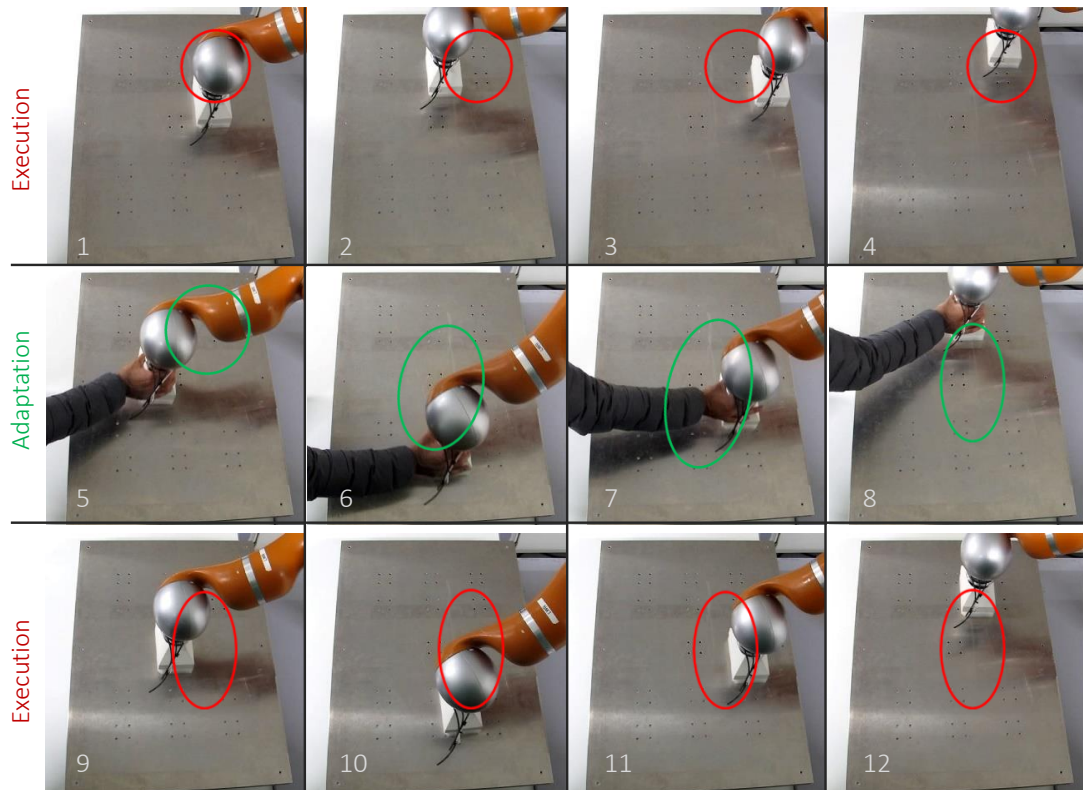
Figure 4.7 – Adaptation of the polishing task during the human-interaction. The robot begins polishing with following the initial DS. As the human demonstrates the desired patterns, the robot adapts the DS and *proactively* follows the human-interaction. As the human retreats, the robot autonomously executed the intended motions.

4.4 Experimental evaluations

The adaptation mechanism is implemented and tested on the Kuka LWR 4+, 7-DOF robotic arm, for two previously described tasks: polishing a surface and pick-and-place. To activate the adaptation upon human interactions, we used a simple threshold on external force (i.e., $||F_{ext}|| > 10N$). The external applied to the end-effector is estimated by the measured torques at the joint-level. Therefore, we avoid to adapt to small tracking errors caused by other uncertainties and mismatched dynamics. In both experiments, the velocities are limited to $0.2m/s$.

4.4.1 Polishing task

Fig. 4.6 shows our setup for the polishing task where the robotic arm is equipped with polishing tool. A flat metallic surface is placed in the workspace of the robot. The robot comes in contact with this surface and follows the polishing pattern generated by the adaptive DS. The adaptation due to the physical interaction of the human is illustrated in a series of snapshots in
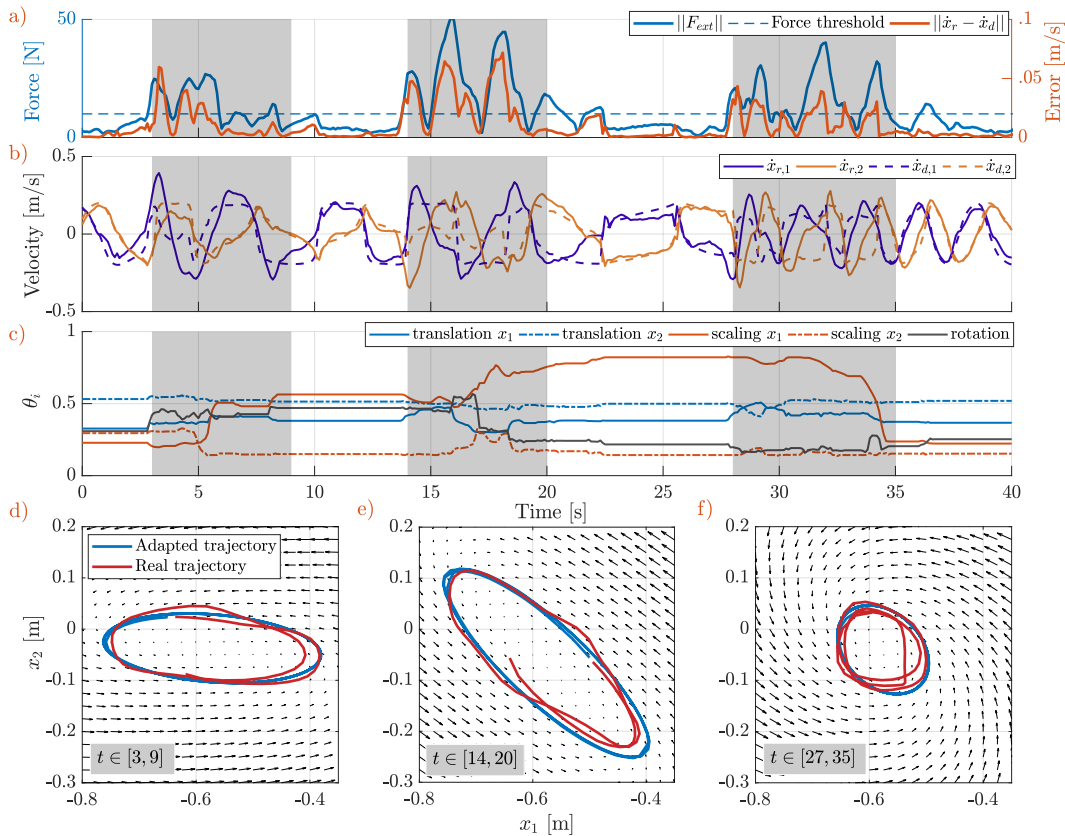
Figure 4.8 – Result of the polishing experiment. **(a)** The norm of the external force and the norm of the tracking error. The dashed line shows the force-threshold which activates the adaptation. **(b)** The desired and real trajectory. Due to the impedance control, the tracking performance is always influenced by the external forces. **(c)** The adaptation of the DS parameters. Bottom row (**d**, **e**, and **f**) shows the adapted DS (i.e., the vector field), the adapted limit cycle, and real trajectory at different time periods. The robot performs the task autonomously (based on the adapted DS) after the human disengages from the interaction.

Fig. 4.7. In the first row (frames 1-4), the robots adapts the surface by executing the initial DS. In the second row (frames 5-8), the human physically interacts with the robots and demonstrates his/her intended desired patterns. As the human leads the interaction, the robot is adapting the DS and *proactively* follows the human-interaction. In the final row (frames 9-12), the robot autonomously performs the human-intended polishing patterns.

Fig. 4.8 shows the analysis of the interaction using the recorded signals. In these recordings, the human interacts with the robot in three separate intervals (i.e., shaded ares). It can be seen by an increase in the external forces and consequently the tracking error in Fig. 4.8.a. The tracking error can be investigated further by inspecting the desired and real velocities depicted in Fig. 4.8.b. Due to the robot compliance, the human is able to demonstrate his/her intention by influencing the real velocity. Fig. 4.8.c shows the adaptation of the parameters which consists of the translation and scaling along both axes and the rotation. It can be
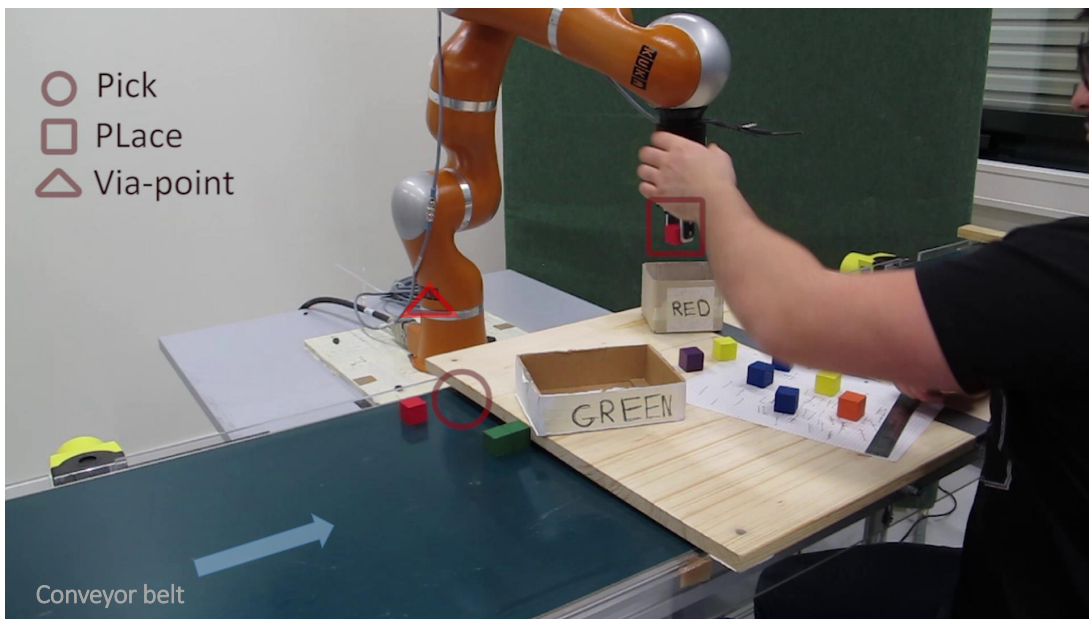
Figure 4.9 – The robotic setup for the adaptive pick-and-place task. The conveyor belt brings a series of objects to the shared workspace of the human and the robot. The objects are required to be examined and placed in their designated boxes. The location of these boxes are only known to the human. Due to the adaptive behavior of the robot, the human performs the high-level aspects of the task and leaves the repetitive parts to the robot.

seen that upon interacting with the robot, the parameters are adapting in order to reduce the error. The bottom row of Fig. 4.8 shows the state of the DS in the three corresponding intervals where the human interacts with the robot. These plots demonstrate the ability of our method to fit the DS (i.e., the vector field) to the demonstrated motions; i.e., to capture the intention of the human user. Moreover, these plots show that the parameterized DS is capable of generating different polishing patterns (i.e., limit cycles). In this experiment, the following hyper-parameters are used: $\epsilon = 0.1$, $h = 0.01$, $\Delta t_s = 5$s, $K = 10$, and $\Delta t = 0.05$s.

4.4.2 Pick-and-place

Fig. 4.9 shows our experimental setup for the adaptive pick-and-place task. In this experiment, we synthesized a production line where different series of objects are required to be placed in designated boxes. The robot performs repetitive pick-and-place using DS-generated motions. The target locations for pick-and-place are adaptive towards human physical interaction. Due to this adaptive behavior, the human only performs the high-level aspects of the task and leaves the repetitive part to the robot. For instance, The human can supervise the task and the robot's performance; e.g., the human can visually inspect the object and removes the faulty cases.

Fig. 4.10 shows a series of snapshots where the human physically interacts with the robot. In
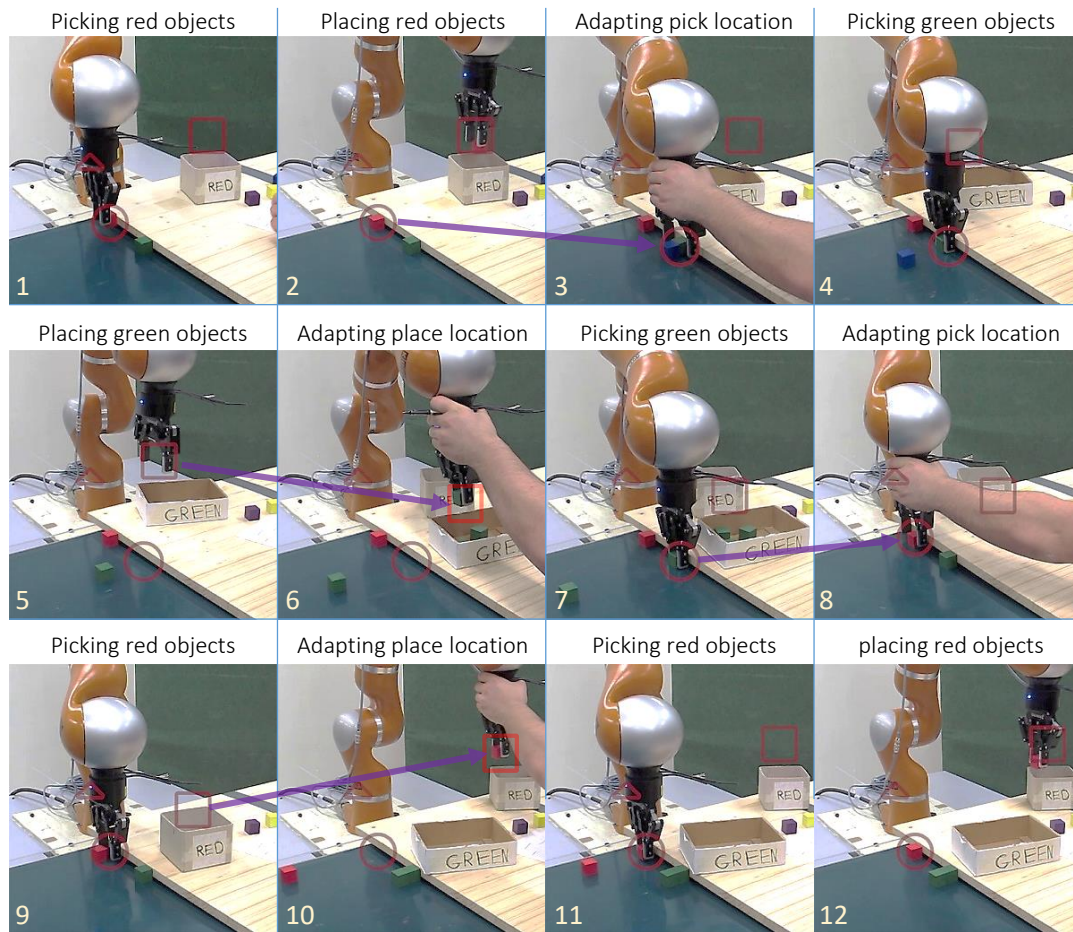
Figure 4.10 – Adaptation of the repetitive pick-and-place task during human-interaction. The robot adapt the target location for picking or placing motion based on the human interaction. This allows the human user to decides for high-level aspect of the task and leave the repetitive part for the robot.

frames 1-2, the robot picks a red object and place it in the designated box. In frame 3, the human decides to change the objects and store the green ones. To do this, the human changes the picking target of the robot by physically demonstrating a new location. This happens several times in the course of interaction in this experiment. For instance, in frames 6 and 10, human adapts the placing target and in frame 9, the picking target.

Fig. 4.11 shows the analysis of the interaction using the recorded signals. Fig. 4.11.a. shows the external forces and the resulting tracking errors induced by the human user. The desired velocity generated by the DS and the real velocity influenced partially by the user are illustrated in Fig. 4.11.b. Fig. 4.11.c shows the adaptation of the normalized parameters: the pick and place target locations. It can be seen that only the parameters of the active DS (either pick or place) are being adapted. Fig. 4.11.d illustrates the human-robot interaction between $2s$ and $12s$. After performing pick, via-point, place, via-point, the robot reaches for the last picking target.
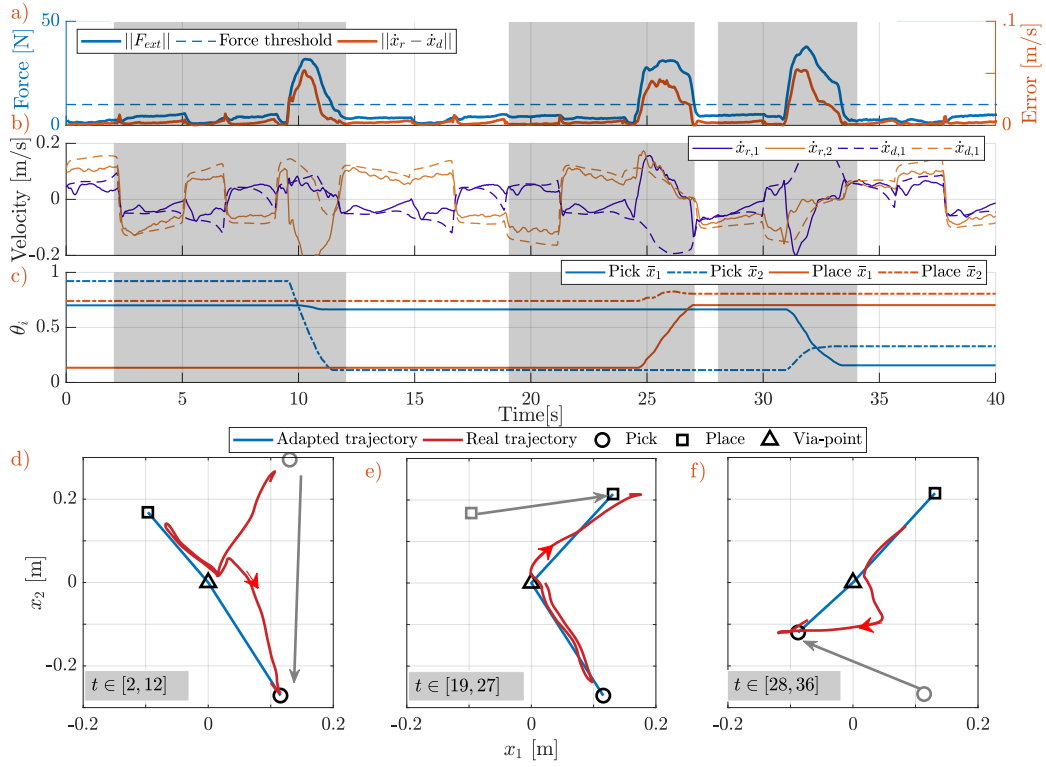
Figure 4.11 – Result of the pick-and-place experiment. **(a)** The norm of the external force and the norm of the tracking error. The dashed line shows the force-threshold which activates the adaptation. **(b)** The desired and real trajectory. **(c)** The adaptation of the DS parameters. Bottom row (**d**, **e**, and **f**) shows the adapted target locations, and real trajectory at different time periods.

However, upon human interaction (the human pulls the robot to a new intended location), the target location for picking adapts accordingly. Fig. 4.11.e-f show similar instances of such interactions where the target locations are adapted. In this experiment, we use the following hyper-parameters: $\epsilon = 0.001$, $h = 0.01$, $K = 1$ (Δt_s not applicable), $\Delta t = 0.05s$, and $K_p = 2$. Moreover, in this implementation, the post-condition for switching between DSs (e.g., from pick to via-point) is (1) to reach the target ($||x - \bar{x}|| < 0.05m$) and (2) the absence of human interaction ($||F_h|| < 10N$). This post-condition allows the human user to adapt the current DS and not switch to the next DS even if it reaches its target.

4.5 Discussion and conclusion

In this chapter, we derived our adaptive mechanism based on tracking error where the performance of the adaptation can be tuned using its set of hyper-parameters. The adaptation rate can be considered as the most important hyper-parameters. The speed of convergence is primarily controlled by the adaptation rate (ϵ) which represents a trade-off between slow convergence and fluctuations in the estimated parameters. Furthermore, the approximation

of the gradient is tuned by h. This parameter needs to be small enough to have a precise estimation of the gradient. However, dealing with a noisy cost-function (due to noisy $\dot{x}$), it needs to be big enough to avoid over-fitting (i.e., to the noise). Finally Δt_s and K can be tuned properly to provide a rich signal for adaptation (Eq. 4.21). Δt_s needs to be large enough to capture the characteristics of both DS and human intention. For example, in the polishing task, we use a Δt_s that includes enough samples from a complete cycle of the motion. Further increment of Δt_s includes information from the past that are no longer relevant. K controls the number of samples from the time-window created by Δt_s. K needs to be tuned properly to have a robust down-sampling while reducing the computational cost. For example, we found $K = 1$ to be sufficient in the pick-and-place experiment. Intuitively, the condition for *persistent excitation* is easier to achieve: input dimension being 2 (i.e., error along x_1 and x_2) and parameter dimension being 2 (i.e., $\bar{x}_1$ and $\bar{x}_2$ since the adaptations of pick and place are mutually exclusive) compared to polishing task where the input dimension is 2, however, there are 5 parameters to adapt. This fact is reflected in the convergence speed of the parameters; compare Fig. 4.8.c with Fig. 4.11 where the latter has faster convergence.

Overall, the proposed adaptive mechanism enables the robot to adapt its motion according to the human interactions and reach a proactive behavior. DS-based Impedance controller, along with a transformation that preserves the stability of the DS, guarantees the overall stability of the control loop. Moreover, the convergence of the parameters (to the intended ones) is guaranteed if the human demonstration satisfies the *persistent excitation* condition (Eq.4.21). Our implementation on the robotic arm for different tasks (i.e., polishing a surface and pick-and-place) proves the efficacy of our method in capturing the human intention. Our experimental results are in line with our analytical analysis in terms of convergence behavior. In conclusion, parameterized dynamical systems (as adaptive motion generators) along with impedance control (providing compliant interaction) proves to be effective to provide seamless and intuitive physical human-robot interaction.

In this chapter, in order to distinguish the human interaction from other undesirable forces (disturbances, frictional forces, etc.), the force-threshold needs to be chosen carefully. A low value results in undesirable adaptation to disturbances, while a high value requires higher human effort to trigger the adaptation. In Chapter 6, we present a more sophisticated and robust method for the detection of human guidance. Furthermore, in the reported experiments in this chapter, the impedance gain presents a trade-off between compliance and tracking precision. We answer this limitation in Chapter 6 by introducing DS-based admittance control. Finally, the adaptation in this chapter is only limited to one task. The robot only adapts either the polishing task or the pick-and-place task. The next chapter we introduce another adaptation methods that allows the robot to switch to the human-intended task.

5 Robotic task adaptation through physical human-interaction

The aim of this chapter is to enable robots to intelligently and compliantly adapt their motions to the intention of a human during physical Human-Robot Interaction (pHRI) in a multi-task setting. We employ a class of parameterized dynamical systems that allows for smooth and adaptive transitions between encoded tasks. To comply with human intention, we propose a mechanism that adapts generated motions (i.e., the desired velocity) to those intended by the human user (i.e., the real velocity) thereby switching to the most similar task. We provide a rigorous analytical evaluation of our method in terms of stability, convergence, and optimality yielding an interaction behavior which is safe and intuitive for the human. We investigate our method through experimental evaluations ranging in different setups: a 3-DoF haptic device, a 7-DoF manipulator and a mobile platform.

5.1   Introduction

As introduced in Section 1.2.2, compliance can be expressed at different levels: *force*, *motion*, *task*. Such compliant behaviors enable individuals to communicate their intentions through physical interactions. In this chapter, we benefit form the compliant behavior offered by DS-based impedance control to recognize the human-intention via trajectories created by human interaction; more precisely, human-induced velocity errors. Moreover, in Chapter 3, we motivated the advantages of model-based intention-recognition for switching across task. In this chapter, we provide a similar formulation where the follower in the interaction (i.e., the robot) has a set of known intentions (i.e., tasks encoded by dynamical systems) for the leader (i.e., the human-user). This formulation allows us to implement intention-recognition capabilities for the robot by comparing human-induced error and the known possible tasks.

As reviewed in Section 2.2.4, the efforts to propose a method to recognize the human intention and adapt the robotic task according during the physical interaction is limited. We complement this body of work by providing adaptation capabilities to these systems, enabling robots to adapt tasks to the intention of the human through physical interaction. More specifically, we contribute to this literature by providing
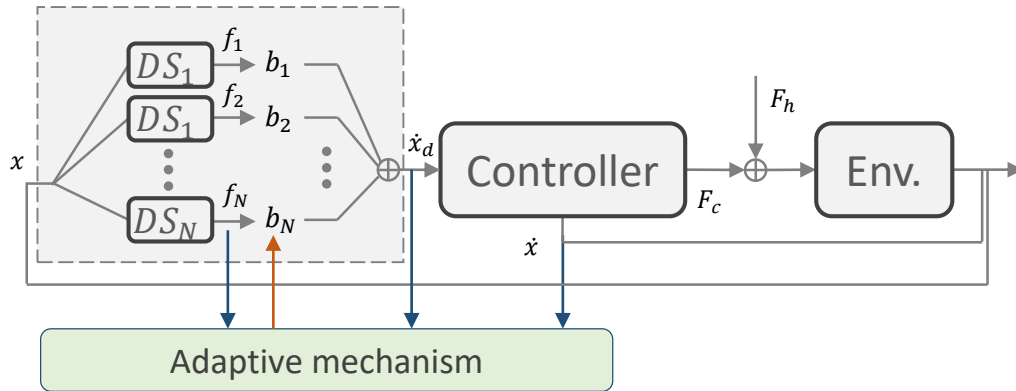
Figure 5.1 – Adaptive dynamical system as motion generators. The dynamical systems in a feedback loop with the controller and the environment. This leads to an active motion generation meaning the generated motion is influenced by the real state of the robot (i.e., the real position x). In this adaptive case, the motion generator is capable of combining several dynamical systems to comply to the intention of the human which enables the robot to transit/switch from one task to another). In this schematics, b_i are task-beliefs which are inferred by a similarity check between real velocity $\dot{x}$ and the corresponding task velocity $(f_i(x))$, and used as output gains to construct the final desired velocity of the motion generator; i.e., $\dot{x}_d$.

1. a dynamical system approach to pHRI that offers:

    (a) a strategy for recognizing human intention

    (b) stable and smooth task transitions

This approach yields compliant physical interaction between human and the robot in practical settings. We propose an adaptive-control framework based on dynamical systems both as motion-generators (which allows for smooth transitions across tasks) and as predictive models (which allows for efficient human-intention recognition and adaptation). We provide a rigorous analytical evaluation of our approach in terms of stability, convergence and optimality. Experimental evaluations on several scenarios show the efficacy of our approach in terms of prediction of human intention, smooth transition between tasks, stable motion generation, safety during contact, human effort reduction, and execution of the tasks.

5.2 Task-Adaptation Using Dynamical Systems

In this section, we propose a novel approach for task-level compliance. Our control scheme is built upon an impedance controller that enables force-level compliance and a set of dynamical systems (DS) defining the tasks known to the robot. For this, we assume that the robot knows

(a) Transition from $f_1(x)$ to $f_2(x)$.

(b) Generated motions.
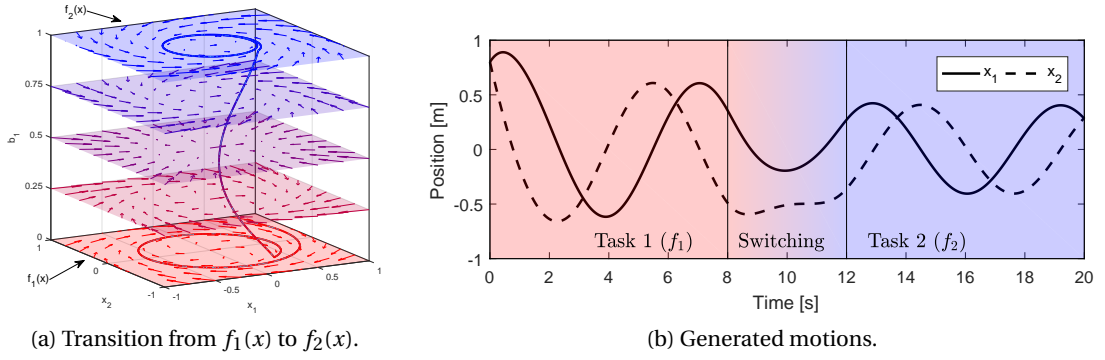
Figure 5.2 – Linear combination of two DS allowing for smooth transition from one task to another. A) clockwise and counter-clockwise rotations encoded by f_1 and f_2 where $b_2 = 1 - b_1$. The trajectory is a generated motion where b_1 is linearly changed from 0 to 1. B) The generated motions stay smooth during the transition.

a set of N possible tasks represented by first order DS, such that the ith task is given by

$$\dot{x}_d = f_i(x) \tag{5.1}$$

Moreover, each DS is globally asymptotically stable at either an attractor or a limit cycle under a continuously differentiable Lyapunov function $V_i(x)$. Given this set of dynamics systems (i.e., f_1 to f_N) each encoding for a task, we introduce the following linear combination as the motion generator.

$$\dot{x}_d = \sum_{i=1}^{N} b_i\, f_i(x) \tag{5.2}$$

where $b_i \in [0, 1]$ are corresponding beliefs for each DS (f_i) which satisfy the following conditions.

$$\sum_{i=1}^{N} b_i = 1 \tag{5.3}$$

This formulation provides smooth transition across task. Fig.5.2 shows a simple example of such linear combination where a *continuous* transition in b_i parameter leads to a *smooth* transition from one task to another.

Although DS are typically used for motion generation (Eq.5.1), they can also be used for task identification; i.e., given a current position and current velocity of the robot, they can evaluate a similarity measure between an arbitrary task and the current velocity, or, equivalently in this context, the result of the interaction between the robot and the human user. We use such similarities in our adaptation mechanism to enforce the task with the highest similarity to the human's current velocity ensuring a smooth transition through the proposed linear combination of DS (Eq.5.2).

We introduce the following adaptation mechanism.

$$\dot{\hat{b}}_i = \epsilon \ (\dot{e}^T f_i(x) + (b_i - 0.5)|f_i(x)|^2) \tag{5.4}$$

$$\dot{B} = \Omega(\dot{\hat{B}}) \tag{5.5}$$

$$b_i \leftarrow b_i + \dot{b}_i \, \Delta t \tag{5.6}$$

$$b_i \leftarrow \max(0, \min(1, b_i)) \tag{5.7}$$

where $\dot{e} = \dot{x} - \dot{x}_d$, $\dot{\hat{B}} = [\dot{\hat{b}}_1, ..., \dot{\hat{b}}_N]$ is a vector of belief-updates, $\epsilon \in \mathbb{R}^+$ is the adaptation rate, $\Omega : N \rightarrow N$ represents a winner-take-all process (which adds an offset such that only the maximum update stay positive), and Δt is the sampling time. $|.|$ denotes the norm-2 of a given vector.

In this adaptation mechanism, belief-updates ($\dot{\hat{b}}_i$) are computed based on the similarities between each DS (f_i) and the real velocity ($\dot{x}$). Broadly speaking, the second term in Eq.5.4 accounts for the inner-similarity between DS. In the second step (Eq.5.5), the beliefs are modified based on an Winner-Takes-All (WTA) process that ensures only one increasing belief and $N-1$ decreasing one. Finally, the beliefs are updated based on a given sampling-time and saturated between 0 and 1. However to ensure proper convergence behavior the WTA process should satisfy the following properties:

1. There is no more than one belief-update with a positive value in $\dot{B}$.

2. The pairwise distances are preserved:

$$(\dot{b}_i - \dot{b}_j)/(\dot{\hat{b}}_i - \dot{\hat{b}}_j) \geq 1 \quad \forall i, j \tag{5.8}$$

3. The update using $\dot{B}$ preserves $\sum\limits_{i=1}^{N} b_i = 1$.

Even though WTA can be implemented in several fashions, we use the following implementation used in this work.

This algorithm takes two inputs: a vector for the current beliefs and their updates (computed based on the adaptation mechanism). Here, we assume that beliefs are between 0 and 1 and the sum is 1. In the first step (line 1), the element with the greatest update is detected as the winner. In case of multiple maximums, one can pick the winner randomly. In the following lines (2–5), we handle the case where the winner is already saturated at 1. In this case, no update is necessary. In lines 6-8, we make sure that only the winner has a positive update. This is done by detecting the second-biggest update-value and setting the baseline in the middle. Again, in case of multiple maximums, one can pick randomly. In the rest of the algorithm, we ensure that the belief-updates sum to zero. This guarantees that the sum of the beliefs stays constant. To do this, we compute the sum of the current updates (S). In doing so, we exclude

---

Algorithm 1: Winner-take-all

   Input : A vector of beliefs $B = [b_1, ..., b_N]$

   Input : A vector of belief-updates $\dot{\hat{B}} = [\dot{\hat{b}}_1, ..., \dot{\hat{b}}_N]$

1 $w \leftarrow \arg\max_i \dot{\hat{b}}_i$ **9** $S \leftarrow 0$

2   **if** $(\,b_w = 1\,)$ **then**   **10**   **for** i **do**

3 $\dot{b}_i \leftarrow 0$ for $\forall i$ **11**   **if** $(\,b_i \neq 0$ or $\dot{b}_i > 0\,)$ **then**

4   return $\dot{B}$ **12** $S \leftarrow S + \dot{b}_i$

5   **end**   **13**   **end**

                              14   **end**

6 $v \leftarrow \arg\max_i \dot{\hat{b}}_i$ $\forall i \neq w$ **15** $\dot{b}_w \leftarrow \dot{b}_w - S$

7 $z \leftarrow (\dot{\hat{b}}_w + \dot{\hat{b}}_v)/2$

8 $\dot{b}_i \leftarrow \dot{\hat{b}}_i - z$ $\forall i$ **16**   return $\dot{B}$

---

those components that are saturated at zero and have negative updates (line 11) since they do not influence the process. Based on the previous steps (line 6–8), it is guaranteed that S has a non-positive value. By adding this value to the winner component, we ensure that the updates — of active components — sum to zero, thus, sum of the beliefs stays one.

Moreover, based on the properties of WTA, the adaptation dynamics can be seen as a set of pairwise competitions. A pairwise distance between two arbitrary DS (e.g., k and l) can be considered as follows that takes on values between -1 and 1.

$$\Delta b_{kl} = b_k - b_l \tag{5.9}$$

Since WTA process preserves the pairwise distances among the beliefs (Eq.5.8), the dynamics of the belief after WTA can be approximated by those before WTA (which has slower dynamics).

$$\Delta \dot{b}_{kl} = \dot{b}_k - \dot{b}_l \simeq \dot{\hat{b}}_k - \dot{\hat{b}}_l \tag{5.10}$$

Using Eq.5.4, we can write

$$\epsilon^{-1} \Delta \dot{b}_{kl} = \dot{e}^T (f_k - f_l) + (b_k - 0.5)|f_k|^2 + (0.5 - b_l)|f_l|^2 \tag{5.11}$$

Note that for a simpler notion, we drop the argument of the DS; i.e., we write f_i instead of $f_i(x)$. Finally, it can be shown that the adaptation rule in Eq. 5.4 is equivalent to the following.

$$\dot{\hat{b}}_i = -\epsilon \left(|\dot{x} - f_i(x)|^2 + 2 \sum_{j \neq i} b_j f_j(x)^T f_i(x) \right) \tag{5.12}$$

5.3 Mathematical analysis

In this section, we study the stability and convergence of the proposed adaptive law.

5.3.1   Optimality

We start by showing that our proposed adaptation methods (Eq.5.4) can be considered as a minimization-operator on the following cost-function based on the error induced by the human.

$$J(B) = \frac{1}{2}(|\dot{e}|^2 + \sum_{i=1}^{N} b_i(1 - b_i)|f_i|^2) \tag{5.13}$$

where $\dot{e} = \dot{x}_r - \dot{x}_d$, and where $B = [b_1, ..., b_N]$ is the belief vector. We can show this by moving along the gradient (with the step size ϵ) as follows:

$$
\begin{aligned}
\dot{b}_i &= -\epsilon \, \frac{\partial J}{\partial b_i} \\
&= -\epsilon \, (\dot{e}^T \frac{\partial \dot{e}}{\partial b_i} + (0.5 - b_i)|f_i|^2) \\
&= -\epsilon \, (-\dot{e}^T \frac{\partial \dot{x}_d}{\partial b_i} + (0.5 - b_i)|f_i|^2) \\
&= \epsilon \, (\dot{e}^T f_i + (b_i - 0.5)|f_i|^2)
\end{aligned}
\tag{5.14}
$$

In this derivation, we assume $\partial \dot{x}/\partial b_i = 0$ since the real velocity is the given input to the adaptive mechanism.

Moreover, a simple approximation of this cost function can be achieved as

$$
\begin{aligned}
\tilde{J}(B) &\simeq |\dot{e}|^2 + |\tilde{f}|^2 \sum_{i=1}^{N} b_i(1 - b_i) \\
&\simeq |\dot{e}|^2 + (1 - b^*)|\tilde{f}|^2
\end{aligned}
\tag{5.15}
$$

where $|f_i| \simeq |\tilde{f}|$ and the summation is approximated by $1 - b^*$, b^* being the maximum b_i. To simplify further, we can scale the cost by $|\tilde{f}|$ and remove the offset.

$$\bar{J}(B) = \tilde{J}(B)/|\tilde{f}|^2 - 1 = |\dot{e}|^2/|\tilde{f}|^2 - b^* \tag{5.16}$$

which shows the adaptation is a trade-off between minimizing the scaled-error and maximizing the maximum-belief. Moreover, in cases without perturbations (i.e., $\dot{e} = 0$ such as the autonomous mode), adaptation maximizes the belief of the most certain task. It is interesting to note that the error function that the adaptation tries to minimize is similar to the one in the impedance control. However, the difference is that the impedance controller tries to bring $\dot{x}$ close to $\dot{x}_d$ whereas in the task-adaptation, the motion generator tries to bring $\dot{x}_d$ (based on possible tasks encoded by the set of f_i) close to $\dot{x}$ assuming that real trajectory has components induced by human based on his/her intention; see Fig.5.3.
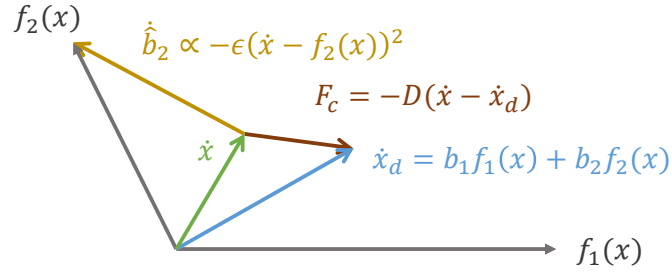
Figure 5.3 – An example of a discrepancy induced by the human guiding the robot away from its current desired trajectory $\dot{x}_d$. The impedance controller (Eq. 2.30) tries to reduce this error by *controlling* $\dot{x}$ toward $\dot{x}_d$ while the adaptation mechanism (Eq.5.4) tries to reduce the same error by *adapting* $\dot{x}_d$ to a DS that is similar to $\dot{x}$ (f_1 in this example).

5.3.2 Convergence

With regard to convergence, in the following, we analyze our adaptation mechanism in two conditions: first, when the user behavior matches the motions encoded in one of the DS, and second, when the user is not exerting any forces and the robot execution becomes autonomous.

Convergence to a demonstrated task

In this section, we assume the human user demonstrates one of the DS to the robot; i.e., $\dot{x} = f_k$. By replacing error as $\dot{e} = f_k - \dot{x}_d$ in Eq. 5.11, we obtain the competition dynamics between the demonstrated task and any other task (f_l).

$$\epsilon^{-1}\Delta\dot{b}_{kl} = (f_k - \dot{x}_d)^T(f_k - f_l) + (b_k - 0.5)|f_k|^2 + (0.5 - b_l)|f_l|^2 \tag{5.17}$$

Using the definition of $\dot{x}_d$ (Eq.5.11) we have

$$\epsilon^{-1}\Delta\dot{b}_{kl} = ((1-b_k)f_k - b_l f_l - \sum_{i\neq k,l} b_i f_i)^T(f_k - f_l) + (b_k - 0.5)|f_k|^2 + (0.5 - b_l)|f_l|^2 \tag{5.18}$$

Defining $\delta_{kl} = \sum_{i\neq k,l} b_i f_i$, we can simplify this to

$$\begin{aligned} 2\epsilon^{-1}\Delta\dot{b}_{kl} &= |f_k|^2 + |f_l|^2 - 2(1+b_l-b_k)f_k^T f_l - 2\delta_{kl}^T(f_k - f_l) \\ &= |f_k - f_l|^2 - 2(b_1 - b_k)f_k^T f_l - 2\delta_{kl}^T(f_k - f_l) \end{aligned} \tag{5.19}$$

To have a convergence to $b_k = 1$, it required to have $\Delta\dot{b}_{kl} > 0$, therefore:

$$|f_k - f_l|^2 > 2(b_1 - b_k)f_k^T f_l + 2\delta_{kl}^T(f_k - f_l) \tag{5.20}$$

This inequality serves as a metric to guarantee the converges to $b_k = 1$ and $b_l = 0$ for all other beliefs. More precisely, this inequality shows that distinguishable tasks (i.e., those with a

smaller inner products) provides a better condition for convergence. Using this condition, we study the possibility of switching from one DS to another over the sate-space in the worst case condition is Section X.x. Moreover, this can be taken into consideration beforehand to design distinguishable DS.

Convergence speed

To investigate how ϵ affects the convergence speed, we consider the case where the current task is $\dot{x}_d = f_l$ and the human demonstration is $\dot{x} = f_k$; i.e., $\dot{e} = f_k - f_l$. This simplifies Eq.5.11 into

$$2\epsilon^{-1}\Delta \dot{b}_{kl} = (1 + 2b_k)|f_k|^2 + (3 - 2b_l)|f_l|^2 - 4f_k^T f_l \tag{5.21}$$

To reach a simple estimation of convergence speed, we assume $f_k^T f_l = 0$ (i.e., the two task are distinguishable) and tasks operate at the same speed ($|f_k|^2 = |f_l|^2 = |f|^2$). This yields

$$\Delta \dot{b}_{kl} = \epsilon |f|^2 (2 + \Delta b_{kl}) \tag{5.22}$$

The analytical solution to this equation with initial condition $\Delta b_{kl} = -1$ ($b_l = 1$ and $b_k = 0$) can be computed as

$$\Delta b_{kl}(t) = \exp(\epsilon |f|^2 t) - 2 \tag{5.23}$$

Then the reaching time T_{reach} to $\Delta b_{kl} = 1$ ($b_l = 0$ and $b_k = 1$) is

$$T_{reach} = \frac{\log(3)}{\epsilon |f|^2} \tag{5.24}$$

For example, for tasks operating around $|f|^2 = 0.1$ and $\epsilon = 8$ as in the Section.5.5.2, we have $T_{reach} = 1.37$ which can be verified in Fig.5.13a. In real-world settings, given the time-scale of noises and other undesirable dynamics (approximated by T_{noise}), to avoid noise-driven adaptation and chatting between undesirable tasks, one should aim for $T_{reach} >> T_{noise}$. For example, considering $30Hz$ noise ($T_{noise} = 1/30$) for a case operating at $|f|^2 = 0.1$ leads to the $\epsilon < 329.6$ as the upper-bound. A better approach to tune ϵ is to aim for a T_{reach} that correspond to a natural human-robot interaction. For example, expecting the robot to recognize and adapt to the human intention in 1 second leads to $\epsilon = 11$. Thereafter, the approximated value can be re-adjusted in the real experiment to achieve the desirable behavior.

Convergence in the absence of human interactions

In the absence of human perturbations on the real velocity, and with the assumption of perfect tracking (i.e., $\dot{e} = 0$), Eq.5.11 can be simplified to

$$\epsilon^{-1}\Delta \dot{b}_{kl} = (b_k - 0.5)|f_k|^2 + (0.5 - b_l)|f_l|^2 \tag{5.25}$$

In this case, when the belief of the dominant task (b_k) is bigger than 0.5, one can make sure that all other beliefs are less than 0.5 (since $\sum b_i = 1$), therefore the terms of the right-hand-side are positive, and consequently, $\Delta \dot{b}_{kl} > 0$. This means that the difference between b_k and b_l increase over time until the saturation points of $b_k = 1$ and $b_l = 0$. Assuming $|f|^2 = |f_k|^2 = |f_l|^2$, we have

$$\epsilon^{-1} \Delta \dot{b}_{kl} = (b_k - 0.5)|f|^2 + (0.5 - 2b_l)|f|^2 = \Delta b_{kl}|f|^2 \tag{5.26}$$

which shows that the beliefs converge exponentially with rate of $\epsilon |f|^2$. By assuming $b_k + b_l = 1$, we have $\Delta b_{kl} = 2b_k - 1$ and $\Delta \dot{b}_{kl} = 2\dot{b}_k$ which changes Eq.5.26 to

$$\dot{b}_k = \epsilon (b_k - 0.5)|f|^2 \tag{5.27}$$

The solution to this equation is

$$b_k(t) = 0.5 + (b_k(0) - 0.5) exp(\epsilon |f|^2 t) \tag{5.28}$$

Therefore the convergence time from $b_k(0) > 0.5$ to $b_k(T_{auto}) = 1$ is

$$T_{auto} \simeq log(\frac{0.5}{b_k(0) - 0.5})/(\epsilon |f|^2) \tag{5.29}$$

Moreover, in Eq.5.26, the particular case of two tasks with equal beliefs ($b_k = b_l = 0.5$) is an unstable equilibrium point for the adaptation where the system generate motions based on $0.5(f_k + f_l)$. Therefore, the adaptation in the autonomous condition is only guaranteed if there is a task with $b_i > 0.5$ which requires the human supervision to ensure that the robot received enough demonstrations before retracting from the physical interaction; e.g., the human retracts only if he/she is confident that the robot switched to the indented task.

5.3.3 Stability of motion-generation

Now, we investigate the stability of the generated motion due to the linear combination of the DS as introduced in Eq.5.2 and time-variation of b_i due to the adaptation mechanism. In our stability analysis, we are concerned with the divergence of the generated motions and spurious attractors/limit-cycles. Here, we only investigate the autonomous case where the human-user does not exert any force. Note that having a stable behavior in the autonomous case provides a satisfactory condition for the stability of the non-autonomous case (where the human is in contact with the robot) for two basic assumptions: First, the human-user increases the passivity of the system (increasing stability margin away from divergent behaviors), and second, our adaptation mechanism is able to adapt to local perturbations of the human-user (rendering void the concept of spurious attractor and limit cycle).

The stability of generated motion Eq.5.2 in the autonomous condition (which can be seen

as a Nonlinear Parametrically-Varying System) is not straight-forward (even for linear cases). Nevertheless, one can ensure the stability when all DS (f_i) are stable under a same Lyapunov. For the following DS

$$\dot{x} = \sum_{i=0}^{N} \alpha_i(t) \, f_i(x) \tag{5.30}$$

where $\alpha_i \in \mathbb{R}^+$ are a set of positive and arbitrary time-varying values, asymptotically converges to an arbitrarily set Ξ over the state x, if a positive definite function $V(x)$ exists such that

1. $V(w) < V(z) \quad \forall w, z \mid w \in \Xi$ and $z \notin \Xi$
2. $(\partial V/\partial x)^T f_i < 0 \quad \forall i$ and $x \notin \Xi$

Although very restrictive in its conditions, this guarantees that the system will not diverge outside Ξ. However, in the case of the adaptation, the $b_i(t)$ do not change arbitrarily. Based on the exponential convergence of beliefs (Eq 5.28), the stability of the motion generation in the autonomous mode can be investigated by focusing on the dominant task. Assuming there is a task a task with $b_k > 0.5$, we can use its Lyapunov function ($V_k(x)$) to investigate the stability of the motion generation in the autonomous condition as follows:

$$\begin{aligned} \dot{V}_k &= (\frac{\partial V_k}{\partial x})^T \dot{x}_d = (\frac{\partial V_k}{\partial x})^T (b_k f_k + \sum_{i \neq k} b_i f_i) \\ &= b_k (\frac{\partial V_k}{\partial x})^T f_k + \sum_{i \neq k} b_i (\frac{\partial V_k}{\partial x})^T f_i \end{aligned} \tag{5.31}$$

Based on the stability of DS, $(\frac{\partial V_k}{\partial x})^T f_k < 0$. We further assume that the perturbations are bounded $|(\frac{\partial V_k}{\partial x})^T f_i| < \psi(x)$. Using this boundary, we have

$$\dot{V}_k < -b_k (\frac{\partial V_k}{\partial x})^T f_k + (1 - b_k)\psi(x) \tag{5.32}$$

Due to the exponential convergence of b_k (Eq. 5.28), for $t > T_{auto}$, the second term vanishes (in finite time) and the stability of kth DS is restored.

5.3.4 Resulting compliance at the force-level

Considering that the stiffness felt by the user (as presented in Section. 2.3.3), we can compute the resulting stiffness as:

$$K(x_s) = \sum_{i=1}^{N} b_i \, K_i(x_s) \leq \sum_{i=1}^{N} b_i \, K_{max}(x_s) = K_{max}(x_s) \tag{5.33}$$

where $K_i(x_s) = x_s^T K x_s = -D x_s^T \partial f_i(x)/\partial x x_s$ is the stiffness of ith DS and $K_{max}(x_s)$ denotes the stiffness of the stiffest DS in x_s direction. This is a conservative upper-bound that shows in transitory states where several DS are active with low b_i; the real resulting stiffness of

the system would be lower than the most stiff possible candidate. By introducing the a DS generating zero velocities (i.e., $f_0(x) = 0$ resulting in $K_0(x_s) \equiv 0$), the resulting stiffness is as follows.

$$
\begin{aligned}
K(x_s) &= \sum_{i=0}^{N} b_i \ K_i(x_s) = b_0 K_0(x_s) + \sum_{i=1}^{N} b_i \ K_i(x_s) \\
&\leq \sum_{i=1}^{N} b_i \ K_{max}(x_s) = (1 - b_0) K_{max}(x_s)
\end{aligned}
\tag{5.34}
$$

This upper-bound shows that the stiffness can be reduced by adapting to this null-DS; i.e., f_0. The advantage of this property is twofold. First, the lower stiffness (i.e, higher compliance) allows the user to provide demonstration or guidance easier. Second, by sensing this compliance, the user can infer the confidence level of the robot resulting in a richer haptic communication.

5.4 Illustrative example with two tasks

For illustrative purposes, we investigate the adaptation mechanism for a simple case with two DS (f_1 and f_2) encoding two arbitrary tasks. Fig.5.4a shows a generic example for computation of belief-updates following Eq.5.4. It can be seen that the second DS (f_2) has a higher similarity to the real velocity ($\dot{x}$); i.e., higher inner-product. Inner-similarity terms (i.e., $f_1^T f_2$) are important in higher number of DS where adaptation favors updates of DS that are less similar to the rest. After few iterations, the motion generator converges to the second DS. Furthermore, regarding the optimality principle (Eq. 5.13), Fig.5.4d shows the decrease in the cost (Eq.5.13). Since, in this example $\dot{x}$ is fixed, the cost is only a function of b_1 and b_2 which is illustrated in Fig.5.4c. It shows that the beliefs are updated in the direction of the gradient. However, the adaptation mechanism constrains the updates on the $b_1 + b_2 = 1$ manifold.

Moreover, the simplicity of having two DS allows us to have the close formulation of the updates after WTA process. Based on Eq.5.11, Algorithm 1, and the unity constraint ($b_1 + b_2 = 1$), we have

$$
\begin{aligned}
2\epsilon^{-1} \ \dot{b}_1 &= \dot{e}^T (f_1 - f_2) + (b_1 - 0.5)(|f_1|^2 + |f_2|^2) \\
2\epsilon^{-1} \ \dot{b}_2 &= \dot{e}^T (f_2 - f_1) + (b_2 - 0.5)(|f_1|^2 + |f_2|^2)
\end{aligned}
\tag{5.35}
$$

where $\dot{e} = \dot{x} - \dot{x}_d$. Each term in this formulation has an interesting interpretation. The first increases the belief if the error has more similarity (in the form of inner product) to a DS compared to other ones. The second term pushes away the belief from the ambiguous point of 0.5. Therefore, for a belief to go from zero to 1, the similarity (the first term) should be strong enough to overcome the stabilization term (the second term). Moreover, in accordance wit Eq.5.25, this equations show that, in zero error condition ($\dot{e} = 0$), the DS with $b_i > 0.5$ tasks over.
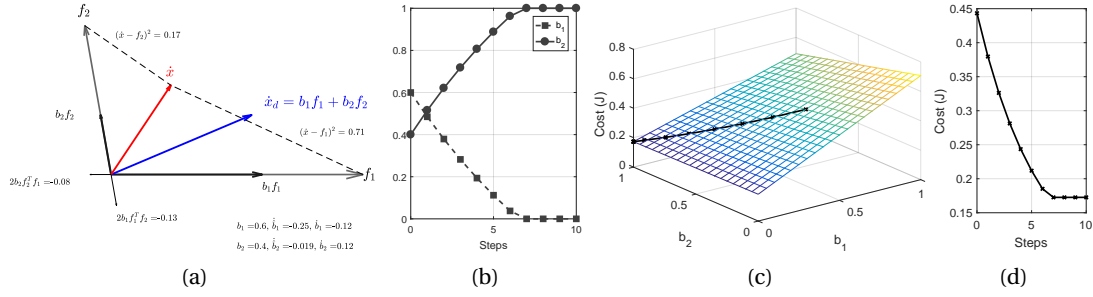
Figure 5.4 – **(a)** Geometrical illustration of the adaptation mechanism in the case of two DS. $\dot{x}$ is the real velocity vector (assumed to be influenced by human), and $\dot{x}_d$ is the desired velocity generated by the two DS (f_1 and f_2) and their corresponding beliefs (b_1,b_2). **(b)** the result of few iterations using $\epsilon = 0.4$. **(c)** The cost function of the adaptation parametrized over b_1 and b_2. **(d)** The decrease in the cost function for each time step.

We now consider the particular case where the real velocity exactly matches the first DS (i.e., $\dot{x} = f_1$). This setting takes place when the human demonstrates a task by overriding the motion. By updating the definition of the error in Eq.5.35, the dynamics of the adaptation simplifies as

$$2\epsilon^{-1}\,\dot{b}_1 = 0.5|f_1 - f_2|^2 + (2b_1 - 1)f_1^T f_2 \tag{5.36}$$

To have a positive update in the worst case scenario ($b_1 = 0$), the DS should satisfy the following inequality.

$$|f_1 - f_2|^2 > 2f_1^T f_2 \tag{5.37}$$

This inequality can be satisfied by any two vectors with inner angles $> \pi/3$. Therefore, to have a guaranteed transition between DS, their vector fields need to have enough dissimilarity. Fig.5.5 shows an example where two similar DS bifurcate to different behaviors. The green-shaded area indicates the part of the state-space where transitions are possible (based on Eq.5.37). However, is some outer regions, it is still possible to transit between similar DS by exaggerating the motion; e.g., $\dot{x} = 1.2f_1 - 0.2f_2$.

5.4.1 Simulated interaction

To simulate a simple human-robot interaction, we consider the following robot's dynamics.

$$M\ddot{x} = F_c + F_h \tag{5.38}$$
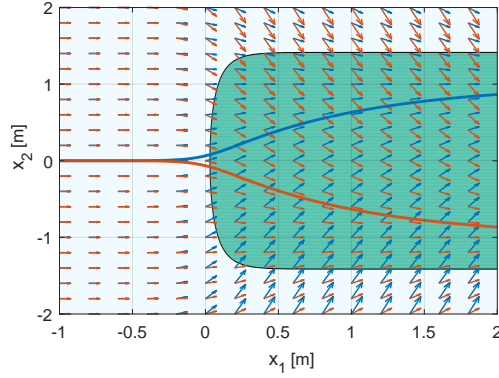
Figure 5.5 – Distinguishably between dynamical systems. Possible transitions between the two DS is shaded in green.

where $x \in \mathbb{R}^2$ represents the robot's position. The mass matrix is set as $M = \text{diag}\{0.82, 0.82\}$. F_c denotes the control force generated by the following impedance controller.

$$F_c = -D(\dot{x} - \dot{x}_d) \tag{5.39}$$

where the damping matrix is to $D = \text{diag}\{30, 30\}$. $\dot{x}_d \in \mathbb{R}^2$ is the desired velocity generated by the adaptive dynamical systems. We use the two dynamical systems illustrated in Fig.5.2 for the motion generation; i.e., $\dot{x}_d = b_1 f_1(x) + b_2 f_2(x)$. Initially, the robot performs the second task; i.e., $b_1 = 0$ and $b_2 = 1$. In Eq. 5.38, $F_h \in \mathbb{R}^2$ represents the forces excreted by a simulated agent. This agent intends to change the task from f_2 to f_1 by applying forces with the following equation.

$$F_h = -30(\dot{x} - f_1(x)) - (1 - b_1)F_c \tag{5.40}$$

In this formulation, the first term tries to executes the second task while the second term resists the robot's execution of the first task. The simulated agent starts interacting with the robot at $t = 0$. However, its forces (F_h) are only active for 0.5 seconds and saturated at $15N$.

Fig.5.6a and Fig.5.6b show the result of the simulated interaction with the adaptation rate (ϵ) set to 10. Fig.5.6a shows how the motion generator adapts with regard to the vector-fields of the DS. It can be seen that only a short demonstration (i.e., the black portion of the trajectory which lasts for $0.3s$) enables the robot to adapt to the intended task. Fig.5.6b shows the adaptations of the beliefs, and power consumptions of the robot and the simulated agent. Its negative sign indicates that the agent is decelerating the motion as the robot moves in accordance with the undesirable DS.
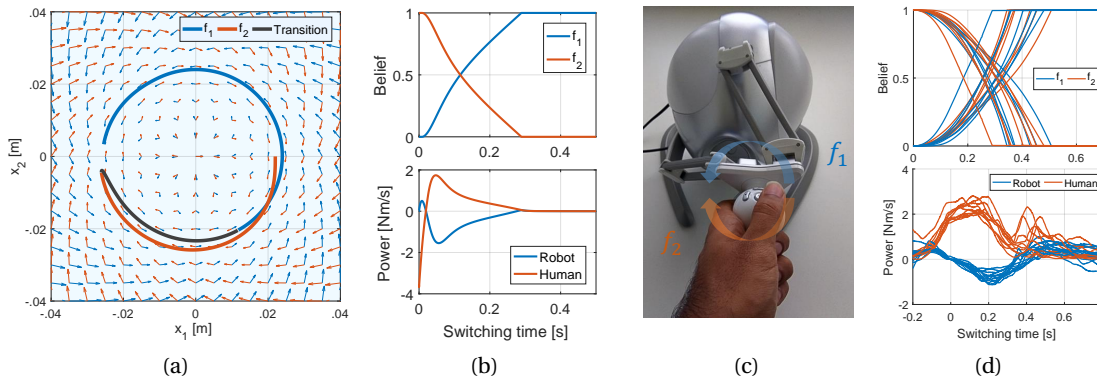
Figure 5.6 – **(a)** The simulated results for adaptation across two tasks where the desired behavior changes from the second DS to the first one based on the interactional forces. **(b)** The evolution of beliefs and the applied power by the robot and by the human during the simulated example. **(c)** The haptic device used to evaluate a simple interaction of our proposed adaptation mechanism with a human-user. **(d)** Switching across the two DS induced by the human during the real interaction.

5.4.2 Real-world interaction

To test our 2-DS example in a realistic scenario, we implemented our approach on a Falcon Novint haptic device where the human user can drive the robot toward his/her desired trajectory; see Fig.5.6c. Hereafter, the robot detects the discrepancy created by the human user and tries to compensate for it by adapting the task to the intention of the human. The results of switching across the two tasks are illustrated in Fig.5.6d; i.e., from the first DS to the second one and vice versa. The switching behavior is consistent across different attempts. The switching time (0.5 seconds which is subjected to the behavior of human-user) is similar to the simulated results (Fig.5.6b). However, the profiles are not as linear as in the simulation, and they tend to behave exponentially. This discrepancy can be explained by the difference between the actual and modeled (Eq.5.40) behavior of a human-user as well as unmodeled dynamics such as damping and friction. Compared to the power exchanges in the simulation, it can be seen that in the simulated scenario, the simulated human applies abrupt and negative power to quickly decelerate the robot and trigger the adaptation mechanism ($\simeq 0.1s$). However, in the real scenario, the human user decelerates the robot much slower ($\simeq 0.2s$) via smaller power benefiting from damping and friction in the hardware. Moreover, after the initial update on the gains ($b_i > 0.4$), no further effort is required from the human. After this phase, the figure shows different arbitrary behaviors from the human; i.e., releasing the device, cooperating with the robot, or trying to switch the DS again.

| A) Linear polish | B) Retreat | C) Circular polish | D) Push down |
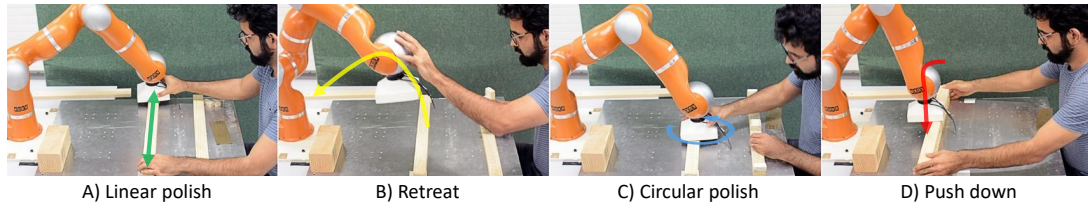
Figure 5.7 – An example of task-adaptation in compliant human-robot interaction. The user and the robot perform a series of manipulation tasks jointly. The robot recognizes the intention of human and adapts its behavior; i.e., switches to the corresponding task. **(A)** The human can ask the robot to polish linearly, **(B)** leave the workspace , **(C)** polish circularly, or **(D)** push down on a object.

5.5 Experimental evaluations

We consider two realistic scenarios (inspired by industrial settings) to evaluate our method in interaction with humans. In the first scenario, the robot and the human-user perform a series of manipulation tasks. In the second scenario, they carry and place heavy objects collaboratively.

5.5.1 Collaboration for manipulation Tasks

In this part, we consider a set of collaborative manipulation task. We consider a working station where the robot and the human polish and assemble a wooden structure; see Fig.5.7. The robot consists of a 7-DOF KUKA LWR 4+ robot with a flat (plastic) end-effector where a sand-paper is attached. The robot is capable of performing four tasks:

1. *Linear polish* (LP): The robot polishes a surface along a line.

2. *Circular polish* (CP): The robot performs a circular motions as to polish a specific location on an object.

3. *Push down* (PD): The robot pushes down on an object and holds it (e.g., to be glued).

4. *Retreat*: The robot retreats and make the workspace fully available to the human-user.

As stated before, each tasks is encoded by a DS; see Appendix B.2.1 for their parameterizations. The generalization provided by the DS enable the robot to perform any of the tasks from any point in its workspace. This is shown in Fig.5.8 where the robot is ready to perform any of the task by following the trajectories generated by the DS. We use the DS-based impedance control (presented in Section 2.3.3) to ensure safe and stable interaction between the robot and its environment. For this experiment, D is set 100 to have a practical balance between tracking and compliance. Moreover, this impedance gain (along with DS-generated trajectories) enables the robot to handle the tasks that requires contact with the environment by generating appropriate forces (F_{imp}) in both contact and non-contact conditions. For
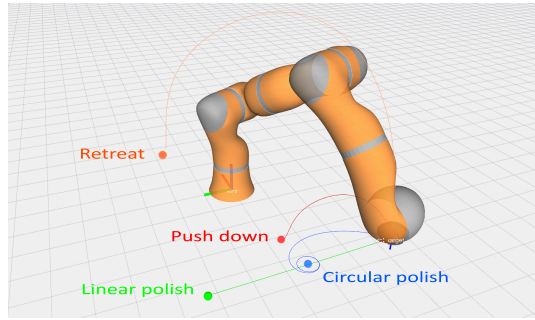
Figure 5.8 – Motion planning using dynamical systems that encodes for different tasks. Each task can be performed form any point in the robot workspace.

the adaptation rate, we use $\epsilon = 3$. For discussion on how to tune this parameter, see Section 5.6.
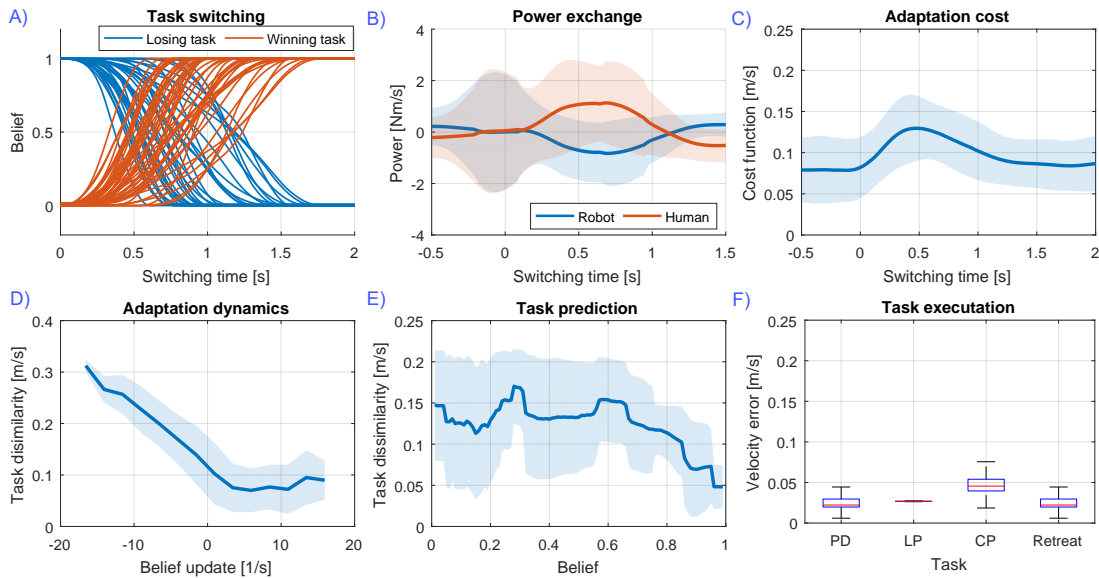
Figure 5.9 – The overall result of the proposed adaptation mechanism for the manipulation tasks using a robot arm. **A)** According the interaction with the human-user, the robot successfully switches from one task to another. **B)** The human-user requires to exchange mechanical power with the robot to demonstrate his/her intention. **C)** The minimization of the adaptation cost (Eq.5.13) upon human perturbations. Note that, to have a comparable units, the root-square of the cost in plotted here. **D)** The dynamics of the adaptation (Eq.5.4) where the dissimilarity of the real velocity to each task affects its belief and vice versa. **E)** Prediction of the human perturbations based on the dissimilarity of the real velocity with each task. **F)** The performance of the robot for execution of each task after adaptation and in absence of human interaction.

Fig.5.9 shows the overall results of the adaptation in this experiment. We systematically assessed all possible switchings across tasks. The first subplot (Fig.5.9.A) shows how, upon human perturbation, the beliefs are adapted. Specifically, the previous task loses its beliefs
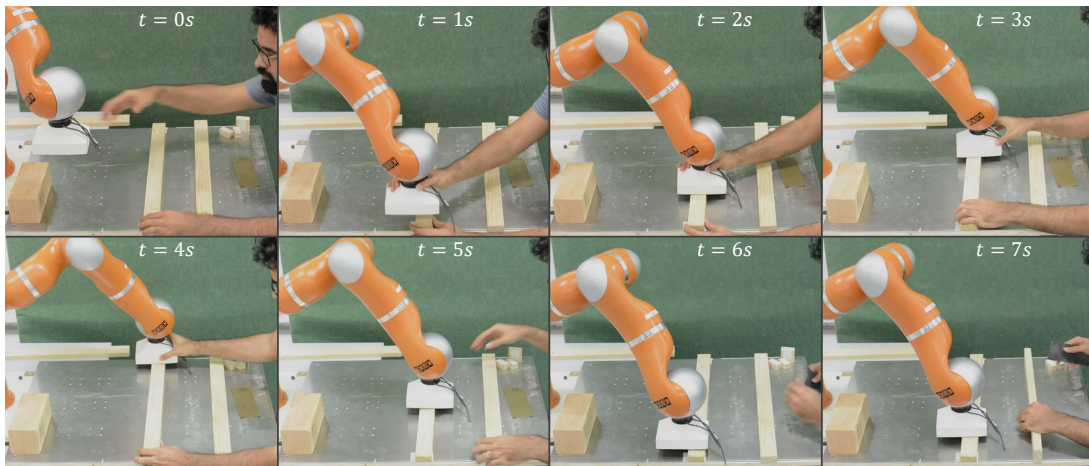
Figure 5.10 – Snapshots of the task-adaptation in the manipulation task. The robot is initially in the retreat task. Staring around $t = 1s$, the human starts to demonstrate the linear polishing task. From $t = 4s$ the robot start to perform the linear polish autonomously.

(falling from 1 to 0) while the new one takes over; the changes in the belief of all other tasks being negligible. It roughly takes 1 second for the belief to rise (from 5% to 95%). However, this rise-time depends on the quality of the human-demonstration, *distinguishability* of the tasks, and the adaptation rate (ϵ). Moreover, the switching behavior is similar to the previous case illustrated in Fig.5.6 where the slower adaptation can be explained by lower value for ϵ; 1.5 compared to 3. This conservative choice of ϵ is to ensure a robust adaptation (i.e., avoiding fluctuations) where the number of possible tasks is higher.

Fig.5.9.B illustrates the power exchange between during the interaction. The human-user spends mechanical power to demonstrate his/her intention. Initially (up to 1 second), the robot rejects the human perturbations when the wining task is still below 0.5. After gaining enough confidence in the new task (i.e., belief higher than 0.5), the robot becomes the active (providing positive effort) and the human the passive partner. The cost of adaptation as formulated in Eq.5.13 is depicted in Fig.5.9.C. It can be seen that, due to human perturbation, the cost (i.e., the first term in Eq.5.13) increases. Before $t = 0.5$, in order to reduce this error, the robot increases its effort to fulfill the losing task until the adaptation activates and beliefs are updated ($0.5 < t < 1$). This reduces the cost since the winning task complies with the human intention and removes his/her perturbation.

Fig.5.9.D. shows the dynamics of our proposed adaptation mechanism (i.e., Eq.5.4). Task dissimilarity is computed as the difference between real velocity ($\dot{x}$) and generated velocity by each DS ($f_i(x)$). This graph is averaged over all possible tasks. It can be seen that a low dissimilarity (high similarity) results in a positive update; i.e., a higher belief for a task. Consequently, the task with highest similarity wins the WTA process and reach $b_i = 1$. Fig.5.9.E shows the prediction capability of our method. It can be seen that, on average, the belief of a
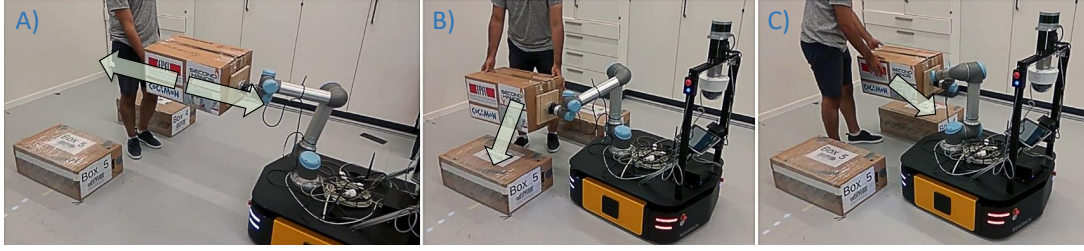
Figure 5.11 – The demonstration of our proposed mechanism in interaction with a human-user. (Left) After an initial movement induced by the human-user, robot adapt to the "forward" DS and performs the task pro-actively. (Center) After an initial push from the human to the left side, the robot switches form "forward" to "place-left" DS resulting in an active assistance behavior. (Right) The human suddenly decides to place the object on the right, and the robot adapts to this intention.

task with a higher similarity to the real velocity has a higher belief. For example, a task that reaches $b_i = 0.9$ has higher similarity to the real velocity compared another task with $b_j = 0.1$. Both Fig.5.9.E and F show that our method adapts the beliefs meaningfully w.r.t. to the real velocity.

Fig.5.9.F shows the performance of the robot during the execution of each task when the belief of the task is 1 and the human is not perturbing the robot. This shows that after adaptation, the robot perform the task satisfactorily in the solo condition. Finally, Fig. 5.10 shows the snapshot during this experiment.

5.5.2   Transportation of heavy objects

We consider a human-robot collaboration task in a warehouse-like scenario where they carry and place a heavy object across the aisles with shelves on each side. However, the initial and target positions of objects are intended by the human and are unknown to the robot. The robot consists of a *Clearpath ridgeback* mobile-robot with *Universal UR5* robotic-arm mounted on top of the base; see Fig.5.11. Using the force-torque sensor (*Robotiq FT300*) the robot is controlled by the following admittance law.

$$\ddot{x}_a = M_a^{-1}[-D_a\dot{x}_a - K_a(x_a - x_e) + F_e + F_c] \tag{5.41}$$

$$\ddot{x}_p = M_p^{-1}[-D_p\dot{x}_p + R_a^p[D_a\dot{x}_a + K_a(x_a - x_e)]] \tag{5.42}$$

where x_a, x_e, K_a, and $D_a \in \mathbb{R}^6$ are the position, equilibrium, stiffness, and damping of the arm respectively. F_e denotes the external forces measured by the sensor, and F_c is the control input. $\dot{x}_a$ and $\ddot{x}_a$ are the desired velocity and acceleration computed by the admittance law. The desired velocities are sent to a low-level velocity-controller to be executed on the robot. M_a

(a) Admittance control.

(b) Encoded tasks.
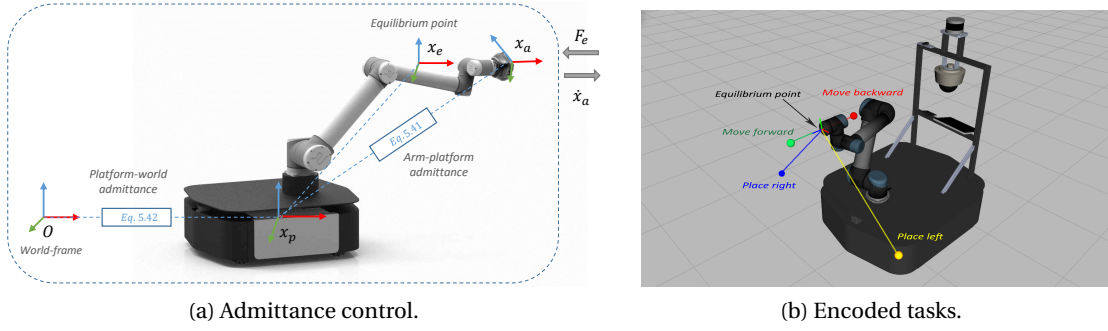
Figure 5.12 – (a) Admittance control of the end-effector of the mobile-base robot. The robot is modeled as two virtual admittance in series; i.e., from the arm (end-effector) to the platform, and from the platform to the global coordinate. (b) Tasks are encoded as simple attractors in the workspace of the arm. Generated motion based on "Move forward/backward" excites the admittance control and moves the platform accordingly, whereas, generated motion using "place left/right" only moves the arm.

and M_p are the simulated mass matrices for the arm and platform respectively. D_p denotes the damping of the platform. The rotation matrix $R_a^p \in \mathbb{R}^{6 \times 6}$ transforms the arm configuration to the platform frame; see Fig.5.12a. Upon any force (F_e or F_c) the admittance control moves the arm and the platform in order to go back to the equilibrium point (i.e., $x_a = x_e$, $\dot{x} = \ddot{x} = 0$). The manner that the admittance control translate the forces into movements of the arm and platform depends on the parameters (M_p, M_a, D_a, D_p, K_a); the robot can be more responsive to forces by moving either the arm or the platform. See Appendix.B.3.2 for the parameters used in this experiment.

The motion of the arm can be controlled using F_c in Eq.5.41. We use this input for our DS-based impedance-control in Section 2.3.3. For the DS, we consider four single-attractor dynamics to encode for four different tasks: 1) *Move Forward* (MF), 2) *Move Backward* (MB), 3) *Place Right* (PR), and 4) *Place Left* (PL); see Appendix B.2.2 for the parameterization of these tasks. Fig.5.12.a shows the location of these attractor with respect to the equilibrium point of the admittance control. Controlling the arm toward the attractor of MF/MB constantly excites the admittance controller and as the result the robot moves forward/backward. However, due a special parameterization of K_a (the stiffness between the arm and the platform) and placement of the attractors, controlling the arm toward PR/PR does not cause the platform to move. For this experiment, the impedance-control gain D is set 200. Given the four tasks, we apply our proposed adaptation mechanism with $\epsilon = 8$.

Fig.5.13 shows the overall results of the adaptation in this experiment. The results are qualitatively similar to the previous experiment in terms of switching behavior, power exchange, and adaptation performance. It can be seen that due to slower motions and stiffer dynamics, more human-effort and longer time are required to switch between tasks. Finally, Fig. 5.14 shows the snapshot during this experiment.
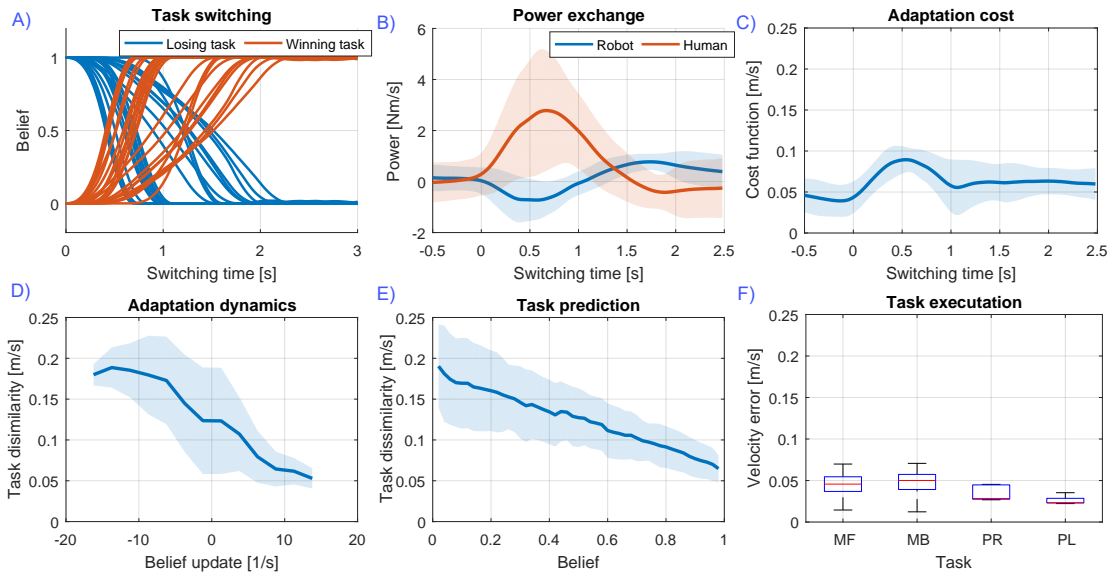
Figure 5.13 – The overall result of the proposed adaptation mechanism for carrying heavy objects. **A)** According the interaction with the human-user, the robot successfully switches from one task to another. **B)** The human-user requires to exchange mechanical power with the robot to demonstrate his/her intention. **C)** The minimization of the adaptation cost (Eq.5.13) upon human perturbations. **D)** The dynamics of the adaptation (Eq.5.4) where the dissimilarity of the real velocity to each task affects its belief and vice versa. **E)** Prediction of the human perturbations based on the dissimilarity of the real velocity with each task. **F)** The performance of the robot for execution of each task after adaptation and in absence of human interaction.
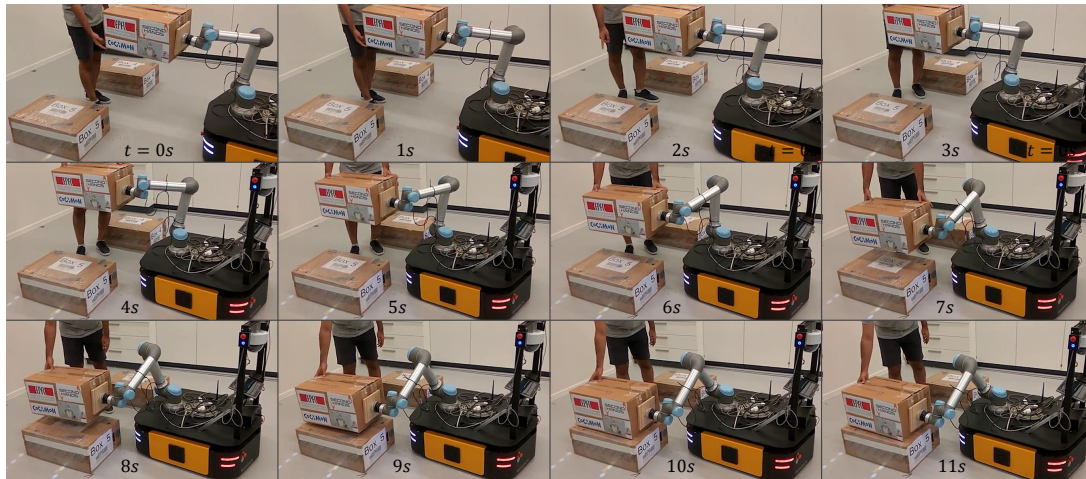
Figure 5.14 – Snapshots of the task-adaptation in the transportation task. The robot is initially performing the "moving forward" task where the human demonstrate a motion that is similar to "place left". Therefore, the robot switches to this task. The robot performs all the tasks autonomously.

5.6   Discussion and conclusion

In this paper, we presented a dynamical-system approach to task-adaptation which enables a robot to comply to the human intention. We extended the DS-based impedance control where, instead of one dynamical system (encoding for one task), several dynamical systems can be considered. We introduced an adaptive mechanism that smoothly switches between different dynamical systems. We rigorously studied the behavior of our method in theory and practice confirming that our adaptive mechanism exhibited robustness to real-world uncertainties (e.g., noisy sensors) and deviation from theory (e.g., imperfect tracking).

To switch from one task to another, the two tasks need to be *"distinguishable"*.   Eq.5.20 provides a theoretical condition on tasks dissimilarity.   However, this condition is under the assumption that the human is perfectly overriding the target task.   This is restrictive assumption in settings where 1) the robot is active at all time and it tries to fulfill its current task, and 2) the human might not know or be able to exactly demonstrate the target task. Thus, it slows down the convergence speed when the robot requires enough dissimilarity to the current task and enough similarity to the target task. If these conditions hold, beliefs are updated proportional to the adaptation rate (ϵ); see Appendix.5.3.2 for more details. In short, the speed of convergence depends on: 1) inner-similarity of the tasks, 2) the adaptation rate and 3) the quality of the human perturbations. Therefore, the convergence behavior can be improved by designing the tasks (encoded by DS) to be dissimilar as possible to produce legible motions Dragan et al. (2013).

Moreover, naive users might require a learning phase to be able to express their intention and achieve a better convergence behavior. Finally, one can increase the convergence speed by increasing the adaptation rate cautiously with respect to the noise and undesirable dynamics; see Appendix.5.3.2. Additionally, to improve the compliant and adaptation behavior of the robot, we can consider a DS that only encodes zero-velocities; i.e., *null-DS*, see Appendix C.3. By adapting to this DS, the human-user is able to stop the robot at any time during the interaction. Moreover, this DS can be used as an intermediary step for switching between two tasks since it reduces the final stiffness felt by the user; see Appendix 5.3.4.

6 | Human guidance recognition for robust robotic reactivity

The goal of this chapter is to answer to the shortcomings of DS-impedance control in Chapter 4 and 5. As discussed in those chapters, the performance of DS-impedance control is limited as tracking and compliant behavior are coupled. Precise tracking and disturbance rejection favor high-impedance whereas proper compliant behavior requires low-impedance gains. To overcome this, we propose a unified control framework based on DS motion planning, admittance control, and an algorithm to detect human-guidance. First, we detect which behavior (tracking or compliance) is required in the course of interaction. Then, we smoothly adapt the robot's behavior accordingly; i.e., compliant when human intended to interact with the robot, and stiff when the task is required to be executed precisely. The idea of this chapter can be seen as an adaptive behavior at the force-level. The related work for this chapter is reviewed in Section 2.1.3 and 2.2.5. In the following, we introduce our control framework and put our approach under rigorous mathematical analysis in terms of stability, passivity, and tracking performance. Furthermore, we conduct several robotic experiments in order to show the efficacy of our method in real-world interaction with human. Discussions and conclusions are presented in the last section.

6.1   Introduction

Two distinct robotic behaviors are necessary for a seamless physical human-robot interaction (pHRI). The first role is the capacity to execute a given task. Most often such task requires high-performance tracking behavior with disturbance rejection capabilities. The second role, on the other hand, is the ability to comply with human interaction forces. This is a crucial capacity as complying with the human forces (i.e., being a passive follower) is the necessary step toward proactivity. Therefore, an efficient control framework for pHRI should 1) identify which role is required, and 2) smoothly and stably transit to the proper behavior. To achieve this, we propose an admittance control architecture along with a human-guidance detection algorithm. This approach enables the robot to 1) precisely track the task-specific velocities, and 2) provide a proper compliant behavior toward human-user. We employ dynamical systems to generate task-specific motion and admittance control to generate velocities that comply
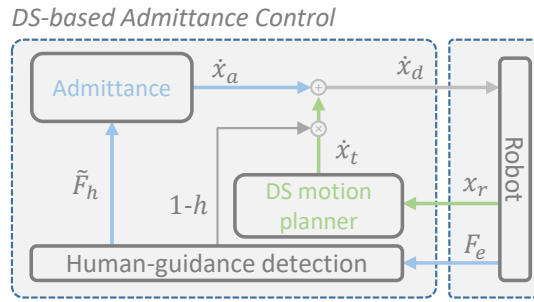
Figure 6.1 – The unified control structure to provide motion-tracking and compliant behavior based on human intention. The inner loops provides the tracking behavior and the outer loop provides the compliance behavior toward the human input. Based on the external forces, we detect if the human demands a compliant behavior. Detected human-guidance (h) attenuates the effect of the motion planner.

with the human forces. Based on an algorithm that recognizes human intentional forces, we combine DS-generated with admittance-generated velocities. This structure enables the robot to reject undesirable perturbations, track the motions precisely, reacts to human-guidance by providing proper compliant behavior, re-plan the motion reactively, and adapt to the human-intended task. Using our proposed framework, the robot smoothly transits across the following different roles:

- **Stiff Leader**: rejecting disturbances and executing the task autonomously.

- **Compliant leader**: complying with the human forces while executing the task.

- **Passive follower**: complying with the human forces and ignoring the task.

- **Proactive follower**: complying with the human forces and adapting to the task.

To detect human-guidance, we assume that intentional forces are consistent over time (as opposed to noises, oscillations, a and short-lived disturbances like shocks). To measure consistency, we compute autocorrelation on the force pattern as a metric to distinguish between intentional (human) guidance and disturbances. Moreover, for reaction/adaptation strategy, we propose a smooth transition between motion tracking and compliant behavior (instead of just varying/adapting the compliance). Our human detection method is independent from the control structure and our reaction strategy is proved to be stable.

Our proposed control architecture is depicted in Fig. 6.1. We assume that the robot is controlled in velocity (either using pure high-gain velocity controller or via velocity-based impedance controller), and position and force feedback are available. In order to obtain reactive motion planning, we employ state-dependent dynamical systems to encode our desired robotic tasks. Furthermore, in order to achieve intelligent compliant behavior, we propose a human-guidance detection algorithm that only passes intentional forces to an admittance controller. This controller structure can be seen as an interplay of two separated control loops:
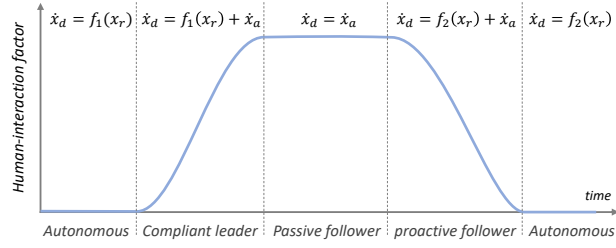
Figure 6.2 – A conceptual illustration for the proposed adaptive method. **(Stiff leader)** The robot starts by performing a task encoded by a dynamical system (f_1). During this period the robot rejects the external disturbances and focuses on the tracking behavior. **(Compliant leader)** The robot detects intentional interactions with human and, as a result, provides complaint behavior while performing the task. **(Passive follower)** The robot neglects the task and provide compliant behavior toward the human-user using the admittance loop. In this phase, the robot observes the motions and recognizes the human-intention; f_2 in this case. **(proactive follower)** Knowing the intended task, the robot starts to actively follow the human guidance which results in human retrieval. **(proactive follower)** The robot starts to autonomously perform the intended task.

the inner loop which aims to provide precise tracking behavior, and the outer loop which aims to provide proper compliance behavior (i.e., to reject the disturbances or to allow for human-interaction). Fig. 6.2 shows how this structure enables the robot to take different roles in the interaction. In the following, we present the formulation for combining DS and admittance-generated motions; i.e., DS-admittance control.

6.2 Motion-compliance Control

We model the robot's end-effector as a rigid-body described in the task space by the state variable $x \in \mathbb{R}^n$ where the measurement of external forces ($F_e \in \mathbb{R}^6$) is available. As illustrated in Fig. 6.1, we assume that the robot is velocity-controlled. We combine the task-specific velocity ($\dot{x}_t$) generated by the robot's nominal DS with the velocity generated by the admittance controller ($\dot{x}_a$), this yields the following equation.

$$\dot{x}_d = (1 - h)\dot{x}_t + \dot{x}_a \tag{6.1}$$

where $h \in [0, 1]$ is a modulation factor that is generated by the human-detection algorithm. Moreover, $\dot{x}_t$ and $\dot{x}_a$ are the velocities generated by the DS and admittance respectively. The desired velocity ($\dot{x}_d$) is sent to the velocity controller to be tracked by the robot. We use a nominal dynamical system for motion planning, given by

$$\dot{x}_t = f(x) \tag{6.2}$$

where $f : \mathbb{R}^n \mapsto \mathbb{R}^n$ generates task-specific velocities ($\dot{x}_t$) for given robot's positions (x). Finally, the compliant behavior is delivered through admittance control with the following formulation.

$$M_a \ddot{x}_a = -D_a \dot{x}_a + \tilde{F}_h \tag{6.3}$$

where M_a and $D_a \in \mathbb{R}^{n \times n}$ are admittance mass and damping matrices. The human-guidance forces ($\tilde{F}_h$) is estimated using our algorithm based on the external forces (F_e).

6.3 Human-guidance detection algorithm

Our human detection algorithm can be seen as a soft switch as follows.

$$\tilde{F}_h = h F_e \quad \text{where} \quad 0 \le h \le 1 \ \ \forall t \tag{6.4}$$

where F_h is the estimated human-force, and h is the human-interaction ratio: $h = 0$ results in stiff behavior whereas $h = 1$ brings out the compliant behavior given by the admittance dynamics. In the following, we show how we compute this ratio. First, in order to understand whether there is a consistent intention behind external forces, we simulate the following virtual admittance.

$$M_a \ddot{\tilde{x}} = -D_a \dot{\tilde{x}} + F_e \tag{6.5}$$

$\dot{\tilde{x}} \in \mathbb{R}^d$ is the virtual state. Using this virtual admittance, we estimate the motion resulting from reacting to F_e. Given $\dot{\tilde{x}}$, we can estimate the persistency of the input using the following powers.

$$\tilde{P}_i = \dot{\tilde{x}}^T F_e \qquad \tilde{P}_o = \dot{\tilde{x}}^T \tilde{F}_h \tag{6.6}$$

where $\tilde{P}_i$ and $\tilde{P}_o$ are the input and output power respectively. Now, we consider an energy tank (with the state E and size E_m) with the following dynamics.

$$\dot{E} = \tilde{P}_i - \tilde{P}_o - (1 - h)\tilde{P}_d \tag{6.7}$$

where $\tilde{P}_d > 0$ is a dissipation rate that is modulated by human-interaction ratio h. This energy is limited between 0 and E_m. The human-guidance ratio h is decided based on the stored energy in the tank as follows.

$$h = \begin{cases} 0 & E \le E_t \\ (E - E_t)/(E_m - E_t) & E > E_t \end{cases} \tag{6.8}$$

where E_t is the threshold triggering the detection of the human-guidance. As it can be seen, positive values of $\tilde{P}_i$ increase the stored energy and consequently increases h. This means that the human must contribute to a positive value of the power over a period of time to generate a response from the robot. Positive power is relevant to the consistency in motion and the indication whether or not there is an intention behind external forces. $\tilde{P}_d$ acts as a forgetting

factor and suppresses the small forces that need to be rejected.

6.3.1 Convergence behavior

In this part, we investigate the convergence behavior of our algorithm. In order to relate our algorithm to methods used in the literature of collision detection (reviewed in Section 2.2.5), we can investigate the time-derivate of h as follows.

$$\dot{h} = \begin{cases} 0 & E \leq E_t \\ \dot{E}/(E_m - E_t) & E > E_t \end{cases} \tag{6.9}$$

By replacing $\dot{E}$ from Eq.6.7 and using $\tilde{P}_o = h\tilde{P}_i$, we have

$$\dot{h} = -\gamma(h - 1) \tag{6.10}$$

where $\gamma = (\tilde{P}_i - \tilde{P}_d)/(E_m - E_t)$. It shows that $\tilde{P}_i > \tilde{P}_d$, $h \to 1$ and otherwise $h \to 0$. The solution to this equation for an arbitrary initial condition ($h(0)$) is

$$h(t) = (h(0) - 1)e^{-\gamma t} + 1 \tag{6.11}$$

In this equation, the rise time (i.e., the time to reach 0.9 from 0) for a fixed γ is $T_r = 2.32\gamma^{-1}$. However, the accumulated energy first needs to pass the triggering value (E_t). Thus, we can compute the trigger time for a constant input power as $T_t = E_t/\tilde{P}_i$. In total, the time to reach $h = 0.9$ when the tank is empty ($E(0) = 0$) for constant $\tilde{P}_i > 0$ is

$$T_u = 2.32(E_m - E_t)/(\tilde{P}_i - \tilde{P}_d) + E_t/\tilde{P}_i \tag{6.12}$$

Same can be derived for the case where the human retreats from the interaction $\tilde{P}_i = 0$. In this case, the required time to reach $h = 0$ from $h(0) = 0.9$ is as follows.

$$T_d = 2.32(E_m - E_t)/\tilde{P}_d \tag{6.13}$$

Note that non-consistent interaction $\tilde{P}_i < 0$ decreases h faster by reducing the energy in the tank. Fig. 6.3 shows the accumulated energy based on the magnitude and duration of an external force. By choosing a level set (i.e., E_m), we can consider the tank as a classifier that passes forces with certain consistency (i,e., magnitude, duration).

It can be seen that in the virtual admittance, $\dot{\tilde{x}}$ is the filtered and scaled version of F_e. Therefore, $\tilde{P}_i$ measures the correlation between F_e and its history; i.e., autocorrelation. This fact is shown with further mathematical details in Section 6.3.2.

Fig. 6.4 shows the results of our detection algorithm for three different types of external forces: Gaussian noise, a persistent force, and a series of impulses. The resulting $\tilde{F}_h$ shows that only the persistent human-input will pass the filter and the other undesirable disturbances are
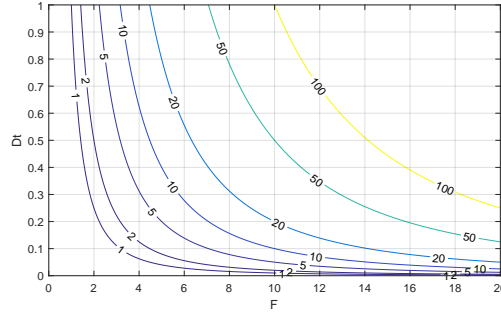
Figure 6.3 – Simulated result for accumulated energy in the storage tank based on the magnitude and duration of an external force with step-function profile.

rejected. Our method exhibits a delay at $t = 3s$ for the detection of the step function. This delay is necessary to ensure that the signal is persistent. Furthermore, we compare our method to low-pass filters with different bandwidths. Even though, low-pass filters can show faster response to the step function, they still suffer in passing the undesirable disturbances.
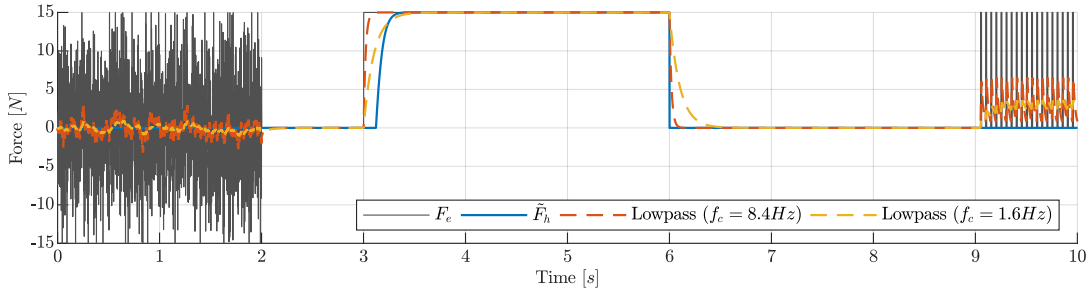
Figure 6.4 – Comparison between our algorithm for human-guidance detection and low-pass filters. The responses are evaluated for Gaussian noise, step function, and a train of impulses. In simulation, we use $E_m = 2$, $E_t = 1$, $\tilde{P}_d = 2$, $M_a = 1$, $D_a = 8$, $dt = 1ms$. The Gaussian noise is generated by $\mathcal{N}(0, 36)$, and impulses last for $10ms$ every $50ms$.

6.3.2   Autocorrelation of external forces

Our human detection algorithm can be investigated from a statistical point of view. First, let's assume diagonal inertia and damping matrix in Eq. 6.5. Let m_j and d_j be the inertia and damping for the j-th dimension ($j \in \{1, ..., n\}$). The admittance dynamics in Eq. 6.5 can be written as a low-pass filter in the following discrete form for each dimension.

$$\dot{\tilde{x}}_j(k) = \beta_j \dot{\tilde{x}}_j(k-1) + (1 - \beta_j)d_j^{-1}F_{e,j} \tag{6.14}$$

where $\dot{\tilde{x}}_j(k)$ is the virtual admittance velocity for the time-step k and j-th dimension. $F_{e,j}$ is the external force in j-th dimension. The filtering factor (β_j) can be computed as $\beta_j = 1 - m_a^{-1}d_j\Delta t$

where Δt is sampling rate. Therefore, the input power at time-step k can be expanded as

$$
\begin{aligned}
\tilde{P}_{in,j}(k) &= \dot{x}_j(k) F_{e,j}(k) \\
&= d_j^{-1}(1 - \beta_j) \sum_{l=1}^{\infty} \beta_j^{l-1} F_{e,j}(k - l) F_{e,j}(k)
\end{aligned}
\tag{6.15}
$$

The accumulated energy due to $\tilde{P}_i$ can be computed as

$$
\begin{aligned}
E_j(n) &= \sum_{k=-\infty}^{n} \tilde{P}_i(k) \\
&= \sum_{k=-\infty}^{n} d_j^{-1}(1 - \beta_j) \sum_{l=1}^{\infty} \beta_j^{l-1} F_{e,j}(k - l) F_{e,j}(k) \\
&= d_j^{-1}(1 - \beta_j) \sum_{l=1}^{\infty} \beta_j^{l-1} \sum_{k=-\infty}^{n} F_{e,j}(k - l) F_{e,j}(k)
\end{aligned}
\tag{6.16}
$$

By defining the autocorrelation function with lag l over the external force at time step n as follows

$$
\rho_j(l) = \sum_{k=-\infty}^{n} F_{e,j}(k) F_{e,j}(k - l)
\tag{6.17}
$$

we can rewrite the energy of the tank as

$$
E_j(n) = d_j^{-1} \frac{\sum_{l=1}^{\infty} \beta_j^{l-1} \rho_j(l)}{\sum_{l=1}^{\infty} \beta_j^{l-1}}
\tag{6.18}
$$

Note that, we used the expansion of $(1 - \beta_j)^{-1}$. Therefore, the input energy is the weighted averaged of autocorrelation with different lags.

6.4 Energy analysis for stability and passivity

In this section, we investigate the passivity of our control architecture. First, we assume the following decomposition for the dynamical system.

$$
f(x) = -\nabla_x V(x) + \tilde{f}(x)
\tag{6.19}
$$

Where $V(x) \in \mathbb{R}^+$ is a potential function and $\tilde{f} : \mathbb{R}^n \mapsto \mathbb{R}^n$ is a residual that accounts for the non-conservative part of the DS. The stability of the motion-generation can be investigated with the assumptions of perfect tracking ($\dot{x} = \dot{x}_t$) as follows.

$$
\dot{V}(x) = \nabla_x V(x) \dot{x}_t = -\|\nabla_x V(x)\|^2 + \nabla_x V(x)^T \tilde{f}(x)
\tag{6.20}
$$

The Lyapunov stability of the DS can be guaranteed if

$$\nabla_x V(x)^T \tilde{f}(x) < ||\nabla_x V(x)||^2 \tag{6.21}$$

which indicates that the conservative part dominates the non-conservative part and vanishes over time.

In the case of perfect tracking ($\dot{x} = \dot{x}_d$), we can write

$$\dot{x} = \bar{h}\dot{x}_t + \dot{x}_a \tag{6.22}$$

where $\bar{h} = 1 - h$. Initially, we limit our analysis to $D_a = d_a \mathbb{I}_n$ where $d_a \in \mathbb{R}^+$. Let's consider the following storage function.

$$W = \frac{1}{2}\dot{x}^T M_a \dot{x} + d_a V(x) \tag{6.23}$$

Using the admittance dynamics (Eq.6.3), the time derivative of this storage function is

$$\dot{W} = \dot{x}^T(\bar{h}M_a\ddot{x}_t - \dot{h}M_a\dot{x}_t - d_a\dot{x}_a + hF_e) + d_a\nabla_x V(x)\dot{x} \tag{6.24}$$

$\ddot{x}_t$ can be computed based on the Jacobian of $f(x)$ as $\ddot{x}_t = f'(x)\dot{x}$.

$$\dot{W} = hF_e^T\dot{x} - \dot{x}^T(d_a\mathbb{I}_n - \bar{h}M_a f'(x))\dot{x} + \bar{h}d_a\dot{x}^T\dot{x}_t + d_a\nabla_x V(x)^T\dot{x} - \dot{h}\dot{x}_t^T M_a\dot{x} \tag{6.25}$$

Using Eq.6.2 and 6.19, we can write

$$\dot{W} = hF_e^T\dot{x} - \dot{x}^T(d_a\mathbb{I}_n - \bar{h}M_a f'(x))\dot{x} + d_a\dot{x}^T(h\nabla_x V(x) + \bar{h}\tilde{f}(x)) - \dot{h}\dot{x}_t^T M_a\dot{x} \tag{6.26}$$

Let's first investigate the two boundary conditions ($h = 1$ and $h = 0$ with $\dot{h} = 0$). For $h = 0$ (the absence of human guidance), we have

$$\dot{W}|_{h=0} = -\dot{x}^T(d_a\mathbb{I}_n - M_a f'(x))\dot{x} + d_a\dot{x}^T\tilde{f}(x) \tag{6.27}$$

The system is stable if $d_a > \lambda_{max}(M_a f'(x))$. This means that forces generated by the damping part of the admittance ($d_a\dot{x}$) should dominate the centrifugal forces generate dy DS ($M_a f'(x)\dot{x}$). Moreover, the non-conservative part of the DS ($\dot{x}^T\tilde{f}(x)$) might violate the stability of the system. Nevertheless, having a damped admittance behavior in $h = 0$ results in $\dot{x}_a \to 0$, therefore $\dot{x} = \dot{x}_t$. Given this, we can rewrite

$$\dot{x}_t^T\tilde{f}(x) = (-\nabla_x V(x) + \tilde{f}(x))^T\tilde{f}(x) = -\nabla_x V(x)^T\tilde{f}(x) + \tilde{f}(x)^2 \tag{6.28}$$

Therefore, the system is stable if $||\tilde{f}(x)||^2 \le \nabla_x V(x)^T\tilde{f}(x)$ which includes $\tilde{f}(x) = 0$. Finally, note that $\dot{W} < 0$ only proves the stability of the system. The passivity of the mapping $F_e \mapsto \dot{x}$ is ill-defined since the term $F_e^T\dot{x}$ does not appear in $\dot{W}$ for $h = 0$.

For $h = 1$ (the presence of human guidance), we have

$$\dot{W}|_{h=1} = F_e^T \dot{x} - d_a ||\dot{x}||^2 + d_a \nabla_x V(x)^T \dot{x} \tag{6.29}$$

The system exchanges energy through the input port $F_e^T \dot{x}$. The passivity of the admittance is guaranteed since $d_a > 0$. The last term (P_h) shows how the human can inject energy into the DS potential function by changing the state of the system.

During the transitions ($\dot{h} = 0$), the DS dissipates energy since $\nabla_x V(x)^T \dot{x}_t < 0$ (from Eq.6.20) and $\bar{h}h > 0$. Since we modulate $\dot{x}_t$ by $(1 - h)$, sudden changes of h result in an acceleration of $-\dot{h}M_a\dot{x}_t$. This temporary energy generation (which is bounded) can either be neglected or handled by setting a limit on the increase of h based on the state of the system. The other solution is to avoid modulating $\dot{x}_t$ (as in Eq.6.1) and to use the following.

$$\dot{x}_d = \dot{x}_t + \dot{x}_a \tag{6.30}$$

This leads to a simpler energy analysis as follows.

$$\dot{W} = hF_e^T \dot{x} - \dot{x}^T (d_a \mathbb{I}_n - M_a f'(x))\dot{x} + d_a \dot{x}^T \tilde{f}(x) \tag{6.31}$$

In this formulation, the desired velocity generated by the DS is always present. This might be a drawback for cases where this velocity perturbs the human during $h = 1$ or deteriorate the compliant behavior. However, in cases where the human guidance has the purpose of small corrections, the presence of this velocity is beneficial. Moreover, in proactive scenarios, even during $h = 1$, it is necessary for the robot to not only rely on $\dot{x}_a$ but also generate and follow $\dot{x}_t$. It is intuitive to see that $\dot{x}_a$ accounts for passive-following behavior and $\dot{x}_t$ can account for pro-active following behavior during $h \neq 0$.

6.4.1 Resulting compliance at the force-level

The variation of h renders a variable-admittance control equivalent to the following.

$$\bar{M}_a \ddot{x}_a = -\bar{D}_a \dot{x}_a + F_e \tag{6.32}$$

where $\bar{M}_a = h^{-1}M_a$ and $\bar{D}_a = h^{-1}D_a$. Here, we have variable admittance control without any loss of stability which is usually the case in impedance controller. This is an advantage of admittance over impedance since we can arbitrary change the admittance ratio. Finally, the passivity of the close-loop system is investigated in Appendix 6.4.

The stiffness of the robot during the detection delay might appear inconvenient to the human user. While this is tolerable when the robot maintains a fixed position, the stiffness of the robot during a fast motion might undermine the comfort and safety of the user. The tracking performance of fast motion can be sacrificed by lowering the stiffness in order to avoid such

issues. To do this, we propose the following formulation for the admittance controller.

$$M_a \ddot{x}_a = -D_a \dot{x}_a + \tilde{h} F_e \qquad (6.33)$$

where

$$\tilde{h} = max\{\underline{h}(\dot{x}), h\} \qquad (6.34)$$

where $\underline{h}$ is a function based on the robot's velocity providing a minimum required compliance. This function can be of the following piecewise linear form.

$$\underline{h}(\dot{x}) = \begin{cases} 0 & \text{for} \quad \dot{x} < \underline{v} \\ (\dot{x} - \underline{v})/(\bar{v} - \underline{v}) & \text{for} \quad \underline{v} < \dot{x} < \bar{v} \\ 1 & \text{for} \quad \bar{v} < \dot{x} \end{cases} \qquad (6.35)$$

where below $\underline{v}$ no additional compliance is required and the robot focuses on tracking performance (unless human guidance is detected which increases h). For velocities higher than $\bar{v}$, the robot tracking performance in sacrificed (only if there are external forces) for safety issues. The linear interpolation part allows for a smooth transition and avoiding the human to experience sudden feeling of blockage or release.

As the initial step in this work, we only used diagonal damping matrices of form $D_a = d\,\mathbb{I}_n$ for simplicity. Similar to previous works Kronander and Billard (2016), we can provide a different damping behavior in the direction of $\dot{x}_t$ vs. other directions. Without any loss of passivity, we can have the following admittance behavior.

$$M_a \ddot{x}_a = -d_a^{\parallel} \dot{x}_a^{\parallel} - d_a^{\perp} \dot{x}_a^{\perp} + h F_e \qquad (6.36)$$

where $\dot{x}_a$ is decomposed into two parts: $\dot{x}_a^{\parallel}$ parallel and $\dot{x}_a^{\perp}$ orthogonal to $\dot{x}_t$ with their respective damping gains ($d_a^{\parallel}$ and $d_a^{\perp}$). The resulting damping matrix is

$$D_a = Q \Lambda Q^T \qquad (6.37)$$

where the columns of $Q \in \mathbb{R}^{n \times n}$ are unit vectors that span R^n and the first column is parallel to $\dot{x}_d s$. Λ is a diagonal matrix with elements equal to $d_a^{\perp}$ except the first one being $d_a^{\parallel}$. The stability and passivity analysis follows the same procedure, only $d_a^{\parallel}$ appears instead of d_a in Eq. 6.26. However, to have a different damping behavior in a specific direction of the space, we can use the following admittance formulation.

$$M_a \ddot{x}_a = -D_a \dot{x}_a + h G F_e \qquad (6.38)$$

where $G \in \mathbb{R}^{n \times n}$ is a diagonal matrix with different diagonal elements. Having these different input gain allows the admittance to exhibit different stiffness in different direction. Similarly, our DS-based admittance controller is also suitable to deliver task-specific compliant behavior.
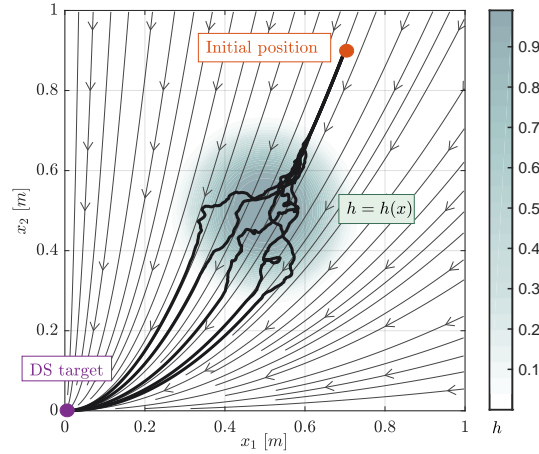
Figure 6.5 – State-dependent compliance through admittance control and state-dependent motion planning through DS. The robot reacts passively to the external force proportionally to h. The external forces are generated using a Gaussian noise. The simulation is repeated five time.

Consider the following controller.

$$M_a \ddot{x}_a = -D_a \dot{x}_a + H(x, \dot{x}) F_e \tag{6.39}$$

where $H : \mathbb{R}^n \mapsto \mathbb{R}^n$ modulates the robot's admittance based on the robot's state. This formulation allows the robot to vary its compliance in different region of the workspace. A simple example is illustrated in Fig. 6.5 where the robot provide a compliant behavior only in the designated region and focuses on the tracking of the DS velocities elsewhere. This mapping can be learned from demonstration and be used in this formulation with any loss of stability and tracking performance.

6.5 Illustrative examples

For our first example, we consider a one-dimensional problem using the following nominal dynamical system for motion generation.

$$\dot{x}_t = -kx \tag{6.40}$$

The results are shown in Fig. 6.6. In this simulation, the DS-impedance loop tries to bring x to zero from any arbitrary initial condition. We tested our algorithm against three types of external forces. In $t \in [0, 2]$, we apply zero-mean Gaussian noise ($\mathcal{N}(0, 1)$). As it can be seen, no energy is accumulated in the tank and h remains at 0. This disturbance is hence rejected and the system performs a perfect tracking of the dynamics generated by Eq. 6.40. In $t \in [3, 6]$, a simulated human applies a state-dependent force for 3 seconds with the intent to bring the
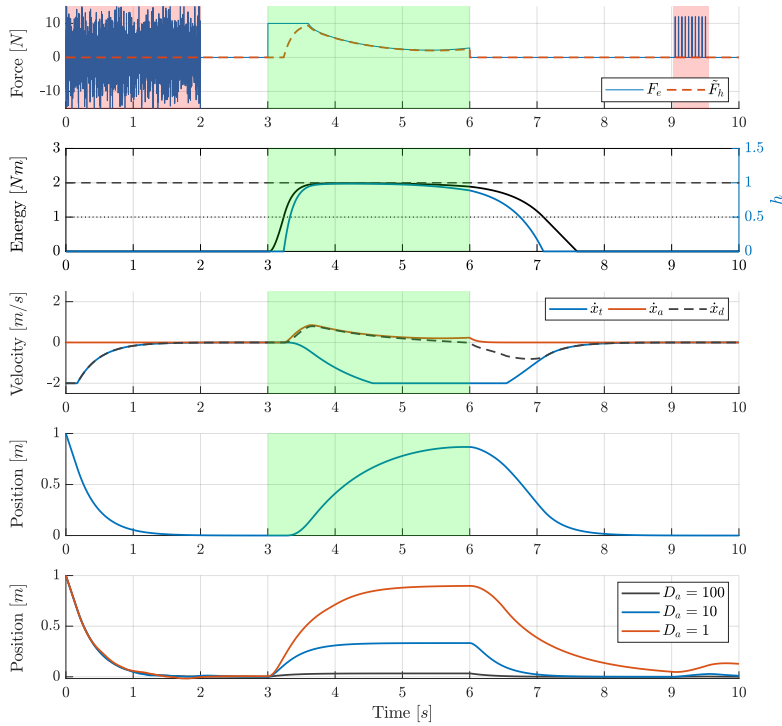
Figure 6.6 – A simulated interaction in a one-dimensional case. The robot rejects the external disturbances such as noises and shocks to deliver a satisfactory tracking behavior. Moreover, the robot detects the human guidance and complies to human intention as to reduce the required effort. Green and shades indicate the human guidance and disturbances respectively. The parameters are specified in Appendix B.3.1.

system to position $x = 1$, using the following applied force.

$$F_e(x, \dot{x}) = -20(x-1) - 10\dot{x} \quad 3 < t < 6 \tag{6.41}$$

The generated forces are saturated to $[-5, 5] N$. Due to the consistency of this external force, the energy increases and h smoothly approaches 1. It can be seen that the estimated human-force F_h, after a short delay, smoothly converges to F_e. As the result, the control loop transit to the admittance mode ($\dot{x}_d = \dot{x}_a$) This allows the simulated-human to reach its goal ($x = 1$) around $t = 6s$ through the expected compliant behavior. Upon human retrieval, the energy of the tank dissipate (due to $\tilde{P}_d$) and control mode switches to motion tracking $\dot{x}_d = \dot{x}_t$. This enables the robot to follow the motion perfectly and reach $x = 0$. At $t = 9s$, we apply a sudden transient forces to the robot ($F_e = 10$ for $5ms$ every $50m$). Due to the lack of consistency, this external force is rejected and the motion-tracking is preserved. The last subgraph shows the results of a fixed admittance controller using different damping gains. This graph clearly shows that the a proper gain for tracking and human-interaction are drastically different; i.e., 100 and 1 respectively. The intimidate values are also ineffective in delivering a satisfactory behavior. Usually, one behavior needs to be sacrificed for the other. One can think of traditional variable
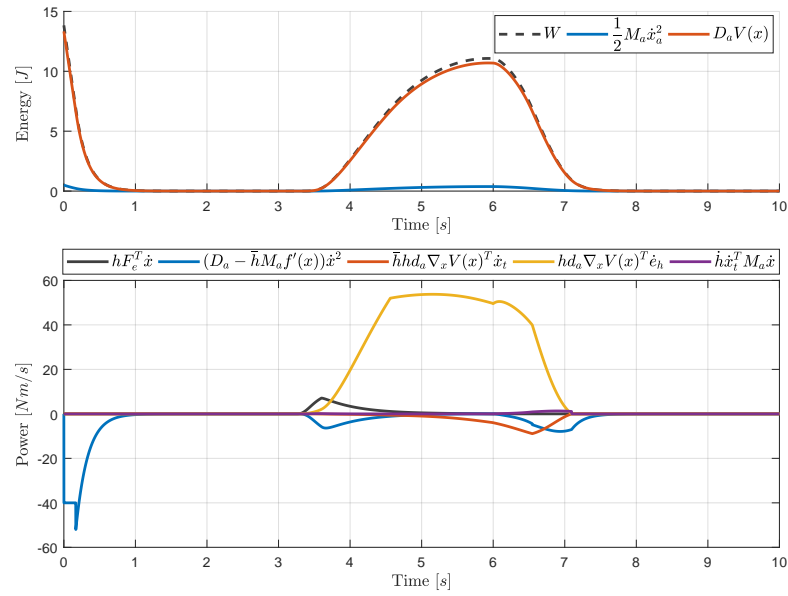
Figure 6.7 – The evolution of energy and power exchanges during the interaction in Fig. 6.6.
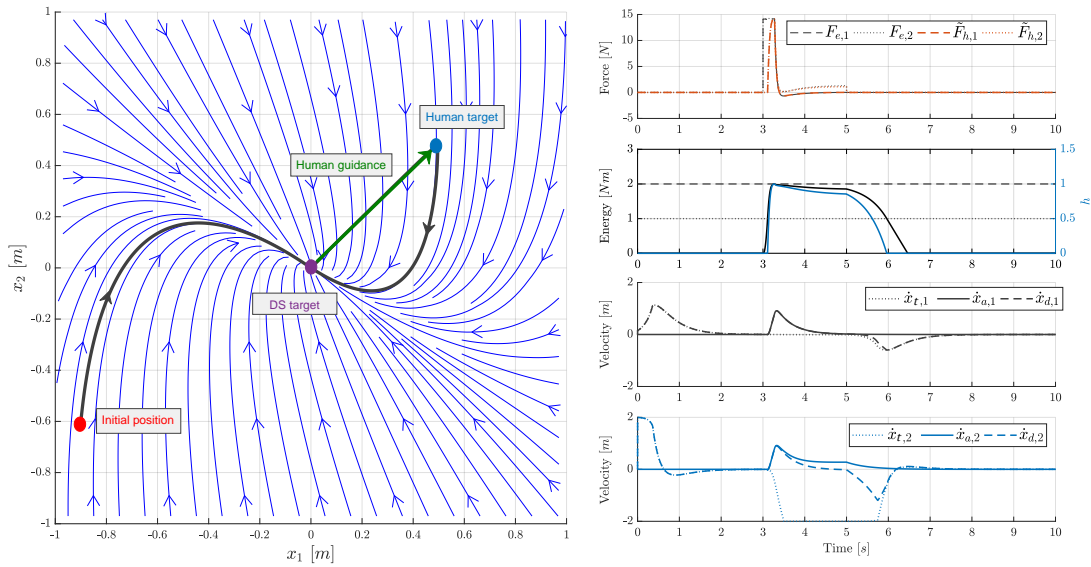
Figure 6.8 – A simulated interaction in a 2-dimensional case. The robot initially tracks the desired velocity generated by the DS. Upon detection of the human-interaction, the robot becomes compliant and passively follows the human motion. After the human-interaction, the robot returns to tracking mode using the DS. The parameters are specified in Appendix B.3.1.

admittance control for this case (i.e., varying D_a over time). However, as discussed before, obtaining a satisfactory tracking behavior and ensuring the stability is not trivial. For better understanding of the energy analysis in Section 6.4, the power exchanges for this simulation are illustrated in Fig. 6.7.

(a)   (b)
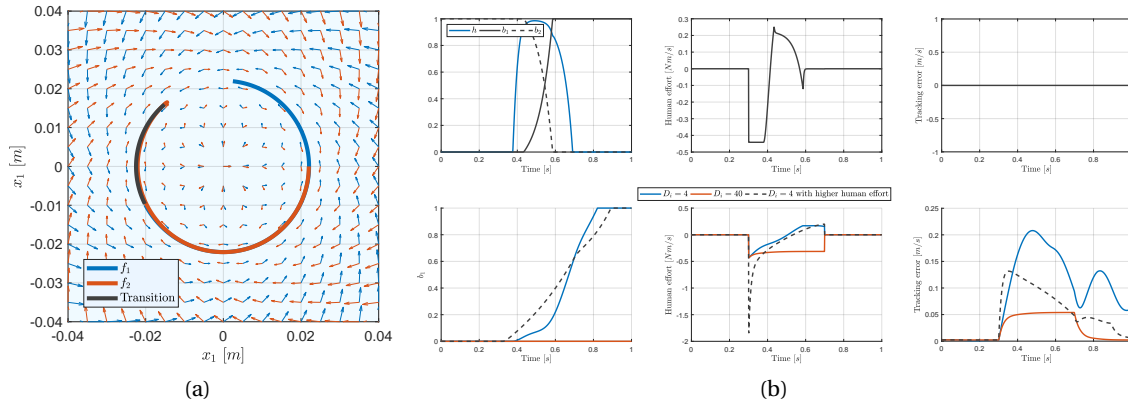
Figure 6.9 – The results for adaptive DS in simulation where the proposed algorithm is used to adapt the motion only to the detected human-guidance. The parameters are specified in Appendix B.3.1.

In our second example, we use a 2-dimensional system to better illustrate the reactivity of DS. Fig. 6.8 shows the simulation results. The robot starts in the tracking mode precisely following the DS vector field. In $t \in [3,6]$, human guidance is detected where the simulated human intends to go to $x = [0.5, 0.5]^T$. Upon detecting human guidance, the robot becomes compliant and the human can drive the robot with small forces (as shown immediately after the detection $t \in [3.5, 6]$). At $t = 6s$, the simulated-human stop excreting forces which results dissipating of the energy in the tank and vanishing h. This enables the robot to go back to motion-tracking mode and approaches the equilibrium point following the vector field. This interaction shows the reactivity of the DS where the generated desired trajectories are different before and after human guidance. This can be advantageous over simple methods where the human guidance are simply damped and the robot smoothly goes back to pre-interaction trajectories.

Fig. 6.9 shows the result for case where we apply motion adaptation using our previous method Khoramshahi and Billard (2018). In this simulated example, two DS are considered: f_1 and f_2 generating clockwise and anti-clockwise motions respectively. In this scenario, the robot starts performing f_2 and a simulated human joins the interaction at $t = 0.3$ and intends to perform f_2. To do so, the simulated human applies forces as $F_e = -20(\dot{x} - f_1(x))$. The first row of plots show the results for our variable admittance control. The first plot shows how the human guidance is detect where h approaches 1 between $t = 0.4$ and 0.6. The second plot shows the human effort starting at $t = 0.3$ and trying to decelerate the robot. After $t = 0.4$ (where the guidance is detected $h \simeq 1$), the human injects energy to demonstrate his/her intention (f_1). The last plot shows the tracking behavior which in this simulation assumed to be a perfect tracking case. The second row of plots shows our comparison with a fixed impedance controller. We tested three different conditions.

A low impedance ($D_i = 4$) results in switching across task, however, the tracking performance

of the robot is unsatisfactory. A High impedance ($D_i = 40$) results in satisfactory tracking behavior, however, the switching is not possible anymore due to limits of human forces ($2N$ in this case). The third case shows where the human can apply higher forces ($20N$) where the switching can take place. It can be seen that in all these three cases, the duration that human tries to decelerate the robot is longer than the variable admittance control. This also results in slower adaptation across tasks. This simulation clearly shows how both compliant and tracking behavior can be achieved through our variable admittance control with human guidance detection.

6.6 Experimental evaluations

For our experiments, we employ a *Clearpath ridgeback* mobile-robot with *Universal UR5* robotic-arm mounted on the top of the base; see Fig. 6.11b. Using the force-torque sensor (*Robotiq FT300*) mounted on the end-effector, we control the arm in admittance mode. For our motion planning, we trained several DS as illustrated in Fig. 6.11a. The details of the admittance control are provided in Appendix .B.3.2. To train these models, we collected 25 demonstrations per task where the human-user moved the end-effector of the robot. We tested our proposed method in the following three different scenarios.

6.6.1 Passive follower using a Null DS

In the first case, we use $\dot{x}_t = 0$ (i.e., $\dot{x}_d = \dot{x}_a$). In this manner, the robot maintains a fixed positions and only reacts to the human guidance. This case is useful when it is required from the robot to maintain the position of an object or a tool in the workspace. The results are shown in Fig. 6.10. The first plot shows the external forces where in $t \in [5, 10]$ and $t \in [25, 30]$ the robot was perturbed. It can be seen that these disturbances are not detected as human guidance and therefore rejected; i.e., the robot maintains its positions. During $t \in [15, 20]$ and $t \in [30, 35]$, human interacts with the robot as to move to a desired position. These human-interactions are shortly (i.e., after around $.5s$) detected and the compliant behavior is provided through admittance as the robot moves in accordance with external forces. Moreover, the comparison between desired and real shows that the robot provides a satisfactory behavior (RMS error of 0.02).

6.6.2 Compliant leader using a nominal DS

In the second case, we use one of the trained DS to perform a reaching task (i.e., *Reach right*). The results are shown in Fig. 6.12. The robot starts from an initial condition and follows the DS velocities to reach its target; i.e., $x = 0$. After reaching the target, the robot rejects the disturbances around $t = 10$ and maintains its position rigidly. Upon the human-guidance at $t = 15$, the robot becomes compliant so as to follow the human guidance passively. When the human retreats from the interaction at $t = 32$, the robot smoothly switches to motion-

planning mode and follows the DS velocities and consequently reach its target. The velocity profiles (plotted separately for each dimension) show how the desired velocity smoothly transit between admittance-velocities and DS-velocities.

6.6.3 Proactive follower using an adaptive DS

Finally, we present an adaptive case where the robot switches between several reaching tasks plotted in Fig. 6.11a. To have the proactive following behavior (i.e., while following, the robot recognize the human intention ands start injecting velocities), we changed our formulation to

$$\dot{x}_d = \dot{x}_a + \dot{x}_t \tag{6.42}$$

In this manner regardless of h (which only affects the admittance control), the robot tries to follow the DS-generated velocities. However, in this case, we use our adaptive mechanism previously presented in Khoramshahi and Billard (2018) to generate $\dot{x}_t$. Given a set of DS
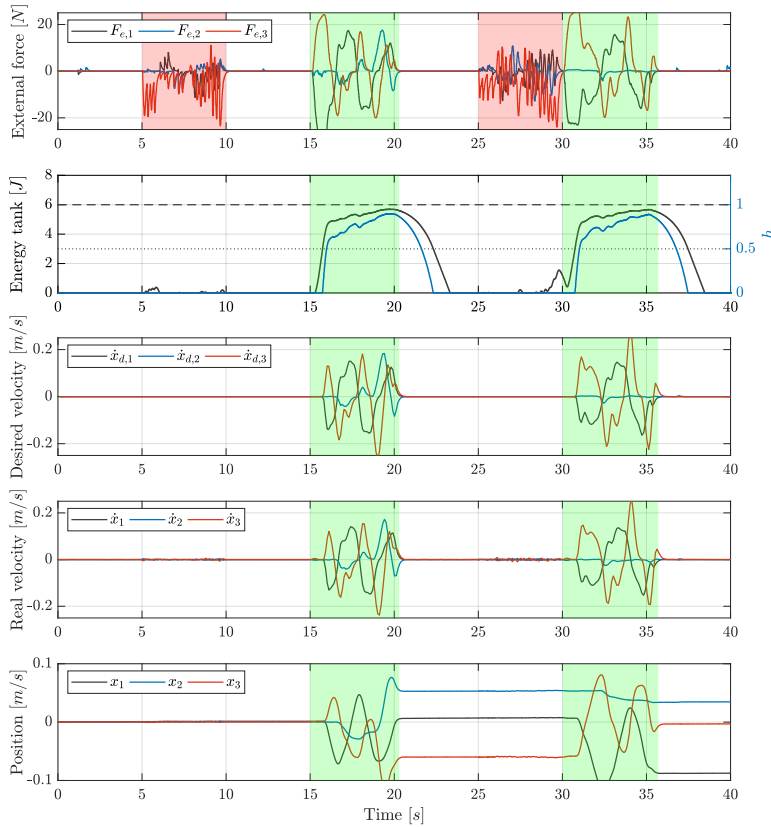
Figure 6.10 – The result of human-robot interaction in the case of null DS ($\dot{x}_t = 0$). A human guidance is presented to the robot and detected during $t \in [15, 20]$ and $t \in [30, 35]$. The disturbances ($t \in [5, 10]$ and $t \in [25, 30]$) are successfully rejected and the robot maintain its position.

for different reaching motions, the adaptive mechanism uses the most similar DS to the human-guidance. The results are illustrated in Fig. 6.13. The robot starts in the retreat task where it makes the workspace available to the human-user. Upon human-guidance, the robot becomes compliant and follows the human motion. While doing so, the robot adapts to the most similar DS (*Reach left* in this case). As human observes that his/her intended task is being performed, he/she leaves the interaction while the robot leads and performs the task autonomously. This transition repeats several times where the robot switches to different tasks. In one case (around $t = 31$), due to partial human-demonstration, the robot initially switch to a task that it is not intended by the user. Therefore, the human stays in the interaction and provides more demonstrations in order to make sure his/her intention is recognized by the robot. Moreover, the results show that disturbances are rejected successful and the robot only complies to the human guidance. Furthermore, we can see that the robot adapts its role based on the human-interaction form *stiff-leader* to *compliant-follower*, *passive-follower* and *proactive-follower*.

In a similar experiment, we designed the robot to reach for different drilling targets. The physical human-robot interaction using our framework is illustrated in Fig. 6.14. In the first 2 frames, the robot is executing its reaching motion for the upper drilling target indicated by a red-cross. In frame 3-4, an accidental shock occurs; i.e. the human-user drops a metallic wrench on the end-effector of the robot. Since this external force is not recognized as human-guidance, the robot remains stiff and maintains its drilling target. In frame 5, the human starts to interact with the robot. Upon recognition of human intentional forces, the robot

(a) Demonstrated trajectories.

(b) Desired trajectory for the end-effector.
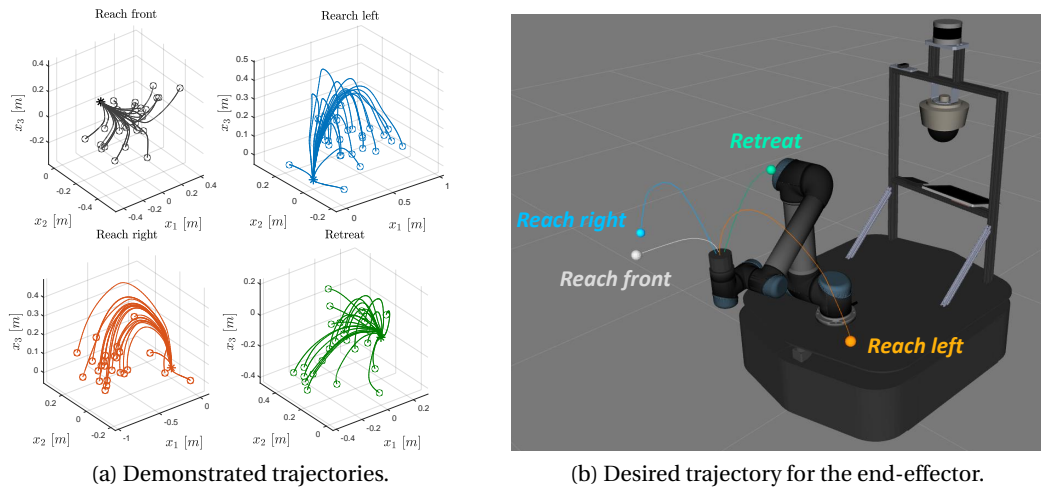
Figure 6.11 – The encoded task for the mobile robot using DS. (a) Generated desired trajectory using the trained DS systems for different reaching tasks. The square and star marker show the initial and target position respectively. (b) Illustration of Clearpath ridgeback mobile-robot with Universal UR5 robotic-arm. The motions are generated by the learned DS from the current position of the end-effector toward the corresponding attractor to perform a specific task.
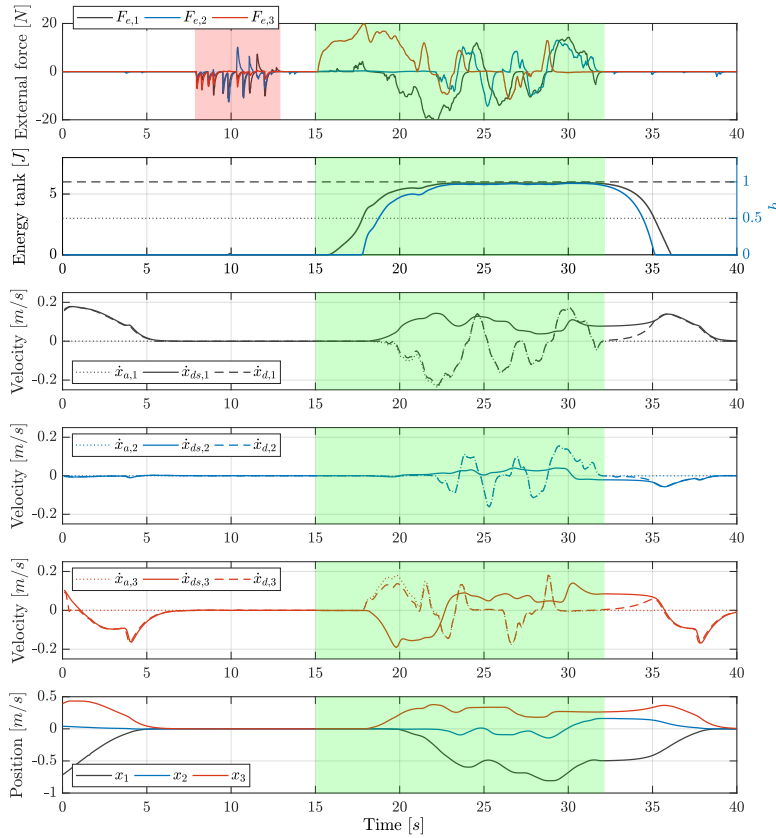
Figure 6.12 – The result of human-robot interaction in the case of a nominal DS (i.e., reaching a target position). The human-guidance is detected during $t \in [18, 35]$ where the human moves the robot compliantly in the workspace regardless of the DS-generated velocities.

complies to the human by introducing admittance-generated velocities. At this moment, the final velocity is a combination of DS (for reaching the upper drilling target) and admittance. Therefore, the robot behavior can be seen as a *compliant leader*. In frame 6, while being compliant toward the human, the robot recognizes the human intended task; i.e., to reach for the lower drilling target. At this stage, the robot behavior can be considered as a *proactive follower*. In frame 7, the human-user retreats from the interaction and the robot performs the task autonomously. In frames 8-11, the robot is acting as a *stiff leader* maintaining its target position and rejecting the disturbances. In frame 12, the robot provides compliant behavior upon human interaction.

6.7 Discussion and conclusion

In this work, we presented a simple detection algorithm for human-guidance during pHRI. We investigated our algorithm theoretically where we showed how external forces consistency (i.e., autocorrelation) can be used for detection of intentional forces. The simulation and experimental results show that this method is effective in distinguishing between dis-
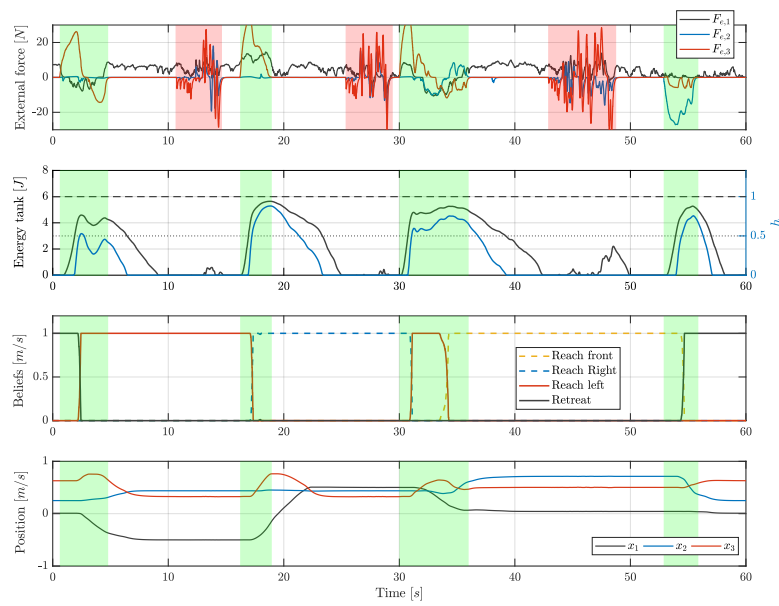
Figure 6.13 – The results for adaptive DS for the robotic arm where the proposed algorithm is used to adapt the motion only to the detected human-guidance.
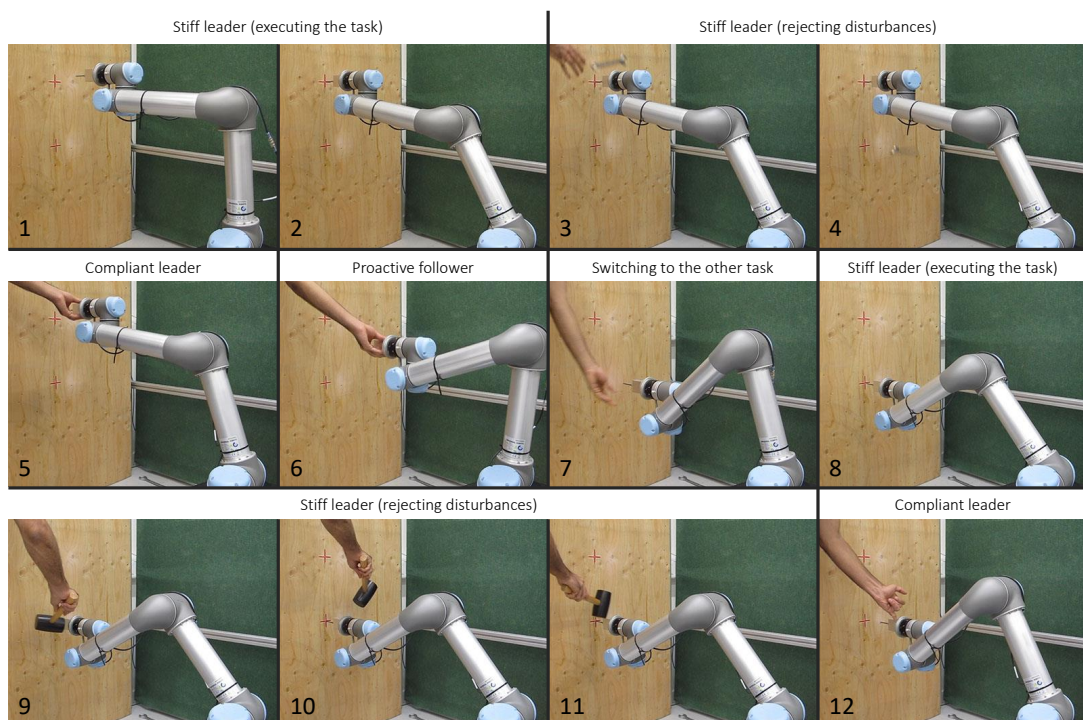
Figure 6.14 – Robotic role adaptation using DS-based admittance control framework. The robot is able to execute its task autonomously and reject disturbances for precise motion tracking. Upon human-interaction, the robot becomes a compliant and adapts to human-intended task.

turbances and human-guidance input. For our detection algorithm , no model of the robot and environment is required, and it is easy to implement (i.e., few algebraic equations). The transparency of its parameters (i.e., their physical meaning) allows for simple tunning in order to filter the disturbances and pass the human-guidance. Furthermore, we presented DS-based variable admittance controller as a tool to deliver both tracking and compliant behaviors. We varied the admittance simply through the *admittance ratio* (i.e., the input gain for the external forces). In this manner, we avoided raising typical instability issues due to the time-variability. Even though the variability of the admittance is limited (i.e., a fixed ratio between inertia and damping part), the resulting behavior is effective in rejecting disturbances and complying to human-guidance forces. Finally, we used the output of our human-detection algorithm (h) to vary the admittance controller yielding a robot that adapts its role based on the human-interaction. In the absence of human-guidance, the robot is autonomous (i.e., a stiff-leader) focusing on the motion tracking and executing the task, while in the presence of human guidance, the robot is a passive follower focusing on tracking human inputs. Moreover, we showed through experimental results that the proactive following behavior can be achieved using adaptive DS. We analyzed our method rigorously and provided sufficient conditions for stability and passivity.

In our detection algorithm for human-guidance, the speed and accuracy are controlled by E_m, E_t, and $\tilde{P}_d$. Lower values result in faster but less accurate detections where the built-up energy due to the disturbances passes the trigger level and is detected as human-guidance. Higher values, on the other hand, lead to more accurate but slower detection where the human is required to exert higher force for a longer time to pass the trigger level. This leaves the designer with a trade-off between speed and accuracy. One practical approach is to investigate the expected disturbances in the environment and set these parameters marginally higher as to filter them. Conversely, one can investigate the expected forces from the human-guidance and set the parameters marginally lower as to detect such guidances. Furthermore, this can be treated as a two-class classification problem which is on our list of future works. Moreover, the autocorrelation notion can be extended to nonlinear cases for early identification a specific force profile. This results in improvement in both detection speed and accuracy of the algorithm.

The admittance control with high-gain velocity control might not be suitable for stiff-contact situations. The delay introduced by the admittance results in unstable interaction with stiff surfaces. A solution for these scenario is to use impedance control instead of a high-gain velocity control. In Appendix C.2, we formulate and analyze this approach in terms of stability and passivity. This control structure is similar to *natural admittance control* proposed by Newman (1992). Hogan and Buerger (2004) shows that this controller is effective in rendering a desire admittance behavior while using high-impedance gain for tracking purposes. Furthermore, the detection algorithm can be extended to distinguish between human forces, hard-contact forces, and disturbances. As we presented the final contribution, in the next chapter, we provide the overall conclusions and discussions.

7 Conclusion

We started this dissertation by describing a fundamental need in physically collaborative robots; i.e., the *proactivity* in their interaction with human users. Proactivity is the ability to recognize other's intended motions and tasks and to act accordingly. In Chapter 1, we introduced the challenges regarding robotic proactivity with regard to 1) safety and compliance interaction, 2) prediction and adaptibility during the interaction, 3) recognizing and complying with the human-intended task, and 4) robustness toward environmental uncertainties. Moreover, in the first chapter, we introduced our approach in reaching robotic proactivity. We followed a state-dependent dynamical system approach throughout this thesis; both in modeling human behavior and designing new controllers. In Chapter 2, we reviewed the related works in the literature of human-human and human-robot interaction. In the subsequent chapters, we proposed several control methods and strategies for robotic proactivity. As the final chapter of this thesis, we summarize the main contributions along with their limitations. Furthermore, we provide discussions for overcoming these limitations that potentially shed lights for defining new directions for future research.

7.1 Contributions

In our first endeavor toward robotic proactivity, we investigated human motion coordination capabilities in Chapter 3. In that chapter, we focused on understanding and modeling human following capacities. For this purpose, we used an adaptive state-dependent dynamical system to explain the follower's behavior. Our results confirmed that individuals follow a prediction of their leaders motion rather than the current observation. Furthermore, we showed that by knowing the possible underlying tasks, individuals exploit contextual cues (such as gaze cues) to improve their motion coordination. More precisely, the follower's ability to recognize the leader's intended task improves the follower's proactivity.

In Chapter 4, we put our findings from the investigation of human behavior in practice. We proposed an online motion-adaptation method for parameterized dynamical systems. This

adaptive capacities allow the robot to proactively follow human demonstrations. Upon human-interaction, the robot adapts its motion-generator based on the human demonstrations. Therefore, instead of passively following the human demonstrations, the robots follows the adapted model which results in a proactive behavior. Such motion adaptation using dynamical systems allows the robot to perform the repetitive and cumbersome parts of the task while the human is able to supervise and modify the task as intended. Our robotic demonstrations for different tasks (polishing and pick-and-place) validate the claim that our proposed method allows the robot to comply and collaborate with the human user on the motion level.

In Chapter 5, we moved from adaptation on the motion-level to the task-level. We proposed a DS formulation to encode for several robotic tasks. This formulation allows the robot to transit across tasks in a smooth and stable manner. Moreover, we proposed an adaptation algorithm which enables the robot to recognize the human-intended task through the physical interaction. Therefore, upon human physical demonstrations, the robot recognizes the underlying intended task and smoothly switches to it. Our experimental evaluation using different robotic platforms confirms that this method is effective in producing proactive behavior; i.e., the robot complies and collaborates with the human on the task-level.

In Chapter 6, we addressed a challenge that was identified in the previously proposed approaches. We realized that it is crucial for the robot to distinguish between intentional and accidental forces; as it is undesirable to adapt to perturbations and accidental forces. Therefore, we proposed an algorithm that distinguishes between intentional and accidental forces. We also extended our control architecture to include an admittance part which generates velocities based on human forces. Using our detection algorithm, the robot is able to reject undesirable disturbances and complies with intentional forces. Our mathematical and experimental evaluation shows that our control strategy is effective in producing proper reactive behavior; i.e., the robot complies only with the human at the force-level.

7.2 Limitations and future work

As aimed initially in this thesis, we reached a proactive robotic behavior for physical collaboration with humans. Even though our dynamical system based approach enabled us for smooth, reactive, and adaptive interaction with human, the robotic tasks were fairly simple. In future works, we will consider more complex tasks which involve 1) physical contact with surfaces and force exertion, 2) kinematic constraints, 3) higher number of sub-tasks/goals, and 4) dynamic environments (e.g., with moving obstacles, robots, and humans). Our current intention-recognition approach is limited and needs to be extended to deal with such complex scenario. Potentially, besides the kinematics/dynamics of the physical interaction, other modalities such as vision can be used to better recognize the human intention and provide assistance. Moreover, it is crucial to assess the human-users' subjective evaluation of our

method. Such user studies can evaluate whether the interaction is natural and the human-user can rely on the robotic assistance.

In the following, we present the limitations of our approach in further details. Furthermore, we discuss possible research directions that can be considered as future work.

7.2.1 Understanding human proactivity for motion coordination

Here, we discuss the limitations that are associated with Chapter 3 where we studied the human ability to proactively coordinate with a leader.

Predictive models with nonlinear terms

In chapter 3, we used a linear dynamical system to investigate the human's following behavior. Our linear model was limited in explaining some aspect of the human behavior; e.g., over and undershoots. Using nonlinear terms in the predictive model can improve the model in creating similar overshoots and undershoots. However, adaptation for such nonlinear models (with a higher number of adaptive parameters) is technically challenging and not so suitable for human's behavior modeling. Technically, for such models with a high number of adaptive parameters, the convergence speed is sacrificed for robustness. Therefore, we argue that the over/undershoots in human's following behavior are artifacts of the tracking rather than the adaptation capabilities. In other words, such artifacts can be modeled and explained by using more realistic controllers rather than the PD controller that we employed in our model.

Moreover, in our model for the follower, we only used a constant delay to account for sensory system processing. In a more realistic setting, we can also consider perception errors modeled as a Gaussian noise. Adaptation of an internal model in this condition might also show robustness toward the uncertainties in perception and deliver a satisfactory tracking behavior.

Follower's visual attention

To understand how leader-intention recognition contributes to follower proactivity, we employed avatar-generated gaze cues in a mirror game setup. In our approach, we did not monitor explicitly the gaze of the human-follower. Instead, we used a questionnaire to assess how participants managed to divide their attention between tracking the robot's hand and looking at the robot's gaze; a five steps rating system (i.e., very easy, easy, normal, hard, very hard); see Appendix A. On average, participants found it easy to divide their attention between the hand and the gaze of the avatar. Nevertheless, incorporating eye trackers and monitoring the subjects' shifts of visual attention could contribute to a finer analysis of the pattern of attention. Such monitoring could provide information on when the human partners pays attention to the avatar/robot's face versus to the avatar/robot's hand.

Robot's gaze behavior

To best of our knowledge, our study in Chapter 3 is the first to investigate the effect of avatars' gaze behavior on social motor coordination. Thus, the results must be considered as exploratory where we used a straightforward gaze model in a simple interaction framework (i.e., the mirror game). We used a simple model for eye-hand coordination, which does not reproduce the exact dynamics of eye-arm coordination found in humans. Modeling more realistic eye-hand coordination for avatars might boost the behavioral realism and improves follower's behavior (Ramaiah et al., 2013; Kipp and Gebhard, 2008; Fu et al., 2008; Liesker et al., 2009). For avatars, reactive gaze behavior to the human gaze can also potentially enrich their realism (Yoshikawa et al., 2006). However, reaching a robust statistical conclusion in face of such a complex behavior of the avatar requires more thorough experimental design with a larger sample size. In our case, we benefited from our simple gaze model. We reached the robust and interpretable results that enabled us to elaborate on effects of gaze on the follower's proactivity.

Metrics and statistical power

To analyze the human's coordination behavior, we used two metrics: reaction time and frequency-dependent-phase. Both metrics captured the beneficial effects of gaze cues. We believe that the second metric was introduced for the first time in this study. Due to a higher effect size in this metric (the entire frequency domain), however, a larger sample size is required to reach substantial statical power in order to draw significant conclusions. Future studies should consider eye tracking to correct for the participants' level of attention to the avatar's gaze in the statistical inferences.

Embodiment: avatar vs. robot vs. human

The embodiment of artificial agents plays an important role in their interactions with human partners. Many works in the literature on social robotics explore this feature. For example, the presence of robotic platforms has been considered a key element in evaluating therapy in the case of autism spectrum disorders (Cazzato et al., 2015). Moreover, Zhao et al. (2016) have recently shown that a robotic referential gaze leads human partners to take the robot's visual perspective. We share the same belief that embodiment can enhance the sense of affiliation. However, it is interesting to see that in our study, a gaze of a simulated robot on a screen can still elicit a sense of realism in the human partner. Replicating the same experiment using the humanoid robot, such as the iCub, in comparison with the avatar case, is an interesting investigation where we can study the difference between simulated and real platforms in the context of social robotics.

The mirror game with physical coupling

In Section 2.1.4, we discussed our rationale for investigating human proactivity using the mirror game framework where the interactions were non-physical. This was a practical choice for this thesis since the focus of the studies in Chapter 3 was on the human proactivity at the motion-level and task-level (rather than force-level). Moreover, the proposed frameworks in the literature of pHRI are limited to point-to-point movements (with known initial and final positions) whereas, in our case, the leader's motions were unconstrained and unknown to the follower. Nevertheless, the mirror game framework can be extended to include the physical coupling between the leader and the follower. For instance, the two individuals can play the mirror game through two haptic devices which are virtually coupled as implemented in Takagi et al. (2017). Such framework can enable us to answer more in-depth questions regarding joint physical interactions. For instance, it would be interesting to investigate whether the follower's tracking behavior (proactivity at the motion-level) and partners' stiffness (proactivity at the force-level) are interlinked.

7.2.2 Designing robotic controllers/algorithms for proactivity

In this part, we discuss the limitations that are associated with Chapter 3-6 where we implemented several robotic strategies to reach proactivity in interactions with a human user.

Designing parametrized dynamical systems

In Chapter 4, we used geometrical transformations (scaling, rotation, and translation) as a mean to modify a robotic task. We showed that such simple transformations are sufficient for simple tasks such as polishing and pick-and-place. Nevertheless, in complex scenarios, the human-intended modification might be indescribable using geometrical transformation of the dynamical system. This issue can be addressed in the learning phase where we directly learn a parameterized DS from demonstrations. For this purpose, the human demonstrates all possible variations of the task with their corresponding label (i.e., the parameter value). For instance, consider the human executing a task with different level of risk-averseness. In this case, each demonstration will consist of $\{x, \dot{x}, \theta\}$; i.e., position, velocity, and θ as the provided label for risk-averseness. Given such extended demonstration, we can learn the DS as $\dot{x}_d = f(x; \theta)$ directly.

Combined motion and task adaptation

In Chapter 4 and 5, we proposed two similar yet distinct approaches to adapt the motion (generated by a single DS) and the task (selected among a series of DS) respectively. It would be of particular interest for further flexibility in robotic motion-planning if the two approaches could be combined: upon human interactions, the robot recognizes whether to fine-tune the current task or to switch to a different one. Indeed, the two adaptive mechanisms can be run

in parallel. However, it is important to safeguard the system from fluctuations (between the adaptation of motion vs. task) and generating undesirable motions. Therefore, it is logical to use lower adaptation rates to ensure robust transitions. Furthermore, it might be necessary to impose a certain set of constraints on the these mechanisms running in parallel; e.g., the activation of one inhibits the other.

From adaptation to learning

Moreover, our adaptive mechanism has the potential to be extended to an interactive learning algorithm where the robot learns a new task based on a mixture of given dynamical systems. For instance, one can consider dependencies for adaptive parameters; e.g., $b_i(x, s)$ depending on the state (x) and other possible contextual signals (s). These dependencies can be learned or approximated while our adaptive mechanism provide an estimation for the parameters. We provide a simple extension in Appendix C.4 where the robot learns (through adaptation) how to combine different primitive dynamics to learn a new task. Such online learning from adaptation has interesting implications in robotic systems. In short, the robot learns from its adaptive behavior, and conversely, uses the learned behaviors in its adaptation mechanism. This interplay between adaptation and learning enables the robot to express what it learns during the interaction and gradually reduces the human supervision and effort. This approach can be useful to move from *learning from demonstration* (in an offline sense) to *learning from interaction* (in an online sense).

Intention misrecognition

Human behavior has a crucial impact on the performance of our adaptation mechanism in Chapter 5; in general, on any online algorithm with a human-in-the-loop. For instance, we experienced cases where the human user falsely assumes that the robot recognized his/her intention and stops the demonstration prematurely. This potentially leads to a misrecognition which we impute more to the human-user rather than the algorithm. Nevertheless, this case shows us the importance of transparency where the human user has a precise inference of the robot's state. As a future work, using synthesized speech or a display indicating the recognized task can improve the transparency of the robot for the human user.

Another important factor for proper recognition of the human-intention is the number of tasks: the condition for "distinguishability" worsens as the number of task increases. As discussed before, lowering the adaptation rate (and relying on a longer portion of the human demonstration) can mitigate the situation. Nevertheless, finding theoretical bounds for the number of tasks as well as the adaptation rate can be beneficial in designing such adaptive systems for more realistic scenarios when the robot knows how to perform numerous tasks.

Motion vs. force-based intention recognition

In Chapter 4, we considered a motion-based intention-recognition strategy. In our adaptation mechanism, we utilize end-effector velocity directly and its position indirectly; i.e., as the input of the DS. Moreover, a certain level of error is tolerated for the execution of our task which does not lead to task-failures. In Chapter 6, we considered force-based intention recognition which is more suitable for delicate tasks where a slight deviation from desired trajectories might lead to failure. However, our approach is limited to distinguishing only between intentional and accidental forces. The ability to recognize the underlying intended-task based on haptic information is useful capacity for collaborative robots. For instance, the robot feels a force at its end-effector and recognizes that the human intends to perform an specific task. Therefore, the robot can temporally stay rigid toward external perturbations while interpreting the forces as to recognize the human intention and carefully plan for the switching. Takeda et al. (2005) and Stefanov et al. (2010) propose statistical models for force-based intention recognition that can be used for such further implementations.

Task-adaptation in redundant robot

Our adaptation mechanism is not limited to non-redundant robots and can be applied to any subset of robotic coordinates. In our experiments, the null-space of the robotic robot was set to a specific configuration (e.g., *elbow-up* for the robotic arm) while the end-effector orientation was set to a fixed angle (e.g., pointing down for robotic arm). Nevertheless, the motion for the end-effector orientation can be embedded into the DS and/or take part in the adaptation. For instance, the motions for the orientation can be generated by and slave-DS and adaptation only take place at the level of linear-velocity commanded by the master-DS. To have adaptation using both position and orientation components, a similarity metric that includes both sub-spaces is then necessary.

Kinematics, dynamics, and other constraints

In this thesis, we treated the robot as a mass-point without any constraints on its kinematics, dynamics, actuator capacities, workspace limits, and so on. However, in more realistic scenarios, such as walking humanoid robots, respecting such constraints is crucial for achieving the desired behavior. Indeed the output of the adaptive dynamical system (i.e., the adapted desired velocities) can be modified to satisfy such constraints. Such modifications (the difference between the original desired velocity and the modified one) might be included or excluded in the final tracking error to be used as the adaptation signal. Including constraint-induced tracking errors might adapt the DS toward respecting the constraints (i.e., treating the modifications due to the constraints similarly to the human demonstrations), but it may generate behaviors that are not aligned with human intentions. Furthermore, instead of modifying the adapted parameters to satisfy the constraints, another approach is to reformulate the adaptation as a constrained optimization problem. However, this might be a challenging

problem since the relation between the adaptive-parameters and the constraint-parameters (often the robot's joint position, velocity, and acceleration) is not straight-forward.

DS-admittance-impedance control and contact tasks

To answer the limitations associated with the impedance control (namely, the coupling between tracking and compliance behavior), we introduced the DS-based admittance control in Chapter 6. However, the admittance approach has its own limitations; mainly, low-performance (and unstable) behavior in interaction with stiff environment. This issue arises from the time-delay introduced by the admittance block; time integration of forces/acceleration to obtain the velocity. From a design perspective, this issue can be mitigated by increasing the control frequency and improving torque-force sensor precisions. From a control perspective, using impedance control (to track the admittance-generated velocity) instead of high-gain velocity controller can improve the robot performance in contacting hard surfaces. We provide a preliminary mathematical formulation for this control structure in Appendix C.2. From an algorithmic perspective, the robot can recognize hard contacts and adapts its impedance and admittance behavior accordingly. We discuss this further in the next subsection. Developing and evaluating this control structure can be an interesting future direction.

Distinguishing between human and hard contact forces

In Chapter 6, we propose an algorithm to distinguish between intentional and accidental forces. To this end, we measure the consistency of the external forces with the assumption that the intentional forces are consistent over a period of time. Our experimental evaluations show that this method is effective in complying to a human user and rejecting undesirable disturbances. Nevertheless, the algorithm cannot distinguish between a human user and a hard contact where both cases leads to consistent forces. To overcome this, one can extend the algorithm to account for difference between the two cases. By modeling the contact dynamics, one might be able to distinguish between a hard contact (which is passive and static) and a human user (which is active and dynamic).

Realism of a human-avatar interaction using avatar gaze cues

In the study reported in Chapter 3, subjective assessment of the avatar's realism was assessed by administering a post-hoc questionnaire. Here we investigate whether introducing active gaze behavior for avatars makes them more realistic and human-like (from the user point of view). As mentioned in Chapter 3, 37 subjects participated in 8 trials of the mirror game. Each subject performed the game in the two conditions (with and without gaze cues). In this within-subject study, the order of the conditions was randomized across participants, and subjective assessment of the avatar's realism was assessed by administering a post-hoc questionnaire. This questionnaire is presented in Fig. A.1. In the following, we discuss the results obtained from this questionnaire in relation to the quantitative assessment reported in Chapter 3.

Please specify the level of difficulty in each condition.

	Very Easy	Easy	Normal	Hard	Very hard
"No gaze" condition					
"With gaze" condition					

How do you rate the behavioral similarity between the robot and the human? (5 for highly human-like behaviour)

	1	2	3	4	5
"No gaze" condition					
"With gaze" condition					

How hard was it to divide your attention between the gaze and the hand?

	Very Easy	Easy	Normal	Hard	Very hard
"With gaze" condition					

Figure A.1 – The questionnaire used post-hoc to the human-avatar experiment.

Figure A.2 – Distributions obtained from the answers to the questionnaire. (A) Difficulty in the "no gaze" condition. (B) Difficulty in the "gaze" condition. (C) Changes in the subjects' opinion from the "no gaze" to the "gaze" condition. (D) Similarity to human behavior in the "no gaze" condition. (E) Similarity to human behavior in the "gaze" condition. (F) Changes in the subjects' opinion form the "no gaze" to the "gaze" condition. In these plots, ratio is calculated by the number of participants in each level divided by the total number of participants.

A.1 Gaze cues lead to natural and cooperative interactions

Analysis of the subjective evaluations from the questionnaires reveals that, in the presence of gaze cues, participants found it not only more human-like/realistic, but also easier to interact with the avatar. Fig A.2 summarizes the response distribution for the first four questions of the questionnaire. Fig A.2.A shows that in the absence of gaze, most of the subjects found it slightly difficult to follow the avatar. whereas, Fig A.2.B shows that, in the presence of gaze, following the avatar is perceived as rather easy. Fig A.2.C shows how presence of gaze cues affected participants' opinion on the level of difficulty. The majority of subjects (60%) perceived the mirror game as easy (by either 1 or 2 steps) in the *gaze cues* condition; see Fig A.2.C. The analysis of variance, presented in Fig. A.3, shows that opinions are significantly shifted toward low difficulty [$F(1,35) = 5.478$, $p = 0.025$].

The second row of Fig A.2 shows subjects' responses to the question about how similar the participants found the robot's behavior compared to human behavior. Fig A.2.D shows a bell-shaped distribution for similarity index in the absence of gaze whereas Fig A.2.E shows a skewed distribution in the presence of gaze implying a high similarity to human behavior when the avatar uses its gaze actively. Fig A.2.F illustrates how presence of gaze cues affected participants' opinions on the level of realism. A majority of subjects (71%) perceived the avatar as more human-like (by either 1, 2, or 3 steps) in the *gaze cues* condition; see Fig A.2.C. The analysis of variance (Fig. A.3) shows that opinions significantly shift toward high realism [$F(1,35) = 17.897$, $p = 0.000$]. In summary, Fig A.2 shows that use of gaze cues made the

interaction easier, and elicited the avatar to be perceived as more human-like and realistic.

Source		Model I					Model II				
		Type III Sum of Squares	df	F	Sig.	Partial η^2	Type III Sum of Squares	df	F	Sig.	Partial η^2
Condition	ReationTime	.003	1	9.445	.004	.213	.001	1	3.933	.056	.109
	Similarity	9.976	1	17.897	.000	.338	6.815	1	12.884	.001	.287
	Difficulty	3.625	1	5.478	.025	.135	3.896	1	5.578	.024	.148
Order	ReationTime	0.000	1	.023	.881	.001	.001	1	1.942	.173	.057
	Similarity	.138	1	.248	.621	.007	1.306	1	2.469	.126	.072
	Difficulty	.382	1	.577	.453	.016	.634	1	.907	.348	.028
Age	ReationTime						.002	2	2.996	.064	.158
	Similarity						1.433	2	1.355	.272	.078
	Difficulty						.745	2	.534	.592	.032
Gender	ReationTime						.000	1	.929	.342	.028
	Similarity						1.418	1	2.680	.111	.077
	Difficulty						.101	1	.145	.706	.005
Error	ReationTime	.011	35				0.009	32			
	Similarity	19.510	35				16.926	32			
	Difficulty	23.159	35				22.352	32			

Figure A.3 – The results of the Repeated Measures ANOVA. In each condition (i.e., *gaze cue* and *no-gaze cue*), the three different measurements done are: 1) the reaction time, 2) the perception of the difficulty of the game, and 3) the perception of the human-similarity. In *Model I*, the effects of conditions and the order of the conditions are studied. In *Model II*, the effects of age and gender are also investigated.

Furthermore, Fig. A.4 shows the Levene's test of equality of variances for the ANOVA analysis in Fig. A.3. This condition is only violated for *Similarity* measure. This was expected as the variances for the two distributions in Fig A.2.D and E are clearly different. For this case, using a non-parametric test (pairwise Wilcoxon Signed-Rank test) shows that the participants rated the gaze condition significantly higher [$z = -3.3234$, $p < 0.01$].

Condition		Model I		Model II	
		F	Sig.	F	Sig.
No gaze	ReactionTime	.351	.981	.383	.971
	Similarity	1.490	.288	1.159	.442
	Difficulty	1.795	.197	1.733	.212
With gaze	ReactionTime	.440	.948	.496	.918
	Similarity	5.577	.008	2.282	.112
	Difficulty	1.289	.373	1.246	.394

Figure A.4 – Equality of variances. The Levene's test of equality of error variances for *Model I* and *Model II* presented in Fig. A.3. For both models df1=28 and df2=8.

In our analysis, no significant effects were detected due to age, gender, and the order of the conditions on the subjective perception. However, we observed a significant effect on reaction time based on the age [$F(1,32) = 2.996$, $p = 0.064$]. In this analysis, to study the effect of age, the participants were categorized in three groups as illustrated in Fig. A.5a. The post-hoc analysis in Fig. A.5b shows that the *Low* group benefits less from the gaze cues compared to *High* group. This comparison is illustrated in Fig. A.6.

Split	range	Number of Participants
Low	[18-19]	11
Mid	[20-22]	11
High	[23-39]	15

(a)

Age (I)	(J)	Mean Difference (I-J)	Std. Error	Sig.	95% Confidence Interval Lower Bound	Upper Bound
Low	Mid	.0134	.0100	.191	-.0071	.0339
	High	.0193	.0093	.047	.0002	.0384
Mid	Low	-.0134	.0100	.191	-.0339	.0071
	High	.0059	.0093	.531	-.0131	.0250
High	Low	-.0193	.0093	.047	-.0383	-.0002
	Mid	-.0059	.0093	.531	-.0249	.0131

(b)

Figure A.5 – a) The split performed on age for the ANOVA analysis in Fig. A.3. b) The post-hoc test for the detected effect of age on the reaction time in Fig. A.3. The multiple comparisons are done based on LSD method. The corresponding distributions are plotted Fig. A.6.
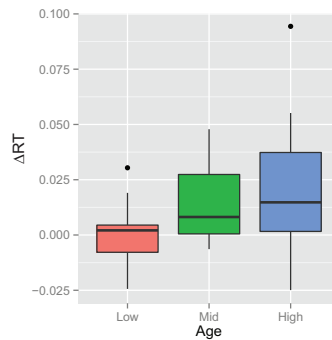
Figure A.6 – The reaction time improvement due to the gaze cues across age. The ANOVA analysis in Fig. A.5b showed that the first group (*Low*) and the last group (*High*) are significantly different.

A.2 Correlation analysis between cooperation and realism

To determine if perception of difficulty (cooperative behavior) and human-likeness (realism) are correlated, we computed a contingency table, see Fig. A.7. This table is computed based the participants' opinions about their performances in the *gaze cues* condition compared to the *no-gaze cue* condition. Fig. A.7 shows that a majority of participants (sum of diagonal elements: 53%), who found the avatar more realistic in the presence of gaze cues, also found the interaction easier. However, no significant dependency between difficulty and realism was detected using Spearman's correlation test in this table.

		Realism Lower	Similar	Higher	Total
Difficulty	Harder	5%	0%	14%	19%
	Similar	3%	5%	14%	22%
	Easier	11%	5%	43%	59%
Total		19%	10%	71%	100%

Figure A.7 – Contingency table for effect of gaze cues on participants' opinion on the difficulty of the interaction and the realism of the avatar.

A.3 Consistency between perceived and measured performance

To determine whether the participants' actual performances are consistent with their impressions, we analyzed their reaction times with respect to their responses in the questionnaire. Fig A.8 compares RT improvements (due to the gaze) for the two groups: (1) the participants who found it harder to follow the avatar with gaze cue, (2) the rest of participants. The ANOVA reveals that these two groups are significantly different $[F(1,34) = 5.495, \ p = 0.025]$; see *Model I* of Fig. A.9 for more details. This means that participants who stated that it is harder to follow the avatar in the presence of the gaze cues, actually had a slower reaction time in the *gaze cues* condition.
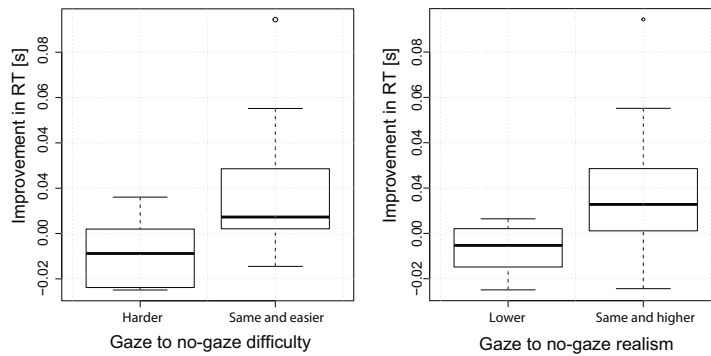
Figure A.8 – Participants' actual performance vs. their perception. Boxplots of ΔRT for the participants who found it (Left) harder to follow with gaze cues compared to the rest of the participants, and (Right) less human-like with gaze cues compared to the rest of the participants.

Crosschecking the ΔRT with the results for realism from the questions reveals interesting facts: The participants who found the presence of gaze cues less human-like have significantly $[F(1,34) = 6.084, \ p = 0.019]$ lower performances in the *gaze cue* condition; see Fig A.8(Right) and *Model II* of Fig. A.9 in the Appendix for more details. Based on this analysis, we can infer that the sense of realism and cooperation (level of difficulty) are related; i.e., cooperation contributes to affiliation and vice versa.

Furthermore, we also asked the participants to report their attentional workload in the questionnaire. The distribution obtained from the answers concerning the division of attention between avatar's gaze and hand is illustrated in Fig. A.10a. In Fig. A.10b, we compare the RT_g distribution of participants who found it hard to divide their attention between the avatar's gaze and hand vs. the rest of the participants. The ANOVA analysis in Fig. A.11 showed that the difference in these distributions is significant. This result shows that the individual who had difficulty dividing their attention between the avatar's gaze and hand had a lower performance in terms of reaction time.

Model		Type III Sum of Squares	df	F	Sig.	Partial η^2
1	Condition	.000	1	1.209	.279	.034
	Order	.000	1	.008	.929	.000
	Diff_dummy	.002	1	5.495	.025	.139
	Error	.009	34			
2	Condition	.000	1	1.087	.304	.031
	Order	.000	1	.008	.930	.000
	Sim_dummy	.002	1	6.084	.019	.152
	Error	.009	34			
3	Condition	.003	1	11.180	.002	.247
	Order	.000	1	.344	.561	.010
	Att_dummy	.001	1	1.911	.176	.053
	Error	.010	34			

Figure A.9 – Crosschecking the result of the motion capture (i.e., RT) with the result of the questionnaire using repeated measures ANOVA. In *Model I*, the effect of perception of difficulty on RT is studied. *Diff_dummy* is 0 for the participants who found it harder to follow the avatar with gaze cue, and 1 for the rest of the participants. In *Model II*, the effect of perception of similarity on RT is studied. *Sim_dummy* is 0 for the participants who found the presence of gaze cues less human-like, and 1 for the rest of the participants. In *Model III*, the effect of attention load on RT is studied. *Sim_dummy* is 1 for the participants who found it very easy, or easy to divide their attention between the avatar's gaze and avatar's hand, and 0 for the rest of the participants.
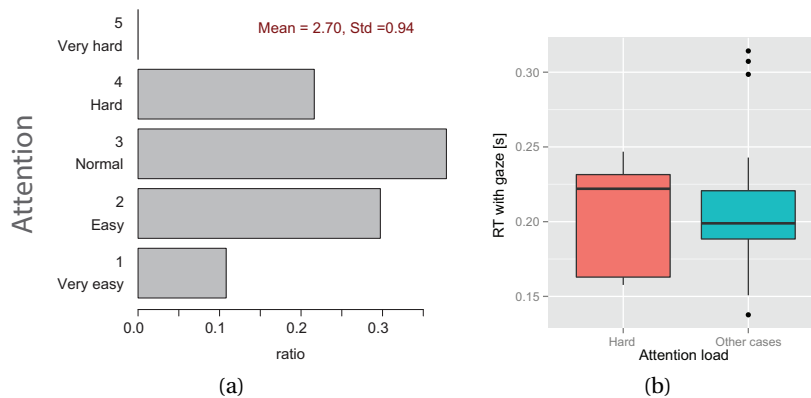
Figure A.10 – a) Participants' attentional workload. The distribution obtained from the answers to the questionnaire concerning the division of attention between avatar's gaze and hand. b) The RT in *gaze cue* condition vs. attention. The RT_g distribution of participants who found it hard to divide their attention between the avatar's gaze and hand compared to the rest of the participants. The ANOVA analysis in Fig. A.11 showed that the difference in these distributions is significant.

Source	Type III Sum of Squares	df	F	Sig.	Partial η^2
Corrected Model	.006	2	1.857	.172	.098
Intercept	1.460	1	898.525	.000	.964
Order	.000	1	.007	.935	.000
Att_dummy	.006	1	3.425	.073	.092
Error	.055	34	.002		
Total	1.648	37			
Corrected Total	.061	36			

Figure A.11 – The effect of attention of the RT. The results of the univariate ANOVA to study the effect of attention on the RT in the *gaze cue* condition. *Att_dummy* is 1 for the participants who found it very easy, or easy to divide their attention between the avatar's gaze and avatar's hand, and 0 for the rest of the participants; see Fig. A.10b. Moreover, Levene's test indicated equal variances [$F(14, 22) = .743, \; p = 0.713$]

A.4   Conclusion

The results of the questionnaire showed that participants perceived the avatar's gaze cues behavior not only as cooperative, but also human-like and realistic. Moreover, we observed that participants perception of similarity and cooperation is correlated with their performance in the game. This suggests that human-similarity, cooperativeness, and the sense of affiliation toward avatars, are highly interlinked. The results of this study could help us design computer-assisted cognitive-remediation therapy for pathologies with abnormal gaze and motor behavior such as schizophrenia. More specifically, these findings may support the design of similar games for studying deficiencies in the ability to interpret other people's gaze, as displayed by individuals suffering from schizophrenia and autism spectrum disorders (ASD) Jayasekera et al. (1996); Langdon and Ward (2012); Roux et al. (2014); Paus (1991). Interpersonal synchrony provides an important foundation for social interaction, in which recent studies suggested that people suffering from schizophrenia and ASD also have deficits in motor coordination Fitzpatrick et al. (2013); Raffard et al. (2015); Varlet et al. (2012, 2013). A recent study in schizophrenia found a causal relationship between impaired attention toward gaze orientation and deficits in theory of mind Roux et al. (2014). The version of the mirror game offered in our study, in which gaze is used as an active cueing device, could serve to design therapeutic games whereby patients are encouraged to process gaze information in order to increase motor synchrony during interactions. Improving interactional synchrony in schizophrenic patients, when engaged in dyadic games with a healthy partner, is shown to be beneficial for the patient and partner alike, as it also increases the motivation and sense of affiliation in the healthy partner Raffard et al. (2015). Previous studies have already shown that schizophrenia patients can benefit from attentional-shaping procedures displayed by a therapist, to enhance neurocognition and functioning Silverstein et al. (2001); Combs et al. (2008); Hooker et al. (2012), or being instructed to pay more attention to facial areas that

contain information about a displayed emotion to enhance emotion recognition Drusch et al. (2014). However, the use of an avatar for therapy in place of a human is advantageous in that the avatar provides a consistent and reliable feedback/behavior without the presence of a therapist.

B Technical details

B.1 Technical details for Chapter 3: avatar gaze control

The following figure (Fig. B.1) shows the control parameters used for robotic avatar behavior.

Parameter	setting
Duration of the,trajectory for the neck actuator	1.0 s
Duration of the,trajectory for the eyes actuator	0.4 s
Oculo-collic reflex,(OCR) gain	0.0
Vestibulo-ocular,reflex (VOR) gain	0.0
Neck roll	Blocked
Neck yaw	[-10,+10] deg
Neck pitch	[-15,+15] deg
Tolerance to gaze at,the target with the neck	5 deg

Figure B.1 – Parameters used in the iCub gaze controller.

B.2 Technical details for Chapter 5: task-adaptation

The adaptation and motion generation is running at 300Hz for both experiments. The control loop of the impedance controller of LWR and the velocity controller of UR5 are running at 200 and 125Hz respectively. The motion planning for all cases is considered in the Cartesian space i.e, the position and the linear velocity of the end-effector (xyz). The orientation of the end-effector is controlled on a set-point. Moreover, the measured velocities are low-pass-filtered with cutoff frequency around 30Hz. In both experiment, we set the control gains experimentally to have a practical balance between compliance and tracking.

B.2.1 DS parametrization for manipulation tasks

The linear polish is generated by the following dynamics:

$$\dot{x}_d = 0.1\,\overrightarrow{p} - 0.8e^{\perp} \tag{B.1}$$

first the first term induce a velocity in the direction of the line and the second term generate a velocity (saturated at $0.25m/s$) to correct for deviation from the line. The direction $\overrightarrow{p}$ between two end-points ($[-.54, .25, .1]$ and $[-.54, -.25, 0.1]$) switches when one is reached.

The circular polish is encoded in the cylindrical coordinates:

$$\dot{r} = -2.7(r - 0.025)$$
$$\dot{\theta} = 2.5 \qquad\qquad\qquad\qquad (B.2)$$
$$\dot{z} = -2.7(z - 0.12)$$

where $r^2 = x^2 + y^2$, and $\theta = atan2(y, x)$, and the center of rotation is $[-.55, 0, .1]$.

The other two tasks (push down and retreat) are created by SEDs Khansari-Zadeh and Billard (2011b) with the following parameters.

$$\pi_1 = 0.35, \ \pi_2 = 0.20, \ \pi_3 = 0.45$$
$$\mu_1 = [35.7, -5.8, -11.4, -2.4, 4.3, 18.0]$$
$$\mu_2 = [0.6, -34.8, 37.4, -0.2, 12.9, 3.1]$$
$$\mu_3 = [-33.6, 10.9, -2.7, 2.6, -0.3, 17.8]$$

$$\Sigma_1 = \begin{bmatrix} 1.3 & -0.2 & 3.0 \\ -0.2 & 0.1 & -5.4 \\ 3.0 & -5.4 & 721.1 \\ -0.8 & 1.2 & -160.7 \\ -0.2 & 0.5 & -79.5 \\ -0.6 & 2.0 & -282.2 \end{bmatrix} \Sigma_2 = \begin{bmatrix} 22.4 & 5.4 & -4.3 \\ 5.4 & 6.7 & 21.1 \\ -4.3 & 21.1 & 136.6 \\ -5.1 & -1.3 & 0.4 \\ -1.7 & 4.8 & 33.3 \\ -0.7 & -10.6 & -58.8 \end{bmatrix} \qquad (B.3)$$

$$\Sigma_3 = \begin{bmatrix} 1.1 & -0.3 & -2.1 \\ -0.3 & 0.2 & -10.3 \\ -2.1 & -10.3 & 922.3 \\ -0.6 & -2.4 & 222.4 \\ 0.2 & 0.9 & -89.9 \\ 0.2 & 4.0 & -348.4 \end{bmatrix}$$

However the attractor of push-down is at $[-.4, 0, .08]$ while the attractor of retreat is at $[-.32, .28, .36]$.

B.2.2   DS parametrization for carrying task

The four tasks has the same dynamics as $\dot{x}_d = -(x_r - x_g)$ with saturated velocity at $0.12 m/s$. However, the location of the attractor (x_g) is set differently for each task as follows.

$$
\begin{aligned}
x_{MF} &= [0.05, 0.47, 0.50] \\
x_{MB} &= [0.05, 0.32, 0.50] \\
x_{PL} &= [-0.3, 0.35, 0.1] \\
x_{PR} &= [0.3, 0.35, 0.1]
\end{aligned}
\tag{B.4}
$$

B.3   Technical details for Chapter 6: human-guidance detection

B.3.1   The simulation parameters for DS-admittance control

The parameters used for the 1D simulations are as follows: $M_a = 1$, $D_a = 10$, $E_m = 2$, $E_t = 1$, $\tilde{P}_d = 2$, $h(0) = 0$, $E(0) = 0$, $\dot{x}(0) = 0$, $x(0) = 1$, $\dot{x}_a(0) = 0$, $dt = 1 ms$. The dynamics system: $\dot{x}_t = -3x$ but saturated in $[-2, 2]$. The external forces:

$$
F_e = \begin{cases}
\mathcal{N}(0, 36) & 0 < t < 2 \\
-20(x-1) - 10\dot{x}_r & 3 < t < 6 \\
10 & 9 < t < 9.005 \\
0 & \text{elsewhere}
\end{cases}
\tag{B.5}
$$

However, the forces for the simulated human (second row) is saturated between 5 and -5, and the pulse (third row) repeats 10 times every $50 ms$.

For the 2D simulation example, we use $M_a = \text{diag}\{2, 2\}$, $D_a = \text{diag}\{4, 4\}$, $E_m = 2$, $E_t = 1$, $\tilde{P}_d = 2$, $h(0) = 0$, $E(0) = 0$, $\dot{x}(0) = [0, 0]$, $x(0) = [-.9, -.6]$, $\dot{x}_a(0) = [0, 0]$, $dt = 1 ms$. The dynamical system is:

$$
f(x) = \begin{bmatrix} -1.5 & 1.5 \\ -2.4 & -6 \end{bmatrix} x
\tag{B.6}
$$

saturated at $2 m/s$.

For the adaptive case (Fig. 6.9), we use $M = \text{diag}\{1, 1\}$, $C = \text{diag}\{0, 0\}$, $\ddot{x}(0) = [0, 0]$, $\dot{x}(0) = [0, 0]$, $x(0) = [.022, 0]$, $D_a = \text{diag}\{2, 2\}$, $M_a = \text{diag}\{0.05, 0.05\}$, $\dot{x}_a(0) = [0, 0]$, $h(0) = 0$, $\tilde{P}_d = .2$, $E(0) = 0$, $E_t = .1$, $E_m = .2$, $dt = 1 ms$. The dynamical system specified in the polar coordinate is:

$$
\begin{cases}
\dot{\theta} = \pm 10 \\
\dot{r} = -15(r - 0.022)
\end{cases}
\tag{B.7}
$$

where $x_1 = r\cos(\theta)$ and $x_2 = r\sin(\theta)$. f_1 represent the counterclockwise and f_2 the clockwise

rotation. The external forces are simulate as

$$F_e = -20(\dot{x} - f_1(x)) \tag{B.8}$$

where the norm of the output is limited to $2N$. In one of the comparisons with impedance control (i.e., higher human effort), we increase this limit to $20N$.

B.3.2 The robot parameters for DS-admittance control

For the arm admittance, we use the following parameters.

$$
\begin{aligned}
M_a &= \text{diag}\{6,6,6,1,1,.5\} \\
D_a &= \text{diag}\{60,60,60,15,15,15\} \\
dt &= 8ms
\end{aligned} \tag{B.9}
$$

However, for the virtual admittance use the following values.

$$
\begin{aligned}
M_a &= \text{diag}\{2,2,2,1,1,1\} \\
D_a &= \text{diag}\{2,2,2,2,2,2\}
\end{aligned} \tag{B.10}
$$

Fro the energy tank, we use $E_m = 4$, $E_t = 2$, $\tilde{P}_d = 2.5$.

Admittance control parametrization for the mobile robot

The parameters used in the admittance control for the mobile-robot are as follows.

$$
\begin{aligned}
M_a &= \text{diag}(1,1,1,.5,.5,.5) \\
D_a &= \text{diag}(25,25,25,5,5,5) \\
K_a &= \text{diag}(10,150,10,5,5,5) \\
M_p &= \text{diag}(100,10,0,0,0,500) \\
D_p &= \text{diag}(500,50,0,0,0,10)
\end{aligned} \tag{B.11}
$$

diag denotes a diagonal matrix with the given values where coordinate system is $(x, y, z, \theta_x, \theta_y, \theta_z)$.

B.4 Source codes

In the following, we provide a reference for the implementation used in this thesis:

- **kuka-lwr-ros** at https://github.com/epfl-lasa/kuka-lwr-ros
  provides the implementations for controlling KUKA LWR 4+ in different control modes including DS-based impedance control.
- **adaptive-polishing** at https://github.com/epfl-lasa/adaptive_polishing

provides the implementation for the adaptation in parameterized dynamical systems (Chapter 4)

- **task-adaptation** at https://github.com/epfl-lasa/task_adaptation
  provides the implementation for the task adaptation method presented in Chapter 5.

- **ds-admittance-control** at https://github.com/epfl-lasa/ds_admittance_control/tree/ridgeback
  provides the implementation for DS-based admittance control with human-guidance detection as presented in Chapter 6.

- **ridgeback-ur5-controller** at https://github.com/epfl-lasa/ridgeback_ur5_controller/tree/devel
  provides several functionalities for the Ridgeback mobile robot with UR5 robotic arm. This includes the DS-based admittance controller.

- **cpr-load-support** at https://github.com/epfl-lasa/cpr_load_support
  provide load support functionality for the Ridgeback mobile robot with UR5 robotic arm. This implementation is based on DS-based admittance control.

B.5 Media

In the following, we provide a external references for the media related to each chapter.

Media for Chapter 4

The experimental demonstration for motion adaptation in the polishing task can be viewed here: https://youtu.be/TGwNkSEMm0M.

The motion adaptation for repetitive pick-and-place is demonstrated here: https://youtu.be/qIcOAtVMNgE.

Media for Chapter 5

The experimental result of the manipulation tasks using Kuka LWR 4+ (Section 5.5.1) can be watched here: https://youtu.be/oqHJ8crB5KY.

The results of the carrying task using the mobile robot (Section 5.5.2) can be viewed here: https://youtu.be/7BjHhV-BkwE

Media for Chapter 6

The result of DS-admittance control with human-guidance detection (Section 6.6.3) can be viewed at https://youtu.be/HrR85-IP-Qo.

Media for DS-based admittance control

A demonstration using DS-admittance control for supporting a load using the Ridgeback mobile robot can be watched here: https://youtu.be/AB7B2HuQdQ0

In another demonstration, we DS-admittance control integrated with tracking and navigation capabilities in order to collaborate with a human for transportation tasks. The demonstration can be viewed here: https://youtu.be/cSRu14MR5mE

Media for DS-based impedance-admittance control

A preliminary implementation of DS-based impedance-admittance control (Section C.2) is demonstrated here: https://youtu.be/-Tj-FUjCYlE

C Further mathematical formulation

C.1 Switching between proactive and passive following behavior

In our proposed method in Section 3, the leader's position and velocity is primarily used for forward prediction.. Here, we extend this model to account for the assumption that human-follower switches between a proactive following behavior (i.e., using the internal model to track leader's future motion) and passive following behavior (i.e., tracking leader's current motion). Therefore, we propose the following dynamics.

$$\ddot{x}_f(t) = f(x_f(t)) + \eta(t)g(e(t)) \tag{C.1}$$

In this model, $f(x(t))$ represents the internal dynamics which can be adapted to the leader's trajectory. Tracking of the leader's trajectory can be achieved by $g(e(t))$ where $e(t) = x_l(t) - x_f(t)$. Switching between relying on the internal model and tracking is simulated by $\eta(t)$. A simple choice for these functions can be:

$$\begin{cases} f(x(t)) = -kx(t) \\ g(e(t)) = K_p e(t) + K_d \dot{e}(t) \\ \eta(t) = \begin{cases} 1 & \text{if } \int_{t-T}^{t} |e(t)| dt > E \\ 0 & \text{otherwise} \end{cases} \end{cases} \tag{C.2}$$

Our choice of $f(x)$ is the most simple oscillatory system as well as PD-controller for tracking dynamics ($g(e)$). Switching between internal model and tracking happens when the integral of the error over last T seconds goes over a threshold E. The performance of such dynamics for a sinusoidal trajectory is shown in Fig. C.1a. The frequency and amplitude of this reference trajectory is smoothly changing from $4\,rad/s$ to $1\,rad/s$ and from $1\,m$ to $2\,m$. For this simulation, $K_p = 60$, $K_d = 15$, $T = 3s$, and $E = 1.5ms$. Setting $k = 16N/m$ consistent with the trajectory is sufficient for good tracking behavior until the leader changes its frequency and amplitude. This sudden change in leader's trajectory creates an error between leader and follower which triggers the tracking dynamics ($\eta = 1$); see Fig. C.1b. Reducing the error and tuning $k = 4N/m$
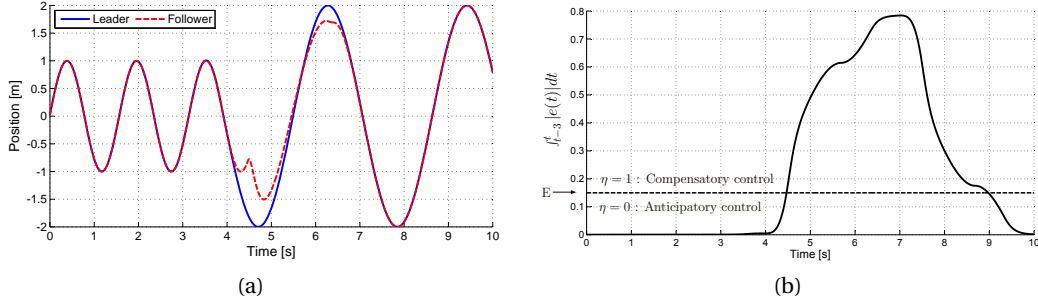
Figure C.1 – (a) Switching between an autonomous internal dynamics and tracking. (b) Switching between anticipatory and compensatory behavior based on the integration of the tracking error.

manually consistent with new frequency makes the internal model sufficient for tracking. Transitory behavior of this model is quite similar to human performance; e.g. undershoot around $27s$ in Fig. 3.7b. Moreover, Fig. C.1b shows how the integration of error triggers the compensatory control and how the absence of tracking error triggers back the anticipatory control; i.e internal model. Switching between anticipatory ($f(x)$) and compensatory ($g(e)$) control has been proposed and studied in action coordination in groups and individuals Knoblich and Jordan (2003). Evaluation of this model –forced dynamical system– for the experimental data requires parameter tuning which lays out of this paper scope.

C.2   DS-based impedance-admittance control

To track Cartesian velocity compliantly, we use the following impedance law proposed by Kronander and Billard (2016):

$$F_c = -d_i(\dot{x} - \dot{x}_d) + (1 - h)Mf'(x)\dot{x} \tag{C.3}$$

Where $D \in \mathbb{R}^+$ is a constant gain. To recall from Chapter 6, we have

$$\dot{x}_d = \dot{x}_t + \dot{x}_a \tag{C.4}$$

where $\dot{x}_t$ is the task-specific velocity generated by a dynamical system, and $\dot{x}_a$ is the admittance-generated velocity which allows the robot to comply the the human user. We slightly modified this controller by adding the second term to improve the tracking performance. In the absence of human-interaction($F_e = 0$ and $h = 0$), and assuming $\dot{x}_d = \dot{x}_t$, we can study the dynamics of the tracking error ($\dot{e} = \dot{x} - \dot{x}_t$) as

$$\ddot{e} = \ddot{x} - \ddot{x}_t \tag{C.5}$$

This leads to

$$\begin{aligned}
\ddot{e} &= -M^{-1}d_i\dot{e} + f'(x)\dot{x} - f'(x)\dot{x} \\
&= -(M^{-1}d_i)\dot{e}
\end{aligned} \tag{C.6}$$

This shows that the error vanishes exponentially since $d_i > 0$ and $M > 0$. The feedback of $\dot{x}$ can be replaced by $\dot{x}_t$ for practical reasons (such noise in the measurements). This way the impedance controller is:

$$F_c = -d_i(\dot{x} - \dot{x}_d) + (1 - h)Mf'(x)\dot{x}_t \tag{C.7}$$

In this case the error dynamics are

$$\begin{aligned}
\ddot{e} &= -M^{-1}d_i\dot{e} + f'(x)\dot{x}_t - f'(x)\dot{x} \\
&= -(M^{-1}d_i + f'(x))\dot{e}
\end{aligned} \tag{C.8}$$

This shows that the error vanishes exponentially if $d_i > \lambda_{max}(Mf'(x))$.

For the energy analysis of the system, consider the following energy function:

$$W = \frac{1}{2}\dot{x}^T M\dot{x} + \alpha\frac{1}{2}\dot{x}_a^T M_a\dot{x}_a + d_i V(x) \tag{C.9}$$

where α is a positive scalar satisfying $\alpha > D/(2\lambda_{min}(D_a))$. The time derivative of this energy function is:

$$\begin{aligned}
\dot{W} &= \dot{x}^T M\ddot{x} + \frac{1}{2}\dot{x}^T \dot{M}\dot{x} + \alpha\dot{x}_a^T M_a\ddot{x}_a + d_i\nabla_x V(x)^T \dot{x} \\
&= \dot{x}^T F_e - \dot{x}^T \underbrace{(d_i\mathbb{I}_d - \bar{h}Mf'(x) - C)}_{\tilde{D}}\dot{x} + d_i\dot{x}^T \dot{x}_d \\
&\quad + \alpha h\dot{x}_a^T F_e - \alpha\dot{x}_a^T D_a\dot{x}_a + d_i\nabla_x V(x)^T \dot{x}
\end{aligned} \tag{C.10}$$

where skew-symmetry of $\dot{M} - 2C$ is used to replace $\dot{M}$. Using $\dot{x}_d = \dot{x}_a + \bar{h}(-\nabla_x V(x) + \tilde{f}(x))$, we have:

$$\begin{aligned}
\dot{W} =& F_e^T(\dot{x} + \alpha h\dot{x}_a) - \dot{x}^T \tilde{D}\dot{x} - \alpha\dot{x}_a^T D_a\dot{x}_a \\
&+ d_i\dot{x}^T \dot{x}_a + hd_i\nabla_x V(x)^T \dot{x} + \bar{h}d_i\tilde{f}(x)^T \dot{x}
\end{aligned} \tag{C.11}$$

using the equality $2\dot{x}^T\dot{x}_a = -(\dot{x} - \dot{x}_a)^2 + \dot{x}^2 + \dot{x}_a^2$, we have

$$\begin{aligned}
\dot{W} =& F_e^T(\dot{x} + \alpha h\dot{x}_a) \\
&- \dot{x}^T(\tilde{D} - \frac{d_i}{2}\mathbb{I}_n)\dot{x} - \dot{x}_a^T(\alpha D_a - \frac{d_i}{2}\mathbb{I}_n)\dot{x}_a - \frac{d_i}{2}(\dot{x} - \dot{x}_a)^2 \\
&+ hd_i\nabla_x V(x)^T \dot{x} + \bar{h}d_i\tilde{f}(x)^T \dot{x}
\end{aligned} \tag{C.12}$$

By introducing human-induced error as $\dot{e}_h = \dot{x} - \bar{h}\dot{x}_t$, we can break one term into two parts as

follows:

$$hD\nabla_x V(x)^T \dot{x} = h\bar{h}D\nabla_x V(x)^T \dot{x}_t + h\nabla_x V(x)^T \dot{e}_h \tag{C.13}$$

This leads us to the following power rates:

$$\dot{W} = P_i + P_d + P_t + P_a + P_h \tag{C.14}$$

where

$$\begin{cases} P_i = F_e^T (\dot{x} + \alpha h \dot{x}_a) \\ P_d = -\dot{x}^T (\frac{d_i}{2}\mathbb{I}_n - \bar{h}Mf'(x) - C)\dot{x} \\ \qquad -\dot{x}_a^T (\alpha D_a - \frac{d_i}{2}\mathbb{I}_n)\dot{x}_a - \frac{d_i}{2}(\dot{x} - \dot{x}_a)^2 \\ P_t = h\bar{h}d_i\nabla_x V(x)^T \dot{x}_t \\ P_a = \bar{h}d_i\dot{x}^T \tilde{f}(x) \\ P_h = hd_i\nabla_x V(x)^T \dot{e}_h \end{cases} \tag{C.15}$$

Here, P_i denotes the power input from the environment. P_{diss} accounts for the dissipations due to impedance and admittance parts. To satisfy passivity, we need to ensure $d_i > 2\lambda_{max}(C + \bar{h}Mf'(x))$. P_t shows that during transitions ($\bar{h}h > 0$), the conservative part of the DS increase the passivity of the system. Note that $\nabla_x V(x)^T \dot{x}_t < 0$. P_a is related to no-conservative part of the motion planning. Energy-tank approach can be used to control this flow of energy to achieve passivity while following temporarily active motions. The last part, P_h denotes the energy that the human user exchanges with the DS.

In this formulation, the damping matrix for the admittance is not required to be of form $d_a\mathbb{I}_n$ and can be any arbitrary positive-definite matrix. Moreover, the resulting variable admittance of this controller (Y) can be formulated as follows:

$$Y = \frac{\partial \dot{x}_r}{\partial F_e} = \frac{1}{d_i}\mathbb{I}_n + \frac{\partial \dot{x}_d}{\partial F_e} = \frac{1}{D_i}\mathbb{I}_n + \frac{\partial \dot{x}_a}{\partial F_e} = \frac{1}{D_i}\mathbb{I}_n + \frac{h}{D_a} \tag{C.16}$$

For small h, the robot exhibits an impedance of size D_i and for higher h (and assuming $D_i \gg D_a$), the robot exhibits an impedance of size $h^{-1}D_a$.

Without any loss of stability, passivity, and tracking performance, we can use an asymmetric impedance matrix

$$F_c = -d_i^{\parallel}(\dot{x}^{\parallel} - \dot{x}_t) - d_i^{\perp}\dot{x}^{\perp} + \bar{h}Mf'(x)\dot{x} \tag{C.17}$$

where $\dot{x}$ is decomposed into two parts: $\dot{x}^{\parallel}$ parallel and $\dot{x}^{\perp}$ orthogonal to $\dot{x}_t$ with their respective damping gains ($d_i^{\parallel}$ and $d_i^{\perp}$). Similar to Eq.6.37, this formulation lead to a asymmetrical

damping matrix D_i. For the passivity analysis, this changes P_{diss} in Eq. C.15 to

$$
\begin{aligned}
P_{diss} = &- \dot{x}^T (\frac{D_i}{2} - \bar{h} M f'(x) - C) \dot{x} - \dot{x}_a^T (\alpha D_a - \frac{d_i^{\|} + d_i^{\perp}}{2} \mathbb{I}_n) \dot{x}_a \\
&- \frac{d_i^{\|}}{2} (\dot{x}^{\|} - \dot{x}_a)^2 - \frac{d_i^{\perp}}{2} (\dot{x}^{\perp} - \dot{x}_a)^2
\end{aligned}
\tag{C.18}
$$

and for P_t, P_a, and P_h, $d_i^{\perp}$ appears instead of d_i.

Task-specific impedance matrix

A further formulation of the impedance controller (in Eq. C.3) is as follow:

$$
F_c = -D\dot{x}_r + \lambda^{\perp} \dot{x}_d + \bar{h} M f'(x) \dot{x}_t
\tag{C.19}
$$

where D (positive definite) has one eigenvector along $\dot{x}_d$ with eigenvalue of λ. Let's decompose $\dot{x}_r$ into two parts: $\dot{x}_r^{\|}$ parallel and $\dot{x}_r^{\perp}$ orthogonal to $\dot{x}_d$. Therefore, the following error dynamics

$$
\ddot{e} = -M^{-1}(-D\dot{x}_r + \lambda^{\perp} \dot{x}_t + M f'(x) \dot{x}_t) - f'(x) \dot{x}_r
\tag{C.20}
$$

can be decomposed into parallel $\dot{e}^{\perp}$ and perpendicular $\dot{e}^{\|}$.

$$
\begin{cases}
\ddot{e}^{\perp} = -(\lambda M^{-1} + f'(x)) \dot{e}^{\perp} \\
\ddot{e}^{\|} = -(M^{-1} D + f'(x)) \dot{e}^{\|}
\end{cases}
\tag{C.21}
$$

Assuming all other eigenvalues of D are equal ($\lambda^{\|}$), the impedance law can be simply seen as:

$$
F_c = -\lambda^{\|} (\dot{x}_r^{\|} - \dot{x}_t) - \lambda^{\perp} \dot{x}_r^{\perp} + \bar{h} M f'(x) \dot{x}_t
\tag{C.22}
$$

C.3 Task adaptation including a null dynamical system

It is possible to include a dynamic DS encoding for zero-velocity (i.e., $f_0(x_r) \equiv 0$) in Eq.5.2 with its corresponding belief b_0. In this case, the constraints in Eq.5.3 should be modified to include b_0 as well. To have the dynamics of the competition between the null-DS and other DS in the autonomous condition, we need to insert $f_0 = 0$ in Eq.5.25 which results in

$$
\Delta \dot{b}_{k0} = (2b_k - 1)|f_k|^2
\tag{C.23}
$$

This equation shows that any DS with belief lower than 0.5 decreases and saturates at 0. Only the confident task – if exists – converges to 1. Therefore, the human can change the task of the robot to a desired one by providing enough demonstrations as to pass this threshold.

C.4 Dynamics approximation and motion learning

Having a series of primitive dynamics (i.e., f_i), and their corresponding beliefs (i.e., b_i), one can consider the following underlying dynamics that governs the human-demonstration.

$$\dot{b} = B(t, x, s, b) \tag{C.24}$$

Where b is a vector including b_i, t is time, x represents the state of the system, and s represents other contextual informations in the interaction (i.e., other than those states (x) used by the dynamical systems f_i). Time-dependency of this model indicates that (or model for) the duration of tasks and their switching times. State-dependency (i.e., x) indicates that the switching between task takes place due a change in the state; e.g., different tasks are desirable in different region of the state-space. Contextual-dependency (i.e., s) indicates the switching between task might occur due to other relevant information during the interaction; e.g., entrance of another human partner, appearance of an obstacle, etc. Finally, the belief-dependency of this model indicates that each task (or primitive dynamics) is decided based on a history of previous task; e.g., the picking an object most certainly followed by a placing the object. All other unknown dynamics and uncertainties can be model as time-variability.

Regarding these underlying dynamics (Eq.C.24), our proposed adaptation mechanism can be seen as an estimator for b under no priors; i.e., assuming $\dot{b} = B(t)$. In the followings, we use this adaptation as a building block for different learning architectures where assume there is a stat-dependency ($\dot{b} = B(x)$), context-dependency ($\dot{b} = B(s)$), or a sequence-dependency ($\dot{b} = B(b)$).

To use the proposed adaptation mechanism in a learning architecture that learns state-dependency (i.e., $\dot{b} = B(x)$ approximation of Eq.C.24), one requires a memory mechanism that associates between the beliefs (i.e., b_i which is being adapted temporally) and other spatial information such as position (x). For this purpose, consider the following state dependency for the beliefs.

$$b_i(x) = \frac{\sum_{m=1}^{M} \Psi_{im}(x)\, \beta_{im}}{\sum_{m=1}^{M} \Psi_{im}(x)} \quad \text{for } i = 1...N \tag{C.25}$$

In this formulation, $\Psi_{im} \geq 0$ is the mth basis function of ith task with its corresponding linear weight β_{im}. We need to impose a set of constraints on our approximators to have positive values summing up to one for b_i. This can be done by using the same set of basis functions for all task ($i = 1...N$) resulting in the disappearance of i subscription for $\Psi_{im}(x)$, and the following constraint on β_{im}.

$$\sum_{i=1}^{N} \beta_{im} = 1 \quad \text{and} \quad 0 \leq \beta_{im} \leq 1. \tag{C.26}$$
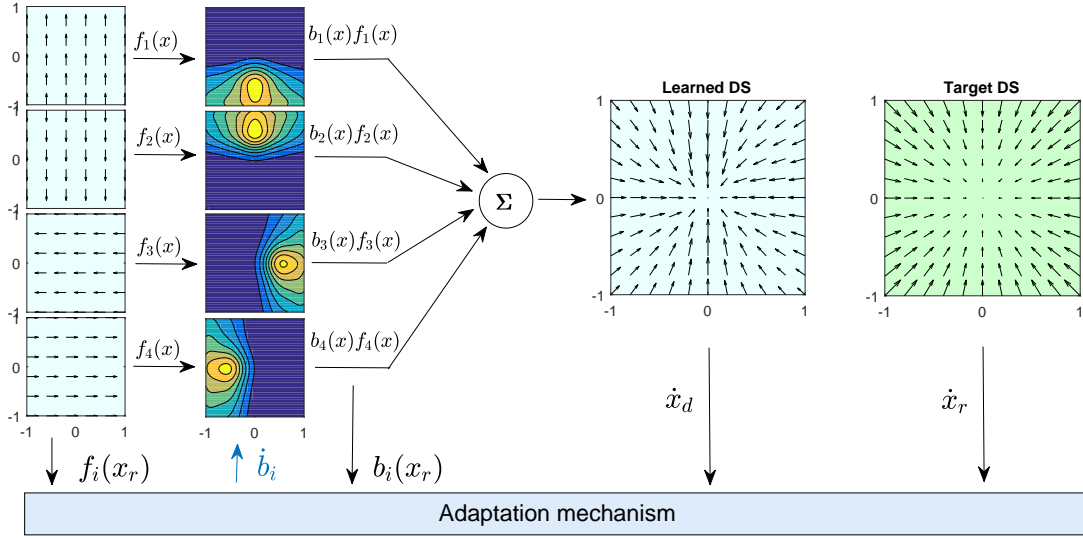
Figure C.2 – An illustrative case of learning a new dynamical task (potentially representing a task) from lower level primitive ones; in this case, four dynamical system (f_1 to f_4) encoding movement in different directions. There are four corresponding function-approximators learning the association between beliefs and the current state ($b_1(x_r)$ to $b_4(x_r)$). In each trial of the learning, a demonstration is simulated from the target dynamical-system (i.e., x_r and $\dot{x}_r$). The architecture adapts the belief temporally ($\dot{b}_i$) and learns them spatially ($b_i(x)$).

Using such assumptions, we can show that

$$\sum_{i=1}^{N} b_i(x) = \sum_{i=1}^{N} \frac{\sum_{m=1}^{M} \Psi_m(x)\beta_{im}}{\sum_{m=1}^{M} \Psi_m(x)}$$

$$= \frac{\sum_{m=1}^{M} \Psi_m(x)(\sum_{i=1}^{N} \beta_{im})}{\sum_{m=1}^{M} \Psi_m(x)} = 1 \tag{C.27}$$

To update the model (i.e., β_{im}), we first compute the updates on task-beliefs ($\dot{b}_i$) using our proposed adaptation mechanism (Eq.5.4). Then, we project the updates of b_i onto the updates of β_{im} as follows.

$$\dot{\beta}_{im} = \frac{\Psi_m(x)\,\dot{b}_i}{\sum_{m=1}^{M} \Psi_m(x)} \tag{C.28}$$

Therefore, the forward integration for the learning parameters is

$$\beta_{im}(t) = \beta_{im}(0) + \int_0^t \dot{\beta}_{im}\, dt \tag{C.29}$$

Appendix C. Further mathematical formulation

By turning the adaptation into a learning mechanism, we are able to approximate a targeted dynamics (i.e., the dynamics that generates $\dot{x}_d$) using a set of given primitive dynamics (i.e., $f_i(x)$). We illustrated a simple case in Fig.C.2 where a targeted dynamics is learned (approximated) by a set of given dynamics. For this case, we used a simple basis function as follows.

$$\Psi_m(x) = exp(-\frac{||x - c_m||_2^2}{2\sigma^2})$$

(C.30)

where c_m represents the center of basis functions which are localized on a 5-by-5 equal distance grid. The width of basis function (σ) is set to 0.25, and adaptation rate (ϵ) is 0.2. In each trial (for 0.5 second and sampling time of $0.05s$), an initial position is randomized, and a motion is generated based on the target dynamics. In the course of this motion generation, the b_i are adapted, and β_{im} are learned online. The learning converges after a few trials (less than 15). It can be seen that our method (due to its WTA process) results in a soft partitioning of the space where in each partition only one primitive dynamics (or task) dominates.

On-line learning from adaptation has interesting implication in robotic system. First, after a few trials the robot can start performing the task. Even though, the initial performance is not satisfactory, it sill reduces the human-effort required to provide further demonstrations. Second, the quality of the learning is decided by the teacher in course of the interaction (as opposed to the reliance on a cost-function or a likelihood function during the offline learning).

Bibliography

Aarno, D. and Kragic, D. (2008). Motion intention recognition in robot assisted applications. *Robotics and Autonomous Systems*, 56(8):692–705. (Cited on page 31).

Abi-Farraj, F., Osa, T., Peters, N. P. J., Neumann, G., and Giordano, P. R. (2017). A learning-based shared control architecture for interactive task execution. In *Proceedings of the IEEE International Conference on Robotics and Automation (ICRA)*, pages 329–335. (Cited on page 30).

Abu-Dakka, F. J., Nemec, B., Jørgensen, J. A., Savarimuthu, T. R., Krüger, N., and Ude, A. (2015). Adaptation of manipulation skills in physical contact with the environment to reference force profiles. *Autonomous Robots*, 39(2):199–217. (Cited on page 30).

Andrist, S., Tan, X. Z., Gleicher, M., and Mutlu, B. (2014). Conversational gaze aversion for humanlike robots. In *Proceedings of the ACM/IEEE International Conference on Human-Robot Interaction (HRI)*, pages 25–32. (Cited on page 25).

Ansuini, C., Cavallo, A., Bertone, C., and Becchio, C. (2014). The visible face of intention: why kinematics matters. *Frontiers in Psychology*, 5:815. (Cited on page 19).

Åström, K. J. and Wittenmark, B. (2013). *Adaptive control*. Courier Corporation. (Cited on pages 10, 45, and 76).

Atkinson, A. P., Dittrich, W. H., Gemmell, A. J., and Young, A. W. (2004). Emotion perception from dynamic and static body expressions in point-light and full-light displays. *Perception*, 33(6):717–746. (Cited on page 19).

Bailenson, J. N., Yee, N., Merget, D., and Schroeder, R. (2006). The effect of behavioral realism and form realism of real-time avatar faces on verbal disclosure, nonverbal disclosure, emotion recognition, and copresence in dyadic interaction. *Presence: Teleoperators and Virtual Environments*, 15(4):359–372. (Cited on page 25).

Bandyopadhyay, T., Chong, Z. J., Hsu, D., Ang Jr, M. H., Rus, D., and Frazzoli, E. (2012). Intention-aware pedestrian avoidance. In *Proceedings of the International Society for Engineers and Researchers*, pages 963–977. (Cited on page 31).

Bibliography

Bavelas, J. B., Coates, L., and Johnson, T. (2002). Listener responses as a collaborative process: The role of gaze. *Journal of Communication*, 52(3):566–580. (Cited on page 19).

Becchio, C., Manera, V., Sartori, L., Cavallo, A., and Castiello, U. (2012). Grasping intentions: from thought experiments to empirical evidence. *Frontiers in Human Neuroscience*, 6:117. (Cited on page 20).

Becchio, C., Sartori, L., Bulgheroni, M., and Castiello, U. (2008). The case of dr. jekyll and mr. hyde: a kinematic study on social intention. *Consciousness and Cognition*, 17(3):557–564. (Cited on page 19).

Bente, G., Eschenburg, F., and Krämer, N. C. (2007). Virtual gaze. a pilot study on the effects of computer simulated gaze in avatar-based conversations. In *Proceedings of the International Conference on Virtual Reality*, pages 185–194. Springer. (Cited on page 25).

Berger, E., Sastuba, M., Vogt, D., Jung, B., and Ben Amor, H. (2015). Estimation of perturbations in robotic behavior using dynamic mode decomposition. *Advanced Robotics*, 29(5):331–343. (Cited on page 12).

Billard, A. (2017). On the mechanical, cognitive and sociable facets of human compliance and their robotic counterparts. *Robotics and Autonomous Systems*, 88:157–164. (Cited on page 8).

Bowman, M. C., Johannson, R. S., and Flanagan, J. R. (2009). Eye–hand coordination in a sequential target contact task. *Experimental Brain Research*, 195(2):273–283. (Cited on page 26).

Brass, M., Schmitt, R. M., Spengler, S., and Gergely, G. (2007). Investigating action understanding: inferential processes versus action simulation. *Current Biology*, 17(24):2117–2121. (Cited on page 19).

Braun, D. A., Ortega, P. A., and Wolpert, D. M. (2009). Nash equilibria in multi-agent motor interactions. *PLoS Computational Biology*, 5(8):e1000468. (Cited on page 22).

Brennan, S. E., Chen, X., Dickinson, C. A., Neider, M. B., and Zelinsky, G. J. (2008). Coordinating cognition: The costs and benefits of shared gaze during collaborative search. *Cognition*, 106(3):1465–1477. (Cited on page 17).

Burdet, E., Ganesh, G., Yang, C., and Albu-Schäffer, A. (2014). Interaction force, impedance and trajectory adaptation: by humans, for robots. In *Proceedings of the International Symposium on Experimental Robotics*, pages 331–345. (Cited on page 23).

Burdet, E., Osu, R., Franklin, D. W., Milner, T. E., and Kawato, M. (2001). The central nervous system stabilizes unstable dynamics by learning optimal impedance. *Nature*, 414(6862):446–449. (Cited on page 22).

Bussy, A., Gergondet, P., Kheddar, A., Keith, F., and Crosnier, A. (2012a). Proactive behavior of a humanoid robot in a haptic transportation task with a human partner. In *Proceedings of the IEEE International Symposium on Robot and Human Interactive Communication (RO-MAN)*, pages 962–967. (Cited on pages 8, 31, and 32).

Bussy, A., Kheddar, A., Crosnier, A., and Keith, F. (2012b). Human-humanoid haptic joint object transportation case study. In *Proceedings of the IEEE International Conference on Intelligent Robots and Systems (IROS)*, pages 3633–3638. (Cited on page 26).

Byrne, D. (1961). Interpersonal attraction and attitude similarity. *The Journal of Abnormal and Social Psychology*, 62(3):713. (Cited on page 25).

Calinon, S., Bruno, D., and Caldwell, D. G. (2014). A task-parameterized probabilistic model with minimal intervention control. In *Proceedings of the IEEE International Conference on Robotics and Automation (ICRA)*, pages 3339–3344. (Cited on pages 28 and 31).

Campeau-Lecours, A., Otis, M. J., and Gosselin, C. (2016). Modeling of physical human–robot interaction: Admittance controllers applied to intelligent assist devices with large payload. *International Journal of Advanced Robotic Systems*, 13(5):1729881416658167. (Cited on page 28).

Cazzato, D., Mazzeo, P. L., Spagnolo, P., and Distante, C. (2015). Automatic joint attention detection during interaction with a humanoid robot. In *Proceedings of the International Conference on Social Robotics*, pages 124–134. (Cited on page 128).

Chauvigné, L. A., Belyk, M., and Brown, S. (2017). Following during physically-coupled joint action engages motion area mt+/v5. *Journal of Integrative Neuroscience*, 16(3):307–318. (Cited on page 22).

Cherubini, A., Passama, R., Crosnier, A., Lasnier, A., and Fraisse, P. (2016). Collaborative manufacturing with physical human–robot interaction. *Robotics and Computer-Integrated Manufacturing*, 40:1–13. (Cited on pages 26 and 28).

Cho, C.-N., Kim, J.-H., Kim, Y.-L., Song, J.-B., and Kyung, J.-H. (2012). Collision detection algorithm to distinguish between intended contact and unexpected collision. *Advanced Robotics*, 26(16):1825–1840. (Cited on page 32).

Cho, S. and Jo, S. (2013). Incremental online learning of robot behaviors from selected multiple kinesthetic teaching trials. *IEEE Transactions on Systems, Man, and Cybernetics*, 43(3):730–740. (Cited on page 30).

Coen-Cagli, R., Coraggio, P., Napoletano, P., Schwartz, O., Ferraro, M., and Boccignone, G. (2009). Visuomotor characterization of eye movements in a drawing task. *Vision Research*, 49(8):810–818. (Cited on page 26).

Cohen, L., Khoramshahi, M., Salesse, R., Bortolon, C., Slowinski, P., Zhaie, C., Tsaneva-Atanasova, K., Di Bernardo, M., Capdevielle, D., Marin, L., et al. (2017a). Effects of facial

Bibliography

emotions on social-motor coordination in schizophrenia. *Joint Action Meeting (JAM)*. (Cited on page 7).

Cohen, L., Khoramshahi, M., Salesse, R. N., Bortolon, C., Słowiński, P., Zhai, C., Tsaneva-Atanasova, K., Bernardo, M., Capdevielle, D., Marin, L., et al. (2017b). Influence of facial feedback during a cooperative human-robot task in schizophrenia. *Scientific Reports*, 7(1):15023. (Cited on pages 7 and 24).

Combs, D. R., Tosheva, A., Penn, D. L., Basso, M. R., Wanner, J. L., and Laib, K. (2008). Attentional-shaping as a means to improve emotion perception deficits in schizophrenia. *Schizophrenia Research*, 105(1):68–77. (Cited on page 139).

Corteville, B., Aertbeliën, E., Bruyninckx, H., De Schutter, J., and Van Brussel, H. (2007). Human-inspired robot assistant for fast point-to-point movements. In *Proceedings of the IEEE International Conference on Robotics and Automation (ICRA)*, pages 3639–3644. (Cited on pages 28, 29, 30, and 32).

Daafouz, J. and Bernussou, J. (2001). Parameter dependent lyapunov functions for discrete time systems with time varying parametric uncertainties. *Systems and Control Letters*, 43(5):355–359. (Cited on page 10).

De Lange, F. P., Spronk, M., Willems, R. M., Toni, I., and Bekkering, H. (2008). Complementary systems for understanding action intentions. *Current Biology*, 18(6):454–457. (Cited on page 19).

De Luca, A., Albu-Schaffer, A., Haddadin, S., and Hirzinger, G. (2006). Collision detection and safe reaction with the dlr-iii lightweight manipulator arm. In *Proceedings of the IEEE/RSJ International Conference on Intelligent Robots and Systems (IROS)*, pages 1623–1630. (Cited on page 32).

De Santis, A., Siciliano, B., De Luca, A., and Bicchi, A. (2008). An atlas of physical human–robot interaction. *Mechanism and Machine Theory*, 43(3):253–270. (Cited on page 8).

D'Entremont, B., Hains, S., and Muir, D. (1997). A demonstration of gaze following in 3-to 6-month-olds. *Infant Behavior and Development*, 20(4):569–572. (Cited on page 18).

Dietrich, A., Wimbock, T., Albu-Schaffer, A., and Hirzinger, G. (2012). Reactive whole-body control: Dynamic mobile manipulation using a large number of actuated degrees of freedom. *IEEE Robotics and Automation Magazine*, 19(2):20–33. (Cited on page 28).

Dragan, A. D., Lee, K. C., and Srinivasa, S. S. (2013). Legibility and predictability of robot motion. In *Proceedings of the ACM/IEEE International Conference on Human-Robot Interaction (HRI)*, pages 301–308. (Cited on page 103).

Drusch, K., Stroth, S., Kamp, D., Frommann, N., and Wölwer, W. (2014). Effects of training of affect recognition on the recognition and visual exploration of emotional faces in schizophrenia. *Schizophrenia Research*, 159(2):485–490. (Cited on page 140).

Duchaine, V. and Gosselin, C. (2009). Safe, stable and intuitive control for physical human-robot interaction. In *Proceedings of the IEEE International Conference on Robotics and Automation (ICRA)*, pages 3383–3388. (Cited on page 28).

Duchaine, V. and Gosselin, C. M. (2007). General model of human-robot cooperation using a novel velocity based variable impedance control. In *Proceedings of Second Joint EuroHaptics conference and Symposium on Haptic Interfaces for Virtual Environment and Teleoperator Systems*, pages 446–451. (Cited on pages 27 and 28).

Emery, N. J., Lorincz, E. N., Perrett, D. I., Oram, M. W., and Baker, C. I. (1997). Gaze following and joint attention in rhesus monkeys (macaca mulatta). *Journal of Comparative Psychology*, 111(3):286. (Cited on page 19).

Engell, A. D. and Haxby, J. V. (2007). Facial expression and gaze-direction in human superior temporal sulcus. *Neuropsychologia*, 45(14):3234–3241. (Cited on page 19).

Evrard, P. and Kheddar, A. (2009). Homotopy switching model for dyad haptic interaction in physical collaborative tasks. In *Proceedings of the EuroHaptics conference and Symposium on Haptic Interfaces for Virtual Environment and Teleoperator Systems*, pages 45–50. (Cited on pages 4, 26, 28, and 32).

Ewerton, M., Maeda, G., Kollegger, G., Wiemeyer, J., and Peters, J. (2016). Incremental imitation learning of context-dependent motor skills. In *Proceedings of the IEEE/RAS International Conference on Humanoid Robots (Humanoids)*, pages 351–358. (Cited on page 30).

Ewerton, M., Neumann, G., Lioutikov, R., Amor, H. B., Peters, J., and Maeda, G. (2015). Learning multiple collaborative tasks with a mixture of interaction primitives. In *Proceedings of the IEEE International Conference on Robotics and Automation (ICRA)*, pages 1535–1542. (Cited on page 31).

Feniger-Schaal, R. and Lotan, N. (2017). The embodiment of attachment: directional and shaping movements in adults' mirror game. *The Arts in Psychotherapy*, 53:55–63. (Cited on page 24).

Ferraguti, F., Preda, N., Manurung, A., Bonfe, M., Lambercy, O., Gassert, R., Muradore, R., Fiorini, P., and Secchi, C. (2015). An energy tank-based interactive control architecture for autonomous and teleoperated robotic surgery. *IEEE Transactions on Robotics*, 31(5):1073–1088. (Cited on page 29).

Ferraguti, F., Secchi, C., and Fantuzzi, C. (2013). A tank-based approach to impedance control with variable stiffness. In *Proceedings of the IEEE International Conference on Robotics and Automation (ICRA)*, pages 4948–4953. (Cited on page 28).

Fitzpatrick, P. D., Richardson, R., and Schmidt, M. (2013). Dynamical methods for evaluating the time-dependent unfolding of social coordination in children with autism. *Frontiers in Integrative Neuroscience*, 7(21.10):3389. (Cited on page 139).

Bibliography

Flanagan, J. R. and Johansson, R. S. (2003). Action plans used in action observation. *Nature*, 424(6950):769–771. (Cited on page 18).

Fogassi, L., Ferrari, P. F., Gesierich, B., Rozzi, S., Chersi, F., and Rizzolatti, G. (2005). Parietal lobe: from action organization to intention understanding. *Science*, 308(5722):662–667. (Cited on page 19).

Foulkes, A. J. M. and Miall, R. C. (2000). Adaptation to visual feedback delays in a human manual tracking task. *Experimental Brain Research*, 131(1):101–110. (Cited on page 20).

Franklin, D. W., Burdet, E., Tee, K. P., Osu, R., Chew, C.-M., Milner, T. E., and Kawato, M. (2008). Cns learns stable, accurate, and efficient movements using a simple algorithm. *Journal of Neuroscience*, 28(44):11165–11173. (Cited on page 23).

Frischen, A., Bayliss, A. P., and Tipper, S. P. (2007). Gaze cueing of attention: visual attention, social cognition, and individual differences. *Psychological Bulletin*, 133(4):694. (Cited on page 19).

Frith, C. D. and Frith, U. (2006). How we predict what other people are going to do. *Brain Research*, 1079(1):36–46. (Cited on page 19).

Fu, Y., Li, R., Huang, T. S., and Danielsen, M. (2008). Real-time multimodal human–avatar interaction. *IEEE Transactions on Circuits and Systems for Video Technology*, 18(4):467–477. (Cited on pages 26 and 128).

Gams, A., Petric, T., Nemec, B., and Ude, A. (2014). Learning and adaptation of periodic motion primitives based on force feedback and human coaching interaction. In *Proceedings of the IEEE International Conference on Humanoid Robots (Humanoids)*, pages 166–171. (Cited on page 31).

Ganesh, G., Albu-Schäffer, A., Haruno, M., Kawato, M., and Burdet, E. (2010). Biomimetic motor behavior for simultaneous adaptation of force, impedance and trajectory in interaction tasks. In *Proceedings of the IEEE International Conference on Robotics and Automation (ICRA)*, pages 2705–2711. (Cited on pages 28 and 30).

Ganesh, G., Takagi, A., Osu, R., Yoshioka, T., Kawato, M., and Burdet, E. (2014). Two is better than one: Physical interactions improve motor performance in humans. *Scientific Reports*, 4:3824. (Cited on pages 18 and 22).

Garau, M., Slater, M., Bee, S., and Sasse, M. A. (2001). The impact of eye gaze on communication using humanoid avatars. In *Proceedings of the ACM SIGCHI Conference on Human Factors in Computing Systems*, pages 309–316. (Cited on page 25).

Garau, M., Slater, M., Vinayagamoorthy, V., Brogni, A., Steed, A., and Sasse, M. A. (2003). The impact of avatar realism and eye gaze control on perceived quality of communication in a shared immersive virtual environment. In *Proceedings of the ACM SIGCHI Conference on Human Factors in Computing Systems*, pages 529–536. (Cited on page 25).

Gentry, S., Feron, E., and Murray-Smith, R. (2005). Human-human haptic collaboration in cyclical fitts' tasks. In *Proceedings of the IEEE/RSJ International Conference on Intelligent Robots and Systems (IROS)*, pages 3402–3407. (Cited on page 21).

Ghadirzadeh, A., Bütepage, J., Maki, A., Kragic, D., and Björkman, M. (2016). A sensorimotor reinforcement learning framework for physical human-robot interaction. In *Proceedings of the IEEE International Conference on Intelligent Robots and Systems (IROS)*, pages 2682–2688. (Cited on pages 27 and 30).

Gmerek, A. and Jezierski, E. (2012). Admittance control of a 1-dof robotic arm actuated by bldc motor. In *Proceedings of the IEEE International Conference on Methods and Models in Automation and Robotics (MMAR)*, pages 633–638. (Cited on page 39).

Gribovskaya, E., Kheddar, A., and Billard, A. (2011). Motion learning and adaptive impedance for robot control during physical interaction with humans. In *Proceedings of the IEEE International Conference on Robotics and Automation (ICRA)*, pages 4326–4332. (Cited on pages 28 and 29).

Grinsted, A., Moore, J. C., and Jevrejeva, S. (2004). Application of the cross wavelet transform and wavelet coherence to geophysical time series. *Nonlinear Processes in Geophysics*, 11(5/6):561–566. (Cited on pages 47 and 65).

Groten, R., Feth, D., Peer, A., and Buss, M. (2010). Shared decision making in a collaborative task with reciprocal haptic feedback-an efficiency-analysis. In *Proceedings of the IEEE International Conference on Robotics and Automation (ICRA)*, pages 1834–1839. (Cited on page 21).

Groten, R., Feth, D., Peer, A., Buss, M., and Klatzky, R. (2009). Efficiency analysis in a collaborative task with reciprocal haptic feedback. In *Proceedings of the IEEE International Conference on Intelligent Robots and Systems (IROS)*, pages 461–466. (Cited on page 22).

Gueugnon, M., Salesse, R. N., Coste, A., Zhao, Z., Bardy, B. G., and Marin, L. (2016). The acquisition of socio-motor improvisation in the mirror game. *Human Movement Science*, 46:117–128. (Cited on page 24).

Haddadin, S., Albu-Schaffer, A., De Luca, A., and Hirzinger, G. (2008). Collision detection and reaction: A contribution to safe physical human-robot interaction. In *Proceedings of the IEEE International Conference on Intelligent Robots and Systems (IROS)*, pages 3356–3363. (Cited on pages 12 and 32).

Haken, H., Kelso, J. S., and Bunz, H. (1985). A theoretical model of phase transitions in human hand movements. *Biological Cybernetics*, 51(5):347–356. (Cited on page 20).

Hart, Y., Noy, L., Feniger-Schaal, R., Mayo, A. E., and Alon, U. (2014). Individuality and togetherness in joint improvised motion. *PLoS One*, 9(2):e87213. (Cited on page 24).

Bibliography

Hashtrudi-Zaad, K. and Salcudean, S. E. (2001). Analysis of control architectures for teleoperation systems with impedance/admittance master and slave manipulators. *The International Journal of Robotics Research*, 20(6):419–445. (Cited on page 28).

Hazara, M. and Kyrki, V. (2016). Reinforcement learning for improving imitated in-contact skills. In *Proceedings of the IEEE/RAS International Conference on Humanoid Robots (Humanoids)*, pages 194–201. (Cited on page 30).

He, S., Ye, J., Li, Z., Li, S., Wu, G., and Wu, H. (2015). A momentum-based collision detection algorithm for industrial robots. In *Proceedings of the IEEE International Conference on Robotics and Biomimetics (ROBIO)*, pages 1253–1259. (Cited on page 32).

Himberg, T., Laroche, J., Bigé, R., Buchkowski, M., and Bachrach, A. (2018). Coordinated interpersonal behaviour in collective dance improvisation: the aesthetics of kinaesthetic togetherness. *Behavioral Sciences*, 8(2):23. (Cited on page 24).

Hogan, N. (1988). On the stability of manipulators performing contact tasks. *Journal on Robotics and Automation*, 4(6):677–686. (Cited on pages 3, 8, and 27).

Hogan, N. and Buerger, S. P. (2004). Impedance and interaction control. In *Robotics and Automation Handbook*, pages 375–398. CRC Press. (Cited on page 124).

Hooker, C. I., Bruce, L., Fisher, M., Verosky, S. C., Miyakawa, A., and Vinogradov, S. (2012). Neural activity during emotion recognition after combined cognitive plus social cognitive training in schizophrenia. *Schizophrenia Research*, 139(1):53–59. (Cited on page 139).

Hove, M. J. and Risen, J. L. (2009). It's all in the timing: Interpersonal synchrony increases affiliation. *Social Cognition*, 27(6):949. (Cited on page 16).

Ikeura, R. and Inooka, H. (1995). Cooperative force control in carrying an object by two humans. In *Proceedings of the IEEE International Conference on Systems, Man, and Cybernetics (SMC)*, volume 3, pages 2307–2311. (Cited on page 22).

Ishiguro, H. (2007). Android science. *Robotics Research*, 28(1):118–127. (Cited on page 24).

Itier, R. J. and Batty, M. (2009). Neural bases of eye and gaze processing: the core of social cognition. *Neuroscience and Biobehavioral Reviews*, 33(6):843–863. (Cited on page 19).

Jain, P. and Nigam, M. (2013). Design of a model reference adaptive controller using modified mit rule for a second order system. *Advance in Electronic and Electric Engineering*, 3(4):477–484. (Cited on page 45).

Jarrassé, N., Charalambous, T., and Burdet, E. (2012). A framework to describe, analyze and generate interactive motor behaviors. *PloS One*, 7(11):e49945. (Cited on page 23).

Jarrassé, N., Paik, J., Pasqui, V., and Morel, G. (2008). How can human motion prediction increase transparency? In *Proceedings of the IEEE International Conference on Robotics and Automation (ICRA)*, pages 2134–2139. (Cited on page 28).

Jayasekera, A., Hellewell, J., Perrett, D., and Deakin, J. (1996). The perception of gaze and attention in schizophrenia. *Schizophrenia Research*, 18(2):218–219. (Cited on page 139).

Jlassi, S., Tliba, S., and Chitour, Y. (2014). An online trajectory generator-based impedance control for co-manipulation tasks. In *Proceedings of the IEEE Symposium on Haptics (HAPTICS)*, pages 391–396. (Cited on pages 28 and 30).

Johansson, G. (1973). Visual perception of biological motion and a model for its analysis. *Perception and Psychophysics*, 14(2):201–211. (Cited on page 19).

Kabir, A. M., Kaipa, K. N., Marvel, J., and Gupta, S. K. (2017). Automated planning for robotic cleaning using multiple setups and oscillatory tool motions. *IEEE Transactions on Automation Science and Engineering*, 14(3):1364–1377. (Cited on page 30).

Kang, S., Komoriya, K., Yokoi, K., Koutoku, T., Kim, B., and Park, S. (2010). Control of impulsive contact force between mobile manipulator and environment using effective mass and damping controls. *International Journal of Precision Engineering and Manufacturing*, 11(5):697–704. (Cited on page 27).

Kastritsi, T., Sidiropoulos, A., and Doulgeri, Z. (2018). A phri framework for modifying a robot's kinematic behaviour via varying stiffness and dynamical system synchronization. In *Proceedings of the IEEE Mediterranean Conference on Control and Automation (MED)*, pages 1–6. (Cited on page 30).

Kendon, A. (1967). Some functions of gaze-direction in social interaction. *Acta Psychologica*, 26:22–63. (Cited on page 19).

Khalil, H. K. (1996). Noninear systems. *New Jersey Prentice-Hall*, 2(5):5–1. (Cited on page 33).

Khansari-Zadeh, S. M. and Billard, A. (2011a). The derivatives of the seds optimization cost function and constraints with respect to the learning parameters. Technical report. (Cited on page 37).

Khansari-Zadeh, S. M. and Billard, A. (2011b). Learning stable nonlinear dynamical systems with gaussian mixture models. *IEEE Transactions on Robotics*, 27(5):943–957. (Cited on pages 3, 9, 29, 31, 36, and 142).

Khansari-Zadeh, S. M. and Khatib, O. (2017). Learning potential functions from human demonstrations with encapsulated dynamic and compliant behaviors. *Autonomous Robots*, 41(1):45–69. (Cited on page 37).

Khatib, O. (1987). A unified approach for motion and force control of robot manipulators: The operational space formulation. *Journal on Robotics and Automation*, 3(1):43–53. (Cited on page 37).

Khoramshahi, M. and Billard, A. (2018). A dynamical system approach to task-adaptation in physical human-robot interaction. *Autonomous Robots*, 1(1):1–20. (Cited on pages 7, 118, and 120).

Bibliography

Khoramshahi, M., Laurens, A., Triquet, T., and Billard, A. (2018). From human physical interaction to online motion adaptation using parameterized dynamical systems. In *Proceedings of IEEE/RSJ International Conference on Intelligent Robots and Systems (IROS)*, pages 1361–1366. (Cited on pages 7 and 29).

Khoramshahi, M., Shukla, A., and Billard, A. (2014). Cognitive mechanism in synchronized motion: An internal predictive model for manual tracking control. In *Proceedings of the IEEE International Conference on Systems, Man, and Cybernetics (SMC)*, pages 765–771. (Cited on pages 6 and 26).

Khoramshahi, M., Shukla, A., and Billard, A. (2015). From joint-attention to joint-action: Effects of gaze on human following motion. *Joint Action Meeting (JAM)*. (Cited on page 6).

Khoramshahi, M., Shukla, A., Raffard, S., Bardy, B. G., and Billard, A. (2016). Role of gaze cues in interpersonal motor coordination: towards higher affiliation in human-robot interaction. *PloS One*, 11(6):e0156874. (Cited on page 6).

Kim, W., Lee, J., Peternel, L., Tsagarakis, N., and Ajoudani, A. (2017a). Anticipatory robot assistance for the prevention of human static joint overloading in human-robot collaboration. *Robotics and Automation Letters*. (Cited on page 26).

Kim, Y. J., Seo, J. H., Kim, H. R., and Kim, K. G. (2017b). Impedance and admittance control for respiratory-motion compensation during robotic needle insertion–a preliminary test. *The International Journal of Medical Robotics and Computer Assisted Surgery*, 13(4). (Cited on page 32).

Kipp, M. and Gebhard, P. (2008). Igaze: Studying reactive gaze behavior in semi-immersive human-avatar interactions. In *Proceedings of the Springer International Conference on Intelligent Virtual Agents*, pages 191–199. (Cited on pages 26 and 128).

Knoblich, G., Butterfill, S., and Sebanz, N. (2011). 3 psychological research on joint action: theory and data. *Psychology of Learning and Motivation-Advances in Research and Theory*, 54:59. (Cited on page 16).

Knoblich, G. and Jordan, J. S. (2003). Action coordination in groups and individuals: learning anticipatory control. *Journal of Experimental Psychology: Learning, Memory, and Cognition*, 29(5):1006. (Cited on page 148).

Konvalinka, I., Vuust, P., Roepstorff, A., and Frith, C. D. (2010). Follow you, follow me: continuous mutual prediction and adaptation in joint tapping. *The Quarterly Journal of Experimental Psychology*, 63(11):2220–2230. (Cited on page 17).

Kouris, A., Dimeas, F., and Aspragathos, N. (2018). A frequency domain approach for contact type distinction in human-robot collaboration. *Robotics and Automation Letters*. (Cited on pages 12 and 32).

Kourtis, D., Knoblich, G., Woźniak, M., and Sebanz, N. (2014). Attention allocation and task representation during joint action planning. *Journal of Cognitive Neuroscience*, 26(10):2275–2286. (Cited on page 17).

Krakauer, J. W. and Mazzoni, P. (2011). Human sensorimotor learning: adaptation, skill, and beyond. *Current opinion in Neurobiology*, 21(4):636–644. (Cited on pages 20, 21, and 51).

Kronander, K. and Billard, A. (2016). Passive interaction control with dynamical systems. *Robotics and Automation Letters*, 1(1):106–113. (Cited on pages 4, 8, 9, 11, 26, 28, 29, 40, 114, and 148).

Kronander, K., Khansari, M., and Billard, A. (2015). Incremental motion learning with locally modulated dynamical systems. *Robotics and Autonomous Systems*, 70:52–62. (Cited on page 9).

Landi, C. T., Ferraguti, F., Sabattini, L., Secchi, C., and Fantuzzi, C. (2017). Admittance control parameter adaptation for physical human-robot interaction. In *Proceedings of the IEEE International Conference on Robotics and Automation (ICRA)*, pages 2911–2916. (Cited on page 32).

Langdon, R. A. and Ward, P. B. (2012). The eyes have it: evidence of heightened sensitivity to other people's eye-gaze in schizophrenia. *Schizophrenia Research*, 136:S362–S363. (Cited on page 139).

Lazzari, S., Mottet, D., and Vercher, J.-L. (2009). Eye-hand coordination in rhythmical pointing. *Journal of motor behavior*, 41(4):294–304. (Cited on page 26).

Lecours, A., Mayer-St-Onge, B., and Gosselin, C. (2012). Variable admittance control of a four-degree-of-freedom intelligent assist device. In *Proceedings of the IEEE International Conference on Robotics and Automation (ICRA)*, pages 3903–3908. (Cited on page 32).

Lee, D. and Ott, C. (2010). Incremental motion primitive learning by physical coaching using impedance control. In *Proceedings of the IEEE/RSJ International Conference on Intelligent Robots and Systems (IROS)*, pages 4133–4140. (Cited on page 30).

Lee, D. and Ott, C. (2011). Incremental kinesthetic teaching of motion primitives using the motion refinement tube. *Autonomous Robots*, 31(2-3):115–131. (Cited on page 30).

Lee, S. H., Suh, I. H., Calinon, S., and Johansson, R. (2015). Autonomous framework for segmenting robot trajectories of manipulation task. *Autonomous Robots*, 38(2):107–141. (Cited on page 31).

Lee, S. Y., Lee, K. Y., Lee, S. H., Kim, J. W., and Han, C. S. (2007). Human-robot cooperation control for installing heavy construction materials. *Autonomous Robots*, 22(3):305. (Cited on page 26).

Bibliography

Leica, P., Roberti, F., Monllor, M., Toibero, J. M., and Carelli, R. (2017). Control of bidirectional physical human–robot interaction based on the human intention. *Intelligent Service Robotics*, 10(1):31–40. (Cited on page 27).

Levy-Tzedek, S., Berman, S., Stiefel, Y., Sharlin, E., Young, J., and Rea, D. (2017). Robotic mirror game for movement rehabilitation. In *Proceedings of the IEEE International Conference on Virtual Rehabilitation (ICVR)*, pages 1–2. (Cited on page 24).

Lewkowicz, D., Delevoye-Turrell, Y., Bailly, D., Andry, P., and Gaussier, P. (2013). Reading motor intention through mental imagery. *Adaptive Behavior*, 21(5):315–327. (Cited on page 20).

Li, Y., Jarrassé, N., and Burdet, E. (2017). Versatile interaction control and haptic identification in humans and robots. In *Geometric and Numerical Foundations of Movements*, pages 187–206. Springer. (Cited on page 28).

Li, Y., Tee, K. P., Chan, W. L., Yan, R., Chua, Y., and Limbu, D. K. (2015). Continuous role adaptation for human–robot shared control. *IEEE Transactions on Robotics*, 31(3):672–681. (Cited on page 26).

Li, Y., Yang, C., and He, W. (2016). Towards coordination in human-robot interaction by adaptation of robot's cost function. In *Proceedings of the International Conference on Advanced Robotics and Mechatronics (ICARM)*, pages 254–259. (Cited on page 28).

Li, Z.-J., Wu, H.-B., Yang, J.-M., Wang, M.-H., and Ye, J.-H. (2018). A position and torque switching control method for robot collision safety. *International Journal of Automation and Computing*, pages 1–13. (Cited on page 32).

Liesker, H., Brenner, E., and Smeets, J. B. (2009). Combining eye and hand in search is suboptimal. *Experimental Brain Research*, 197(4):395–401. (Cited on pages 26 and 128).

Lim, B., Ra, S., and Park, F. C. (2005). Movement primitives, principal component analysis, and the efficient generation of natural motions. In *Proceedings of the IEEE International Conference on Robotics and Automation (ICRA)*, pages 4630–4635. (Cited on page 10).

Loula, F., Prasad, S., Harber, K., and Shiffrar, M. (2005). Recognizing people from their movement. *Journal of Experimental Psychology: Human Perception and Performance*, 31(1):210. (Cited on page 19).

Lydon, J. E., Jamieson, D. W., and Zanna, M. P. (1988). Interpersonal similarity and the social and intellectual dimensions of first impressions. *Social Cognition*, 6(4):269. (Cited on page 25).

MacDorman, K. F., Green, R. D., Ho, C.-C., and Koch, C. T. (2009). Too real for comfort? uncanny responses to computer generated faces. *Computers in Human Behavior*, 25(3):695–710. (Cited on page 25).

Madan, C. E., Kucukyilmaz, A., Sezgin, T. M., and Basdogan, C. (2015). Recognition of haptic interaction patterns in dyadic joint object manipulation. *IEEE Transactions on Haptics*, 8(1):54–66. (Cited on page 22).

Maeda, G., Ewerton, M., Osa, T., Busch, B., and Peters, J. (2017a). Active incremental learning of robot movement primitives. In *Proceedings of the International Conference on Robot Learning (CORL)*. (Cited on page 30).

Maeda, G. J., Neumann, G., Ewerton, M., Lioutikov, R., Kroemer, O., and Peters, J. (2017b). Probabilistic movement primitives for coordination of multiple human–robot collaborative tasks. *Autonomous Robots*, 41(3):593–612. (Cited on pages 9 and 31).

Maeda, Y., Hara, T., and Arai, T. (2001). Human-robot cooperative manipulation with motion estimation. In *Proceedings of the IEEE International Conference on Intelligent Robots and Systems (IROS)*, pages 2240–2245. (Cited on page 28).

Makarov, M., Caldas, A., Grossard, M., Rodriguez-Ayerbe, P., and Dumur, D. (2014). Adaptive filtering for robust proprioceptive robot impact detection under model uncertainties. *IEEE/ASME Transactions on Mechatronics*, 19(6):1917–1928. (Cited on page 32).

Manera, V., Becchio, C., Cavallo, A., Sartori, L., and Castiello, U. (2011a). Cooperation or competition? discriminating between social intentions by observing prehensile movements. *Experimental Brain Research*, 211(3-4):547–556. (Cited on page 19).

Manera, V., Becchio, C., Schouten, B., Bara, B. G., and Verfaillie, K. (2011b). Communicative interactions improve visual detection of biological motion. *PLoS One*, 6(1):e14594. (Cited on page 19).

Manera, V., Schouten, B., Becchio, C., Bara, B. G., and Verfaillie, K. (2010). Inferring intentions from biological motion: a stimulus set of point-light communicative interactions. *Behavior Research Methods*, 42(1):168–178. (Cited on page 19).

Marsh, K. L., Richardson, M. J., and Schmidt, R. C. (2009). Social connection through joint action and interpersonal coordination. *Topics in Cognitive Science*, 1(2):320–339. (Cited on page 17).

Mason, M. F., Tatkow, E. P., and Macrae, C. N. (2005). The look of love gaze shifts and person perception. *Psychological Science*, 16(3):236–239. (Cited on page 25).

Masumoto, J. and Inui, N. (2013). Two heads are better than one: both complementary and synchronous strategies facilitate joint action. *Journal of Neurophysiology*, 109(5):1307–1314. (Cited on page 22).

Masumoto, J. and Inui, N. (2015). Motor control hierarchy in joint action that involves bimanual force production. *Journal of Neurophysiology*, 113(10):3736–3743. (Cited on page 22).

Mateeff, S., Genova, B., and Hohnsbein, J. (1999). The simple reaction time to changes in direction of visual motion. *Experimental Brain Research*, 124(3):391–394. (Cited on page 57).

Bibliography

Meadows, M. S. (2007). *I, avatar: The culture and consequences of having a second life.* New Riders. (Cited on page 24).

Medina, J. R., Duvallet, F., Karnam, M., and Billard, A. (2016). A human-inspired controller for fluid human-robot handovers. In *Proceedings of the IEEE/RAS International Conference on Humanoid Robots (Humanoids)*, pages 324–331. (Cited on page 29).

Medina, J. R., Lawitzky, M., Mörtl, A., Lee, D., and Hirche, S. (2011). An experience-driven robotic assistant acquiring human knowledge to improve haptic cooperation. In *Proceedings of the IEEE International Conference on Intelligent Robots and Systems (IROS)*, pages 2416–2422. (Cited on page 28).

Medina, J. R., Lee, D., and Hirche, S. (2012). Risk-sensitive optimal feedback control for haptic assistance. In *Proceedings of the IEEE International Conference on Robotics and Automation (ICRA)*, pages 1025–1031. (Cited on page 28).

Melendez-Calderon, A. (2012). *Investigating sensory-motor interactions to shape rehabilitation.* PhD thesis, Imperial College London. (Cited on page 18).

Melendez-Calderon, A., Komisar, V., and Burdet, E. (2015). Interpersonal strategies for disturbance attenuation during a rhythmic joint motor action. *Physiology and Behavior*, 147:348–358. (Cited on page 22).

Miall, R. and Jackson, J. (2006). Adaptation to visual feedback delays in manual tracking: evidence against the smith predictor model of human visually guided action. *Experimental Brain Research*, 172(1):77–84. (Cited on page 20).

Minato, T., Shimada, M., Ishiguro, H., and Itakura, S. (2004). Development of an android robot for studying human-robot interaction. In *Proceedings of the International Conference on Industrial, Engineering and Other Applications of Applied Intelligent Systems*, pages 424–434. (Cited on page 24).

Minato, T., Shimada, M., Itakura, S., Lee, K., and Ishiguro, H. (2005). Does gaze reveal the human likeness of an android? In *Proceedings of the IEEE International Conference on Development and Learning*, pages 106–111. (Cited on page 24).

Minato, T., Shimada, M., Itakura, S., Lee, K., and Ishiguro, H. (2006). Evaluating the human likeness of an android by comparing gaze behaviors elicited by the android and a person. *Advanced Robotics*, 20(10):1147–1163. (Cited on page 24).

Modares, H., Ranatunga, I., Lewis, F. L., and Popa, D. O. (2016). Optimized assistive human–robot interaction using reinforcement learning. *IEEE Transactions on Cybernetics*, 46(3):655–667. (Cited on page 28).

Mol, N., Smisek, J., Babuška, R., and Schiele, A. (2016). Nested compliant admittance control for robotic mechanical assembly of misaligned and tightly toleranced parts. In *Proceedings of the IEEE International Conference on Systems, Man, and Cybernetics (SMC)*, pages 002717–002722. (Cited on page 28).

Mori, M., MacDorman, K. F., and Kageki, N. (2012). The uncanny valley [from the field]. *Robotics and Automation Magazine*, 19(2):98–100. (Cited on page 25).

Mussa-Ivaldi, F. A., Hogan, N., and Bizzi, E. (1985). Neural, mechanical, and geometric factors subserving arm posture in humans. *Journal of Neuroscience*, 5(10):2732–2743. (Cited on page 22).

Mutlu, B., Kanda, T., Forlizzi, J., Hodgins, J., and Ishiguro, H. (2012). Conversational gaze mechanisms for humanlike robots. *ACM Transactions on Interactive Intelligent Systems (TiiS)*, 1(2):12. (Cited on page 25).

Mutlu, B., Shiwa, T., Kanda, T., Ishiguro, H., and Hagita, N. (2009). Footing in human-robot conversations: how robots might shape participant roles using gaze cues. In *Proceedings of the ACM/IEEE International Conference on Human-Robot Interaction (HRI)*, pages 61–68. (Cited on page 25).

Naeem, M., Prasad, G., Watson, D. R., and Kelso, J. (2012). Functional dissociation of brain rhythms in social coordination. *Clinical Neurophysiology*, 123(9):1789–1797. (Cited on page 20).

NaturalPoint (2018). Optitrack. https://www.optitrack.com. [Online; accessed 10-October-2018]. (Cited on page 62).

Neumann, K. and Steil, J. J. (2015). Learning robot motions with stable dynamical systems under diffeomorphic transformations. *Robotics and Autonomous Systems*, 70:1–15. (Cited on page 10).

Newman, W. S. (1992). Stability and performance limits of interaction controllers. *Journal of Dynamic Systems, Measurement, and Control*, 114(4):563–570. (Cited on page 124).

Noohi, E. and Žefran, M. (2017). Estimating human intention during a human–robot cooperative task based on the internal force internal force model. In *Trends in Control and Decision-Making for Human–Robot Collaboration Systems*, pages 83–109. Springer. (Cited on page 31).

Noy, L., Dekel, E., and Alon, U. (2011). The mirror game as a paradigm for studying the dynamics of two people improvising motion together. *Proceedings of the National Academy of Sciences*, 108(52):20947–20952. (Cited on pages 4, 23, 46, and 55).

Noy, L., Levit-Binun, N., and Golland, Y. (2015). Being in the zone: physiological markers of togetherness in joint improvisation. *Frontiers in Human Neuroscience*, 9:187. (Cited on page 24).

Oba, Y., Yamada, Y., Igarashi, K., Katsura, S., and Kakinuma, Y. (2016). Replication of skilled polishing technique with serial–parallel mechanism polishing machine. *Precision Engineering*, 45:292–300. (Cited on page 30).

Bibliography

Oguz, S. O., Kucukyilmaz, A., Sezgin, T. M., and Basdogan, C. (2010). Haptic negotiation and role exchange for collaboration in virtual environments. In *Proceedings of the IEEE Symposium on Haptics (HAPTICS)*, pages 371–378. (Cited on page 22).

Ott, C., Mukherjee, R., and Nakamura, Y. (2010). Unified impedance and admittance control. In *Proceedings of the IEEE International Conference on Robotics and Automation (ICRA)*, pages 554–561. (Cited on page 39).

Oztop, E., Wolpert, D., and Kawato, M. (2005). Mental state inference using visual control parameters. *Cognitive Brain Research*, 22(2):129–151. (Cited on page 16).

Pattacini, U. (2011). *Modular cartesian controllers for humanoid robots: Design and implementation on the icub*. PhD thesis, Ph. D. dissertation, RBCS, Italian Institute of Technology, Genova. (Cited on page 60).

Paus, T. (1991). Two modes of central gaze fixation maintenance and oculomotor distractibility in schizophrenics. *Schizophrenia Research*, 5(2):145–152. (Cited on page 139).

Perrett, D., Smith, P., Potter, D., Mistlin, A., Head, A., Milner, A., and Jeeves, M. (1985). Visual cells in the temporal cortex sensitive to face view and gaze direction. *Proceedings of the Royal Society of London B: Biological Sciences*, 223(1232):293–317. (Cited on page 19).

Perrin, N. and Schlehuber-Caissier, P. (2016). Fast diffeomorphic matching to learn globally asymptotically stable nonlinear dynamical systems. *Systems and Control Letters*, 96:51–59. (Cited on page 10).

Peternel, L., Petrič, T., and Babič, J. (2017a). Robotic assembly solution by human-in-the-loop teaching method based on real-time stiffness modulation. *Autonomous Robots*, pages 1–17. (Cited on page 26).

Peternel, L., Petrič, T., Oztop, E., and Babič, J. (2014). Teaching robots to cooperate with humans in dynamic manipulation tasks based on multi-modal human-in-the-loop approach. *Autonomous robots*, 36(1-2):123–136. (Cited on page 26).

Peternel, L., Tsagarakis, N., Caldwell, D., and Ajoudani, A. (2017b). Robot adaptation to human physical fatigue in human–robot co-manipulation. *Autonomous Robots*, pages 1–11. (Cited on page 31).

Petrič, T., Babič, J., et al. (2016). Cooperative human-robot control based on fitts' law. In *Proceedings of the IEEE/RAS International Conference on Humanoid Robots (Humanoids)*, pages 345–350. (Cited on page 27).

Pickering, M. J. and Clark, A. (2014). Getting ahead: forward models and their place in cognitive architecture. *Trends in Cognitive Sciences*, 18(9):451–456. (Cited on page 17).

Pistillo, A., Calinon, S., and Caldwell, D. G. (2011). Bilateral physical interaction with a robot manipulator through a weighted combination of flow fields. In *Proceedings of the IEEE/RSJ*

International Conference on Intelligent Robots and Systems (IROS), pages 3047–3052. (Cited on page 31).

Prinz, W. (1997). Perception and action planning. *European Journal of Cognitive Psychology*, 9(2):129–154. (Cited on page 20).

Quintero, C. P., Tatsambon, R., Gridseth, M., and Jägersand, M. (2015). Visual pointing gestures for bi-directional human robot interaction in a pick-and-place task. In *Proceedings of the IEEE International Symposium on Robot and Human Interactive Communication (RO-MAN)*, pages 349–354. (Cited on page 30).

Raffard, S., Bortolon, C., Cohen, L., Khoramshahi, M., Salesse, R. N., Billard, A., and Capdevielle, D. (2018). Does this robot have a mind? schizophrenia patients' mind perception toward humanoid robots. *Schizophrenia Research*, 197:585–586. (Cited on page 7).

Raffard, S., Bortolon, C., Khoramshahi, M., Salesse, R. N., Burca, M., Marin, L., Bardy, B. G., Billard, A., Macioce, V., and Capdevielle, D. (2016). Humanoid robots versus humans: How is emotional valence of facial expressions recognized by individuals with schizophrenia? an exploratory study. *Schizophrenia Research*, 176(2-3):506–513. (Cited on page 7).

Raffard, S., Salesse, R. N., Marin, L., Del-Monte, J., Schmidt, R. C., Varlet, M., Bardy, B. G., Boulenger, J.-P., and Capdevielle, D. (2015). Social priming enhances interpersonal synchronization and feeling of connectedness towards schizophrenia patients. *Scientific Reports*, 5. (Cited on page 139).

Ramaiah, M., Vijay, A., Sharma, G., and Mukerjee, A. (2013). Head motion animation using avatar gaze space. In *Proceedings of the IEEE International Symposium on Virtual Reality (VR)*, pages 95–96. (Cited on pages 25 and 128).

Ranasinghe, A., Dasgupta, P., Althoefer, K., and Nanayakkara, T. (2015). Identification of haptic based guiding using hard reins. *PloS One*, 10(7):e0132020. (Cited on page 22).

Ranatunga, I., Cremer, S., Popa, D. O., and Lewis, F. L. (2015). Intent aware adaptive admittance control for physical human-robot interaction. In *Proceedings of the IEEE International Conference on Robotics and Automation (ICRA)*, pages 5635–5640. (Cited on page 32).

Ranatunga, I., Lewis, F. L., Popa, D. O., and Tousif, S. M. (2017). Adaptive admittance control for human–robot interaction using model reference design and adaptive inverse filtering. *IEEE Transactions on Control Systems Technology*, 25(1):278–285. (Cited on page 28).

Ravichandar, H. C. and Dani, A. (2015). Human intention inference and motion modeling using approximate em with online learning. In *Proceedings of the IEEE/RSJ International Conference on Intelligent Robots and Systems (IROS)*, pages 1819–1824. (Cited on page 31).

Reed, K., Peshkin, M., Colgate, J. E., and Patton, J. (2004). Initial studies in human-robot-human interaction: Fitts' law for two people. In *Proceedings of the IEEE International Conference on Robotics and Automation (ICRA)*, volume 3, pages 2333–2338. (Cited on page 21).

Bibliography

Reed, K., Peshkin, M., Hartmann, M. J., Grabowecky, M., Patton, J., and Vishton, P. M. (2006a). Haptically linked dyads. *Psychological Science-Cambridge*, 17(5):365. (Cited on pages 21 and 22).

Reed, K. B., Peshkin, M., Hartmann, M. J., Colgate, J. E., and Patton, J. (2005). Kinesthetic interaction. In *Porceedings of the IEEE International Conference on Rehabilitation Robotics*. (Cited on page 22).

Reed, K. B., Peshkin, M., Hartmann, M. J., Patton, J., Vishton, P. M., and Grabowecky, M. (2006b). Haptic cooperation between people, and between people and machines. In *Proceedings of the IEEE International Conference on Intelligent Robots and Systems (IROS)*, pages 2109–2114. (Cited on pages 17 and 22).

Reed, K. B. and Peshkin, M. A. (2008). Physical collaboration of human-human and human-robot teams. *IEEE Transactions on Haptics*, 1(2):108–120. (Cited on page 22).

Richardson, M. J. and Johnston, L. (2005). Person recognition from dynamic events: The kinematic specification of individual identity in walking style. *Journal of Nonverbal behavior*, 29(1):25–44. (Cited on page 19).

Roux, P., d'Arc, B. F., Passerieux, C., and Ramus, F. (2014). Is the theory of mind deficit observed in visual paradigms in schizophrenia explained by an impaired attention toward gaze orientation? *Schizophrenia Research*, 157(1):78–83. (Cited on page 139).

Rozo, L., Calinon, S., Caldwell, D., Jiménez, P., and Torras, C. (2013). Learning collaborative impedance-based robot behaviors. In *Proceedings of the AAAI Conference on Artificial Intelligence*, pages 1422–1428. (Cited on page 27).

Sakamoto, D., Kanda, T., Ono, T., Ishiguro, H., and Hagita, N. (2007). Android as a telecommunication medium with a human-like presence. In *Proceedings of the ACM/IEEE International Conference on Human-Robot Interaction (HRI)*, pages 193–200. (Cited on page 24).

Salehian, S. S. M., Khoramshahi, M., and Billard, A. (2016). A dynamical system approach for softly catching a flying object: Theory and experiment. *IEEE Transactions on Robotics*, 32(2):462–471. (Cited on page 7).

Sallnäs, E.-L. and Zhai, S. (2003). Collaboration meets fitts' law: Passing virtual objects with and without haptic force feedback. In *Proceedings of the IFIP Interational Conference on Human-Computer Interaction*, pages 97–104. (Cited on page 21).

Sartori, L., Becchio, C., Bara, B. G., and Castiello, U. (2009). Does the intention to communicate affect action kinematics? *Consciousness and Cognition*, 18(3):766–772. (Cited on pages 17 and 19).

Sartori, L., Becchio, C., and Castiello, U. (2011). Cues to intention: the role of movement information. *Cognition*, 119(2):242–252. (Cited on pages 8, 17, and 19).

Sauser, E. L., Argall, B. D., Metta, G., and Billard, A. G. (2012). Iterative learning of grasp adaptation through human corrections. *Robotics and Autonomous Systems*, 60(1):55–71. (Cited on page 30).

Sawers, A., Bhattacharjee, T., McKay, J. L., Hackney, M. E., Kemp, C. C., and Ting, L. H. (2017). Small forces that differ with prior motor experience can communicate movement goals during human-human physical interaction. *Journal of Neuroengineering and rehabilitation*, 14(1):8. (Cited on pages 8 and 22).

Schindlbeck, C. and Haddadin, S. (2015). Unified passivity-based cartesian force/impedance control for rigid and flexible joint robots via task-energy tanks. In *Proceedings of the IEEE International Conference on Robotics and Automation (ICRA)*, pages 440–447. (Cited on pages 29 and 30).

Schmidt, R., Fitzpatrick, P., Caron, R., and Mergeche, J. (2011). Understanding social motor coordination. *Human Movement Science*, 30(5):834–845. (Cited on page 16).

Schulz, R. (2017). Collaborative robots learning spatial language for picking and placing objects on a table. In *Proceedings of the ACM International Conference on Human Agent Interaction*, pages 329–333. (Cited on page 30).

Sebanz, N., Bekkering, H., and Knoblich, G. (2006). Joint action: bodies and minds moving together. *Trends in Cognitive Sciences*, 10(2):70–76. (Cited on pages 16, 17, and 19).

Sebanz, N. and Knoblich, G. (2009). Prediction in joint action: What, when, and where. *Topics in Cognitive Science*, 1(2):353–367. (Cited on pages 8, 17, 18, 19, 20, and 21).

Sebanz, N., Knoblich, G., and Prinz, W. (2005). How two share a task: corepresenting stimulus-response mappings. *Journal of Experimental Psychology: Human Perception and Performance*, 31(6):1234. (Cited on page 17).

Senju, A. and Johnson, M. H. (2009). The eye contact effect: mechanisms and development. *Trends in Cognitive Sciences*, 13(3):127–134. (Cited on page 19).

Shadmehr, R. and Mussa-Ivaldi, F. A. (1994). Adaptive representation of dynamics during learning of a motor task. *The Journal of Neuroscience*, 14(5):3208–3224. (Cited on page 22).

Shahriari, E., Kramberger, A., Gams, A., Ude, A., and Haddadin, S. (2017). Adapting to contacts: Energy tanks and task energy for passivity-based dynamic movement primitives. In *Proceedings of the IEEE/RAS International Conference on Humanoid Robotics (Humanoids)*, pages 136–142. (Cited on pages 11 and 29).

Silverstein, S. M., Menditto, A. A., and Stuve, P. (2001). Shaping attention span: An operant conditioning procedure to improve neurocognition and functioning in schizophrenia. *Schizophrenia Bulletin*, 27(2):247. (Cited on page 139).

Skewes, J. C., Skewes, L., Michael, J., and Konvalinka, I. (2015). Synchronised and complementary coordination mechanisms in an asymmetric joint aiming task. *Experimental Brain Research*, 233(2):551–565. (Cited on page 22).

Słowiński, P., Alderisio, F., Zhai, C., Shen, Y., Tino, P., Bortolon, C., Capdevielle, D., Cohen, L., Khoramshahi, M., Billard, A., et al. (2017). Unravelling socio-motor biomarkers in schizophrenia. *npj Schizophrenia*, 3(1):8. (Cited on pages 7 and 24).

Slowinski, P., Rooke, E., Di Bernardo, M., and Tanaseva-Atanasova, K. (2014). Kinematic characteristics of motion in the mirror game. In *Proceedings of the IEEE International Conference on Systems, Man, and Cybernetics (SMC)*. (Cited on page 24).

Smith, O. J. (1959). A controller to overcome dead time. *ISA Journal*, 6(2):28–33. (Cited on page 20).

Sommer, N., Kronander, K., and Billard, A. (2017). Learning externally modulated dynamical systems. In *Proceedings of the IEEE/RSJ International Conference on Intelligent Robots and Systems (IROS)*. (Cited on page 29).

Stefanov, N., Peer, A., and Buss, M. (2009). Role determination in human-human interaction. In *Proceedings of the EuroHaptics Conference and Symposium on Haptic Interfaces for Virtual Environment and Teleoperator Systems*, pages 51–56. (Cited on page 22).

Stefanov, N., Peer, A., and Buss, M. (2010). Online intention recognition for computer-assisted teleoperation. In *Proceedings of the IEEE International Conference on Robotics and Automation (ICRA)*, pages 5334–5339. (Cited on page 131).

Steptoe, W., Wolff, R., Murgia, A., Guimaraes, E., Rae, J., Sharkey, P., Roberts, D., and Steed, A. (2008). Eye-tracking for avatar eye-gaze and interactional analysis in immersive collaborative virtual environments. In *Proceedings of the ACM Conference on Computer Supported Cooperative work*, pages 197–200. (Cited on page 25).

Strabala, K. W., Lee, M. K., Dragan, A. D., Forlizzi, J. L., Srinivasa, S., Cakmak, M., and Micelli, V. (2013). Towards seamless human-robot handovers. *Journal of Human-Robot Interaction*, 2(1):112–132. (Cited on page 26).

Takagi, A., Bagnato, C., and Burdet, E. (2016). Facing the partner influences exchanges in force. *Scientific Reports*, 6:35397. (Cited on page 22).

Takagi, A., Ganesh, G., Yoshioka, T., Kawato, M., and Burdet, E. (2017). Physically interacting individuals estimate the partner's goal to enhance their movements. *Nature Human Behaviour*, 1(3):0054. (Cited on pages 17, 18, 22, and 129).

Takagi, A., Usai, F., Ganesh, G., Sanguineti, V., and Burdet, E. (2018). Haptic communication between humans is tuned by the hard or soft mechanics of interaction. *PLoS Computational Biology*, 14(3):e1005971. (Cited on page 22).

Takeda, T., Kosuge, K., and Hirata, Y. (2005). Hmm-based dance step estimation for dance partner robot -ms dance-. In *Proceedings of the IEEE/RSJ International Conference on Intelligent Robots and Systems (IROS)*, pages 3245–3250. (Cited on page 131).

Tanwani, A. K. and Calinon, S. (2017). A generative model for intention recognition and manipulation assistance in teleoperation. In *Proceedings of the IEEE/RSJ International Conference on Intelligent Robots and Systems (IROS)*, pages 43–50. IEEE. (Cited on page 31).

Thoroughman, K. A. and Shadmehr, R. (2000). Learning of action through adaptive combination of motor primitives. *Nature*, 407(6805):742. (Cited on page 10).

Tikhanoff, V., Cangelosi, A., Fitzpatrick, P., Metta, G., Natale, L., and Nori, F. (2008). An open-source simulator for cognitive robotics research: the prototype of the icub humanoid robot simulator. In *Proceedings of the ACM Workshop on Performance Metrics for Intelligent Systems*, pages 57–61. (Cited on page 58).

Todorov, E. and Jordan, M. I. (2002). Optimal feedback control as a theory of motor coordination. *Nature Neuroscience*, 5(11):1226. (Cited on page 23).

Tomasello, M. (1995). Joint attention as social cognition. *Joint Attention: Its Origins and Role in Development*, pages 103–130. (Cited on pages 17 and 19).

Tomasello, M., Hare, B., Lehmann, H., and Call, J. (2007). Reliance on head versus eyes in the gaze following of great apes and human infants: the cooperative eye hypothesis. *Journal of Human Evolution*, 52(3):314–320. (Cited on page 18).

Townsend, E. C., Mielke, E. A., Wingate, D., and Killpack, M. D. (2017). Estimating human intent for physical human-robot co-manipulation. *arXiv preprint arXiv:1705.10851*. (Cited on page 20).

Tykal, M., Montebelli, A., and Kyrki, V. (2016). Incrementally assisted kinesthetic teaching for programming by demonstration. In *Proceedings of the ACM/IEEE International Conference on Human-Robot Interaction (HRI)*, pages 205–212. (Cited on page 30).

Valdesolo, P., Ouyang, J., and DeSteno, D. (2010). The rhythm of joint action: Synchrony promotes cooperative ability. *Journal of Experimental Social Psychology*, 46(4):693–695. (Cited on page 17).

van der Wel, R. P., Knoblich, G., and Sebanz, N. (2011). Let the force be with us: dyads exploit haptic coupling for coordination. *Journal of Experimental Psychology: Human Perception and Performance*, 37(5):1420. (Cited on pages 8, 18, and 22).

van Schie, H. T., van Waterschoot, B. M., and Bekkering, H. (2008). Understanding action beyond imitation: reversed compatibility effects of action observation in imitation and joint action. *Journal of Experimental Psychology: Human Perception and Performance*, 34(6):1493. (Cited on page 17).

Bibliography

Vanderborght, B., Albu-Schäffer, A., Bicchi, A., Burdet, E., Caldwell, D. G., Carloni, R., Catalano, M., Eiberger, O., Friedl, W., Ganesh, G., et al. (2013). Variable impedance actuators: A review. *Robotics and Autonomous Systems*, 61(12):1601–1614. (Cited on page 28).

Varlet, M., Filippeschi, A., Ben-sadoun, G., Ratto, M., Marin, L., Ruffaldi, E., and Bardy, B. G. (2013). Virtual reality as a tool to learn interpersonal coordination: Example of team rowing. *PRESENCE: Teleoperators and Virtual Environments*, 22(3):202–215. (Cited on page 139).

Varlet, M., Marin, L., Raffard, S., Schmidt, R. C., Capdevielle, D., Boulenger, J.-P, Del-Monte, J., and Bardy, B. G. (2012). Impairments of social motor coordination in schizophrenia. *PLoS One*, 7(1):e29772. (Cited on page 139).

Vesper, C., Abramova, E., Bütepage, J., Ciardo, F., Crossey, B., Effenberg, A., Hristova, D., Karlinsky, A., McEllin, L., Nijssen, S. R., et al. (2017). Joint action: mental representations, shared information and general mechanisms for coordinating with others. *Frontiers in Psychology*, 7:2039. (Cited on page 17).

Vesper, C., Butterfill, S., Knoblich, G., and Sebanz, N. (2010). A minimal architecture for joint action. *Neural Networks*, 23(8):998–1003. (Cited on pages 17 and 18).

Volcic, R. and Lappe, M. (2009). Keeping an eye on each other: gaze behaviour in joint action. In *Abstracts of the European Conference on Visual Perception*, volume 38, pages 174–174. (Cited on pages 18, 19, and 26).

Wang, W., Li, R., Chen, Y., and Jia, Y. (2018). Human intention prediction in human-robot collaborative tasks. In *Proceedings of the ACM/IEEE International Conference on Human-Robot Interaction (HRI)*, pages 279–280. (Cited on page 31).

Wang, Z., Yuan, J., and Buss, M. (2008). Modelling of human haptic skill: A framework and preliminary results. In *Proceedings of the International Federation of Automatic Control (IFAC)*, volume 41, pages 14761–14766. (Cited on page 23).

Wolpert, D. M., Doya, K., and Kawato, M. (2003). A unifying computational framework for motor control and social interaction. *Philosophical Transactions of the Royal Society of London B: Biological Sciences*, 358(1431):593–602. (Cited on pages 20 and 21).

Wolpert, D. M., Miall, R. C., and Kawato, M. (1998). Internal models in the cerebellum. *Trends in Cognitive Sciences*, 2(9):338–347. (Cited on pages 20 and 51).

Yang, C., Ganesh, G., Haddadin, S., Parusel, S., Albu-Schaeffer, A., and Burdet, E. (2011). Human-like adaptation of force and impedance in stable and unstable interactions. *IEEE Transactions on robotics*, 27(5):918–930. (Cited on page 23).

Yoshikawa, Y., Shinozawa, K., Ishiguro, H., Hagita, N., and Miyamoto, T. (2006). Responsive robot gaze to interaction partner. In *Proceedings of the International Conference on Robotics: Science and Systems*. (Cited on pages 25 and 128).

Zhai, C., Alderisio, F., Tsaneva-Atanasova, K., and Di Bernardo, M. (2014). A novel cognitive architecture for a human-like virtual player in the mirror game. In *Proceedings of the IEEE International Conference on Systems, Man, and Cybernetics (SMC)*, pages 754–759. (Cited on page 23).

Zhao, X., Cusimano, C., and Malle, B. F. (2016). Do people spontaneously take a robot's visual perspective? In *Proceedings of the ACM/IEEE International Conference on Human-Robot Interaction (HRI)*, pages 133–134. (Cited on page 128).

Mahdi Khoramshahi

Curriculum Vitae

EPFL, ME A3 434, Station 9
Lausanne 1015, Switzerland
✆ *(+41) 21 69 35961*
✉ *mahdi.khoramshahi@epfl.ch*

Education

2014–2018 **PhD in Robotics and Intelligent Systems**, *École Polytechnique Fédérale de Lausanne, Institute of Microengineering*, Lausanne, Switzerland.
PhD thesis: From human-intention recognition to compliant-motion control using dynamical systems in physical human-robot interaction. Supervisor: Prof. Aude Billard

2009–2012 **M.S. in Electrical Engineering (Control Systems)**, *University of Tehran, Department of Electrical and Computer Engineering*, Tehran, Iran.
Master thesis: A Study on effects of flexible Spine on stability and energy consumption of a quadruped robot. Supervisor: Prof. Majid Nili Ahmadabadi

2004–2009 **B.S. in Electrical Engineering (Control Systems)**, *Sharif University of Technology, Department of Electrical Engineering*, Tehran, Iran.

Projects and Research Experience

2017–2018 **SecondHands**, *European project (H2020-ICT-2014-1)*, Designing robotic systems that can offer help to a maintenance technician in a pro-active manner, EPFL, Switzerland.
Researcher

2014–2016 **AlterEgo**, *European project (FP7-ICT-600610)*, Designing new human-artificial agent interactions through the concept of similarity in order to enhance human social competence, EPFL, Switzerland.
Researcher

2013–2014 **Design of energy efficient walking systems**, *Exploitation and modification of natural dynamics through design and control for reaching energy efficient system*, Cognitive Robotics Laboratory, University of Tehran, Supervisors: Prof. Majid Nili Ahmadabadi.
Research assistance

2012–2013 **Multi-Terrain Locomotion of Water-Running robots**, *Closed-loop control of a quadruped water-runner robot*, NanoRobotics Laboratory, Carnegie Mellon University, Supervisors: Prof. Metin Sitti.
Scholar visitor

2011–2012 **Bobcat: a quadruped robot with flexible spine**, *Design and control implementation of a quadruped robot with flexible spine*, Biorobotics Laboratory (BioRob), École Polytechnique Fédérale de Lausanne (EPFL), Supervisors: Prof. Auke Jan Ijspeert, Dr. Alexander Sprowitz.
Internship

Journals:

2018 **Dynamical System Approach to Task-Adaptation in Physical Human-Robot Interaction.**, *Mahdi Khoramshahi*, *Aude Billard*, Autonomous Robots 2018.

– **Does this robot have a mind? Schizophrenia patients' mind perception toward humanoid robots.**, *Stéphane Raffard, Catherine Bortolon, Laura Cohen, Mahdi Khoramshahi, Robin Salesse, Aude Billard, Delphine Capdevielle*, Schizophrenia Research 2018.

– **Influence of facial feedback during a cooperative human-robot task in schizophrenia.**, *Laura Cohen, Mahdi Khoramshahi, Robin Salesse, Catherine Bortolon, Piotr Slowinski, Chao Zhai, Krasimira Tsaneva-Atanasova, Mario Di Bernardo, Delphine Capdevielle, Ludovic Marin, Richard C. Schmidt, Benoit G. Bardy, Aude Billard, Stéphane Raffard* , Nature - Scientific Reports 2018.

2017 **Unravelling socio-motor biomarkers in schizophrenia.**, *Piotr Slowinski, Francesco Alderisio, Chao Zhai, Yuan Shen, Peter Tino, Catherine Bortolon, Delphine Capdevielle, Laura Cohen, Mahdi Khoramshahi, Aude Billard, Robin Salesse, Mathieu Gueugnon, Ludovic Marin, Benoit G. Bardy, Mario Di Bernardo, Stéphane Raffard, Krasimira Tsaneva-Atanasova*, Schizophrenia npj.

– **Adaptive Natural Oscillator to Exploit Natural Dynamics for Energy Efficiency.**, *Mahdi Khoramshahi, Rezvan Nasiri, Mohammad Shushtari, Aude Ijspeert, Majid Nili Ahmadabadi*, Robotics and Autonomous Systems 2017.

2016 **Role of Gaze Cues in Interpersonal Motor Coordination: Towards Higher Affiliation in Human-Robot Interaction**, *Mahdi Khoramshahi, Ashwini Shukla, Stéphane Raffard, Benoit G. Bardy, Aude Billard*, PLoS ONE.

– **Adaptation in Variable Parallel Compliance: Towards Energy Efficiency in Cyclic Tasks**, *Rezvan Nasiri, Mahdi Khoramshahi, Mohammad Shushtari, Aude Ijspeert, Majid Nili Ahmadabadi*, Transactions on Mechatronics.

– **A Dynamical System Approach for Catching Softly a Flying Object: Theory and Experiment**, *Seyed Sina Mirrazavi Salehian, Mahdi Khoramshahi, Aude Billard*, Transactions on Mechatronics.

– **Humanoid robots versus humans: How is emotional valence of facial expressions recognized by individuals with schizophrenia? An exploratory study**, *stÃ©phane Raffard, Catherine Bortolon, Mahdi Khoramshahi, Robin Salesse, Marianna Burca, Ludovic Marin, Benoit G. Bardy, Aude Billard, ValÃ©rie Macioce, Delphine Capdevielle*, Schizophrenia Research.

2013 **Piecewise linear spine for speed-energy efficiency trade-off in quadruped robots.**, *Mahdi Khoramshahi, Hamed Jalaly Bidgoly, Soroosh Shafiee, Ali Asaei, Auke Jan Ijspeert, Majid Nili Ahmadabadi*, Robotics and Autonomous Systems.

Conference Proceedings and abstracts:

2018 **From Human Physical Interaction To Online Motion Adaptation Using Parameterized Dynamical Systems**, *Mahdi Khoramshahi, Antoine Laurens, Thomas Triquet, Aude Billard*, International Conference on Intelligent Robots and Systems.

- **Intention-based motion-adaptation using dynamical systems with human in the loop**, *Mahdi Khoramshahi*, *Aude Billard*, Machine Learning in Robot Motion Planning.

2017 **Effects of Facial Emotions on Social-motor Coordination in Schizophrenia**, *Laura Cohen*, *Mahdi Khoramshahi*, *Robin Salesse*, *Catherine Bortolon*, *Piotr Slowinski*, *Chao Zhai*, *Krasimira Tsaneva-Atanasova*, *Mario Di Bernardo*, *Delphine Capdevielle*, *Ludovic Marin*, *Richard C. Schmidt*, *Benoit G. Bardy*, *Aude Billard*, *Stéphane Raffard*, Joint Action Meetings.

2016 **Design of a Nonlinear Adaptive Natural Oscillator: Towards Natural Dynamics Exploitation in Cyclic Tasks**, *Rezvan Nasiri*, *Mahdi Khoramshahi*, *Majid Nili Ahmadabadi*, International Conference on Intelligent Robots and Systems.

2015 **From joint-attention to joint-action: Effects of gaze on human following motion**, *Mahdi Khoramshahi*, *Ashwini Shukla*, *Aude Billard*, Joint Action Meetings.

2014 **Cognitive mechanism in synchronized motion: An internal predictive model for manual tracking control**, *Mahdi Khoramshahi*, *Ashwini Shukla*, *Aude Billard*, International Conference on Intelligent Robots and Systems.

- **Natural Dynamics Modification for Energy Efficiency: A Data-driven Parallel Compliance Design Method**, *Mahdi Khoramshahi*, *Atoosa Parsa*, *Auke Ijspeert*, *Majid Nili Ahmadabadi*, International Conference on Robotics and Automation.

- **Energy Efficient Locomotion with Adaptive Natural Oscillator**, *Mahdi Khoramshahi*, *Rezvan Nasiri*, *Auke Ijspeert*, *Majid Nili Ahmadabadi*, Dynamic Walking.

- **Robust Walking using Piecewise Linear Spring**, *Mahdi Khoramshahi*, *Ali Asaei*, *Auke Ijspeert*, *Majid Nili Ahmadabadi*, Dynamic Walking.

2013 **Benefits of an Active Spine Supported Bounding Locomotion With a Small Compliant Quadruped Robot**, *Mahdi Khoramshahi*, *Alexander Sprowitz*, *Alexandre Tuleu*, *M. N. Ahmadabadi*, *Auke Ijspeert*, International Conference on Robotics and Automation.

- **Angular motion control using a closed-loop CPG for a water-running robot**, *Nithish Thatte*, *Mahdi Khoramshahi*, *Auke Jan Ijspeert*, *Metin Sitti*, Dynamic Walking.

- **Use Your Spine! Effect of Active Spine Movements on Horizontal Impulse and Cost of Transport in a Bounding, Quadruped Robot**, *Alexander Sprowitz*, *Emilie Badri*, *Mahdi Khoramshahi*, *Alexandre Tuleu*, *Auke Ijspeert*, Dynamic Walking.

- **Exploiting natural dynamics of nonlinear compliance using adaptive oscillators**, *Mahdi Khoramshahi*, *Auke Jan Ijspeert*, *Majid Nili Ahmadabadi*, Adaptive Motion of Animal and Machine.

Skills and qualifications

Automation control Expert with several years of experience in designing controllers and algorithms with application in robotics including linear, nonlinear, adaptive, optimal control methods.

Machine Learning	Experience in Reinforcement Learning (Q-learning, Policy Improvement, etc.), dimension reduction (PCA, LDA, etc.), regression (GMR, SVR, GP, etc.), clustering (GMM, K-means, etc.), classification (Linear models, SVM, Neural Networks, Nearest Neighbor)
Signal Processing	Experience with time-series, filtering, and forecasting with applications in robotic and control systems
Statistical analysis	Experience with design of experiments, hypothesis testing, and performing statistical analysis using parametric and non-parametric models.
Programming languages	$C/C++$ software development (with focus on control architectures for real-time robotic applications), Matlab (as primary language for scientific computing, machine learning, and control systems design), and R/Stata (with focus on statistical inferences)
Operation Systems	Ubuntu/Linux, Windows
Tools	Latex (with long experience with scientific typesetting), Microsoft office, Adobe Photoshop and Premiere (with intermediate knowledge for image and video editing), Git, SVN

Teaching Experience

2017	Robotic Practicals, EPFL, Lausanne
2016	Robotic Practicals, EPFL, Lausanne
2015	Robotic Practicals, EPFL, Lausanne
2011	Distributed Artificial Intelligence, University of Tehran, Iran
2010	Machine learning, University of Tehran, Iran
–	Robotics, University of Tehran, Iran

Languages

English	Proficient
Farsi	Mother tongue
French	Intermediate (B1)

Interests

- Music (playing guitar, bass guitar, and piano) and Chess
- Cinema, photography, and philosophy